

# Acta Naturae

## Organism-Level Tumor Models in Zebrafish *Danio rerio*



**MOLECULAR APPROACHES  
TO SAFE AND CONTROLLED  
ENGINEERED T-CELL  
THERAPY**  
P. 16

**REVERSIBLE CYCLIC  
THERMAL INACTIVATION  
OF OLIGOPEPTIDASE B FROM  
*Serratia proteamaculans***  
P. 65



# Comprehensive solutions for cell analysis



- Cell lines and primary cells
- Traditional and specialized culture media
- Sterilizing filtration



- Biochemical reagents
- Water purification systems
- Cell counting and analysis
- Cryopreservation



## An extensive range and top quality of cell lines from our partner, the European Collection of Authenticated Cell Cultures (ECACC):

- 4000 animal and human cell lines;
- Cells of 45 animal species and 50 tissue types;
- 370 B-lymphoblastoid cell lines for which human leukocyte antigen (HLA) typing data are available;
- 480 hybridoma cell lines secreting monoclonal antibodies;
- DNA, RNA, and cDNA extracted from the cell lines from our collection;

[SIGMAaldrich.com/ECACC](https://www.sigmaaldrich.com/ECACC)

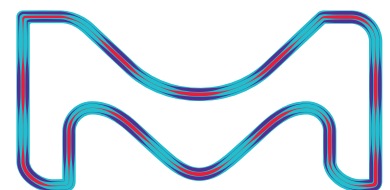
### LLC Merck

Valovaya Str., 35, Moscow, 115054, Russia;

Tel. +7 (495) 937-33-04

E-mail: [mm.russia@merckgroup.com](mailto:mm.russia@merckgroup.com), [ruorder@sial.com](mailto:ruorder@sial.com)

[SIGMAaldrich.com/cellculture](https://www.sigmaaldrich.com/cellculture)  
[MERCKmillipore.com/cellculture](https://www.merckmillipore.com/cellculture)

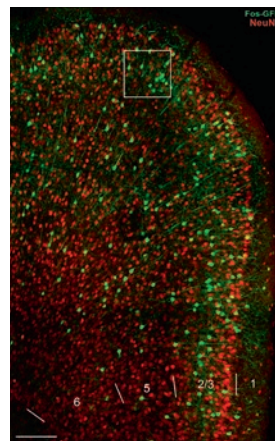


SIGMA-ALDRICH® is now MERCK

# Cognitive Tagging of Neurons: CRE-Mediated Genetic Labeling and Characterization of the Cells Involved in Learning and Memory

O. I. Ivashkina, N. S. Vorobyeva, A. M. Gruzdeva, M. A. Roshchina, K. A. Toropova, K. V. Anokhin

In this study, authors describe use of Cre-mediated recombination to obtain a permanent genetic labeling of the brain neuronal networks activated during a new experience in animals. This method utilizes bitransgenic Fos-Cre-eGFP mice in which a green fluorescent protein is expressed upon tamoxifen-induced Cre-recombination only in the cells where immediate early gene *c-fos* expression takes place due to the new experience. Authors also showed that a combination of genetic Cre-eGFP labeling with immunohistochemical staining of the endogenous *c-Fos* protein allows one to identify and compare the neuronal populations that are activated during two different episodes of new experiences in the same animal. This new approach can be used in a wide spectrum of tasks that require imaging and a comparative analysis of cognitive neuronal networks.

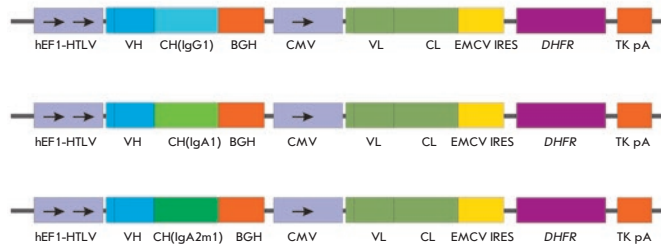


Experience-dependent Cre-recombination takes place only in neurons

# The Development and Study of Recombinant Immunoglobulin A to Hemagglutinins of the Influenza Virus

T. K. Aliev, I. G. Dement'yeva, V. A. Toporova, V. V. Argentova, L. P. Pozdnyakova, M. N. Bokov, Yu. A. Votchitseva, D. A. Dolgikh, S. D. Varfolomeyev, P. G. Sveshnikov, M. P. Kirpichnikov

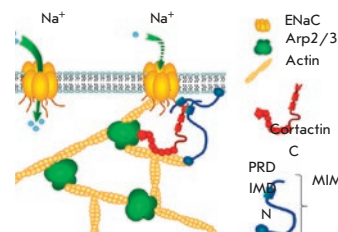
Authors obtained recombinant variants of human antibody FI6 broadly specific to hemagglutinins of the influenza A virus. On the basis of a bi-promoter (CMV, hEF1-HTLV) vector, they developed genetic constructs for the expression of the heavy and light chains of the immunoglobulins of IgA1-, IgA2m1-, and IgG-isotypes. Authors performed an immunohistochemical characterization and studied their interactions with influenza A strains of the H1N1- and H3N2-subtypes.



Expression cassettes of bi-promotor plasmids for the production of FI6 antibodies of different isotypes.

# Role of the Scaffold Protein MIM in the Actin-Dependent Regulation of Epithelial Sodium Channels (ENaC)

L. S. Shuyskiy, V. V. Levchenko, Y. A. Negulyaev, A. V. Staruschenko, D. V. Ilatovskaya  
Epithelial Sodium Channels (ENaCs) are expressed in different organs and tissues, particularly in the cortical collecting duct (CCD) in the kidney, where they fine tune sodium reabsorption. Dynamic rearrangements of the cytoskeleton are one of the common mechanisms of ENaC activity regulation. In previous studies, authors showed that the actin-binding proteins cortactin and Arp2/3 complex are involved in the cytoskeleton-dependent regulation of ENaC and that their cooperative work decreases a channel's probability of remaining open; however, the specific mechanism of interaction between actin-binding proteins and ENaC is unclear. In this study, authors propose a new component for the protein machinery involved in the regulation of ENaC, the missing-in-metastasis (MIM) protein.



Suggested scheme of actin-dependent regulation of ENaC by the actin-binding proteins MIM, cortactin, and the Arp2/3 complex

## Founders

Ministry of Education and  
Science of the Russian Federation,  
Lomonosov Moscow State University,  
Park Media Ltd

## Editorial Council

*Chairman:* A.I. Grigoriev  
*Editors-in-Chief:* A.G. Gabibov, S.N. Kochetkov

V.V. Vlassov, P.G. Georgiev, M.P. Kirpichnikov,  
A.A. Makarov, A.I. Miroshnikov, V.A. Tkachuk,  
M.V. Ugryumov

## Editorial Board

*Managing Editor:* V.D. Knorre

K.V. Anokhin (Moscow, Russia)  
I. Bezprozvanny (Dallas, Texas, USA)  
I.P. Bilenkina (Moscow, Russia)  
M. Blackburn (Sheffield, England)  
S.M. Deyev (Moscow, Russia)  
V.M. Govorun (Moscow, Russia)  
O.A. Dontsova (Moscow, Russia)  
K. Drauz (Hanau-Wolfgang, Germany)  
A. Friboulet (Paris, France)  
M. Issagouliants (Stockholm, Sweden)  
A.L. Konov (Moscow, Russia)  
M. Lukic (Abu Dhabi, United Arab Emirates)  
P. Masson (La Tronche, France)  
V.O. Popov (Moscow, Russia)  
I.A. Tikhonovich (Moscow, Russia)  
A. Tramontano (Davis, California, USA)  
V.K. Švedas (Moscow, Russia)  
J.-R. Wu (Shanghai, China)  
N.K. Yankovsky (Moscow, Russia)  
M. Zouali (Paris, France)

*Project Head:* N.V. Soboleva

*Editor:* N.Yu. Deeva

*Designer:* K.K. Oparin

*Art and Layout:* K. Shnaider

*Copy Chief:* Daniel M. Medjo

Phone/Fax: +7 (495) 727 38 60

E-mail: vera.knorre@gmail.com, actanaturae@gmail.com

Reprinting is by permission only.

© ACTA NATURAE, 2018

Номер подписан в печать 27 июня 2018 г.

Тираж 200 экз. Цена свободная.

Отпечатано в типографии «МИГ ПРИНТ»

# CONTENTS

## REVIEWS

L. A. Dobrynina, M. R. Zabitova,  
L. A. Kalashnikova, E. V. Gnedovskaya,  
M. A. Piradov

**Hypertension and Cerebral  
Microangiopathy (Cerebral Small Vessel  
Disease): Genetic and Epigenetic Aspects  
of Their Relationship. . . . . 4**

R. S. Kalinin, A. V. Petukhov, V. D. Knorre,  
M. A. Maschan, A. V. Stepanov, A.G. Gabibov  
**Molecular Approaches to Safe  
and Controlled Engineered T-cell Therapy. . . 16**

I. V. Mizgirev, D. R. Safina, I. V. Demidyuk,  
S. V. Kostrov  
**Organism-Level Tumor Models  
in Zebrafish *Danio rerio*. . . . . 24**

## RESEARCH ARTICLES

T. K. Aliev, I. G. Dement'yeva,  
V. A. Toporova, V. V. Argentova,  
L. P. Pozdnyakova, M. N. Bokov,  
Yu. A. Votchitseva, D. A. Dolgikh,  
S. D. Varfolomeyev, P. G. Sveshnikov,  
M. P. Kirpichnikov

**The Development and Study  
of Recombinant Immunoglobulin A  
to Hemagglutinins of the Influenza Virus. . . . 30**

O. I. Ivashkina, N. S. Vorobyeva,  
A. M. Gruzdeva, M. A. Roshchina,  
K. A. Toropova, K. V. Anokhin  
**Cognitive Tagging of Neurons:  
CRE-Mediated Genetic Labeling and  
Characterization of the Cells Involved  
in Learning and Memory** .....37

E. A. Komech, I. V. Zvyagin,  
M. V. Pogorelyy, I. Z. Mamedov,  
D. A. Fedorenko, Y. B. Lebedev  
**Characterization of the T-cell Repertoire  
after Autologous HSCT in Patients with  
Ankylosing Spondylitis** .....48

N. A. Nikitenko, E. S. Gureeva, A. A. Ozerov,  
A. I. Tukhvatulin, F. M. Izhaeva, V. S. Prassolov,  
P. G. Deryabin, M. S. Novikov, D. Y. Logunov  
**1-(4-Phenoxybenzyl) 5-Aminouracil  
Derivatives and Their Analogues –  
Novel Inhibitors of Human Adenovirus  
Replication**.....58

M. V. Ovchinnikova, A. G. Mikhailova,  
D. M. Karlinsky, V. A. Gorlenko, L. D. Rumsh  
**Reversible Cyclic Thermal  
Inactivation of Oligopeptidase B from  
*Serratia proteamaculans***.....65

I. V. Ryzhova, A. D. Nozdrachev, T. V. Tobias,  
E. A. Vershinina  
**Soluble Guanylate Cyclase As the Key  
Enzyme in the Modulating Effect of NO  
on Metabotropic Glutamate Receptors** .....71

A. A. Stakheev, L. V. Samokhvalova,  
O. D. Mikityuk, S. K. Zavriev  
**Phylogenetic Analysis and Molecular  
Typing of Trichothecene-Producing  
*Fusarium* Fungi from Russian Collections** .....79

E. F. Khaziev, D. V. Samigullin,  
A. N. Tsentsevitsky, E. A. Bukharaeva,  
E. E. Nikolsky  
**ATP Reduces the Entry of Calcium Ions  
into the Nerve Ending by Blocking L-type  
Calcium Channels** .....93

L. S. Shuyskiy, V. V. Levchenko,  
Y. A. Negulyaev, A. V. Staruschenko,  
D. V. Ilatovskaya  
**Role of the Scaffold Protein MIM  
in the Actin-Dependent Regulation  
of Epithelial Sodium Channels (ENaC)** .....97

**Guidelines for Authors**..... 104



**IMAGE ON THE COVER PAGE**  
(see the article by Mizgirev *et al.*)

# Hypertension and Cerebral Microangiopathy (Cerebral Small Vessel Disease): Genetic and Epigenetic Aspects of Their Relationship

L. A. Dobrynina\*, M. R. Zabitova, L. A. Kalashnikova, E. V. Gnedovskaya, M. A. Piradov

Research center of neurology, Volokolamskoe Shosse 80, Moscow, 125367, Russia

\*E-mail: dobrla@mail.ru

Received May 03, 2017; in final form April 24, 2018

Copyright © 2018 Park-media, Ltd. This is an open access article distributed under the Creative Commons Attribution License, which permits unrestricted use, distribution, and reproduction in any medium, provided the original work is properly cited.

**ABSTRACT** Hypertension (HT) and its cerebral complications are extremely vexing medical and social problems. Despite the obvious association between hypertension and the clinical and neuroimaging features of cerebral microangiopathy (CMA) (also known as cerebral small vessel disease), the causal links between them remain ambiguous. Besides, antihypertensive therapy as the only way to manage these patients does not always prevent brain damage. Knowledge about the key factors and mechanisms involved in HT and CMA development is important for predicting the risk of cerebral complications and developing new approaches to their prevention and treatment. At present, genome-wide association studies and other approaches are used to investigate the common hereditary mechanisms of HT and CMA development, which will explain a large number of CMA cases not associated with hypertension, lack of a correlation between HT severity and the degree of cerebral injury, and failure of antihypertensive therapy to prevent CMA progression. Epigenetic markers likely play a modulating role in the development of these diseases.

**KEYWORDS** genetics, epigenetics, arterial hypertension, cerebral microangiopathy, small vessel disease, neuroimaging.

**ABBREVIATIONS** HT – hypertension, CMA – cerebral microangiopathy, WMH – white matter hyperintensities, LI – lacunar infarct, GWAS – genome-wide association study, RAAS – renin-angiotensin-aldosterone system, CADASIL – cerebral autosomal dominant arteriopathy with subcortical infarcts and leukoencephalopathy, CARASIL – cerebral autosomal recessive arteriopathy with subcortical infarcts and leukoencephalopathy, RVCL – retinal vasculopathy with cerebral leukodystrophy.

## INTRODUCTION

For many decades, hypertension (HT) has been one of the leading pathologies in the structure of morbidity and mortality in populations across the world. On average, HT is diagnosed in every third adult and has an age-dependent pattern and a tendency to increase in its incidence rate with the next decades [1–4]. The cerebral complications of HT develop very early, dominate, and contribute the most to the structure of HT-associated mortality [5–7]. HT-associated lesions in small cerebral arteries, arterioles, capillaries, and venules lead to the development of the progressive cerebral microangiopathy (CMA) (in Russia, it is included in a broader concept termed dyscirculatory encephalopathy; in the foreign literature, it is referred to as small vessel disease) that is one of the main causes of strokes and dementia [5, 8–14]. At present, there is an understanding of the relationship between white matter hyperinten-

sities (WMH, previously known as leukoaraiosis), which is a recognized neuroimaging marker of CMA, and the duration and profile of HT, cognitive impairments/dementia, disability, and risk of stroke and death [10, 15–24], as well as the possibility of delaying the progression of WMH and cognitive impairments by using adequate antihypertensive therapy [11, 25, 26]. The latter is implicitly confirmed by the recent Framingham study that demonstrated a reduction in the rate of vascular dementia in subjects with secondary and higher education, which was presumably related to their greater awareness, access to medical care, and adherence to therapy. However, the reduced prevalence of most vascular risk factors in these people, including HT control, could not adequately explain the reduction in the rate of dementia [27]. In addition, the absence of a direct correlation between the severity of HT and the degree of clinical and neuroimaging manifestations of

CMA, which is well-known in clinical practice, as well as the risk of CMA in middle-aged and elderly individuals without HT is indicative of the ambiguity of the relationships between CMA and HT and inapplicability of antihypertensive therapy as the only management option for CMA patients to arrest the progression of CMA.

Epidemiological analysis has revealed a high coefficient of heritability of leukoaraiosis in family and twin studies (55–71%) [28], as well as a more than 1/3 (36%) overlap between the hereditary factors controlling pulse pressure and indicators of fractional anisotropy of the white matter [29]. In this regard, the close relationship between HT and CMA may be explained by common genetic disorders.

The influence of common environmental factors, including diet and lifestyle, on the development of both diseases may indicate an involvement of common epigenetic mechanisms of gene expression regulation. This is in line with the Framingham study results [27]. Adherence to a healthy lifestyle and diet, more anticipated among individuals with high education, may be one of the explanations for the reduced dementia in such populations.

### GENETICS OF HT AND CMA

The main aspects of genetic studies of HT and CMA are as follows:

- investigation of monogenic (Mendelian) forms;
- analysis of the candidate genes associated with known signs/mechanisms of disease development; and
- genome-wide association studies (GWAS) – clarification of the nucleotide variants associated with HT and CMA.

### Monogenic forms of HT and CMA

The number of monogenic (Mendelian) forms of HT and CMA known to date is small. Monogenic forms of HT are characterized by a very low prevalence in the population [30]. Despite pathogenetic heterogeneity, they are all associated with mutations in the components of the renin-angiotensin-aldosterone system (RAAS), which ultimately lead to impairment of urinary sodium excretion. Below, we provide a list of the main genes whose mutations are associated with particular forms of CMA (Table 1). The best known monogenic forms of CMA include CADASIL, caused by a mutation in the *NOTCH3* receptor gene located on chromosome 19q12; CARASIL (mutations in the *HTRA1* gene encoding serine peptidase 1, which is located on chromosome 10q25); an autosomal dominant form of COL4A1 (the *COL4A1* gene encoding collagen type IV  $\alpha 1$ , which is mapped on chromosome 13q34); RVCL (the *TREX1* gene encoding DNase III exhibiting 3'–5' exonuclease

activity, which occurs on chromosome 3p21); and the Fabry disease (X-linked disease caused by mutations in the *GLA* gene encoding  $\alpha$ -galactosidase A, chromosome Xq22) [31]. In all these forms of CMA, an altered protein product leads to a loss of the structural and functional integrity of small arteries with subsequent secondary injury to the brain substance. CADASIL is the most commonly diagnosed hereditary CMA. Its estimated prevalence is 4.6/100,000 in the adult population, and the mutation rate in the *NOTCH3* gene is 10.7/100,000 adults [32]. Most CADASIL patients have no HT, but when it is present in carriers of certain polymorphisms in the *NOTCH3* gene, the risk of injury to the white matter increases [33]. Accurate information about the prevalence of other monogenic CMAs is unavailable, and HT occurrence has not been analyzed.

### Candidate genes for HT and CMA

The main directions in the search for the candidate genes associated with individual risk of the disease include the investigation of the genes that are the key components of RAAS, endothelium, hemostasis, inflammation and immune response, neurotrophic factors, etc. (Table 2) (the names of the genes/polymorphisms/proteins are given in accordance with international nomenclature <https://www.ncbi.nlm.nih.gov/genome/guide/human/>).

Apparently, impaired functioning of the RAAS is central in the development of HT. The imbalance in the functioning of RAAS components is associated with vasoconstriction, electrolyte imbalance with sodium and water retention, and vascular remodeling [30]. The role of angiotensinogen (*AGT*), the angiotensin-converting enzyme (*ACE*), and aldosterone synthase (*CYP11B2*) genes in these processes has been the best studied. Studies of the significance of angiotensin II receptor type 1 and 2 (*AGTR1*, *AGTR2*) and renin genes yielded controversial results [34–36].

### The *AGT* gene of angiotensinogen (chromosome 1q42).

The *AGT* gene belongs to the serpin gene superfamily, is expressed in the brain, liver, heart, adipose tissue, kidney, and vascular walls, and encodes a precursor of angiotensin II (AGTII) – a physiological regulator of blood pressure (BP) and water-salt metabolism. Among the large number of molecular variants of the *AGT* gene, only the polymorphisms rs699C > T (codon M235T) and rs4762C > T (codon T174M) have been shown to be associated with HT and plasma angiotensinogen levels in Europeans and white Americans [37, 38]. Attempts to reproduce these studies have led to ambiguous results [39, 40].

According to [41], the homozygous genotype of the codon M235T of the *AGT* gene is associated, signifi-

**Table 1.** Monogenic forms of CMA

| Disease       | Locus | Gene          | Protein                                   | Mode of inheritance | Clinical manifestations  | MRI findings  | Morphological changes in the vascular wall                                |
|---------------|-------|---------------|---|---------------------|--|---|---|
| CADASIL       | 19q12 | <i>NOTCH3</i> | NOTCH3-receptor                           | Autosomal dominant  | Migraine with aura, lacunar strokes, cognitive impairments/dementia, mental disorders  | WMH in the temporal lobe poles and external capsules, subcortical LIs         | Accumulation of osmiophilic deposits                                      |
| CARASIL       | 10q25 | <i>HTRA1</i>  | HtrA, serine peptidase 1                  | Autosomal recessive | Cognitive disorders, lacunar strokes, alopecia, low back pain  | Subcortical LIs   | Extensive smooth muscle cell degeneration                                 |
| COL4A1        | 13q34 | <i>COL4A1</i> | $\alpha$ 1-collagen type IV               | Autosomal dominant  | Porencephaly, infantile cerebral palsies, Axenfeld-Rieger anomaly, nephropathy, cramps, cataract, retinal hemorrhages                        | WMH, LI, subcortical microhemorrhages   | Basement membrane damage  |
| RVCL          | 3p21  | <i>TREX1</i>  | DNase III with 3'-5'-exonuclease activity | Autosomal dominant  | Retinal vasculopathy, migraine, cognitive impairments, mental disorders, Raynaud's phenomenon, hepatic cirrhosis, nephropathy, osteonecrosis | Subcortical LIs, WMH  | Basement membrane damage  |
| Fabry disease | Xq22  | <i>GLA</i>    | $\alpha$ -galactosidase A                 | X-linked            | Angiokeratomas, acroparesthesias, damage to the kidneys and heart, changes in the facial skull   | WMH and LI in the vertebral-basilar system, dolichoectasia of the main artery | Accumulation of lysosomal deposits in endothelial and smooth muscle cells |

cantly and independently of HT, to the progression of brain injury in CMA, but not with carotid atherosclerosis, which suggests that this genotype is a genetic marker of progressive brain injury in CMA. However, the number of lacunae detected in the brain of carriers of this genotype was significantly smaller than that in heterozygous carriers [35]. The latter is explained by a probable involvement of angiotensinogen in clotting processes. This is indirectly confirmed by the relationship, independent of increased BP, between an *AGT* gene polymorphism and the development of lacunar infarct [35]. An investigation of polymorphisms C521T (T174M, T207M) and rs699 (T704C) of the *AGT* gene in a Transbaikalian population failed to establish any link with the development of chronic cerebral ischemia (most likely associated with CMA) [42]. An analysis of a group of 410 adults (aged 50–75 years) with CMA-specific changes revealed by MRI demonstrated that the four most common mutations in the gene promoter were combined into haplotypes. In this case, the B-haplotype (–6:A, –20:C, –153:G, –218:G) was an HT-independent risk factor of changes in the brain. The (B/B) homozygosity of this haplotype was found to increase eight-fold or more the risk of brain injury in CMA [43]. As was shown later,

the B haplotype enhances the main transcriptional activity of the *AGT* promoter in astrocytes (the main site of *AGT* synthesis in the brain), which suggests a potential association between white matter injury and impaired RAAS activity [44]. A later study found no relationship between single polymorphisms in the *ACE* and *AGT* genes and white matter injury in CMA. The exception was the polymorphism –20A > C in the *AGT* promoter region, which was associated with leukoaraiosis in HT patients [45]. Recently, in healthy elderly subjects, a relationship was established between the M268T polymorphism (previously M235T) of the *AGT* gene and a loss of the microstructure of some white matter regions. This was assessed by MRI fractional anisotropy [46].

*The ACE gene of the angiotensin-converting enzyme (chromosome 17q23).* The angiotensin-converting enzyme converts angiotensin 1 into a potent angiotensin-2 vasopressor, cleaves bradykinin (stimulant of endothelial NO formation) to inactive metabolites, and regulates the release of aldosterone. HT is better associated with the insertion-deletion (I/D) polymorphism in intron 16 of the *ACE* gene, which is identified by the presence/absence of Alu repeats. A combination

**Table 2.** Association of candidate genes with MRI markers of CMA and/or HT

| Gene           | Polymorphism   | Association   |   |
|----------------|--|---|---|
|                |  | MRI markers of CMA  | HT                                      |
| <i>AGT</i>     | rs699  | Lacunes [35, 41], WMH [41]<br>Loss of white matter tract microstructure [46]<br>Not verified [42, 45] | Found [37, 8]<br>Not verified [39, 40]  |
| <i>AGT</i>     | rs4762   | Not verified [42]   | Found [37, 38]<br>Not verified [39, 40] |
| <i>AGT</i>     | -20A>C   | WMH [45]  | Found [45]                              |
| <i>ACE</i>     | I/D<br>Alu-sequences                                       | WMH [52–55]<br>Not verified [46]  | Found [47–52]                           |
| <i>CYP11B2</i> | rs1799998  | WMH, expansion of perivascular spaces [36, 56]  | No data                                 |
| <i>NOS1</i>    | rs3782218  | Contradictory data  | Found [59]                              |
| <i>NOS3</i>    | rs3918226  | Contradictory data  | Found [59]                              |
| <i>NOS3</i>    | rs3918227  | Contradictory data  | Found [59]                              |
| <i>EDN1</i>    | rs5370   | Not verified [45]   | Found [63, 64]                          |
| <i>MTHFR</i>   | rs1801133  | WMH, LI [65, 66]<br>Not verified [55, 67, 68]   | Found [65, 66]                          |
| <i>PLAT</i>    | rs2020918  | LI [71, 72]   | No data                                 |
| <i>FGB</i>     | rs1800790  | LI [73]   | No data                                 |
| <i>IL1B</i>    | rs16944  | LI [78], WMH [81]   | No data                                 |
| <i>IL6</i>     | rs1800795  | LI [79], WMH [80]   | Not verified [74]                       |
| <i>IL6</i>     | rs1800796  | LI [80]   | Found [75]                              |
| <i>TNFA</i>    | rs1800629  | No data   | Found [75]                              |
| <i>MMP2</i>    | rs243865   | WMH [85]  | No data                                 |
| <i>MMP2</i>    | rs1030868<br>rs2241145<br>rs2287074<br>rs2287076<br>rs7201 | LI [84]   | No data                                 |
| <i>MMP9</i>    | rs3918242  | No data   | Found [78]                              |
| <i>CRP</i>     | rs3091244  | WMH [81]  | No data                                 |
| <i>VEGF</i>    | rs2010963  | LI [86]   | Found [86]                              |
| <i>BDNF</i>    | rs6265   | WMH [87]  | No data                                 |

of II+ID alleles of the I/D polymorphism with a daily intake of more than 2,300 mg of salt was found to be associated with HT and subsequent obesity [47]. The D allele of I/D polymorphism was found to be associated with diastolic and systolic HT, daily variability of HT, and injury to target organs [48–52]. The D/D genotype was shown to play a significant role in the development of CMA-associated cerebral lesions [53, 54] and in the prediction of the risk of this lesion [55].

**The aldosterone synthase gene (*CYP11B2*, chromosome 8q24.3).** Aldosterone synthase catalyzes the synthesis of aldosterone from deoxycorticosterone. Aldosterone increases tubular reabsorption of Na<sup>+</sup> and elimination of K<sup>+</sup>, which enhances the ability of tissues to retain water. The protective effect of the C allele of polymorphism rs1799998 (-344T> C) of *CYP11B2* is manifest-

ed in leukoaraiosis and the expansion of perivascular spaces [36, 56].

**Genes affecting endothelial function**

These genes include the *NOS1* gene encoding neuronal NO synthase (nNOS) (chromosome 12q24.2-q24.3) and the *NOS3* gene of endothelial NO synthase (eNOS) (chromosome 7q35-q36). NO plays an important role in maintaining the homeostasis of the endothelium. Impairment of NO production leads to failure of physiological vasodilation, increased aggregation and adhesion of platelets, proliferation and migration of smooth muscle cells, and inflammation – the main pathophysiological mechanisms of HT and CMA. Inhibition of the *NOS1* gene in the medulla oblongata and hypothalamus is associated with the pathogenesis of systemic hypertension [57]. A genome-wide association study for

ischemic stroke risk factors identified *NOS1* as a potential candidate gene [58]. Among the 58 single nucleotide substitutions in the *NOS* genes associated with HT, there were the polymorphic sites rs3782218 in *NOS1* and rs3918226 and rs3918227 in *NOS3* [59]. The data published by Russian researchers who have studied the association between the polymorphisms rs1799983 (G298A, G894T) and 4a/4b of the *NOS3* gene and HT and the remodeling of the wall of large cerebral arteries are contradictory [60–62]. There are no stably reproducible results concerning the significance of *NOS* polymorphisms in the development of CMA.

**The endothelin-1 gene (*EDN1*, chromosome 6p24.1).** The polymorphism rs5370G > T (codon K198N) of the *EDN1* gene encoding a potent vasoconstrictor, endothelin has been shown to be associated with the development of HT [63, 64]. The role of the polymorphisms in endothelin and endothelin receptor genes in CMA has not been verified [45].

**The methylenetetrahydrofolate reductase gene (*MTHFR*, chromosome 1p36.22).** Methylenetetrahydrofolate reductase is involved in the conversion of homocysteine to methionine in the presence of cofactors (vitamins B6 and B12) and a substrate (folic acid). Most population-based studies have confirmed the association between the polymorphism rs1801133C > T (C677T) in the *MTHFR* gene and hyperhomocysteinemia and CMA (WMH volume or lacunar infarcts) in patients with and without HT [65, 66]. However, a significant number of studies have found no evidence of association between the polymorphism C677T and WMH [55, 67, 68]. Studies that have evaluated the total effect of carriage of several polymorphisms have revealed significant worsening of CMA (WMH, lacunar infarcts) when a C677T variant of the *MTHFR* gene was combined with the D/D genotype of the I/D polymorphism of the *ACE* gene. At the same time, combination of one of the genotypes 2/2, 2/3, 4/4, or 4/3 of the *APOE* gene (chromosome 19q13, apolipoprotein E) with the *MTHFR* C677T or *ACE* D/D genotype can act as an independent genetic risk factor for leukoaraiosis [69, 70].

### Genes of the hemostasis system

There is contradictory data on the association between the polymorphism rs2020918 (–7351C/T) in the tissue plasminogen activator gene (*PLAT*, or *TPA*) and the development of lacunar infarcts [71, 72]. The AA genotype of polymorphism rs1800790 (455G/A) of the fibrinogen gene (*FGB*) has been demonstrated to be associated with an increased risk of multiple lacunar infarcts [73].

### Genes of immune response and inflammation

The largest number of studies that have explored the pathogenetic significance of mutations in the genes of inflammation are devoted to genetic variants of cytokines. The polymorphisms rs1800796 (572G > C) of the interleukin-6 gene (*IL6*) [74] and rs1800629 (308G > A) of the *TNF $\alpha$*  gene encoding tumor necrosis factor alpha have been found to be associated with the development of HT in the Asian population [75]. *TNF $\alpha$*  gene polymorphisms also affect the course of HT in the population of the Russian Central Chernozem Region [76]. The polymorphism rs3918242 (–1562C > T) in the matrix metalloproteinase-9 gene (*MMP9*) is associated with a risk of HT [77].

A study of the polymorphism rs16944 (–511C > T) in the interleukin-1 $\beta$  gene (*IL1B*) revealed a prevalence of the T/T genotype in patients with lacunar strokes compared to other stroke subtypes. An analysis with allowance for concomitant factors demonstrated that the T/T genotype of the *IL1B* gene (polymorphism 511C > T) was an independent risk factor of strokes in CMA [78]. The C/C genotype of the polymorphism rs1800795 (–174G > C) of the *IL6* gene has been shown to be associated with lacunar stroke and an increased risk of WMH [79, 80], and the polymorphism rs1800796 (–572G > C) has been associated with the development of asymptomatic infarcts [80]. Worsening of WMH was detected in old and elderly subjects without neurological deficiency, homozygous carriers of the *IL1B* rs16944 (–511C > T) T allele and T allele at position –286 (rs3091244) of the C-reactive protein gene (*CRP*) [81]. There is an increase in the carriage rate of homozygous variants of polymorphisms –31CC of the *IL1B* gene, –174GG of the *IL6* gene, –197AA of the *IL17A* gene, and –166ArgArg of the *IL17F* gene, as well as the alleles IL-1 $\beta$ -31C of the *IL1B* gene and IL17F-166Arg of the *IL17F* gene in elderly patients (Transbaikalian population of Russia) with chronic ischemia most likely associated with CMA [82]. No association of the haplotypes/polymorphisms of the *CRP* gene with CMA has been detected [83]. It has been demonstrated that carriage of the allelic variants rs1030868:g.T, rs2241145:g.C, rs2287074:g.A, rs2287076:g.C, and rs7201:g.C of the *MMP2* gene is associated with a risk of lacunar infarcts; the rs7201:g.C allele is an independent risk factor for their development [84]; and the C/C genotype of the *MMP2* gene (rs243865, 1306T > C) plays an independent predictive role in the development of leukoaraiosis [85].

### Genes of trophic factors

The polymorphism rs2010963 (–634G > C) of the vascular endothelial growth factor gene (*VEGF*) was found to be associated with the development of lacunar stroke

in [86]. The multidirectional effect of homozygous carriage of various Val66Met (rs6265) codon alleles of the brain-derived neurotrophic factor gene (*BDNF*) in WMH and cognitive disorders has been revealed: the Met allele is protective, and the Val allele is damaging [87].

Therefore, a significant number of genes selected based on data on the causes and mechanisms of disease development have been studied to date. The identified and reproducible associations of polymorphisms of these genes with HT and CMA suggest that these polymorphisms are risk factors for the diseases. However, most researchers have indicated that the cumulative data explain only a small part of HT and CMA cases and their course manifestations, and that the rather frequent contradictions in the results are due to the impossibility of reproducing them in other samples [88]. The data on an HT-independent association of mutations in the key pathogenetic factors, e.g., the TT genotype (M235T polymorphism) and B haplotype of the *AGT* gene, with the development and progression of CMA confirm the ambiguity of the relationships between CMA and HT. In addition, the dependence of the clinical significance of mutations on environmental factors, in particular the development of HT and obesity in carriers of the *ACE* gene I/D polymorphism and the effect of a high daily salt uptake [47], confirm the need for a clarification of the effect of environmental factors on gene expression when studying the mechanisms of HT and CMA. An approach based on an investigation of candidate genes has some limitations in assessing the various possible variants of interaction and overlap of inherited features.

### GENOME-WIDE ASSOCIATION STUDIES (GWAS)

To date, several genome-wide studies aimed at clarifying the loci associated with HT and CMA have been performed (Table 3). However, only a few of these studies have identified loci with genome-wide significance ( $p < 5 \times 10^{-8}$ ).

The Global Blood Pressure Genetics (BPGen) consortium and the Cohorts for Heart and Ageing Research in Genome Epidemiology (CHARGE) consortium analyzed 34,433 and 29,136 individuals, respectively, and identified eight loci associated with HT, three of which were common to both studies [89, 90]. Later, the International Consortium for Blood Pressure Genome-Wide Association Studies (ICBP GWAS) analyzed the data of 200,000 individuals and identified 29 loci, six of which had been previously identified as significant for HT [91]. Many of these loci are considered as potential candidates, including the *NPPA* and *NPPB* genes encoding natriuretic peptides.

In 2011, the CHARGE consortium performed the first genome-wide association study for WMH in 9,361

stroke-free individuals of European descent (mean age 69.5 years; 42.6% males) [92]. Six single-nucleotide polymorphisms (with a genome-wide level of significance) associated with a high risk of WMH were identified. Of these, rs3744028 in the *TRIM65* gene had the most significant association with WMH severity. The polymorphisms were mapped to a single genetic locus – a 17q25 chromosome region containing seven major genes: *WBP2*, *TRIM65*, *TRIM47*, *MRPL38*, *FBF1*, *ACOX1*, and *UNC13D*. All these genes are involved in the processes of neuroinflammation and immune system functioning. The results of this meta-analysis could be reproduced in subsequent studies [93–95].

In 2015, the results of a multi-ethnic genome-wide association study for WMH were published [96]. The study involved 21,079 middle-aged dementia- and stroke-free individuals selected from 29 population-based cohorts: European ( $n=17,936$ ), African ( $n=1,943$ ), Hispanic ( $n=795$ ), and Asian ( $n=405$ ). The obtained data confirmed the association of a 17q25 chromosome region with a risk of WMH; also, three loci (chromosomes 10q24, 1q22, and 2p16.1) associated with WMH in more than one population were identified. The genetic loci regulating systolic and diastolic HT were shown to be associated with the development of WMH. A new chromosome 10q24 locus containing genome-wide significant polymorphisms in the introns of the *PDCD11*, *NEURL*, *SH3PXD2A*, *TAF5*, and *CALHM1* genes is associated with the development of brain tumors (medulloblastomas, astrocytomas, gliomas), with *CALHM1* being associated with both the regulation of calcium homeostasis and formation of amyloid beta. Earlier, the polymorphism rs2984613 (chromosome 1q22; *PMF1* and *SLC25A44* genes) had been found to be associated with non-lobar intracerebral hemorrhage [97].

In 2015, the results of a genome-wide association study for white matter lesion progression in elderly individuals of European descent were also published [98]. Progression of white matter lesions was observed in 1,085 (14%) participants in the study, which was indicative of the low significance of genetic factors in the progression of this lesion in the elderly. The findings were explained by a possible omission of significant polymorphisms, a relatively short follow-up period to assess the contribution of genetic factors to progression, and the age of the study participants. A potential role of genetic factors in white matter lesion progression in young people was suggested.

Thus, the performed genome-wide association studies for WMH and HT have revealed the loci whose genes are associated with both WMH and HT variability. Understanding the biological functions of these genes and evaluating their overlap and interaction will shed light on the molecular mechanisms of WMH, their

**Table 3.** Results of genome-wide association studies (GWAS) for HT and CMA

| Study   | Single nucleotide polymorphism   | Locus  | P-value   |  |
|---|--|--|---|--|
|   |  |  | Systolic BP   | Diastolic BP   |
| <b>HT</b>   |  |  |   |  |
| Global BPGen (Global Blood Pressure Genetics) [89]<br>Sample size – 34,433 individuals  | rs17367504<br>rs11191548<br>rs12946454<br>rs16998073<br>rs1530440<br>rs653178<br>rs1378942<br>rs16948048   | <b>1p36</b><br><b>10q24</b><br>17q21<br>4q21<br>10q21<br><b>12q24</b><br><b>15q24</b><br>17q21   | $1 \times 10^{-5}$<br>$3 \times 10^{-17}$<br>$4 \times 10^{-6}$   | $7 \times 10^{-9}$<br>$3 \times 10^{-6}$<br>$1 \times 10^{-7}$<br>$6 \times 10^{-8}$<br>$5 \times 10^{-6}$   |
| CHARGE (The Cohorts for Heart and Ageing Research in Genome Epidemiology) [90]<br>Sample size – 29,136 individuals                | rs1004467<br>rs381815<br>rs2681492<br>rs2681472<br>rs3184504<br>rs9815354<br>rs11014166<br>rs2384550<br>rs6495122  | <b>10q24</b><br>11p15<br>12q21<br>12q21<br>12q24<br>3p22<br>10p12<br><b>12q24</b><br><b>15q24</b>  | $1.99 \times 10^{-6}$<br>$5.76 \times 10^{-7}$<br>$3.01 \times 10^{-11}$<br><br>$5.73 \times 10^{-7}$   | $3.74 \times 10^{-8}$<br>$1.68 \times 10^{-8}$<br>$7.88 \times 10^{-7}$<br>$8.82 \times 10^{-7}$<br>$1.32 \times 10^{-7}$<br>$8.10 \times 10^{-7}$   |
| ICBP GWAS (International Consortium for Blood Pressure Genome-Wide Association Studies) [91]<br>Sample size – 200,000 individuals | rs2932538<br>rs13082711<br>rs419076<br>rs13107325<br>rs13139571<br>rs1173771<br>rs11953630<br>rs1799945<br>rs805303<br>rs4373814<br>rs932764<br>rs7129220<br>rs633185<br>rs2521501<br>rs17608766<br>rs1327235<br>rs6015450<br>rs17367504<br>rs3774372<br>rs1458038<br>rs1813353<br>rs4590817<br>rs11191548<br>rs381815<br>rs17249754<br>rs3184504<br>rs10850411<br>rs1378942<br>rs12940887 | 1p13<br>3p24<br>3q26<br>4q24<br>4q32<br>5p13<br>5q33<br>6p22<br>6p21<br>10p12<br>10q23<br><b>11p15</b><br>11q22<br>15q26<br>17q21<br>20p12<br>20q13<br><b>1p36</b><br><b>3p22</b><br>4q21<br>10p12<br><b>10q21</b><br>10q24<br><b>11p15</b><br>12q21<br><b>12q24</b><br><b>12q24</b><br><b>12q24</b><br><b>17q21</b> | $1.2 \times 10^{-9}$<br>$1.5 \times 10^{-6}$<br>$1.8 \times 10^{-13}$<br>$3.3 \times 10^{-14}$<br>$1.2 \times 10^{-6}$<br>$1.8 \times 10^{-16}$<br>$3.0 \times 10^{-11}$<br>$7.7 \times 10^{-12}$<br>$1.5 \times 10^{-11}$<br>$4.8 \times 10^{-11}$<br>$7.1 \times 10^{-16}$<br>$3.0 \times 10^{-12}$<br>$1.2 \times 10^{-17}$<br>$5.2 \times 10^{-19}$<br>$1.1 \times 10^{-10}$<br>$1.9 \times 10^{-8}$<br>$3.9 \times 10^{-23}$<br>$8.7 \times 10^{-22}$<br>0.39<br>$1.5 \times 10^{-23}$<br>$2.6 \times 10^{-12}$<br>$4.0 \times 10^{-12}$<br>$6.9 \times 10^{-26}$<br>$5.3 \times 10^{-11}$<br>$1.8 \times 10^{-18}$<br>$3.8 \times 10^{-18}$<br>$5.4 \times 10^{-8}$<br>$5.7 \times 10^{-23}$<br>$1.8 \times 10^{-10}$ | $9.9 \times 10^{-10}$<br>$3.8 \times 10^{-9}$<br>$2.1 \times 10^{-12}$<br>$2.3 \times 10^{-17}$<br>$2.2 \times 10^{-10}$<br>$9.1 \times 10^{-12}$<br>$3.8 \times 10^{-11}$<br>$1.5 \times 10^{-15}$<br>$3.0 \times 10^{-11}$<br>$4.4 \times 10^{-10}$<br>$8.1 \times 10^{-7}$<br>$6.4 \times 10^{-8}$<br>$2.0 \times 10^{-15}$<br>$1.9 \times 10^{-15}$<br>0.017<br>$1.4 \times 10^{-15}$<br>$5.6 \times 10^{-23}$<br>$3.5 \times 10^{-19}$<br>$9.0 \times 10^{-14}$<br>$8.5 \times 10^{-25}$<br>$2.3 \times 10^{-15}$<br>$1.3 \times 10^{-12}$<br>$9.4 \times 10^{-13}$<br>$5.3 \times 10^{-10}$<br>$1.2 \times 10^{-14}$<br>$3.6 \times 10^{-25}$<br>$5.4 \times 10^{-10}$<br>$2.7 \times 10^{-26}$<br>$2.3 \times 10^{-14}$ |
| <b>WMH</b>  |  |  |   |  |
| CHARGE (The Cohorts for Heart and Ageing Research in Genome Epidemiology) [92]<br>Sample size – 9,361 individuals                 | rs3744028<br>rs1055129<br>rs3744017<br>rs936393<br>rs9894383<br>rs11869977   | 17q25  | $4.0 \times 10^{-9}$<br>$4.1 \times 10^{-8}$<br>$7.3 \times 10^{-9}$<br>$6.8 \times 10^{-9}$<br>$5.3 \times 10^{-9}$<br>$5.7 \times 10^{-9}$  |  |
| Multi-ethnic GWAS [96]<br>Sample size – 21,079 individuals  | rs72848980<br>rs7894407<br>rs7214628<br>rs12357919<br>rs7909791<br>rs78857879<br>rs2984613<br>rs11679640   | <b>17q25</b><br><b>17q25</b><br><b>17q25</b><br>10q24.33<br>10q24.33<br>2p16.1<br>1q22<br>2p21   | $2.6 \times 10^{-9}$<br>$2.6 \times 10^{-8}$<br>$5.1 \times 10^{-9}$<br>$1.5 \times 10^{-8}$<br>$2.9 \times 10^{-9}$<br>$1.5 \times 10^{-8}$<br>$2.0 \times 10^{-8}$<br>$2.1 \times 10^{-6}$  |  |

\*Loci identified in different studies are shown in bold

relationships with HT, and their involvement in aging and the development of degenerative lesions. The results thus obtained confirm the multifactorial character of diseases and the dependence of their course on combinations of and interaction between the factors. However, at present, the cumulative effect of the GWAS-identified HT loci explains less than 3% of clinically significant HT variability [99].

### EPIGENETICS OF HT AND CMA

Epigenetic studies of HT and CMA are not numerous and are mainly devoted to the influence of potentially modifiable environmental factors, lifestyle, and diet on gene expression [100].

The main mechanisms of epigenetic modulation of gene expression include DNA methylation, chromatin modifications (including histones), and microRNA regulation [101–103].

### DNA methylation

Methylation regulates gene activity through attaching a methyl group to DNA cytosine bases, which disrupts RNA synthesis and, accordingly, translation. Functionally, hypermethylation should lead to the silencing of the gene, and hypomethylation should lead to gene activation [100].

Protein deficiency in the diet of pregnant rats was found to lead to hypomethylation of the *ACE* gene promoter, causing a predisposition to both HT and cognitive impairment in rat offspring [104]. An inverse correlation between *ACE* gene methylation, angiotensin converting enzyme activity, and systolic BP is observed in children. In this case, the methylation level in children with the DD genotype and low weight is significantly lower than that in children with normal weight [105]. As was demonstrated in a Chinese population, the risk of HT depends on the methylation level of the CpG1 and CpG2-5 sites of the *ADD1* gene (adducin) in females and males, respectively, as well as those of the *ADD1* promoter regardless of gender [106]. Hypermethylation of the *HSD11B2* gene promoter (hydroxysteroid 11-beta dehydrogenase 2) leads to impaired conversion of cortisol to cortisone, an increased tetrahydrocortisol/tetrahydrocortisone ratio (active metabolites of cortisol and cortisone), and the development of HT in humans [107, 108]. Hypomethylation of the *NKCC1* gene (Na-K-2Cl cotransporter-1) in hypertensive rats is associated with increased *NKCC1* activity and the development of HT [109]. A relationship between the methylation and expression of the *NET* gene (norepinephrine transporter) in patients with HT and panic attacks was established [110].

The only microarray analysis of DNA methylation in CMA revealed differently methylated genes asso-

ciated to the onset and progression of leukoaraiosis. For example, the *NDRG1* gene located on chromosome 8q24 was hypermethylated (the cytoplasmic protein encoded by this gene is involved in the protection of the myelin sheath in the peripheral nervous system, cell differentiation, tumor metastasis and hypoxia, inflammatory response, etc.) and the *BRUNOL4* gene or the *CELF4* gene (chromosome 18q12, BRUNO-like 4 protein involved in mRNA stabilization) was hypomethylated compared to the control group with a normal neuroimaging picture [111].

### Histone modification

Histones (H1/H5, H2A, H2B, H3, and H4) are the main chromatin proteins involved in the packaging of DNA into nucleosomes in the nucleus. The involvement of histones in the mechanisms of epigenetic regulation of nuclear processes is enabled by a 20-amino-acid mobile N-terminal fragment (tail) of the nucleosome. Modification of the N-terminal fragment, which involves various enzymes (arginine methylation, lysine acetylation, serine and threonine phosphorylation, ubiquitination, etc.), affects the interaction between histones and DNA. Dissociation of the histone makes DNA packing less dense and more accessible to regulatory proteins, which leads to an increase in gene activity, while denser packaging reduces gene activity. For example, acetylation of histones enhances transcription, while deacetylation inhibits it; methylation of lysine inhibits transcription, and methylation of arginine activates transcription; hypermethylation or monomethylation of lysine can have the opposite effect – turn off or activate target genes [112].

The enzymatic cascades triggered by aldosterone upon hypomethylation of histone H3 Lys79 are associated with activation of the epithelial Na<sup>+</sup> channel gene promoter, which leads to an increase in the number of Na channels in the distal parts of the nephron, enhanced cAMP-mediated reabsorption of sodium, and development of HT [113]. Hypermethylation of histone H3 caused by deficiency in lysine-specific demethylase 1 (LSD-1) leads to the development of HT in mice on a high-salt diet [114]. A transgenic mouse model was used to demonstrate the possibility of triggering sympathetic activation upon primary stimulation of B2-adrenergic receptors via the acetylation of histones H3 and H4, followed by turning-off of the *WNK4* gene promoter (serine-threonine kinase). This led to overexpression of the Na<sup>+</sup>Cl<sup>-</sup> cotransporter and epithelial Na<sup>+</sup> channels, sodium reabsorption, and the development of HT [115]. Acetylation of H3 in area postrema neurons was shown to be associated with a change in the sensitivity of the catecholaminergic neurons of the medul-

lary cardiovascular center, followed by sympathetic brainstem activation and HT [116].

### MicroRNA regulation

MicroRNAs (miR) are endogenous noncoding RNAs ~22 nucleotides in length that regulate gene activity both at the transcriptional level, preventing the transfer of information from DNA to mRNA, and at the translation stage, which leads to a destruction of synthesized mRNA. At least 30% of human genes are believed to be regulated by microRNAs [117]. Activation of miR-21 expression by angiotensin II in human adrenal gland cells was shown to result in increased aldosterone secretion and enhanced cell proliferation [118]. MiR-124 and miR-135a influence the expression of the mineralocorticoid receptor gene *NR3C2* involved in the mechanisms of familial hypertension and renal salt balance maintenance [119]. An increase in the miR-320 and miR-26b levels and a decrease in the miR-21 level are observed in salt-sensitive Dahl rats. A presumed target of miR-320 is the insulin-like growth factor-1 receptor. The vascular remodeling observed in a high-salt diet is believed to be associated with inactivation of these receptors [120]. There is a relationship between miR-143, miR-145, miR-21, miR-133, and miR-1 and changes in vascular smooth muscle cells and vascular bed remodeling in HT. The peripheral blood mononuclear cells in HT patients are characterized by a low level of miR-143, miR-145, and miR-133 and a high level of miR-21 and miR-1 compared to those in a control group. A correlation between the expression of miR-143, miR-145, and miR-133 and daily diastolic BP in HT [121] has been shown. As demonstrated in a culture of human adrenal cortex cells, miR-24 participates in the epigenetic regulation of aldosterone and cortisol synthesis via action on 11 $\beta$ -hydroxylase (CYP11B), the key enzyme in the synthesis of these hormones [122].

A study of the role of microRNA in the development of leukoaraiosis in CMA [111] revealed eight differentially expressed microRNAs associated with the regulation of pathogenetic gene activity and the molecular mechanisms of leukoaraiosis. It should be noted that the significance of these putative pathogenetic genes was confirmed by the results of GWAS (*TRIM65*, *ACOX1*), searches for candidate genes (*AGTR2*, *MTHFR*, *BDNF*, *MMP3*, *MMP13*), gene expression profiles (*CCR5*, *IL6*, *MAF*, *CALM1*, *COL24A1*, *EPHB2*, *MAP1B*, *CYB5A*, *CDC6*, *CTSC*), and epigenetic studies (*HLA-DQA1*, *TGFBR3*, *CD80*, *WDR41*, *RNF39*, *KIAA1199*, *AAK1*). Most of these genes are associated with inflammation in the CNS [111].

The study of the role of the epigenetic dysregulation mechanisms that lead to impaired gene expression in HT and CMA is at its very inception. Given their direct

association with cerebrovascular risk factors, epigenetic mechanisms could be thought to play a significant role in the development of age-dependent multifactorial diseases. The probability of such a suggestion is enhanced by the overlap between the results of epigenetic studies and the data of studies of candidate genes, genome-wide studies on the significance of inflammation, the immune response, and RAAS components in the development of CMA. It is crucial to clarify the pathogenetically important epigenetic markers in the blood and cerebrospinal fluid and the possibility of using them to assess injury to the brain and small vessels, given the impossibility of direct intravital visualization and the importance of indirect methods for assessing progressive injury to the brain and small vessels. The topicality of studying epigenetic dysregulation mechanisms has to do not only with the high social impact of the diseases, which only increases as a population tends to live longer, but also with their potential reversibility due to the association with modifiable cerebrovascular risk factors. We suggest that microRNA-regulated processes play an important role in the development of CMA. Our suggestion is based on the leading role played by endothelial disorders in the development of CMA [10] and on the dependence of the expression of major endothelial function regulators on the activity of Dicer ribonuclease and, respectively, microRNA [123].

### CONCLUSION

Investigations of the genetic basis of HT and CMA have identified new molecular targets that could be potentially important in understanding the pathogenetic mechanisms of these diseases and how to correct them therapeutically. However, it is impossible at this point to explain why, given the obvious role of heredity, genetic data do not fully explain the patterns of predisposition to these diseases or do not allow one to predict their development. One of the approaches that could be explored in order to resolve this contradiction may be to investigate the interactions between gene-metabolic and other regulatory networks and the genes associated with the studied diseases. The immediate objective should be the search for epigenetic markers that are associated with various variants of the course of HT and CMA, which would enable to differentiate significant environmental factors at the individual level. This would become the basis for the search for new approaches to the prevention and treatment of these diseases. Reproducibility of results may be achieved through the formation of homogeneous groups of patients and use of uniform standards for assessing brain injury (neuroimaging phenomena and terms) and methods of laboratory diagnostics and post-processing. ●

## REFERENCES

1. Oganov R.G., Timofeeva T.N., Koltunov I.E., Konstantinov V.V., Balanova Y.A., Kapustina A.V., Lel'chuk, I.N., Shal'nova S.A., Deev A.D. // *Kardiovaskulyarnaya terapiya i profilaktika*. 2011. V.10. №1. P. 9–13.
2. Chazova I.E., Oshchepkova E.V. // *Vestnik RAMN*. 2013. № 2. P. 4–11.
3. Lewington S., Clarke R., Qizilbash N., Peto R., Collins R.; Prospective Studies Collaboration. // *Lancet*. 2002. V. 360. P. 1903–1913.
4. Mancía G., Fagard R., Narkiewicz K., Redón J., Zanchetti A., Böhm M., Christiaens T., Cifkova R., De Backer G., Dominiczak A., et al. // *J. Hypertension*. 2013. V. 31. № 7. P. 1281–1357.
5. Dahlöf B. // *Am. J. Cardiol*. 2007. V. 100. № 3. P. 17J–24J.
6. Feigin V.L., Abajobir A.A., Abate K.H., Abd-Allah F., Abdulle A.M., Abera S.F., Abyu G.Y., Ahmed M.B., Aichour A.N., Akinyemi R.O., et al. // *Lancet Neurol*. 2017. V. 16. № 11. P. 877–897.
7. Feigin V.L., Krishnamurthi R., Bhattacharjee R., Parmar P., Theadom A., Hussein T., Purohit M., Hume P., Abbott M., Rush E., et al. // *Stroke*. 2015. V. 46. № 6. P. 1740–1747.
8. Shmidt E.V., Maksudov G.A. // *Zhurnal nevrologii i psichiatrii im S.S. Korsakova*. 1971. № 71(1). P. 3–11.
9. Vereshchagin N.V., Morgunov V.A., Gulevskaya T.S. *Patologiya golovnogogo mozga pri ateroskleroze i arterial'noj gipertonii*. M.: Medicina, 1997. P. 228.
10. Pantoni L., Gorelick F.B. *Cerebral Small Vessel Disease*. UK: Cambridge Univ. Press, 2014. P. 1–360.
11. Gorelick P.B., Scuteri A., Black S.E., Decarli C., Greenberg S.M., Iadecola C., Launer L.J., Laurent S., Lopez O.L., Nyenhuis D., et al. // *Stroke*. 2011. V. 42. № 9. P. 2674–2701.
12. Meissner A. // *Cerebrovascular Diseases*. 2016. V. 42. № 3–4. P. 255–262.
13. Perrotta M., Lembo G., Carnevale D. // *Int. J. Mol. Sci*. 2016. V. 17. № 347. P. 1–11.
14. Gakidou E., Afshin A., Abajobir A.A., Abate K.H., Ababafati C., Abbas K.M., Abd-Allah F., Abdulle A.M., Abera S.F., Aboyans V., et al. // *Lancet*. 2017. V. 16. № 90 (10100). P. 1345–1422.
15. Dufouil C., de Kersaint-Gilly A., Besançon V., Levy C., Auffray E., Brunnereau L., Alépérovitch A., Tzourio C. // *Neurology*. 2001. V. 56. № 7. P. 921–926.
16. de Leeuw F.E., de Groot J.C., Oudkerk M., Wittteman J.C., Hofman A., van Gijn J., Breteler M.M., et al. // *Brain*. 2002. V. 125. № 4. P. 765–762.
17. van Dijk E.J., Breteler M.M., Schmidt R., Berger K., Nilsson L.G., Oudkerk M., Pajak A., Sans S., de Ridder M., Dufouil C., et al. // *Hypertension*. 2004. V. 44. № 5. P. 625–630.
18. van Dijk E.J., Prins N.D., Vrooman H.A., Hofman A., Koudstaal P.J., Breteler M.M. // *Stroke*. 2008. V. 39. № 10. P. 2712–2719.
19. Firbank M.J., Wiseman R.M., Burton E.J., Saxby B.K., O'Brien J.T., Ford G.A. // *J. Neurol*. 2007. V. 254. № 6. P. 713–721.
20. Debette S., Markus H.S. // *British Medical J*. 2010. V. 341. № c3666. P. 1–9.
21. LADIS Study Group, Poggesi A., Pantoni L., Inzitari D., Fazekas F., Ferro J., O'Brien J., Hennerici M., Scheltens P., Erkinjuntti T., et al. // *Cerebrovasc. Dis*. 2011. V. 32. № 6. P. 577–588.
22. Verhaaren B.F., Vernooij M.W., de Boer R., Hofman A., Niessen W.J., van der Lugt A., Ikram M.A. // *Hypertension*. 2013. V. 61. № 6. P. 1354–1359.
23. Abraham H.M., Wolfson L., Moscufo N., Guttman C.R., Kaplan R.F., White W.B. // *J. Cereb. Blood Flow Metab*. 2016. V. 36. № 1. P. 132–142.
24. Filomena J., Riba-Liena I., Vinyoles E. Tovar J.L., Mundet X., Castañé X., Vilar A., López-Rueda A., Jiménez-Baladó J., Cartanyà A., et al. // *Hypertension*. 2015. V. 66. № 3. P. 634–640.
25. Godin O., Tzourio C., Maillard P., Mazoyer B., Dufouil C. // *Circulation*. 2011. V. 123. № 3. P. 266–273.
26. Chang-Quan H., Hui W., Chao-Min W., Zheng-Rong W., Jun-Wen G., Yong-Hong L., Yan-You L., Qing-Xiu L. // *Int. J. Clin. Pract*. 2011. V. 65. № 12. P. 1295–1305.
27. Satizabal C.L., Beiser A.S., Chouraki V., Chêne G., Dufouil C., Seshadri S. // *N. Engl. J. Med*. 2016. V. 374. № 6. P. 523–532.
28. Hara K. // *Rinsho Shinkeigaku*. 2010. V. 50. № 11. P. 852–854.
29. Kochunov P., Glahn D.C., Lancaster J., Winkler A., Karlsgodt K., Olvera R.L., Curran J.E., Carless M.A., Dyer T.D., Almasy L., et al. // *Hypertension*. 2011. V. 57. № 2. P. 330–335.
30. Singh M., Singh A.K., Pandey P., Chandra S., Singh K.A., Gambhir I.S. // *Clin. Exp. Hypertension*. 2016. V. 38. № 3. P. 268–277.
31. Choi J.C. // *J. Stroke*. 2015. V. 17. № 1. P. 7–16.
32. Moreton F.C., Razvi S.S., Davidson R., Muir K.W. // *Acta Neurol. Scand*. 2014. V. 130. № 3. P. 197–203.
33. Schmidt H., Zeginigg M., Wiltgen M., Freudenberger P., Petrovic K., Cavalieri M., Gider P., Inzinger C., Fornage M., Debette S., et al. // *Brain*. 2011. V. 134. № 11. P. 3384–3397.
34. Sierra C., Coca A., Gómez-Angelats E., Poch E., Sobrino J., de la Sierra A. // *Hypertension*. 2002. V. 39. № 2. P. 343–347.
35. Takami S., Imai Y., Katsuya T., Ohkubo T., Tsuji I., Nagai K., Satoh H., Hisamichi S., Higaki J., Ogihara T. // *Am. J. Hypertens*. 2000. V. 13. № 2. P. 121–127.
36. Brenner D., Labreuche J., Pico F., Scheltens P., Poirier O., Cambien F., Amarenco P.; GENIC Investigators. // *J. Neurol*. 2008. V. 255. № 7. P. 993–1000.
37. Jeunemaitre X., Soubrier F., Kotelevtsev Y.V., Lifton R.P., Williams C.S., Charru A., Hunt S.C., Hopkins P.N., Williams R.R., Lalouel J.M., et al. // *Cell*. 1992. V. 71. № 1. P. 169–180.
38. Jeunemaitre X., Inoue I., Williams C., Charru A., Tichet J., Powers M., Sharma A.M., Gimenez-Roqueplo A.P., Hata A., Corvol P., Lalouel J.M. // *Am. J. Hum. Genet*. 1997. V. 60. № 6. P. 1448–1460.
39. Kunz R., Kreutz R., Beige J., Distler A., Sharma A.M. // *Hypertension*. 1997. V. 30. № 6. P. 1331–1337.
40. Staessen J.A., Kuznetsova T., Wang J.G., Emelianov D., Vlietinck R., Fagard R. // *J. Hypertens*. 1999. V. 17. № 1. P. 9–17.
41. Schmidt R., Schmidt H., Fazekas F., Launer L.J., Niederkorn K., Kapeller P., Lechner A., Kostner G.M. // *Hypertension*. 2001. V. 38. № 1. P. 110–115.
42. Strambovskaya N.N. // *Sibirskij medicinskij zhurnal*. 2014. № 1. P. 72–75.
43. Schmidt H., Fazekas F., Kostner G.M., van Duijn C.M., Schmidt R. // *Stroke*. 2001. V. 32. № 2. P. 405–412.
44. Schmidt H., Aulchenko Y.S., Schweighofer N., Schmidt R., Frank S., Kostner G.M., Ott E., van Duijn C. // *Stroke*. 2004. V. 35. № 11. P. 2592–2597.
45. Gormley K., Bevan S., Markus H.S. // *Cerebrovasc. Dis*. 2007. V. 23. № 2–3. P. 148–155.
46. Salminen L.E., Schofield P.R., Pierce K.D., Zhao Y., Luo

- X., Wang Y., Laidlaw D.H., Cabeen R.P., Conturo T.E., Tate D.F., et al. // *Behav. Brain Res.* 2016. V. 296. P. 85–93.
47. Zhang L., Miyaki K., Araki J., Song Y., Kimura T., Omae K., Muramatsu M. // *Hypertens. Res.* 2006. V. 29. № 1. P. 751–758.
48. Pontremoli R., Ravera M., Viazzi F., Nicoletta C., Berruti V., Leoncini G., Giacobelli F., Bezante G.P., Sacchi G., Ravazzolo R., et al. // *Kidney Int.* 2000. V. 57. № 2. P. 561–569.
49. Julve R., Chaves F.J., Rovira E., Pascual J.M., Miralles A., Armengod M.E., Redon J. // *Blood Press. Monit.* 2001. V. 6. № 1. P. 27–32.
50. Jimenez P.M., Conde C., Casanegra A., Romero C., Tabares A.H., Orías M. // *J. Renin Angiotensin Aldosterone Syst.* 2007. V. 8. № 1. P. 42–44.
51. Cosenso-Martin L.N., Vaz-de-Melo R.O., Pereira L.R., Cesarino C.B., Yugar-Toledo J.C., Cipullo J.P., de Souza Pinhel M.A., Souza D.R., Vilela-Martin J.F. // *Eur. J. Med. Res.* 2015. V. 20. № 1. P. 1–9.
52. Orlova N.V., Sitnikov V.F., Chukaeva I.I., Prohin A.V. // *Medicinskij al'manah.* 2011. № 3(16). P. 81–84.
53. Amar K., MacGowan S., Wilcock G., Lewis T., Scott M. // *Int. J. Geriatr. Psychiatry.* 1998. V. 13. № 9. P. 585–590.
54. Purandare N., Oude Voshaar R.C., Davidson Y., Gibbons L., Hardicre J., Byrne J., McCollum C., Jackson A., Burns A., Mann D.M. // *J. Am. Geriatr. Soc.* 2006. V. 54. № 9. P. 1395–1340.
55. Paternoster L., Chen W., Sudlow C.L. // *Stroke.* 2009. V. 40. № 6. P. 2020–2026.
56. Tran T., Cotlarciuc I., Yadav S., Hasan N., Bentley P., Levi C., Worrall B.B., Meschia J.F., Rost N., Sharma P. // *J. Neurol. Neurosurg. Psychiatry.* 2016. V. 87. № 3. P. 260–266.
57. Toda N., Ayajiki K., Okamura T. // *J. Hypertens.* 2009. V. 27. № 10. P. 1929–1940.
58. Meschia J.F., Nalls M., Matarin M., Brott T.G., Brown R.D. Jr., Hardy J., Kissela B., Rich S.S., Singleton A., Hernandez D., et al. // *Stroke.* 2011. V. 42. № 10. P. 2726–2732.
59. Levinsson A., Olin A.C., Björck L., Rosengren A., Nyberg F. // *Nitric Oxide.* 2014. V. 39. P. 1–7.
60. Yakovleva O.I., Vahrameeva N.V., Larionova V.I., Bogdanova M.A., Konradi O.A. // *Arterial'naya gipertenziya.* 2005. V. 11. № 3. P. 195–200.
61. Bairova T.A., Dolgih V.V., Bimbaev A.B.–Zh., Tugutova I.A., Hojkova O.Ch. // *Byulleten' VSNC SO RAMN.* 2007. № 3(55). P. 64–65.
62. Kuznecova T.Yu., Gavrilov D.V., Samohodskaya L.M., Postnov A.Yu., Bojcov S.A. // *Sibirskij medicinskij zhurnal.* 2010. V. 25. № 2(1). P. 33–38.
63. Jin J.J., Nakura J., Wu Z., Yamamoto M., Abe M., Tabara Y., Yamamoto Y., Igase M., Kohara K., Miki T. // *Hypertension.* 2003. V. 41. № 1. P. 163–167.
64. Tiret L., Poirier O., Hallet V., McDonagh T.A., Morrison C., McMurray J.J., Dargie H.J., Arveiler D., Ruidavets J.B., Luc G., et al. // *Hypertension.* 1999. V. 33. № 5. P. 1169–1174.
65. Hassan A., Hunt B.J., O'Sullivan M., Bell R., D'Souza R., Jeffery S., Bamford J.M., Markus H.S. // *Brain.* 2004. V. 127. № 1. P. 212–219.
66. Hong E.D., Taylor W.D., McQuoid D.R., Potter G.G., Payne M.E., Ashley-Koch A., Steffens D.C. // *Am. J. Geriatr. Psychiatry.* 2009. V. 17. № 10. P. 847–855.
67. Rutten-Jacobs L.C., Traylor M., Adib-Samii P., Thijs V., Sudlow C., Rothwell P.M., Boncoraglio G., Dichgans M., Meschia J., Maguire J., et al. // *Stroke.* 2016. V. 47. № 3. P. 646–651.
68. Lau L.M., van Meurs J.B., Uitterlinden A.G., Smith A.D., Refsum H., Johnston C., Breteler M.M. // *Neurobiol. Aging.* 2010. V. 31. № 11. P. 2020–2022.
69. Szolnoki Z., Somogyvári F., Kondacs A., Szabó M., Fodor L. // *Acta Neurol. Scand.* 2001. V. 104. № 5. P. 281–287.
70. Szolnoki Z., Somogyvári F., Kondacs A., Szabó M., Fodor L., Bene J., Melegh B. // *Acta Neurol. Scand.* 2004. V. 109. № 3. P. 222–227.
71. Jannes J., Hamilton-Bruce M.A., Pilotto L., Smith B.J., Mullighan C.G., Bardy P.G., Koblar S.A. // *Stroke.* 2004. V. 35. № 5. P. 1090–1094.
72. Sun X., Lai R., Li J., Luo M., Wang Y., Sheng W. // *PLoS One.* 2013. V. 8. № 1. P. 1–8.
73. Martiskainen M., Pohjasvaara T., Mikkelsen J., Mäntylä R., Kunnas T., Laippala P., Ilveskoski E., Kaste M., Karhunen P.J., Erkinjuntti T. // *Stroke.* 2003. V. 34. № 4. P. 886–891.
74. Ma H., Sun G., Wang W., Zhou Y., Liu D., Tong Y., Lu Z. // *Medicine (Baltimore).* 2016. V. 95. № 2. P. 1–15.
75. Li Y.Y. // *PLoS One.* 2012. V. 7. № 4. P. 1–7.
76. Krivoshej I.V. // *Nauchnye vedomosti.* 2013. № 25(168). V. 24. P. 165–69.
77. Yang W., Lu J., Yang L., Zhang J. // *Iran J. Public Health.* 2015. V. 44. № 11. P. 1445–1452.
78. Dziedzic T., Slowik A., Pera J., Szczudlik A. // *Cerebrovasc. Dis.* 2005. V. 20. № 5. P. 299–303.
79. Chamorro A., Revilla M., Obach V., Vargas M., Planas A.M. // *Cerebrovasc. Dis.* 2005. V. 19. № 2. P. 91–95.
80. Fornage M., Chiang Y.A., O'Meara E.S., Psaty B.M., Reiner A.P., Siscovick D.S., Tracy R.P., Longstreth W.T. Jr. // *Stroke.* 2008. V. 39. № 7. P. 1952–1959.
81. Raz N., Yang Y., Dahle C.L., Land S. // *Biochim. Biophys. Acta.* 2012. V. 1822. № 3. P. 361–369.
82. Knyazeva A.S., Strambovskaya N.N. // *Byulleten' VSNC SO RAMN.* 2014. № 1(95). P. 30–34.
83. Reitz C., Berger K., de Maat M.P., Stoll M., Friedrichs F., Kardys I., Wittman J.C., Breteler M.M. // *Stroke.* 2007. V. 38. № 8. P. 2356–2359.
84. Fatar M., Stroick M., Steffens M., Senn E., Reuter B., Bukow S., Griebe M., Alonso A., Lichtner P., Bugert P. // *Cerebrovasc. Dis.* 2008. V. 26. № 2. P. 113–119.
85. Zhang M., Zhu W., Yun W., Wang Q., Cheng M., Zhang Z., Liu X., Zhou X., Xu G. // *J. Neurol. Sci.* 2015. V. 356. № 1–2. P. 61–64.
86. Kim O.J., Hong S.H., Oh S.H., Kim T.G., Min K.T., Oh D., Kim N.K. // *Stroke.* 2011. V. 42. № 9. P. 2393–2402.
87. Huang C.C., Liu M.E., Chou K.H., Yang A.C., Hung C.C., Hong C.J., Tsai S.J., Lin C.P. // *Psychoneuroendocrinology.* 2014. V. 39. P. 94–103.
88. Lupton S.J., Chiu C.L., Lind J.M. // *Twin Res. Hum. Genet.* 2011. V. 14. № 4. P. 295–304.
89. Newton-Cheh C., Johnson T., Gateva V., Tobin M.D., Bochud M., Coin L., Najjar S.S., Zhao J.H., Heath S.C., Eyheramendy S., et al. // *Nat. Genet.* 2009. V. 41. № 6. P. 666–676.
90. Levy D., Ehret G.B., Rice K., Verwoert G.C., Launer L.J., Dehghan A., Glazer N.L., Morrison A.C., Johnson A.D., Aspelund T., et al. // *Nat. Genet.* 2009. V. 41. № 6. P. 677–687.
91. International Consortium for Blood Pressure Genome-Wide Association Studies, Ehret G.B., Munroe P.B., Rice K.M., Bochud M., Johnson A.D., Chasman D.I., Smith A.V., Tobin M.D., Verwoert G.C., et al. // *Nature.* 2011. V. 478. № 7367. P. 103–109.
92. Fornage M., Debette S., Bis J.C., Schmidt H., Ikram M.A., Dufouil C., Sigurdsson S., Lumley T., DeStefano A.L., Fazzekas F., et al. // *Ann. Neurol.* 2011. V. 69. № 6. P. 928–939.
93. Verhaaren B.F., de Boer R., Vernooij M.W., Rivadeneira F., Uitterlinden A.G., Hofman A., Krestin G.P., van der Lugt

- A., Niessen W.J., Breteler M.M., et al. // *Stroke*. 2011. V. 42. № 11. P. 3297–3279.
94. Adib-Samii P., Rost N., Traylor M., Devan W., Biffi A., Lanfranconi S., Fitzpatrick K., Bevan S., Kanakis A., Valant V., et al. // *Stroke*. 2013. V. 44. № 6. P. 1609–1615.
95. Tabara Y., Igase M., Okada Y., Nagai T., Uetani E., Kido T., Ochi N., Takita R., Yamamoto M., Kohara K., et al. // *Eur. J. Neurol.* 2013. V. 20. № 5. P. 860–862.
96. Verhaaren B.F., Debette S., Bis J.C., Smith J.A., Ikram M.K., Adams H.H., Beecham A.H., Rajan K.B., Lopez L.M., Barral S., et al. // *Circ. Cardiovasc. Genet.* 2015. V. 8. № 2. P. 398–409.
97. Woo D., Falcone G.J., Devan W.J., Brown W.M., Biffi A., Howard T.D., Anderson C.D., Brouwers H.B., Valant V., Battey T.W., et al. // *Am. J. Hum. Genet.* 2014. V. 94. № 4. P. 511–521.
98. Hofer E., Cavalieri M., Bis J.C., DeCarli C., Fornage M., Sigurdsson S., Srikanth V., Trompet S., Verhaaren B.F., Wolf C., et al. // *Stroke*. 2015. V. 46. № 11. P. 3048–3057.
99. Munroe P.B., Barnes M.R., Caulfield M.J. // *Circ. Res.* 2013. V. 112. № 10. P. 1365–1379.
100. Raftopoulos L., Katsi V., Makris T., Tousoulis D., Stefanadis C., Kallikazaros I. // *Life Sci.* 2015. V. 129. P. 22–26.
101. Liang M., Cowley A.W.Jr, Mattson D.L., Kotchen T.A., Liu Y. // *Semin. Nephrol.* 2013. V. 33. № 4. P. 392–399.
102. Wang J., Gong L., Tan Y., Hui R., Wang Y. // *J. Hum. Hypertens.* 2015. V. 29. № 10. P. 575–582.
103. Wise I.A., Charchar F.J. // *Int. J. Mol. Sci.* 2016. V. 17. № 4. P. 2–14.
104. Goyal R., Goyal D., Leitzke A., Gheorghe C.P., Longo L.D. // *Reprod. Sci.* 2010. V. 17. № 3. P. 227–238.
105. Rangel M., dos Santos J.C., Ortiz P.H., Hirata M., Jasilionis M.G., Araujo R.C., Ierardi D.F., Franco Mdo C., et al. // *PLoS One.* 2014. V. 9. № 8. P. 1–8.
106. Zhang L.N., Ji L.D., Fei L.J., Yuan F., Zhang Y.M., Xu J., et al. // *Biomed. Res. Int.* 2013. V. 2013. P. 1–5.
107. Friso S., Pizzolo F., Choi S.-W., Guarini P., Castagna A., Ravagnani V., Carletto A., Pattini P., Corrocher R., Olivieri O. // *Atherosclerosis.* 2008. V. 199. № 2. P. 323–327.
108. Udali S., Guarini P., Moruzzi S., Choi S.W., Friso S. // *Mol. Aspects Med.* 2013. V. 34. № 4. P. 883–901.
109. Lee H.A., Baek I., Seok Y.M., Yang E., Cho H.M., Lee D.Y., Hong S.H., Kim I.K. // *Biochem. Biophys. Res. Commun.* 2010. V. 396. № 2. P. 252–257.
110. Esler M., Eikelis N., Schlaich M., Lambert G., Alvarenga M., Kaye D., El-Osta A., Guo L., Barton D., Pier C., et al. // *Ann. N. Y. Acad. Sci.* 2008. V. 1148. P. 338–348.
111. Lin Q., Huang W.Q., Tzeng C.M. // *Rev. Neurosci.* 2015. V. 26. № 3. P. 343–358.
112. Millis R.M. // *Curr. Hypertens. Rep.* 2011. V. 13. № 1. P. 21–28.
113. Zhang D., Yu Z.Y., Cruz P., Kong Q., Li S., Kone B.C. // *Kidney Int.* 2009. V. 75. № 3. P. 260–267.
114. Pojoga L.H., Williams J.S., Yao T.M., Kumar A., Raffetto J.D., do Nascimento G.R., Reslan O.M., Adler G.K., Williams G.H., Shi Y., et al. // *Am. J. Physiol. Heart Circ. Physiol.* 2011. V. 301. № 5. P. H1862–H1871.
115. Mu S., Shimosawa T., Ogura S., Wang H., Uetake Y., Kawakami-Mori F., Marumo T., Yatomi Y., Geller D.S., Tanaka H., et al. // *Nat. Med.* 2011. V. 17. № 5. P. 573–580.
116. Irmak M.K., Sizlan A. // *Med. Hypotheses.* 2006. V. 66. № 5. P. 1000–1007.
117. Ouyang Y.B., Stary C.M., Yang G.Y., Giffard R. // *Curr. Drug Targets.* 2013. V. 14. № 1. P. 90–101.
118. Romero D.G., Plonczynski M.W., Carvajal C.A., Gomez-Sanchez E.P., Gomez-Sanchez C.E. // *Endocrinology.* 2008. V. 149. № 5. P. 2477–2483.
119. Söber S., Laan M., Annilo T. // *Biochem. Biophys. Res. Commun.* 2010. V. 391. № 1. P. 727–732.
120. Ling S., Nanhwan M., Qian J., Kodakandla M., Castillo A.C., Thomas B., Liu H., Ye Y. // *J. Mol. Cell Cardiol.* 2013. V. 65. P. 127–136.
121. Kontaraki J.E., Marketou M.E., Zacharis E.A., Parthenakis F.I., Vardas P.E. // *J. Hum. Hypertens.* 2014. V. 28. № 8. P. 510–516.
122. Robertson S., MacKenzie S.M., Alvarez-Madrazo S., Diver L.A., Lin J., Stewart P.M., Fraser R., Connell J.M., Davies E. // *Hypertension.* 2013. V. 62. № 3. P. 572–578.
123. Suárez Y., Fernández-Hernando C., Pober J.S., Sessa W.C. // *Circ. Res.* 2007. V. 100. № 8. P. 1164–1173.

# Molecular Approaches to Safe and Controlled Engineered T-cell Therapy

R. S. Kalinin<sup>1</sup>, A. V. Petukhov<sup>1</sup>, V. D. Knorre<sup>1</sup>, M. A. Maschan<sup>2</sup>, A. V. Stepanov<sup>1\*</sup>, A.G. Gabibov<sup>1</sup>

<sup>1</sup>M.M. Shemyakin and Yu.A. Ovchinnikov Institute of Bioorganic Chemistry, Russian Academy of Sciences, Miklukho-Maklaya Str. 16 /10, Moscow, 117997, Russia

<sup>2</sup>Dmitrii Rogachev Federal Research Center for Pediatric Hematology, Oncology and Immunology, Samory Mashela Str. 1, Moscow, 117997, Russia

\*E-mail: stepanov.aleksei.v@gmail.com

Received December 7, 2017; in final form, May 14, 2018

Copyright © 2018 Park-media, Ltd. This is an open access article distributed under the Creative Commons Attribution License, which permits unrestricted use, distribution, and reproduction in any medium, provided the original work is properly cited.

**ABSTRACT** Chimeric antigen receptor-modified T-cell therapy (CAR-T therapy) is one of the fastest developing areas of immuno-oncology. Over the past decade, it has revolutionized the cell therapy modality and expedited its pace of development, from optimization of the structure of chimeric antigen receptors and animal model experiments to successful clinical application. The initial designs of the CAR configuration focused on increasing T-cell activation, cytotoxicity, and persistence. However, the first attempts to treat patients with CAR T cells have demonstrated the need for increased safety and controlled activation of genetically modified T cells. Herein, we summarize the different molecular approaches to engineering chimeric antigen receptors for reducing the potential clinical risks of T-cell therapy.

**KEYWORDS** chimeric antigen receptors, T-cells, cell therapy, cancer cells.

## INTRODUCTION

Adoptive cell immunotherapy was first used to treat metastatic sarcoma in 1985 and remains one of the most promising trends in cancer treatment [1, 2]. In this therapy, autologous T cells are isolated, activated, expanded, and infused back into the patient, resulting in partial regression or eradication of the tumor [3–6]. Application of autologous T cells prevents the development of the graft-versus-host disease (GVHD) and, importantly, enhances the persistence of therapeutically active cells [7–9]. However, adoptive immunotherapy shows lack of effectiveness in most cases [10]. The next step in the evolution of this therapy was to engineer T cells that could specifically recognize tumor cells and circumvent their immunosuppressive mechanisms. One of the ways to modify T cells is to insert an artificial T-cell receptor (TCR) targeting tumor-associated antigens (TAAs) [11]. Unfortunately, TCR-modified T cells can recognize only the proteasome-processed antigens presented by major histocompatibility complex class I (MHC I). The most recent approach, which consists in modifying T cells with chimeric antigen receptor (CAR) genes, is devoid of these shortcomings: this method helps T cells recognize the native antigens presented on the cancer cell membrane irrespective of MHC I. In terms of its structure, a CAR consists of three functional components: the extracellular antigen recognition domain; the transmembrane domain; and the intracel-

lular component that comprises the T-cell activation domain of CD3 $\zeta$  and, depending on what “generation” a receptor belongs to, different costimulatory domains (*Figure A*) [12]. Z. Eshhar and colleagues (the Weizmann Institute of Science, Israel) were the first to report on the use of a technique employing MHC I-independent recombinant antigen receptors back in the late 1980s [13]. This approach eventually evolved into the CAR T-cell therapy and yielded promising results in studies focused on hematological malignancies. Thus, clinical trials of CAR-modified T cells (CAR T cells) targeting the B-lymphocyte antigen CD19 have demonstrated that they are efficacious in the treatment of chemotherapy-resistant tumors of B-cell origin [14–18]. Finally, the Food and Drug Administration (FDA) in 2017 approved CAR T-cell products (Kymriah manufactured by Novartis and Yescarta manufactured by Kite Pharma) targeting CD19 for the treatment of acute lymphoblastic leukemia (ALL).

## THE RISKS ASSOCIATED WITH CAR T-CELL THERAPY

The earliest clinical trials of CAR-T therapy demonstrated its exceptional efficacy. Infusion of modified T cells resulted in an exponential increase in the T-cell count and active elimination of tumor cells already after the first several weeks [19]. The dark side of such an efficacious therapy is the high risk of developing systemic and life-threatening adverse events, primarily

hypercytokinemia (cytokine storm, cytokine cascade, and cytokine release syndrome) or the tumor lysis syndrome [20–23]. These complications may trigger the multiple organ dysfunction syndrome and eventually cause death. These T cell-induced complications can be eliminated using cytostatic and cytotoxic corticosteroids [24]; however, these medications suppress all T cells and cause a number of side effects, such as systemic organ failure [25]. Another problem related to the application of CAR T cells consists in their nonspecific cytotoxicity; this issue becomes especially topical in the treatment of solid tumors as it is arduous to choose specific TAAs for this type of tumors [26–29]. Thus, clinical trials aimed at evaluating CAR T cells targeting carbonic anhydrase IX, which is hyperexpressed in renal cell carcinoma cells but is also present in normal tissues, including liver, have revealed that CAR T cells exhibit the nonspecific cytotoxicity that causes complications in patients [26, 28]. Furthermore, the use of HER2-specific CAR for a patient with metastatic colon cancer results in a rapid and intense cross reaction to healthy lung cells expressing HER2 at low levels and patient death immediately after the infusion of CAR T cells [30]. The methods for controlling the expansion and cytotoxicity of T cells already infused into a patient need further elaboration in order to improve safety and eliminate the current drawbacks, such as delayed cross-reactivity and toxicity after a successful CAR T-cell therapy [6, 31]. Herein, we summarize the different molecular approaches to safe and controlled T-cell therapy.

#### **APPLICATION OF THE HERPES SIMPLEX VIRUS THYMIDINE KINASE (HSV-TK) GENE**

Herpes simplex virus thymidine kinase has long been used in both laboratory and clinical studies to induce cell death. HSV-TK phosphorylates ganciclovir to ganciclovir monophosphate, which is further stepwise converted to di- and triphosphates by cellular kinases (*Figure B*) [32–34]. Ganciclovir triphosphate is incorporated into DNA during the elongation and replication stages, thus disrupting the DNA polymerase function and causing cell death [35, 36]. Ganciclovir phosphorylated by viral thymidine kinase causes ligand-independent CD95 aggregation, which induces the formation of a Fas-associated protein with a death domain (FADD) and activates caspase-8 [37]. Elimination of the modified cells using ganciclovir and cells carrying the HSV thymidine kinase gene is the best studied technique with verified safety and efficacy [34, 38]. However, this approach also has some drawbacks consisting in the immunogenicity of HSV-TK [39]. Clinical trials have revealed that T-cell elimination is not a fast process as it requires DNA replication for the nucleotide analogue to

be incorporated into the genome [38, 40]. Furthermore, this therapy cannot be performed if a patient has a herpes infection. Despite the apparent limitations of the approach, neither acute toxicity nor an immunogenic response to HSV-TK has been observed in clinical trials evaluating allogeneic HSV-TK-transduced T cells [41]. In two patients, ganciclovir was used to treat GVHD and complete elimination of HSV-TK<sup>+</sup> was achieved; however, GVHD was successfully mitigated in only one patient. No immune response to HSV-TK was observed in the clinical trial [42], but GVHD did not occur in this study (possibly, because of the immunocompromised status of the patients and the low dose of infused T cells).

#### **APPLICATION OF CHEMICALLY INDUCIBLE CASPASE-9**

The use of chimeric molecules based on pro-apoptotic signaling proteins that are capable of dimerization and activation in the presence of low-molecular-weight compounds is an interesting and promising approach to a controlled induction of apoptosis in CAR T cells [43, 44]. One of the most vivid examples is chimeric caspase-9 (iCasp9) [45], which consists of two key components: truncated caspase-9 and a fragment of the FKPB12-binding protein carrying a F36V mutation (FK506). This chimeric protein is dimerized in the presence of rimiducid (AP1903), thus inducing the apoptotic cascade (*Figure B*). The iCasp9 system is apparently advantageous over HSV-TK. First, it consists of human gene products exhibiting low potential immunogenicity. Second, administration of the medicinal product does not produce significant adverse effects and results in selective elimination of CAR T cells only [46]. In addition, iCasp9 remains functionally active even in T cells that exhibit enhanced expression of anti-apoptotic proteins [43, 47–49]. The key advantage of iCasp9 over HSV-TK is that the former system acts very rapidly. Exposure to AP1903 for several hours leads to the elimination of CAR T cells. The efficacy of iCasp9 was proved for CAR T cells with different targets (CD19, CD20, and CD30). Clinical trials involving patients with lymphoma (NCT02274584) have also demonstrated that this approach is safe and efficacious [50].

#### **ELIMINATION OF CAR T CELLS BY MONOCLONAL ANTIBODIES**

In the past decade, monoclonal antibodies (mAbs) have been routinely used in cancer therapy. Novel chimeric antigen receptors have been designed using therapeutic antibody variable domains. Interestingly, some antibodies that have already passed all the required clinical trials and have been approved by the FDA can be used for eliminating CAR T cells if patients develop complications from cellular therapy [51–53]. In order to elimi-

nate T cells by mAbs, a proper antigen needs to appear on the surface of CAR T cells (Figure C). The same antigen can be employed to select CART<sup>+</sup> cells following the modification of T cells [9]. The pioneering studies in this area were the experiments on the transduction of T cells with a CD20 molecule and infusion of anti-CD20 monoclonal antibodies, which proved themselves to be effective in the therapy of lymphoproliferative disorders of B-cell nature [54–56]. A similar system has been designed for the truncated form of the epidermal growth factor receptor (tEGFR) and acts as a target for the currently marketed medicinal product cetuximab [52]. tEGFR has undergone several clinical trials; however, application of cetuximab has not been found justifiable enough. In some studies, the mAb epitope was integrated into the sequence of the extracellular domain of the CAR. This approach was employed in a preclinical study where a 10-aa tag of c-myc was inserted into the recombinant TCR sequence [9, 51]. However, when considering mAbs for clinical application, one should take into account the intrinsic cytotoxicity of the antibody and the possible complications [9].

### SELF-/NONSELF DISCRIMINATION

Researchers have for a long time faced the problem of the choice of a TAA that would target tumor cells only, since it is extremely difficult to select unique antigens for most types of cancer cells. However, it is possible to select deterministic antigen patterns that are typical both of healthy and tumor cells. Fedorov et al. [57] suggested using an additional inhibitory chimeric receptor (iCAR) that protects normal cells against the nonspecific cytotoxicity of CAR T cells: when interacting with the antigens of healthy cells, it transmits an inhibitory signal (Figure D). The iCAR-modified cells inhibit the signals from the main CAR through the extracellular domain of PD-1 or CTLA-4. The key advantage of this approach is that the inhibitory effect is reversible and the T cells can still function when they subsequently encounter a tumor cell [57]. Such factors as proper selection of the expression level of the chimeric receptor, the balance between the affinities of the recognition domains, variability of the set of antigens presented on cancer and healthy cells, as well as the individual characteristics of each patient, significantly limit the clinical application of iCARs [57].

### ELIMINATION OF A CELL CARRYING A CERTAIN COMBINATION OF ANTIGENS

The problem of searching for tumor-specific antigens is especially relevant for solid tumors [58]. Therefore, it has been suggested that the selectivity and safety of CAR T cells can be enhanced if two receptors targeting different tumor antigens are expressed. It is not until

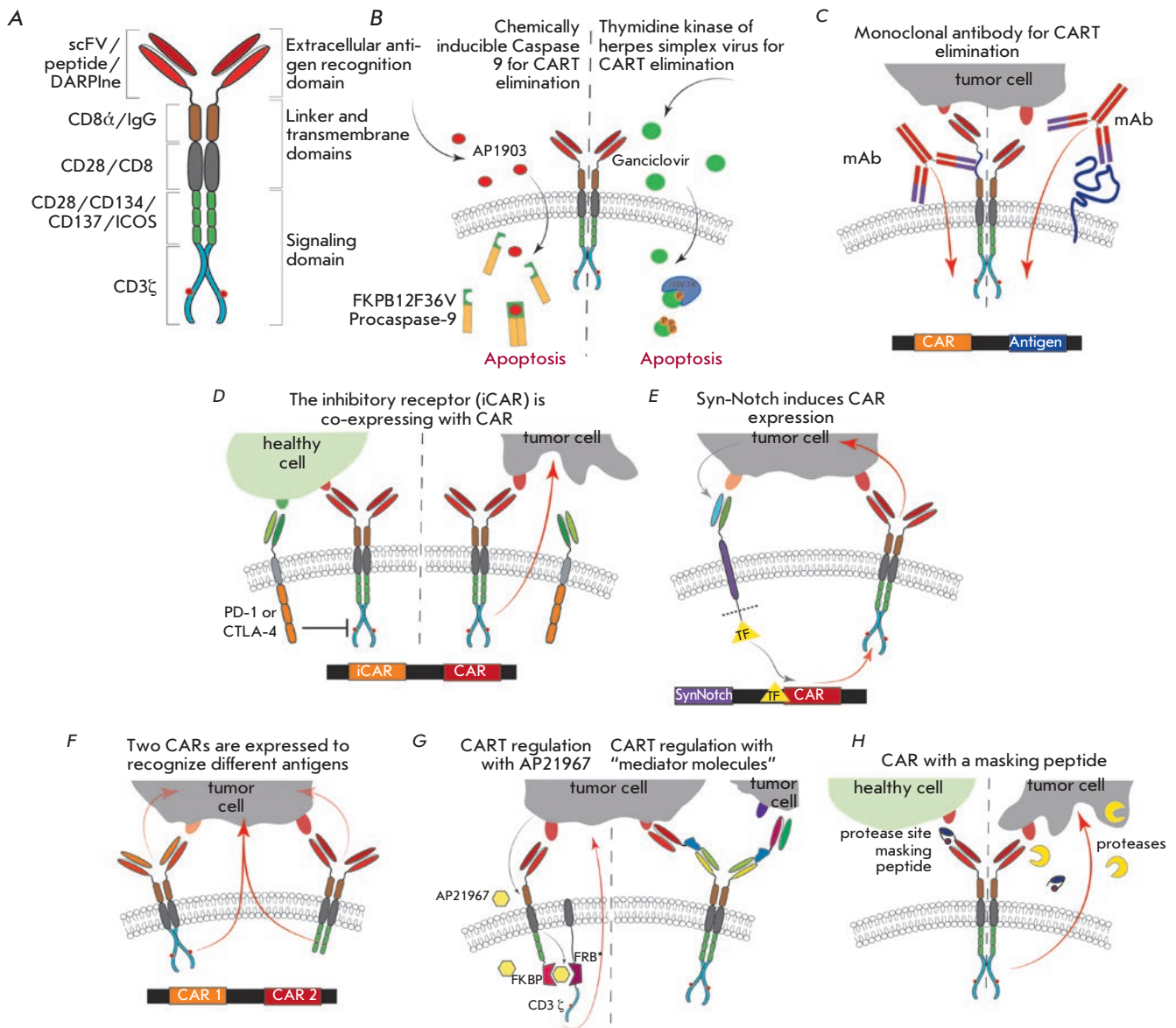
all the CARs (one receptor may contain the CD3 $\zeta$  stimulatory domain, while the other may carry CD28) have recognized their targets that a T cell receives stimulation sufficient for its activation (Figure F) [59–63]. This dual targeting system allows one to significantly reduce the intensity of adverse effects even in the absence of a specific tumor antigen [62]. W. Wilkie et al. compared CAR-modified T cells carrying two receptors and control CAR-modified T cells having one receptor with all its intracellular domains and found that despite the identical efficacy *in vivo*, the level of interleukin-2 secretion was significantly lower in the T cells with two receptors [63]. However, when using dual-targeted CARs, one should take into account that the efficiency of cell elimination and proliferation will directly depend on the balance between the signals from two receptors, with the optimal balance lying in a rather narrow range. A strong difference in the quantities of the two target antigens presented on tumor cells or the absence of one antigen may render cellular therapy ineffective.

In another strategy, a synthetic Notch receptor (syn-Notch) was designed: this receptor binds to the second antigen on a tumor cell and triggers the expression of CAR inside the T cells via transcription factors (Figure E) [64]. In its turn, CAR binds to its antigen presented on the tumor cell and activates the cytotoxicity of this CAR-modified T cell. Localized suppression of tumor cells is achieved thanks to this mechanism, without the risk of exhibiting nonspecific cytotoxicity with respect to healthy tissues.

Hence, using two different antigens present on tumor cells for recognition broadens the possible range of target antigens for CAR T cells and simultaneously reduces the toxicity that would be observed for conventional CAR T cells. However, neither this method nor modification of iCARs allows real-time control over CAR T cells and the intensity of their activity [65]. The constantly updated human protein reference databases are another solution to the problem of searching for an antigen that targets healthy cells [66]. MHC can also be a promising antigen that discriminates between healthy cells and tumor ones: it is expressed on the surface of almost all healthy cells, while MHC expression in cancer cells is downregulated to suppress the immune response [67].

### CONTROLLING THE EXPRESSION OF THE CHIMERIC ANTIGEN RECEPTOR GENE

Since activation and the cytotoxicity of modified T cells directly depend on the quantity of the receptor presented on the cell membrane, the effectiveness of cell therapy can be controlled by regulating the expression of the chimeric antigen receptor gene. Inducible promoters have been used to regulate gene expression



The methods used to regulate CAR T cells. **A** – the general structure of CAR. **B** – elimination of CAR by exogenous molecules. In the right-hand side of the Figure, HSV-TK phosphorylates ganciclovir to ganciclovir monophosphate, which is further sequentially converted to the di- and triphosphate forms by cellular kinases. Ganciclovir triphosphate is incorporated into DNA at the elongation and replication stages, resulting in cell death. In the left-hand side of the Figure, the truncated variant of caspase-9 and the FK506 fragment are dimerized in the presence of rimiducid (AP1903) and induce the apoptotic cascade. The antigen targeting monoclonal antibodies, which is capable of eliminating CAR T cells, is added to the surface of CAR T cells or to the linker domain of CAR. **D** – iCAR interacts with the antigen present on healthy cells and inhibits the CAR function via the intracellular domain of PD-1 or CTLA-4. This inhibition is reversible, which allows T cells to function when they subsequently encounter a tumor cell. **E** – after the additional receptor (synNotch) interacts with one tumor antigen, transcription factors (TFs) induce expression of CAR, which recognizes the second antigen and induces cytotoxicity. **F** – CAR T cells are sufficiently activated only when two CARs interact with two different tumor antigens. **G** – modular CARs. The left-hand side of the Figure shows that the activation ability of CARs is restored only upon dimerization of the protein binding FK 506 (FKBP) with the T2089L mutant of FKBP-rapamycin (FRB\*) via the exogenously inserted rapamycin analogue (AP21967). In the right-hand side of the Figure: CAR is activated only through an exogenous “mediator molecule.” **H** – modification of the extracellular domain of CAR by a masking peptide, which is cleaved in the tumor microenvironment, thus allowing CAR to bind to its antigen.

over the past decades. The tetracycline-responsive promoter system is a convenient tool for regulating gene expression in eukaryotic cells. CAR expression in modified T cells can be regulated through dosed insertion of a regulatory molecule. In one case, doxycycline inhibited CAR expression [68]. Contrariwise, CAR was expressed only in the presence of doxycycline in another case [69]. The convenience of this method is that it allows one to regulate cytotoxicity and that CAR-T cells are cultured *ex vivo*, where the functional status and the phenotype are not affected by the presence of CAR, unlike upon permanent CAR expression. However, *in vivo* experiments have revealed that the components of the tetracycline-responsive promoter system are immunogenic [68].

### CONTROLLING THE ACTIVATION OF THE CHIMERIC ANTIGEN RECEPTOR

As already mentioned, chimeric antigen receptors consist of three key domains: the antigen recognition, the transmembrane, and the signaling domains. The direct relationship between antigen binding and receptor activation ensures the high efficiency of CAR T cells. In order to control the intensity of signal transmission from the antigen recognition domain to the signaling one, the receptor structure has been significantly modified by dividing it into two portions: the antigen-binding extracellular component and the intracellular component carrying the signaling domains. Both components carry the heterodimerization domains (FKBP and FRB\*), which are hybridized in the presence of AP21967, a rapamycin analogue that is less immunosuppressive than rapamycin [70, 71]. Therefore, the immunoreactivity of therapeutic CAR T cells depends on the tumor antigen and the low-molecular-weight agent, whose concentration can be dosed (*Figure G*). An analysis of the therapeutic potential has demonstrated that AP21967-dependent CAR T cells and regular CAR T cells are equally effective, both *in vitro* and *in vivo* [65]. Meanwhile, this technique necessitates the design of novel classes of controller drugs optimized for clinical application in combination with therapeutically modified cells [65, 72–74].

### “MEDIATOR MOLECULES” HYBRIDIZING WITH THE EXTRACELLULAR CAR DOMAIN AND THE TUMOR ANTIGEN

It is possible to modulate both the intensity of signal transduction from the antigen recognition domain to the signaling one and the level of antigen recognition. The so-called “mediator molecules” (*Figure G*) show the greatest potential. These molecules are proteins or low-molecular-weight compounds with one end interacting with the tumor antigen and the other one in-

teracting with CAR-modified T cells -- the so-called switchable (universal) CAR-T cells [75, 76]. The modularity of this approach allows one to broaden the range of antigens, while using the same CAR T cells. By adjusting the doses of “mediator molecules” one can regulate the intensity of the T-cell response and prevent the development of hypercytokinemia or the tumor lysis syndrome [77]. This strategy could be highly potent in polyclonal and recurrent tumors, when the T-cell response needs to be redirected [78, 79]. Either antibodies fused to a nonimmunogenic antigen targeted by CAR T cells or CARs targeting the Fc fragment of a therapeutic monoclonal antibody can be used as such “mediator molecules” [75–77, 80–84]. This approach has been implemented using recombinant anti-CD19 antibodies carrying the nonimmunogenic epitope of the GCN4 yeast transcription factor, which was in its turn targeted by the antigen recognition epitope of CAR T cells [77]. The same CAR T cells were successfully redirected using antibodies targeting CD20 modified by the GCN4 epitope [77]. The direct dependence between the phenotype of CAR T cells and concentration of mediator molecules was rather interesting: low doses of these molecules significantly increased the count of central memory T cells. Along with antibodies, modified natural polypeptides or their fragments carrying the hypervariable peptide segments responsible for molecular recognition can also be applied [85]. Well-known affinity pairs, such as the biotin–avidin pair, can also be used [76]. The same principle was employed to design fluorescein isothiocyanate (FITC)-conjugated antibodies targeting CD19 or FITC-conjugated folic acid. These “mediator molecules” are recognized by universal anti-FITC-CAR T cells [83, 86]. CD16-CAR T cells targeting the Fc domain of antibodies are currently being developed as universal CAR T cells. This will enable application of monoclonal antibodies in CAR T cell therapy [80–82].

Hence, switchable CAR T cells represent a promising new paradigm in cellular therapy which has the potential to enhance the safety and universality of CAR T cells. This approach will make production of CAR T cells simpler and reduce the cost of treatment. Being capable of redirecting therapy by changing “mediator molecules,” physicians could immediately adjust their treatment strategy. This method is especially relevant in preventing relapse after the development of mutations making the target tumor antigen disappear, as well as for effective therapy of tumors with heterogeneous expression of antigens [77, 79, 83]. Nevertheless, it remains disputable whether mediator molecules can be used in solid tumor therapy, since their tumor-penetrating ability is limited, which reduces the effectiveness of local activation and function of CAR T cells,

while conventional CAR T cells can migrate into the tumor tissue [87, 88].

### **MASKING THE ANTIGEN RECOGNITION DOMAIN OF THE CHIMERIC ANTIGEN RECEPTOR**

The toxicity of CAR T therapy in dealing with solid tumors can be mitigated by modifying the antigen-binding domain of CAR with the masking peptide [89], which resides at the N-terminus of the chimeric antigen receptor, before the antigen-binding domain, and screens the recognition function of CAR (*Figure H*). A distinctive feature of some tumor types is that they contain specific proteases that hydrolyze the linker connecting the masking peptide and the antigen recognition domain of CAR. After the cleavage, CAR T cells can recognize the antigen presented on the tumor cell surface [89]. This approach enables use of the antigens presented on healthy cells for CAR-modified T cell therapy.

### **APPLICATION OF MRNA TO MODIFY T CELLS**

After they are administered to a patient, CAR T cells actively proliferate and differentiate into one of several T cell lineages. The new T cells also carry the CAR gene, which stimulates their activation. For most types of cancer, there is no need for the presence of therapeutic T cells during the entire life of a patient. Furthermore, it can cause additional complications and restoration of a patient's immune status after therapy. Transfecting CAR-coding mRNA into T cells is one of the methods used to temporarily modify T cells with CARs [90]. This approach has been successfully used both *in vitro* and *in vivo* to study CD19- and mesothelin-specific CARs [90, 91]. Mesothelin-specific CARs have been subsequently successfully applied to treat

pancreatic cancer [92, 93]. Electroporation of mRNA cells is carried out *in vitro* to avoid the potentially dangerous integration of the viral vector into a human's genome [90, 91]. Unfortunately, a single infusion of CAR T cells is insufficient, which makes treatment more expensive and complex. However, multiple infusions of CAR T cells allow one to regulate the count of persisting cells and intensiveness of treatment [90] to avoid excessive cytokine release, the tumor lysis syndrome, and cytotoxicity with respect to healthy cells.

### **CONCLUSIONS**

The successful application of CAR-modified T cells *in vivo* and FDA approval of their use on patients with acute lymphoblast leukemia have made CAR T-cell therapy the most widely discussed and promising potential treatment for various types of cancer and even autoimmune diseases. However, a closer look and clinical trials have revealed that chimeric antigen receptors are not devoid of drawbacks and carry certain risks for patients. Therefore, it is safety and the possibility to control the therapy that matters most rather than its effectiveness. Many bioengineering techniques and approaches have been used to design next-generation CARs that are safer and can be controlled. Each of the reported approaches has its own advantages and drawbacks. However, thanks to the new approaches, cellular therapy can now be used at much earlier stages of cancer, thus significantly increasing the patient's chances for a favorable outcome and reducing the risks of potential complications. ●

*This study was supported by the Russian Science Foundation (grant No. 17-74-30019).*

### **REFERENCES**

- Rosenberg S.A., Lotze M.T., Muul L.M., Leitman S., Chang A.E., Ettinghausen S.E., Matory Y.L., Skibber J.M., Shiloni E., Vetto J.T. // *N. Engl. J. Med.* 1985. V. 313. № 23. P. 1485–1492.
- Rosenberg S.A., Mulé J.J. // *Surgery.* 1985. V. 98. № 3. P. 437–444.
- Galluzzi L., Vacchelli E., Eggermont A., Fridman W.H., Galon J., Sautès-Fridman C., Tartour E., Zitvogel L., Kroemer G. // *Oncoimmunology.* 2012. V. 1. № 3. P. 306–315.
- Restifo N.P., Dudley M.E., Rosenberg S.A. // *Nat. Rev. Immunol.* 2012. V. 12. № 4. P. 269–281.
- Rosenberg S.A., Restifo N.P. // *Science.* 2015. V. 348. № 6230. P. 62–68.
- Kalos M., June C.H. // *Immunity.* 2013. V. 39. № 1. P. 49–60.
- de Bueger M., Bakker A., van Rood J.J., van der Woude F., Goulmy E. // *J. Immunol. Baltim. Md 1950.* 1992. V. 149. № 5. P. 1788–1794.
- Ringdén O., Labopin M., Gorin N.C., Schmitz N., Schaefer U.W., Prentice H.G., Bergmann L., Jouet J.P., Mandelli F., Blaise D., et al. // *Br. J. Haematol.* 2000. V. 111. № 4. P. 1130–1137.
- Minagawa K., Zhou X., Mineishi S., Di Stasi A. // *Pharm. Basel Switz.* 2015. V. 8. № 2. P. 230–249.
- Kershaw M.H., Westwood J.A., Darcy P.K. // *Nat. Rev. Cancer.* 2013. V. 13. № 8. P. 525–541.
- Schumacher T.N.M. // *Nat. Rev. Immunol.* 2002. V. 2. № 7. P. 512–519.
- Ramos C.A., Dotti G. // *Expert Opin. Biol. Ther.* 2011. V. 11. № 7. P. 855–873.
- Gross G., Waks T., Eshhar Z. // *Proc. Natl. Acad. Sci. USA.* 1989. V. 86. № 24. P. 10024–10028.
- Porter D.L., Levine B.L., Kalos M., Bagg A., June C.H. // *N. Engl. J. Med.* 2011. V. 365. № 8. P. 725–733.
- Porter D.L., Kalos M., Zheng Z., Levine B., June C. // *J. Cancer.* 2011. V. 2. P. 331–332.
- Kochenderfer J.N., Dudley M.E., Feldman S.A., Wilson W.H., Spaner D.E., Maric I., Stetler-Stevenson M., Phan G.Q., Hughes M.S., Sherry R.M., et al. // *Blood.* 2012. V. 119. № 12. P. 2709–2720.

17. Brentjens R.J., Davila M.L., Riviere I., Park J., Wang X., Cowell L.G., Bartido S., Stefanski J., Taylor C., Olszewska M., et al. // *Sci. Transl. Med.* 2013. V. 5. № 177. P. 177ra38.
18. Grupp S.A., Kalos M., Barrett D., Aplenc R., Porter D.L., Rheingold S.R., Teachey D.T., Chew A., Hauck B., Wright J.F., et al. // *N. Engl. J. Med.* 2013. V. 368. № 16. P. 1509–1518.
19. Kalos M., Levine B.L., Porter D.L., Katz S., Grupp S.A., Bagg A., June C.H. // *Sci. Transl. Med.* 2011. V. 3. № 95. P. 95ra73.
20. Brentjens R.J., Riviere I., Park J.H., Davila M.L., Wang X., Stefanski J., Taylor C., Yeh R., Bartido S., Borquez-Ojeda O., et al. // *Blood.* 2011. V. 118. № 18. P. 4817–4828.
21. Xu X.-J., Zhao H.-Z., Tang Y.-M. // *Leuk. Lymphoma.* 2013. V. 54. № 2. P. 255–260.
22. Xu Y., Zhang M., Ramos C.A., Durett A., Liu E., Dakhova O., Liu H., Creighton C.J., Gee A.P., Heslop H.E., et al. // *Blood.* 2014. V. 123. № 24. P. 3750–3759.
23. Davila M.L., Riviere I., Wang X., Bartido S., Park J., Curran K., Chung S.S., Stefanski J., Borquez-Ojeda O., Olszewska M., et al. // *Sci. Transl. Med.* 2014. V. 6. № 224. P. 224ra25.
24. Akpek G., Lee S.M., Anders V., Vogelsang G.B. // *Biol. Blood Marrow Transplant. J. Am. Soc. Blood Marrow Transplant.* 2001. V. 7. № 9. P. 495–502.
25. Ferrara F., Mele G., Palmieri S., Pedata M., Copia C., Riccardi C., Izzo T., Criscuolo C., Musto P. // *Hematol. Oncol.* 2009. V. 27. № 4. P. 198–202.
26. Lamers C.H.J., Langeveld S.C.L., Groot-van Ruijven C.M., Debets R., Sleijfer S., Gratama J.W. // *Cancer Immunol. Immunother. CII.* 2007. V. 56. № 12. P. 1875–1883.
27. Johnson L.A., Morgan R.A., Dudley M.E., Cassard L., Yang J.C., Hughes M.S., Kammula U.S., Royal R.E., Sherry R.M., Wunderlich J.R., et al. // *Blood.* 2009. V. 114. № 3. P. 535–546.
28. Lamers C.H., Sleijfer S., van Steenbergen S., van Elzakker P., van Krimpen B., Groot C., Vulto A., den Bakker M., Oosterwijk E., Debets R., et al. // *Mol. Ther. J. Am. Soc. Gene Ther.* 2013. V. 21. № 4. P. 904–912.
29. Sadelain M., Brentjens R., Riviere I. // *Cancer Discov.* 2013. V. 3. № 4. P. 388–398.
30. Morgan R.A., Yang J.C., Kitano M., Dudley M.E., Laurencot C.M., Rosenberg S.A. // *Mol. Ther. J. Am. Soc. Gene Ther.* 2010. V. 18. № 4. P. 843–851.
31. Uttenthal B.J., Chua I., Morris E.C., Stauss H.J. // *J. Gene Med.* 2012. V. 14. № 6. P. 386–399.
32. Moolten F.L. // *Cancer Res.* 1986. V. 46. № 10. P. 5276–5281.
33. Tiberghien P., Reynolds C.W., Keller J., Spence S., Deschaseaux M., Certoux J.M., Contassot E., Murphy W.J., Lyons R., Chiang Y. // *Blood.* 1994. V. 84. № 4. P. 1333–1341.
34. Bonini C., Ferrari G., Verzeletti S., Servida P., Zappone E., Ruggieri L., Ponzoni M., Rossini S., Mavilio F., Traversari C., et al. // *Science.* 1997. V. 276. № 5319. P. 1719–1724.
35. Oliveira G., Greco R., Lupo-Stanghellini M.T., Vago L., Bonini C. // *Curr. Opin. Hematol.* 2012. V. 19. № 6. P. 427–433.
36. Greco R., Oliveira G., Stanghellini M.T.L., Vago L., Bondanza A., Peccatori J., Cieri N., Markt S., Mastaglio S., Bordignon C., et al. // *Front. Pharmacol.* 2015. V. 6. P. 95.
37. Beltinger C., Fulda S., Kammertoens T., Meyer E., Uckert W., Debatin K.M. // *Proc. Natl. Acad. Sci. USA.* 1999. V. 96. № 15. P. 8699–8704.
38. Traversari C., Markt S., Magnani Z., Mangia P., Russo V., Ciceri F., Bonini C., Bordignon C. // *Blood.* 2007. V. 109. № 11. P. 4708–4715.
39. Riddell S.R., Elliott M., Lewinsohn D.A., Gilbert M.J., Wilson L., Manley S.A., Lupton S.D., Overell R.W., Reynolds T.C., Corey L., et al. // *Nat. Med.* 1996. V. 2. № 2. P. 216–223.
40. Ciceri F., Bonini C., Stanghellini M.T.L., Bondanza A., Traversari C., Salomoni M., Turchetto L., Colombi S., Bernardi M., Peccatori J., et al. // *Lancet Oncol.* 2009. V. 10. № 5. P. 489–500.
41. Maury S., Rosenzweig M., Redjoul R., Marçais A., Khaard A., Cherai M., Cabanne L., Churlaud G., Suarez F., Socié G., et al. // *Leukemia.* 2014. V. 28. № 12. P. 2406–2410.
42. Zhan H., Gilmour K., Chan L., Farzaneh F., McNicol A.M., Xu J.-H., Adams S., Fehse B., Veys P., Thrasher A., et al. // *PloS One.* 2013. V. 8. № 10. P. e77106.
43. Di Stasi A., Tey S.-K., Dotti G., Fujita Y., Kennedy-Nasser A., Martinez C., Straathof K., Liu E., Durett A.G., Grilley B., et al. // *N. Engl. J. Med.* 2011. V. 365. № 18. P. 1673–1683.
44. Zhou X., Di Stasi A., Tey S.-K., Krance R.A., Martinez C., Leung K.S., Durett A.G., Wu M.-F., Liu H., Leen A.M., et al. // *Blood.* 2014. V. 123. № 25. P. 3895–3905.
45. Iliuucci J.D., Oliver S.D., Morley S., Ward C., Ward J., Dalgarno D., Clackson T., Berger H.J. // *J. Clin. Pharmacol.* 2001. V. 41. № 8. P. 870–879.
46. Straathof K.C., Pulè M.A., Yotnda P., Dotti G., Vanin E.F., Brenner M.K., Heslop H.E., Spencer D.M., Rooney C.M. // *Blood.* 2005. V. 105. № 11. P. 4247–4254.
47. Quintarelli C., Vera J.F., Savoldo B., Giordano Attianese G.M.P., Pule M., Foster A.E., Heslop H.E., Rooney C.M., Brenner M.K., Dotti G. // *Blood.* 2007. V. 110. № 8. P. 2793–2802.
48. Ramos C.A., Asgari Z., Liu E., Yvon E., Heslop H.E., Rooney C.M., Brenner M.K., Dotti G. // *Stem Cells Dayt. Ohio.* 2010. V. 28. № 6. P. 1107–1115.
49. Gargett T., Brown M.P. // *Cytotherapy.* 2015. V. 17. № 4. P. 487–495.
50. Budde L.E., Berger C., Lin Y., Wang J., Lin X., Frayo S.E., Brouns S.A., Spencer D.M., Till B.G., Jensen M.C., et al. // *PloS One.* 2013. V. 8. № 12. P. e82742.
51. Kieback E., Charo J., Sommermeyer D., Blankenstein T., Uckert W. // *Proc. Natl. Acad. Sci. USA.* 2008. V. 105. № 2. P. 623–628.
52. Wang X., Chang W.-C., Wong C.W., Colcher D., Sherman M., Ostberg J.R., Forman S.J., Riddell S.R., Jensen M.C. // *Blood.* 2011. V. 118. № 5. P. 1255–1263.
53. Philip B., Kokalaki E., Mekkaoui L., Thomas S., Straathof K., Flutter B., Marin V., Marafioti T., Chakraverty R., Lynch D., et al. // *Blood.* 2014. V. 124. № 8. P. 1277–1287.
54. Introna M., Barbui A.M., Bambacioni F., Casati C., Gaipa G., Borleri G., Bernasconi S., Barbui T., Golay J., Biondi A., et al. // *Hum. Gene Ther.* 2000. V. 11. № 4. P. 611–620.
55. Serafini M., Manganini M., Borleri G., Bonamino M., Imberti L., Biondi A., Golay J., Rambaldi A., Introna M. // *Hum. Gene Ther.* 2004. V. 15. № 1. P. 63–76.
56. Griffioen M., van Egmond E.H.M., Kester M.G.D., Willems R., Falkenburg J.H.F., Heemskerk M.H.M. // *Haematologica.* 2009. V. 94. № 9. P. 1316–1320.
57. Fedorov V.D., Themeli M., Sadelain M. // *Sci. Transl. Med.* 2013. V. 5. № 215. P. 215ra172.
58. Zhang E., Xu H. // *J. Hematol. Oncol. J Hematol Oncol.* 2017. V. 10. № 1. P. 1.
59. Grada Z., Hegde M., Byrd T., Shaffer D.R., Ghazi A., Brawley V.S., Corder A., Schönfeld K., Koch J., Dotti G., et al. // *Mol. Ther. Nucleic Acids.* 2013. V. 2. P. e105.
60. Maher J., Brentjens R.J., Gunset G., Riviere I., Sadelain M. // *Nat. Biotechnol.* 2002. V. 20. № 1. P. 70–75.
61. Seton-Rogers S. // *Nat. Rev. Cancer.* 2016. V. 16. № 3. P. 128–129.

62. Kloss C.C., Condomines M., Cartellieri M., Bachmann M., Sadelain M. // *Nat. Biotechnol.* 2013. V. 31. № 1. P. 71–75.
63. Wilkie S., van Schalkwyk M.C.L., Hobbs S., Davies D.M., van der Stegen S.J.C., Pereira A.C.P., Burbridge S.E., Box C., Eccles S.A., Maher J. // *J. Clin. Immunol.* 2012. V. 32. № 5. P. 1059–1070.
64. Morsut L., Roybal K.T., Xiong X., Gordley R.M., Coyle S.M., Thomson M., Lim W.A. // *Cell.* 2016. V. 164. № 4. P. 780–791.
65. Wu C.-Y., Roybal K.T., Puchner E.M., Onuffer J., Lim W.A. // *Science.* 2015. V. 350. № 6258. P. aab4077.
66. Uhlen M., Oksvold P., Fagerberg L., Lundberg E., Jonnasson K., Forsberg M., Zwahlen M., Kampf C., Wester K., Hober S., et al. // *Nat. Biotechnol.* 2010. V. 28. № 12. P. 1248–1250.
67. Campoli M., Ferrone S. // *Oncogene.* 2008. V. 27. № 45. P. 5869–5885.
68. Ginhoux F., Turbant S., Gross D.A., Poupiot J., Marais T., Lone Y., Lemonnier F.A., Firat H., Perez N., Danos O., et al. // *Mol. Ther. J. Am. Soc. Gene Ther.* 2004. V. 10. № 2. P. 279–289.
69. Sakemura R., Terakura S., Watanabe K., Julamanee J., Takagi E., Miyao K., Koyama D., Goto T., Hanajiri R., Nishida T., et al. // *Cancer Immunol. Res.* 2016. V. 4. № 8. P. 658–668.
70. Choi J., Chen J., Schreiber S.L., Clardy J. // *Science.* 1996. V. 273. № 5272. P. 239–242.
71. Bayle J.H., Grimley J.S., Stankunas K., Gestwicki J.E., Wandless T.J., Crabtree G.R. // *Chem. Biol.* 2006. V. 13. № 1. P. 99–107.
72. Bishop A., Buzko O., Heyeck-Dumas S., Jung I., Kraybill B., Liu Y., Shah K., Ulrich S., Witucki L., Yang F., et al. // *Annu. Rev. Biophys. Biomol. Struct.* 2000. V. 29. P. 577–606.
73. Banaszynski L.A., Chen L.-C., Maynard-Smith L.A., Ooi A.G.L., Wandless T.J. // *Cell.* 2006. V. 126. № 5. P. 995–1004.
74. Park J.S., Rhau B., Hermann A., McNally K.A., Zhou C., Gong D., Weiner O.D., Conklin B.R., Onuffer J., Lim W.A. // *Proc. Natl. Acad. Sci. USA.* 2014. V. 111. № 16. P. 5896–5901.
75. Tamada K., Geng D., Sakoda Y., Bansal N., Srivastava R., Li Z., Davila E. // *Clin. Cancer Res. Off. J. Am. Assoc. Cancer Res.* 2012. V. 18. № 23. P. 6436–6445.
76. Urbanska K., Lanitis E., Poussin M., Lynn R.C., Gavin B.P., Kelderman S., Yu J., Scholler N., Powell D.J. // *Cancer Res.* 2012. V. 72. № 7. P. 1844–1852.
77. Rodgers D.T., Mazagova M., Hampton E.N., Cao Y., Ramadoss N.S., Hardy I.R., Schulman A., Du J., Wang F., Singer O., et al. // *Proc. Natl. Acad. Sci. USA.* 2016. V. 113. № 4. P. E459–468.
78. Lee D.W., Kochenderfer J.N., Stetler-Stevenson M., Cui Y.K., Delbrook C., Feldman S.A., Fry T.J., Orentas R., Sabin M., Shah N.N., et al. // *Lancet Lond. Engl.* 2015. V. 385. № 9967. P. 517–528.
79. Evans A.G., Rothberg P.G., Burack W.R., Huntington S.F., Porter D.L., Friedberg J.W., Liesveld J.L. // *Br. J. Haematol.* 2015. V. 171. № 2. P. 205–209.
80. Clémenceau B., Congy-Jolivet N., Gallot G., Vivien R., Gaschet J., Thibault G., Vié H. // *Blood.* 2006. V. 107. № 12. P. 4669–4677.
81. Kudo K., Imai C., Lorenzini P., Kamiya T., Kono K., Davidoff A.M., Chng W.J., Campana D. // *Cancer Res.* 2014. V. 74. № 1. P. 93–103.
82. D'Aloia M.M., Caratelli S., Palumbo C., Battella S., Arriga R., Lauro D., Palmieri G., Sconocchia G., Alimandi M. // *Cytotherapy.* 2016. V. 18. № 2. P. 278–290.
83. Ma J.S.Y., Kim J.Y., Kazane S.A., Choi S.-H., Yun H.Y., Kim M.S., Rodgers D.T., Pugh H.M., Singer O., Sun S.B., et al. // *Proc. Natl. Acad. Sci. USA.* 2016. V. 113. № 4. P. E450–458.
84. Cao Y., Rodgers D.T., Du J., Ahmad I., Hampton E.N., Ma J.S.Y., Mazagova M., Choi S.-H., Yun H.Y., Xiao H., et al. // *Angew. Chem. Int. Ed Engl.* 2016. V. 55. № 26. P. 7520–7524.
85. Skerra A. // *Curr. Opin. Biotechnol.* 2007. V. 18. № 4. P. 295–304.
86. Kim M.S., Ma J.S.Y., Yun H., Cao Y., Kim J.Y., Chi V., Wang D., Woods A., Sherwood L., Caballero D., et al. // *J. Am. Chem. Soc.* 2015. V. 137. № 8. P. 2832–2835.
87. Shimizu Y., van Seventer G.A., Horgan K.J., Shaw S. // *Immunol. Rev.* 1990. V. 114. P. 109–143.
88. Salmon H., Franciszkiewicz K., Damotte D., Dieu-Nos-jean M.-C., Validire P., Trautmann A., Mami-Chouaib F., Donnadieu E. // *J. Clin. Invest.* 2012. V. 122. № 3. P. 899–910.
89. Han X., Bryson P.D., Zhao Y., Cinay G.E., Li S., Guo Y., Siriwon N., Wang P. // *Mol. Ther. J. Am. Soc. Gene Ther.* 2017. V. 25. № 1. P. 274–284.
90. Zhao Y., Moon E., Carpenito C., Paulos C.M., Liu X., Brennan A.L., Chew A., Carroll R.G., Scholler J., Levine B.L., et al. // *Cancer Res.* 2010. V. 70. № 22. P. 9053–9061.
91. Barrett D.M., Zhao Y., Liu X., Jiang S., Carpenito C., Kalos M., Carroll R.G., June C.H., Grupp S.A. // *Hum. Gene Ther.* 2011. V. 22. № 12. P. 1575–1586.
92. Maus M.V., Haas A.R., Beatty G.L., Albelda S.M., Levine B.L., Liu X., Zhao Y., Kalos M., June C.H. // *Cancer Immunol. Res.* 2013. V. 1. P. 26–31.
93. Beatty G.L., Haas A.R., Maus M.V., Torigian D.A., Soulen M.C., Plesa G., Chew A., Zhao Y., Levine B.L., Albelda S.M., et al. // *Cancer Immunol. Res.* 2014. V. 2. № 2. P. 112–120.

# Organism-Level Tumor Models in Zebrafish *Danio rerio*

I. V. Mizgirev<sup>1</sup>, D. R. Safina<sup>2\*</sup>, I. V. Demidyuk<sup>2</sup>, S. V. Kostrov<sup>2</sup>

<sup>1</sup>N.N. Petrov National Medical Research Center of Oncology, Ministry of Health of Russia, Leningradskaya Str., 68, Pesochnyy Settlement, St. Petersburg, 197758, Russia

<sup>2</sup>Institute of Molecular Genetics, Russian Academy of Sciences, Kurchatov Sq., 2, Moscow, 123182, Russia

\*E-mail: nauruz@mail.ru

Received November 15, 2017; in final form May 14, 2018

Copyright © 2018 Park-media, Ltd. This is an open access article distributed under the Creative Commons Attribution License, which permits unrestricted use, distribution, and reproduction in any medium, provided the original work is properly cited.

**ABSTRACT** Development and implementation of adequate organism-level models is one of the key elements in biomedical research that focuses on experimental oncology. Over the last decade, studies using Zebrafish (*Danio rerio*) have gained in popularity in this area of research. This review describes the various approaches that have been used in developing highly effective models for oncological (clinical term, better cancer or tumor) studies based on *D. rerio*. Priority is given to transplantation models of cancer and their application to optically transparent *D. rerio* lines, including clonal ones, and utilization tumors of various origins bearing fluorescent labels. The combination of tumor transplantation at organism-level models in transparent clonal *D. rerio* lines with fluorescent microscopy, FACS-fractionation of tumor cell subsets, and transcription analysis can result in one of the most promising research approaches in providing new information on tumor formation and growth.

**KEYWORDS** Zebrafish, *Danio rerio*, molecular oncology, syngeneic, allogeneic and xenogeneic transplantation, transparent fish lines, bioimaging.

## INTRODUCTION

Cancer is one of the most significant problems of modern medicine. Cancer mortality ranks second in industrial countries and is projected to claim first rank in the future [1]. In this context, the development of biological models providing unique opportunities for studying the mechanisms of initiation and progression of malignant neoplasms in order to improve the effectiveness of novel antitumor therapies is among the top priorities in modern oncology.

Most of the current approaches are based primarily on the use of human and other mammalian cells *in vitro*. Despite their obvious advantages, these models have a number of significant limitations. First of all, the results obtained using these approaches are out of the whole organism context. For example, 1) *in vitro* models do not reflect the developmental stage or age of the organism; and 2) it is impossible to evaluate *in vitro* some organism-mediated effects on tumor growth, such as the influence of the tissue microenvironment, the hormonal and metabolic status, the immune system, etc. Obviously, *in vitro* studies should be supplemented with *in vivo* organism-level models. Rodents are the central organism-level model in cancer research. Transplantable tumor lines that can be

serially engrafted to inbred recipients are considered as the “gold standard” in experimental oncology, since they provide high penetrance of synchronously developing tumors. On the other hand, standard *in vivo* tumor growth models using rodents are hard to adapt to modern technologies for high-throughput screening of antitumor agents because of the high cost and labor-intensity of such studies. It should also be emphasized that the model does not allow high-throughput bioimaging of tumor development, including the changes taking place in the tumor microenvironment *in vivo*, which is a significant drawback in the analysis of fine mechanisms of tumor progression. Therefore, researchers have begun focusing on alternative tumor models which can compete with rodents in terms of the translational significance of experiments for clinical practice and that are much more informative and efficient.

In recent years, the freshwater fish *Danio rerio* (zebrafish) has become an increasingly popular model. This is due to its small size (2.5–4 cm), relatively short lifespan, as well as the possibility of laying up to several hundreds eggs per week from one female, *ex utero* development, transparency of embryos and larvae, the relative simplicity of maintenance and breeding,

and the existence of numerous mutant and transgenic lines.

It should be emphasized that the *D. rerio* model is perfectly adapted to the use of modern molecular and genetic. The genome of this organism has been mapped and sufficiently annotated [www.ncbi.nlm.nih.gov/genom/GRCz11]. Methods for precise editing of the zebrafish genome have become relatively simple and efficient, including targeted mutations using the ZFNs (zinc finger nucleases) platform [2–4] and the recently thoroughly elaborated CRISPR/Cas9 system [8]. The method of high-throughput insertional mutagenesis using retroviruses [5] and transposon elements has also been developed [6, 7]. Various genetically engineered *D. rerio* lines harboring oncogenes have been developed to induce tumors. Several of these tumors have been adapted to transplantable models. Recently, considerable attention has been focused on xenograft transplantation of human tumor cells.

#### ***D. rerio* MODELS BASED ON INDUCED TUMORS**

The pioneering studies by Stanton [9] and Khudoley [10] on hepatic tumor induction with chemical carcinogens laid the foundation for tumor growth modeling in *D. rerio*. This model remains one of the most popular tools used to study various aspects of tumor growth in fish (Fig. 1).

Furthermore, many new models have been generated by introducing vector DNA containing different oncogenes controlled by tissue-specific promoters into *D. rerio* zygotes [11], and they resulted in efficient induction of embryonic rhabdomyosarcomas [12], melanomas [13], hepatocellular carcinomas [14], and various types of leukemia [15–17].

Importantly, many genetically induced tumors express fluorescent protein-reporters, which enable to determine the time of tumor onset and investigate its growth and dissemination based on increased level and spatial distribution of fluorescence [18]. Some of these models use genetic constructs with regulatory elements to control the timing of tumor onset. In particular, induction of hepatocellular carcinomas by KRASV12 under the control of doxycycline [19] and mifepristone [20] has been developed. However, most of the above-mentioned models still possess limitations, such as a low incidence and long and variable latent period of tumor onset, which makes it difficult to use them, for example, for the screening of potential drugs.

#### **TRANSPLANTATION MODEL BASED ON *D. rerio***

Studies aimed at developing malignant growth models based on the transplantation of labeled mammalian or fish tumor cells into the organism of *D. rerio* are be-

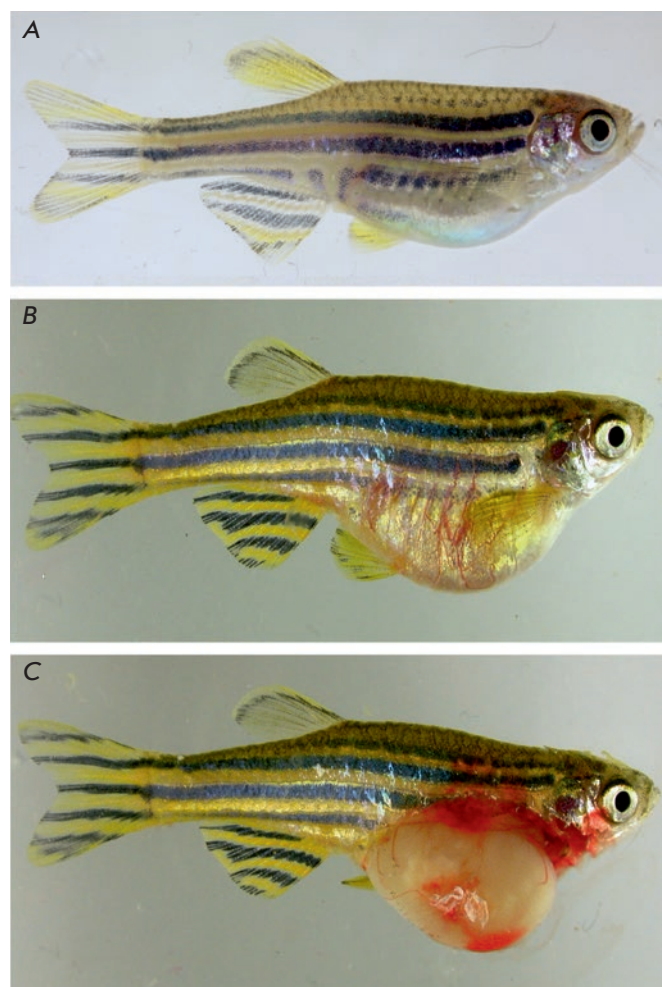


**Fig. 1.** *D. rerio* with a carcinogen-induced hepatic tumor. A – healthy fish; B – fish with induced hepatocarcinoma; C – the same fish with an opened abdominal cavity. Tumor induction was carried out according to the procedure described in Khudoley [10].

ing carried out in many laboratories around the world [21–25].

However, until recently, all attempts at using transplantation models based on *D. rerio* in cancer research faced a number of significant limitations. In particular, for a long time, a tumors could only be transplanted to sublethally irradiated fish or embryos at the early developmental stages.

At the same time, the approach associated with the use of sublethal gamma irradiation was not that convenient due to the high mortality of fish, as well as the quite rapid recovery of the immune system in survived animals [26].

The technique of xenogeneic transplantation of tumor cells, including human [27] and rodent [28] cells, into *D. rerio* embryos seems more attractive and has witnessed intensive development in recent years. Tumor cells transplanted into embryos at early developmental stages (before the age of 48 hours) are not rejected because of the immaturity of the embryonic immune system and can survive in the recipient organism for several days. In some cases, these cells may migrate (“metastasize”) some distance from the injection site [29] and produce angiogenic factors stimulating the growth of blood vessels [30–32]. Nevertheless, this type of transplantation models also exhibit some limitations related, for example, the temperature conditions optimal for fish embryos at 28°C, which are not optimal for mammalian cell growth. However, it should be noted that *D. rerio* can be maintained for some time at a higher temperature, up to 35°C, which is more adequate for mammalian cells, without significant loss in their survival rate [33]. Recently, xenotransplantation of tumors into *D. rerio* embryos has been successfully used to assess the sensitivity of tumors obtained from patients to the action of various drugs and their combinations in order to select the optimal strategy of drug therapy [34]. Previously, such studies were carried out only in athymic NOD/SCID mice. However, the prospects for a widespread use of this approach in clinical oncology are extremely limited due to its high cost and the labor-intensity of such studies.

Unfortunately, all attempts at developing inbred *D. rerio* lines similar to inbred mammalian ones using standard inbreeding techniques have failed due to the reduced fertility of fish after several rounds of closely related crossing.

The problem of heterologous tissue transplantation into the organism of *D. rerio* has largely been solved thanks to the development of three new experimental approaches. The first one is based on the production of homozygous diploid clonal lines of *D. rerio* [35], which for the first time enabled the transplantation of tumor or normal cells from one fish to another within the same line without graft rejection. The possibility of constructing such lines was first demonstrated by Streisinger et al. [36]. The double-heat shock method was used to generate clonal lines [37]. For this purpose, oocytes from *D. rerio* were fertilized *in vitro* with UV-inactivated sperms and then subjected to a short thermal shock to block the first cell cleavage. Survived embryos (approximately 0.5% of heat-shock treated zygotes) were grown to adult state. This procedure leads to the development of completely homozygous diploid fish, which, nevertheless, are genetically different from each other. At the second stage, the oocytes obtained from each of the homozygous females are subjected

to the next round of fertilization with UV-irradiated sperm, followed by heat shock. The offspring obtained from each homozygous female are genetically identical (clones) to this female and to each other because of the initial homozygosity of the mother organism. Clonal lines are further maintained by crossing the fish within one clone with each other. It should be noted that the sex of *D. rerio* is determined not by sex chromosomes but by physiological factors acting at early developmental stages, and, therefore, the offspring produced by clonal fish crossing will include both males and females. These lines are characterized by complete genetic identity and full homozygosity of the animals within each clone. This is a direct analogue of inbred rodent strains.

Clonal zebrafish lines consisting of genetically identical animals have been proven to be a convenient model for serial transplantation of tumor cells. Some tumor strains originating from the nitrosodiethylamine-induced hepatic and pancreatic carcinomas of clonal fish have undergone more than 20 consecutive passages without signs of rejection. In later studies, the clonal fish lines CG1 and CG2 were used to induce and subsequently transplant fluorescent reporter-labeled rhabdomyosarcoma [38] and leukemia cells [39] to syngeneic recipients. In that situation, the small sizes of the *D. rerio* larvae and embryos make them an ideal tool for large-scale transplantation of tumor cells to hundreds of syngeneic recipients within a short period of time.

The second approach, which has been under development since recently, is based on the use of immunodeficient fish lines [40] similar to athymic NOD/SCID mice [41]. The model enables quite effective allogeneic transplantation of malignant and normal tissues to a recipient. However, it must be emphasized that immunodeficient animals cannot be used to study, for example, a number of the aspects of tumor interaction with the host organism.

In this regard, another approach based on the recently developed double transplantation technique appears especially promising [42]. The approach is based on engraftment of lethally irradiated tumor cells into *D. rerio* embryos at the early developmental stages (up to 48 hours after fertilization). It has been shown that these cells persist in the recipient organism for about 2 weeks, do not affect its viability but lead to the development of specific immunological tolerance to this tumor without causing global immunodeficiency. Three months after primary transplantation, these animals can be injected with non-irradiated cells of the corresponding tumor. These cells successfully form tumor nodes and are capable of metastasizing. The approach was tested on various human tumor cell lines, including

hepatocarcinoma and prostate cancer. Thus, this model enables transplantation of allogeneic and xenogeneic tumors to adult fish and quite accurately simulates spontaneous tumor growth in the host organism.

**TRANSPLANTATION MODELS BASED ON TRANSPARENT LINES OF *D. rerio***

The loss of fish body wall transparency with growth due to the production of pigment cells, i.e. chromatophores producing black (melanophores), light-reflecting (iridophores), and yellow (xanthophores) pigments in the skin, eyes, and peritoneal lining, is another limitation in the use of *D. rerio* as an organism-level tumor model. This significantly complicates the bioimaging analysis of the development of the transplanted or induced tumors in the animal's body. However, optically transparent lines (*ruby*, *casper*, *sheer*) have been developed [43, 44] which lack most pigment cells and, as a result, have transparent body walls through which all visceral organs, as well as transplanted normal and tumorous tissue, can be visualized (Fig. 2, 3). Therefore, transparent lines are an almost ideal model for real-time non-invasive study of tumor growth *in vivo*. Obviously, generation of clonal optically transparent lines, as well as combining transparent lines with double-transplantation technology, should be the next step.

Generation of optically transparent clonal *D. rerio* lines makes the use of fluorescently labeled tumors for transplantation highly promising. Generation of these tumors by mosaic expression of transgenes containing various oncogenes, in combination with fluorescent reporters, has been demonstrated previously for clonal *D. rerio* lines [38, 39]. Chemical carcinogen-induced tu-



Fig. 2. Three-week old *D. rerio*, transparent line *sheer*.



Fig. 3. Carcinogen-induced hepatocellular carcinoma in a transparent *sheer* line of *D. rerio*. Tumor was induced according to the procedure described in Khudoley [10].

mors in fish which are phenotypically very similar to human tumors might be very desirable for bioimaging of cancer development and progression. This is being accomplished by chemical carcinogenesis in transgenic *D. rerio* sublines based on clonal line CG2 expressing a fluorescent marker ubiquitously: i.e. in all tissue types. Any tumor induced in fish that belong to one of these sublines will bear a fluorescent label and can be transplanted to non-transgenic syngeneic CG2 fish (Fig. 4).

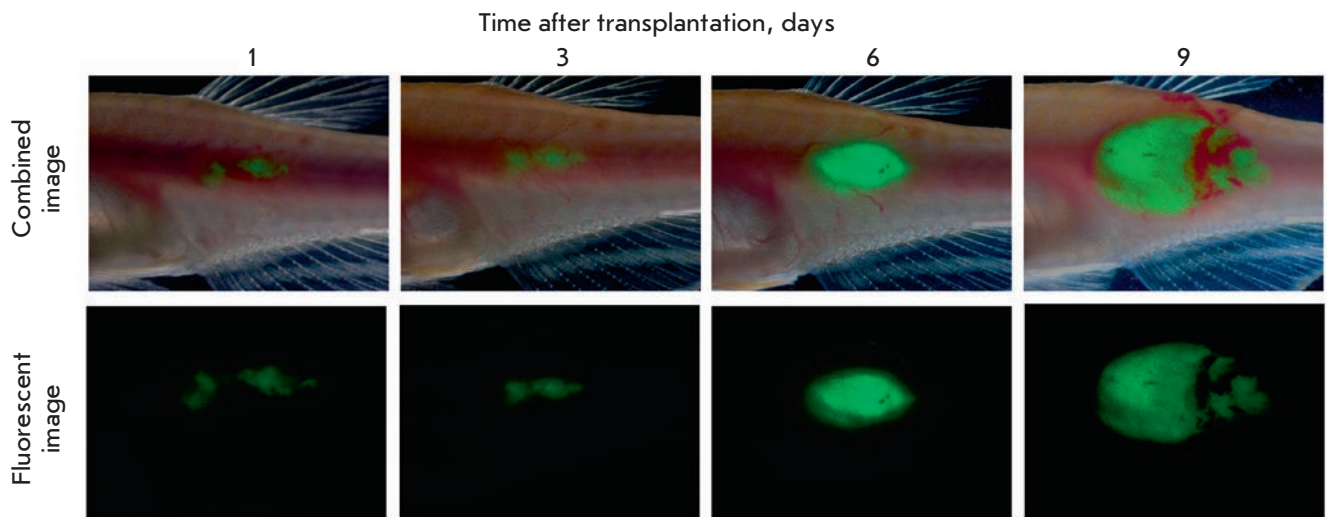


Fig. 4. Green fluorescent protein-labeled rhabdomyosarcoma grown in the clonal line of *D. rerio*. Intramuscular transplantation, the 4<sup>th</sup> passage.

The implementation of this technique in clonal transparent lines of *D. rerio* will result in a transplantation model that provides exceptional capabilities for detailed bioimaging of tumor growth.

### PROSPECTS OF MODEL DEVELOPMENT

One of the most interesting strategies in the development of models based on *D. rerio* includes its combination with modern approaches to transcriptome analysis. At present, transcriptome analysis of a number of tumors of *D. rerio* of various geneses (hepatocellular carcinoma, melanoma, rhabdomyosarcoma, etc.) is carried out using microarrays and RNA sequencing technology. The results have been compared to those obtained when analyzing corresponding human tumors. The finding that the transcriptome changes accompanying tumor growth in humans and *D. rerio* are conserved was the main conclusion of these studies [45, 46]. This conclusion is extremely important for further development of this system, since it indicates the possibility of its use for a detailed analysis of the mechanisms of the onset and development of human tumors and high-throughput screening of antitumor agents. Detailed study of the interaction between the tumor and surrounding stromal tissue is one of the most promising areas, which provides hope for the development of new approaches to the therapy of tumor diseases [47]. To date, it is clear that a microenvironment represented primarily by fibroblasts, endothelial cells, pericytes,

leukocytes, and the extracellular matrix is an integral part of a tumor and is directly involved in the control over its formation, growth, and progression. In turn, tumor cells have an active remodeling effect on the surrounding tissue. Therefore, the tumor growth process involves a complex set of various interactions that change with tumor progression. Obviously, any analysis of the interaction between a tumor and stromal tissue is impossible without the use of organism-level models. The most common, currently used systems are based on immunodeficient rodent lines, which provide a combination of an organism-level model, fluorescent microscopy, FACS analysis of cell subpopulations, and transcription analysis [48]. However, the *D. rerio* model is gaining in popularity, especially where high-resolution microscopy is warranted [49, 50]. It is very likely that implementation of these approaches, in combination with a syngeneic transplantation model based on optically transparent *D. rerio* lines, will provide fundamentally new insight into understanding tumor growth and its interaction with its microenvironment. ●

*This study was supported by the Russian Foundation for Basic Research as the part of scientific projects No. 18-04-00319 and 17-00-00189, and the Presidium of the Russian Academy of Sciences as the part of the Research Programs Fundamental Research for Biomedical Technologies and Molecular and Cell Biology.*

### REFERENCES

- Jemal A., Siegel R., Ward E., Hao Y., Xu J., Murray T., Thun M.J. // *CA Cancer J. Clin.* 2008. V. 58. № 2. P. 71–96.
- Reyon D., Kirkpatrick J.R., Sander J.D., Zhang F., Voytas D.F., Joung J.K., Dobbs D., Coffman C.R. // *BMC Genomics.* 2011. V. 12. P. 83.
- Cifuentes D., Xue H., Taylor D.W., Patnode H., Mishima Y., Cheloufi S., Ma E., Mane S., Hannon G.J., Lawson N.D., et al. // *Science.* 2010. V. 328. № 5986. P. 1694–1698.
- Siekman A.F., Standley C., Fogarty K.E., Wolfe S.A., Lawson N.D. // *Genes Dev.* 2009. V. 23. № 19. P. 2272–2277.
- Amsterdam A., Nissen R.M., Sun Z., Swindell E.C., Farrington S., Hopkins N. // *Proc. Natl. Acad. Sci. USA.* 2004. V. 101. № 35. P. 12792–12797.
- Kwan K.M., Fujimoto E., Grabher C., Mangum B.D., Hardy M.E., Campbell D.S., Parant J.M., Yost H.J., Kanki J.P., Chien C.B. // *Dev. Dyn.* 2007. V. 236. № 11. P. 3088–3099.
- Villefranc J.A., Amigo J., Lawson N.D. // *Dev. Dyn.* 2007. V. 236. № 11. P. 3077–3087.
- Li M., Zhao L., Page-McCaw P.S., Chen W. // *Trends Genet.* 2016. V. 32. № 12. P. 815–827.
- Stanton M.F. // *J. Natl. Cancer Inst.* 1965. V. 34. P. 117–130.
- Khudoley V.V. // *Natl. Cancer Inst. Monogr.* 1984. V. 65. P. 65–70.
- Etchin J., Kanki J.P., Look A.T. // *Methods Cell Biol.* 2011. V. 105. P. 309–337.
- Chen E.Y., Langenau D.M. // *Methods Cell Biol.* 2011. V. 105. P. 383–402.
- Bootorabi F., Manouchehri H., Changizi R., Barker H., Palazzo E., Saltari A., Parikka M., Pincelli C., Aspatwar A. // *Int. J. Mol. Sci.* 2017. V. 18. № 7. P. 1550.
- Nguyen A.T., Emelyanov A., Koh C.H., Spitsbergen J.M., Lam S.H., Mathavan S., Parinov S., Gong Z. // *Dis. Model Mech.* 2011. V. 4. № 6. P. 801–813.
- Langenau D.M., Traver D., Ferrando A.A., Kutok J.L., Aster J.C., Kanki J.P., Lin S., Prochownik E., Trede N.S., Zon L.I., et al. // *Science.* 2003. V. 299. № 5608. P. 887–890.
- Teittinen K.J., Grönroos T., Parikka M., Rämetsä M., Lohi O. // *Leuk. Res.* 2012. V. 36. № 9. P. 1082–1088.
- Moore F.E., Langenau D.M. // *Adv. Hematol.* 2012. V. 2012. P. 478164.
- Ignatius M.S., Langenau D.M. // *Methods Cell Biol.* 2011. V. 105. P. 437–459.
- Li Z., Zheng W., Wang Z., Zeng Z., Zhan H., Li C., Zhou L., Yan C., Spitsbergen J.M., Gong Z. // *Dis. Model Mech.* 2013. V. 6. № 2. P. 414–423.
- Nguyen A.T., Emelyanov A., Koh C.H., Spitsbergen J.M., Parinov S., Gong Z. // *Dis. Model Mech.* 2012. V. 5. № 1. P. 63–72.
- Le X., Pugach E.K., Hettmer S., Storer N.Y., Liu J., Wills A.A., DiBiase A., Chen E.Y., Ignatius M.S., Poss K.D., et al. // *Development.* 2013. V. 140. № 11. P. 2354–2356.

22. Li Z., Zheng W., Li H., Li C., Gong Z. // *PLoS One*. 2015. V. 10. № 7. P. e0132319.
23. Kaufman C.K., Mosimann C., Fan Z.P., Yang S., Thomas A.J., Ablain J., Tan J.L., Fogley R.D., van Rooijen E., Hagedorn E.J., et al. // *Science*. 2016. V. 351(6272). P. 2197.
24. Moore F.E., Garcia E.G., Lobbardi R., Jain E., Tang Q., Moore J.C., Cortes M., Molodtsov A., Kasheta M., Luo C.C., et al. // *J. Exp. Med.* 2016. V. 213. № 6. P. 979–992.
25. Tulotta C., He S., van der Ent W., Chen L., Groenewoud A., Spaik H.P., Snaar-Jagalska B.E. // *Adv. Exp. Med. Biol.* 2016. V. 916. P. 239–263.
26. Langenau D.M., Ferrando A.A., Traver D., Kutok J.L., Hezel J.P., Kanki J.P., Zon L.I., Look A.T., Trede N.S. // *Proc. Natl. Acad. Sci. USA*. 2004. V. 101. № 19. P. 7369–7374.
27. Jung D.W., Oh E.S., Park S.H., Chang Y.T., Kim C.H., Choi S.Y., Williams D.R. // *Mol. Biosyst.* 2012. V. 8. № 7. P. 1930–1939.
28. Nicoli S., Ribatti D., Cotelli F., Presta M. // *Cancer Res.* 2007. V. 67. № 7. P. 2927–2931.
29. Marques I.J., Weiss F.U., Vlecken D.H., Nitsche C., Bakkers J., Lagendijk A.K., Partecke L.I., Heidecke C.D., Lerch M.M., Bagowski C.P. // *BMC Cancer*. 2009. V. 9. P. 128.
30. Tran T.C., Sneed B., Haider J., Blavo D., White A., Aiyejorun T., Baranowski T.C., Rubinstein A.L., Doan T.N., Dingleline R., et al. // *Cancer Res.* 2007. V. 67. № 23. P. 11386–11392.
31. Rouhi P., Lee S.L., Cao Z., Hedlund E.M., Jensen L.D., Cao Y. // *Cell Cycle*. 2010. V. 9. № 5. P. 913–917.
32. Zhao C., Wang X., Zhao Y., Li Z., Lin S., Wei Y., Yang H. // *PLoS One*. 2011. V. 6. № 7. P. e21768.
33. Marques I.J., Weiss F.U., Vlecken D.H., Nitsche C., Bakkers J., Lagendijk A.K., Partecke L.I., Heidecke C.D., Lerch M.M., Bagowski C.P. // *BMC Cancer*. 2009. V. 9. P. 128.
34. Fior R., Póvoa V., Mendes R.V., Carvalho T., Gomes A., Figueiredo N., Ferreira M.G. // *Proc. Natl. Acad. Sci. USA*. 2017. V. 114. № 39. P. 8234–8243.
35. Mizgirev I.V., Revskoy S.Y. // *Cancer Res.* 2006. V. 66. № 6. P. 3120–3125.
36. Streisinger G., Walker C., Dower N., Knauber D., Singer F. // *Nature*. 1981. V. 291. № 5813. P. 293–296.
37. Mizgirev I., Revskoy S. // *Nat. Protocols*. 2010. V. 5. № 3. P. 383–394.
38. Ignatius M.S., Chen E., Elpek N.E., Fuller A., Tenente I.M., Clagg R., Liu S., Blackburn J.S., Linardic C.M., Rosenberg A., et al. // *Cancer Cell*. 2012. V. 21. № 5. P. 680–693.
39. Mizgirev I.V., Revskoy S. // *Cancer Biol. Ther.* 2010. V. 9. № 11. P. 895–902.
40. Moore J.C., Tang Q., Yordán N.T., Moore F.E., Garcia E.G., Lobbardi R., Ramakrishnan A., Marvin D.L., Anselmo A., Sadreyev R.I., et al. // *J. Exp. Med.* 2016. V. 213. № 12. P. 2575–2589.
41. Ito M., Hiramatsu H., Kobayashi K., Suzue K., Kawahata M., Hioki K., Ueyama Y., Koyanagi Y., Sugamura K., Tsuji K., et al. // *Blood*. 2002. V. 100. P. 3175–3182.
42. Zhang B., Shimada Y., Hirota T., Ariyoshi M., Kuroyanagi J., Nishimura Y., Tanaka T. // *Transl. Res.* 2016. V. 170. P. 89–98.e3.
43. White R.M., Sessa A., Burke C., Bowman T., LeBlanc J., Ceol C., Bourque C., Dovey M., Goessling W., Burns C.E., et al. // *Cell Stem Cell*. 2008. V. 2. № 2. P. 183–189.
44. Ren J.Q., McCarthy W.R., Zhang H., Adolph A.R., Li L. // *Vision Res.* 2002. V. 42. № 3. P. 293–299.
45. Lam S.H., Wu Y.L., Vega V.B., Miller L.D., Spitsbergen J., Tong Y., Zhan H., Govindarajan K.R., Lee S., Mathavan S., et al. // *Nat. Biotechnol.* 2006. V. 24. № 1. P. 73–75.
46. Lam S.H., Gong Z. // *Cell Cycle*. 2006. V. 5. № 6. P. 573–577.
47. Pietras K., Östman A. // *Exp. Cell Res.* 2010. V. 316. № 8. P. 1324–1331.
48. Yang N., Huang B., Tsinkalovsky O., Brekkå N., Zhu H., Leiss L., Enger P.Ø., Li X., Wang J. // *Cancer Cell Int.* 2014. V. 14. № 1. P. 541.
49. Wang J., Cao Z., Zhang X.M., Nakamura M., Sun M., Hartman J., Harris R.A., Sun Y., Cao Y. // *Cancer Res.* 2015. V. 75. № 2. P. 306–315.
50. Vittori M., Breznik B., Gredar T., Hrovat K., Bizjak Mali L., Lah T.T. // *Radiol. Oncol.* 2016. V. 50. № 2. P. 159–167.

# The Development and Study of Recombinant Immunoglobulin A to Hemagglutinins of the Influenza Virus

T. K. Aliev<sup>1\*</sup>, I. G. Dement'yeva<sup>2</sup>, V. A. Toporova<sup>3</sup>, V. V. Argentova<sup>4</sup>, L. P. Pozdnyakova<sup>2</sup>, M. N. Bokov<sup>2</sup>, Yu. A. Votchitseva<sup>4</sup>, D. A. Dolgikh<sup>3,4</sup>, S. D. Varfolomeyev<sup>1</sup>, P. G. Sveshnikov<sup>2</sup>, M. P. Kirpichnikov<sup>3,4</sup>

<sup>1</sup>Lomonosov Moscow State University, Department of Chemistry, Leninskie gory 1, bldg. 3, Moscow, 119991, Russia

<sup>2</sup>Russian Research Center for Molecular Diagnostics and Therapy, Simferopolsky Blvd. 8, Moscow, 117149, Russia

<sup>3</sup>Shemyakin-Ovchinnikov Institute of Bioorganic Chemistry, Russian Academy of Sciences, Miklukho-Maklaya Str. 16/10, Moscow, 117997, Russia

<sup>4</sup>Lomonosov Moscow State University, Faculty of Biology, Leninskie gory 1, bldg. 12, Moscow, 119991, Russia

\*E-mail: ta12345@list.ru

Received November 15, 2017; in final form April 16, 2018

Copyright © 2018 Park-media, Ltd. This is an open access article distributed under the Creative Commons Attribution License, which permits unrestricted use, distribution, and reproduction in any medium, provided the original work is properly cited.

**ABSTRACT** We obtained recombinant variants of human antibody FI6 broadly specific to hemagglutinins of the influenza A virus. On the basis of a bi-promoter (CMV, hEF1-HTLV) vector, we developed genetic constructs for the expression of the heavy and light chains of the immunoglobulins of IgA1-, IgA2m1-, and IgG-isotypes. Following transfection and selection, stable Chinese hamster ovary (CHO) cell lines were produced. The antibodies of IgA1-, IgA2m1-, and IgG-isotypes were purified from culture media. We performed an immunochemical characterization and studied their interactions with influenza A strains of the H1N1- and H3N2-subtypes. It was shown that recombinant FI6 variants of the IgA-isotype retain the properties of the parental IgG antibody to demonstrate specificity to all the strains tested. The strongest binding was observed for the H1N1 subtype, which belongs to hemagglutinins of phylogenetic group I.

**KEYWORDS** Influenza A virus, broadly neutralizing antibodies, immunoglobulin A, IgA1, IgA2m1, recombinant antibodies.

**ABBREVIATIONS** IAV – influenza A virus MES – 2-(*N*-morpholino)ethanesulfonic acid; ELISA – enhanced light immunosorbent assay;  $K_d$  – dissociation constant.

## INTRODUCTION

Passive immunotherapy with antibodies targeting viral capsid components is a promising strategy in the design of new drugs against influenza viruses [1, 2]. This approach is of particular importance because of the high antigenic variation of surface influenza A virus (IAV) proteins that decreases the efficacy of vaccines and low-molecular therapeutic agents. In recent years, neutralization of monoclonal antibodies (mABs) cross-protective against diverse IAV serotypes have been pursued in the design of broad spectrum antivirals [3–7]. A large-scale screening of more than 100,000 individual, cultured antibody-producing B cells selected from several donors with significant heterosubtypic immunity against several IAV subtypes, has been a great success [8]. A unique antibody FI6 that targets

the recombinant and natural hemagglutinins of phylogenetic groups I and II was found. The broad specificity of this antibody appears to be associated with the targeting of a conserved epitope in the F subdomain of hemagglutinin, which is less mutation-prone than the HA1 domain. Transfer of this antibody at a dose of 2–20 mg/kg into mice and ferrets after lethal H1N1 and H5N1 challenge conferred full protection. The discovery of this broad-spectrum antibody opens up myriad opportunities for the creation of different recombinant immunoglobulins on its basis.

The respiratory tract is the major route for IAV entry into host cells; hence, intranasal administration of neutralizing antibodies can significantly enhance the effect of passive immunotherapy [9, 10]. The intranasal delivery of recombinant immunoglobulin A, the most

prevalent antibody at human mucosal sites, appears as a very intriguing option [11]. Class A immunoglobulins come in various isoforms (monomer, dimer, secretory form) and, thus, employ different mechanisms for virus neutralization. IgA-isotype antibodies can block virus interaction with the surface of human cells, neutralize the viral particles inside cells, and facilitate the destruction of infected cells by attracting and activating neutrophils [12].

The aim of this study was to produce recombinant variants of antibody FI6 of IgA-isotype and to compare its immunochemical properties with those of IgG-isotype.

## EXPERIMENTAL

### Construction of the bi-promoter vector for the expression of recombinant FI6 IgG1-isotype antibodies

We had previously synthesized [13] cDNA sequences of the variable domain of the heavy FI6VHv3 and light FI6VKv2 chains of antibody FI6 [8].

A fragment with a nucleotide sequence encoding the leader peptide MAWVWTLFLMAAAQSAQA and the untranslated regulatory region were fused to the 5'-end region of the previously synthesized cDNA of the heavy chain variable domain FI6VHv3 through splicing by overlap extension polymerase chain reaction (SOE-PCR). To create the bi-promoter expression cassette, the SOE-PCR DNA fragment was treated with *NheI* and *Bsp120I* restrictases and cloned into the pSK+/hEF1-HTLV-BGH plasmid, pretreated with the same restrictases [14] containing the hEF1-HTLV hybrid promoter, the full-length IgG1 constant region and polyadenylation site BGH, all flanked with *MluI* restriction sites. Thus, a pSK+/hEF1-HTLV-FI6HG1-BGH plasmid was obtained.

Similar to the heavy chain, human antibody light chain cDNA adapted to expression in eukaryotic cells was obtained. Using SOE-PCR, we spliced cDNA of the leader peptide MKSQTQVFVLLLLCVSGAHG, previously synthesized cDNA of the variable domain of the FI6VKv2 light chain, and cDNA of the constant domain of human kappa-isotype. The resulting DNA fragment was treated with *NheI* and *Sfr274I* restrictases and cloned into the pOptiVEC plasmid (Invitrogen, USA) that was pretreated with the same restrictases and carried a preliminarily inserted *MluI* restriction site near the 5'-end of the promoter. In this way, a pOpti-FI6L plasmid containing the light-chain gene of antibody FI6 under the cytomegalovirus promoter (CMV) control was obtained.

At the final stage of pBiPr-ABiG1FI6 bi-promoter plasmid creation, the *MluI*-*MluI* fragment (2500 bp)

from the pSK+/hEF1-HTLV-FI6HG1-BGH plasmid was inserted into the pOpti-FI6L dephosphorylated vector pretreated with the *MluI* restrictase.

### Construction of bi-promoter plasmids for the expression of recombinant FI6 IgA1- and IgA2m1-isotype antibodies

The constant heavy-chain domains of IgA1- and IgA2m1-isotypes were obtained as follows. Exons of the corresponding genes were amplified using the human chromosomal DNA template and specific oligonucleotide primers and cloned into an intermediate vector, pAL-TA (Eurogen, Russia). Exons of the constant domains of the same isotopes were spliced by SOE-PCR. The obtained fragments were treated with *SacI* and *Sfr274I* restrictases; each of these fragments, the *NheI*-*SacI* fragment from pSK+/hEF1-HTLV-FI6HG1-BGH containing cDNA of the leader peptide MAWVWTLFLMAAAQSAQA and cDNA of the variable heavy-chain region of antibody FI6, was cloned into the pSK+/hEF1-HTLV-BGH vector pretreated with *NheI* and *Sfr274I* restrictases. Thus, the plasmids pSK+/hEF1-HTLV-FI6HA1-BGH and pSK+/hEF1-HTLV-FI6HA2m1-BGH were obtained that contained the hEF1-HTLV promoter, cDNA of the leader peptide MAWVWTLFLMAAAQSAQA, the variable heavy-chain region of antibody FI6, cDNA of the constant domain of human IgA1- or IgA2m1-isotype (respectively), and an untranslated region which includes the polyadenylation site BGH flanked by *MluI* restriction sites.

At the final stage of creation of pBiPr-ABiG1FI6 and pBiPr-ABiG2m1FI6 bi-promoter vectors, fragments *MluI*-*MluI* (2500 bp) from the plasmids pSK+/hEF1-HTLV-FI6HA1-BGH and pSK+/hEF1-HTLV-FI6HA2m1-BGH, respectively, were inserted into the pOpti-FI6L dephosphorylated vector pretreated with *MluI* restrictase.

### Preparation of cell lines producing recombinant antibodies

CHO DG44 cells (Invitrogen, USA) were transfected with linearized pBiPr-ABiG1FI6, pBiPr-ABiG2m1FI6, and pBiPr-ABiG1FI6 plasmids using the Lipofectamine 3000 reagent (Invitrogen, USA) according to the standard protocol. Primary selection of transfected cells was performed using the CD OptiCHO medium (Invitrogen, USA) with addition of 8 mM *L*-glutamine (Gibco, USA), 0.1% Pluronic F-68 (Gibco, USA), and a 1X antibiotic/antimycotic solution (Gibco, USA). Fluorescent screening and selection of the producer clones were performed to obtain a stable cell line. The cells were seeded on a semi-solid CloneMedia medium (Molecular Devices, USA) with the addition of mouse an-

tibodies to the constant domains of human immunoglobulins G (Molecular Devices, USA) or A (Russian Research Center for Molecular Diagnostics and Therapy, Russia) depending on the isotype of the FITC-labeled recombinant antibodies. After 14 days of cell cultivation, some producing clones were selected using the ClonePix FL device (Molecular Devices, USA) based on fluorescence intensity. The selected clones were cultured in the presence of increasing methotrexate concentrations from 20 to 500 nM to enhance productivity.

### Extraction and purification of recombinant antibodies

The culture of cells producing recombinant antibodies was grown in spinner flasks with a 500 mL working volume. For this,  $2.5\text{--}3.0 \times 10^5$  cells/mL were seeded in a 300 mL CD OptiCHO medium and grown for 14–18 days in a CO<sub>2</sub>-incubator at 37°C, 8% CO<sub>2</sub> and a stirring rate of the spinner of 50–70 rpm.

The culture fluid was centrifuged at 4000 g; 50 mM 2-(N-morpholino)ethanesulfonic acid (MES) and 150 mM NaCl were added to the supernatant, pH 5.7.

The culture fluid containing FI6-IgG was loaded on the Protein G-Sepharose 4B Fast Flow column (diameter 2.5 cm, gel height 3.5 cm, volume 17 mL), pre-equilibrated with a MES solution pH 5.7, at a recirculation rate of 42 mL/h ( $8.6 \text{ mL/h} \times \text{cm}^2$ ) for 21 h at 4°C. Antibodies were eluted with 0.1 M glycine buffer at pH 2.7 and an elution rate of 70 mL/h. Immediately after the eluate was obtained, pH was adjusted to ~7.5 with 2 M Tris and concentrated using the 30000 NMWL ultrafiltration membrane to a volume of  $\approx 1.5\text{--}2$  mL and dialyzed against a phosphate buffer (200X volume) at pH 7.4 overnight.

For affine chromatography of FI6-IgA1 and FI6-IgA2m1, an immunosorbent based on FabH A3

mouse monoclonal antibodies (mABs) (Russian Research Center for Molecular Diagnostics and Therapy, Russia) to human immunoglobulin kappa-chain was obtained. Antibodies were immobilized on activated BrCN-sepharose according to Kavran et al. [15]. The immobilization degree of FabH A3 antibodies was 5 mg per 1 mL of sepharose. The pH of the culture fluid containing FI6-IgA antibodies was adjusted to 8.0 with a 1 M Tris solution and loaded on the column via recirculation for 18 h at a rate of 15 mL/h. For the elution of the FI6-IgA1 and FI6-IgA2m1 antibodies, 0.1 M sodium-acetate buffer, pH 3.0; 0.5 M NaCl; 0.1 M glycine buffer, pH 2.5; 0.5 M NaCl; 0.1 M glycine buffer, pH 2.0; 0.5 M NaCl were consecutively used. All eluates were neutralized with a 1 M Tris solution.

### Immunochemical analysis of recombinant antibodies

In this work, we used highly purified relic and current strains of IAV produced by Hytest Ltd. (Turku, Finland) and the Research Institute of Influenza RAMS (St. Petersburg, Russia) obtained from infected chicken embryos by successive ultracentrifugation in a sucrose density gradient and inactivation with merthiolate for 24 hours (Table 1). Virus inactivation was confirmed on a MDCK cell culture.

Recombinant antibody titration was performed by indirect, enhanced light immunosorbent assay (ELISA). The inactivated IAV strains were sorbed at a concentration of 5 µg/mL at 4°C overnight in 50 µL of a 0.1 M carbonate buffer at pH 9.2–9.4 in the wells of a 96-well-plate with high binding capacity (Corning-Costar, Netherlands). FabH A3 mABs conjugated to horseradish peroxidase were used as the secondary antibody for detection.

For Western blot, electrophoretic separation of influenza A virus strain A/Solomon Islands/03/06 in 10%

**Table 1.** Characterization of the viral samples used in the work

| Manufacturer                    | Serotype           | Strain/year of isolation         |
|---------------------------------|--------------------|----------------------------------|
| Hytest Ltd 8IN73                | Influenza A (H1N1) | A/Taiwan/1/86                    |
| Hytest Ltd 8IN73-2              | Influenza A (H1N1) | A/Beijing/262/95                 |
| Hytest Ltd 8IN73-3              | Influenza A (H1N1) | A/New Caledonia/20/99            |
| Hytest Ltd 8IN73-4              | Influenza A (H1N1) | A/Solomon Islands/03/06          |
| Research Institute of Influenza | Influenza A (H1N1) | A/California/07/09               |
| Hytest Ltd 8IN74                | Influenza A (H3N2) | A/Samara/222/99=A/Shangdong/9/93 |
| Hytest Ltd 8IN74-1              | Influenza A (H3N2) | A/Panama/2007/99                 |
| Hytest Ltd 8IN74-2              | Influenza A (H3N2) | A/Kiev/301/94                    |
| Hytest Ltd 8IN74-3              | Influenza A (H3N2) | A/Wisconsin/67/05                |
| Hytest Ltd 8IN74-4              | Influenza A (H3N2) | A/Brisbane/10/07                 |
| Research Institute of Influenza | Influenza A (H3N2) | A/Sydney/5/97                    |
| Hytest Ltd 8IN75-2              | Influenza B        | B/Tokio/53/99                    |

polyacrylamide gel upon non-reducing conditions was performed. Electrophoretic transfer (electroblotting) of proteins from the gel to the nitrocellulose membrane S045A330R (Advantec MFS, Inc., USA) was conducted. Transferred proteins were detected on the nitrocellulose membrane by indirect ELISA. The membrane was blocked with a 5% casein solution for 1 h at room temperature on a shaker, rinsed three times with PBS-T (10 mM  $K_2HPO_4$ , pH 7.5, 0.145 M NaCl, 0.1% Tween 20), and incubated for 1 h on a shaker at room temperature. After three times rinsing, the membrane was incubated with a solution of corresponding recombinant antibodies at a concentration of 1  $\mu$ g/mL in a phosphate-salt buffer for 1 h at 37°C. After three times rinsing with PBS-T, the membrane was incubated with FabH A3 mABs conjugated to horseradish peroxidase for 1 h at 37°C. Western blots were stained by adding a substrate (3,3-diaminobenzidine, 4-chlorine-1-naphthol and hydrogen peroxide).

$K_d$  of the antigen-antibody complex was estimated according to Friguier et al. [16]. At the first stage, mABs at a constant concentration of 1 nM (150 ng/mL) were incubated with an inactivated antigen of the influenza A(H1N1)/Solomon Islands/03/06 strain in a concentration range of 0.1–10 nM (10–1000 ng/mL) for 2 h at room temperature with constant stirring on a shaker to achieve a thermodynamic equilibrium in a three-component system: free antigen, free antibody, and an antigen-antibody complex. At the second stage, the concentrations of free antibodies were measured by solid-phase ELISA with an antigen immobilized on the wellplate. At the final stage, the  $K_d$  value was estimated using the Klotz equation [17] from the values of the total antigen concentration and free recombinant antibody concentration.

## RESULTS AND DISCUSSION

Recombinant immunoglobulins were generated using nucleotide sequences encoding the variable domains of the heavy FI6VHv3 and light FI6VKv2 chains of a broad-spectrum neutralizing antibody FI6 [8]. Such modified sequences differ from the sequences encoding the heavy and light chains of immunoglobulin FI6 by the fact that they contain less somatic mutations and correspond more to the variable domain germ-line sequences of human immunoglobulin.

Recombinant IgA1- and IgA2m1-isotype antibodies were obtained to study the ability of the FI6 antibody to interact with IAV of IgA-isotype. The IgG1-isotype antibody FI6 was obtained as a positive control.

Human immunoglobulin A comes in two isotypes – IgA1 and IgA2. IgA1 dominates in the serum, while the proportion of IgA2 is higher in secretions [18]. The most significant structural differences between these

isotypes are associated with the hinge region. IgA1 has a 13-amino-acid-longer hinge than IgA2, resulting in more flexible antigen-binding sites for the IgA1-isotype antibodies. This advantage renders IgA1 more susceptible to proteolytic cleavage at the hinge region compared to IgA2 [12]. IgA2-isotype antibody comes in two allotypes: IgA2m1 and IgA2m2, which differ in the number of glycosylation sites and, most significantly, the location of inter-chain disulfide bonds [19, 20]. IgA2m1 lacks disulfide bonds between the constant domain of the light chain and the constant domain of the heavy chain (CH1), which are typical for the structure of immunoglobulins. In this case, the disulfide bond forms between the constant domains of light chains and the interaction between the light and heavy chain is non-covalent.

For the expression of recombinant antibodies in CHO cells, we had previously developed a bi-promoter vector which was effective in producing antibodies. This expression vector contains two transcription units, and pCMV and hEF1-HTLV promoters that control the transcription of heavy and light antibody chains in one plasmid. The plasmid also contains the dihydrofolate reductase gene (*DHFR*), which is translated with an independent ribosomal binding site. During amplification of the *DHFR* gene copies in the chromosome of producer lines by means of methotrexate (MTX) selective pressure, this vector allows simultaneous increase in the light- and heavy-chain gene copy numbers. Three expression plasmids different in the constant domains of immunoglobulin heavy chains were obtained (*Fig. 1*).

Stable cell lines based on CHO DG44 cells were generated for the production of recombinant immunoglobulins. Recombinant IgG and IgA antibodies were isolated from a serum-free culture medium. After affinity chromatography, recombinant IgG and IgA-isotype antibodies were analyzed using polyacrylamide gel electrophoresis upon reducing and non-reducing conditions (*Fig. 2*).

An analysis of gel electrophoresis showed that the size of the detected protein fragments reflects the features of the location of inter-chain disulfide bonds in each of the studied isotopes. Thus, two bands corresponding to the light and heavy chains of the immunoglobulins appear on the electrophoregrams of IgG- and IgA1-isotype antibodies upon reducing conditions. The IgA2m1-isotype antibody was found to have a unique location of the inter-chain disulfide bonds characteristic of this isotype. As mentioned previously, IgA2m1-isotype antibodies lack an inter-chain disulfide bond between the constant domain of the light chain and the CH1-domain of the heavy chain, which is common to most immunoglobulins. Herewith, the constant domains of the light chains are interconnected by a di-

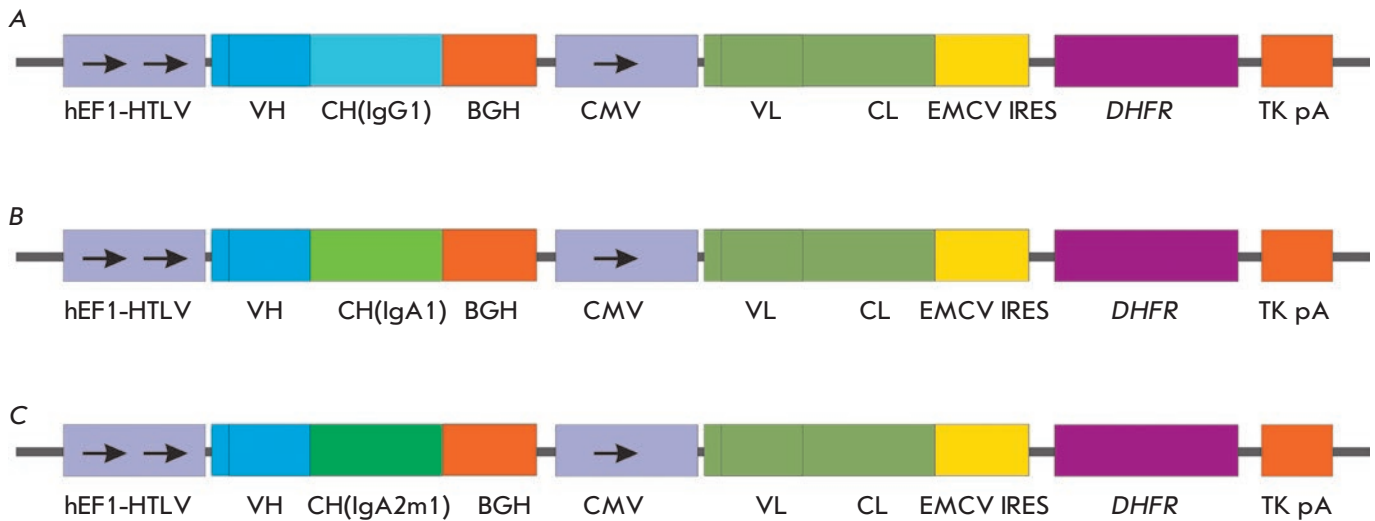


**Fig. 1.** Expression cassettes of bi-promotor plasmids for the production of FI6 antibodies of different isotypes. A. Plasmid pBiPr-ABlgG1FI6. B. Plasmid pBiPr-ABlgA1FI6. C. Plasmid pBiPr-ABlgA2m1FI6. hEF1-HTLV – hybrid promoter from plasmid pMG, combining the promoter of an elongation factor EF-1a and 5'-untranslated region of the human T-cell leukemia virus HTLV; VH – variable domain of an antibody heavy chain; CH(IgG1), CH(IgA1), CH(IgA2m1) – constant domains of human immunoglobulin heavy chains of IgG1-, IgA1-, IgA2m1-isotypes, respectively; BGH – polyadenylation site BGH; CMV – promoter/enhancer of early genes of human cytomegalovirus; VL – variable domain of an antibody light chain; CL – constant domain of an antibody light chain; EMCV IRES – internal ribosome entry site (IRES) of the encephalomyocarditis virus; DHFR – dihydrofolate reductase gene; TK pA – herpes virus thymidine kinase polyadenylation signal.

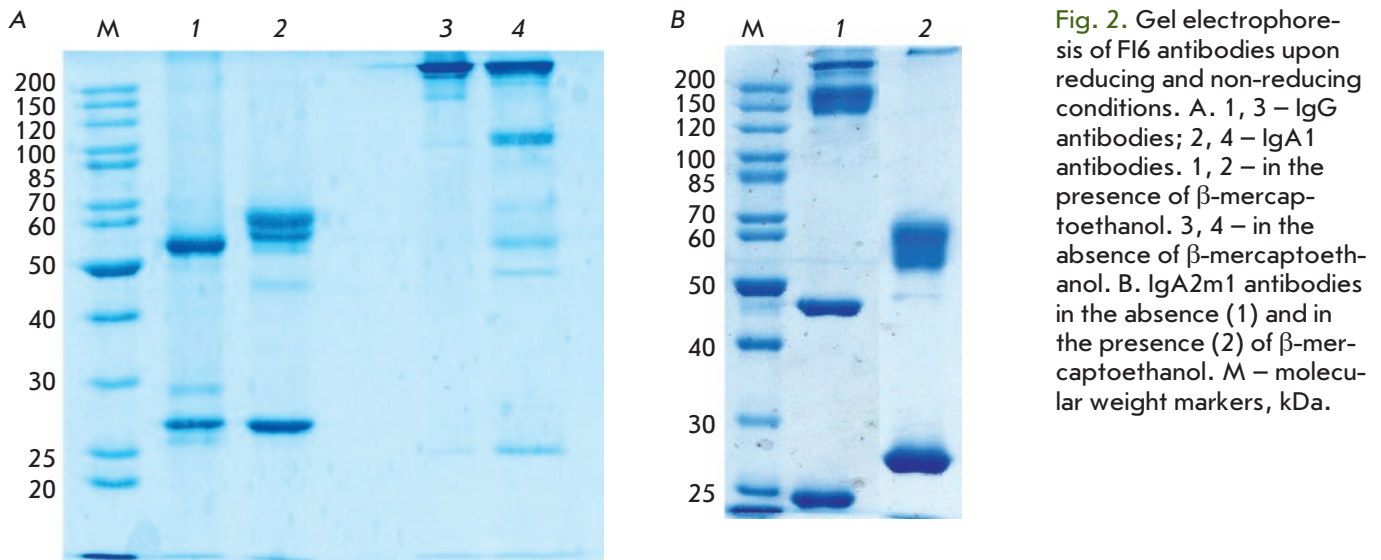


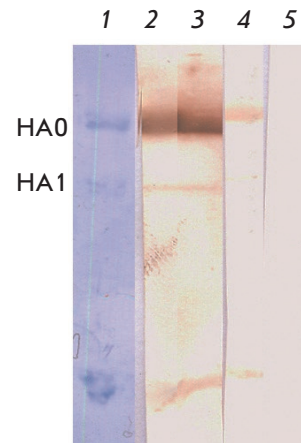
**Fig. 2.** Gel electrophoresis of FI6 antibodies upon reducing and non-reducing conditions. A. 1, 3 – IgG antibodies; 2, 4 – IgA1 antibodies. 1, 2 – in the presence of β-mercaptoethanol. 3, 4 – in the absence of β-mercaptoethanol. B. IgA2m1 antibodies in the absence (1) and in the presence (2) of β-mercaptoethanol. M – molecular weight markers, kDa.

sulfide bond. Dimers of the light (~46 kDa) and heavy chains (~105 kDa) are found on gel electrophoregrams (Fig. 2B) upon non-reducing conditions.

The antigen-binding activity of the recombinant proteins was studied by Western blotting with an inactivated A/Solomon Islands/03/06 H1N1 influenza strain (Fig. 3).

Western blot data confirm the ability of the recombinant antibodies to recognize the native hemagglutinin of IAV. Western blotting confirmed previous results on the Fab-fragment of the FI6 IgG1-isotype antibody [13] indicating that antibody FI6 can interact with both whole HA0 hemagglutinin and the HA1 and HA2 fragments formed during hydrolysis of the whole protein in

**Fig. 3.** Western blot of FI6 recombinant antibodies with the proteins of the influenza A virus, strain A/Solomon Islands/03/06 (H1N1). Lane 1. Influenza A virus proteins before transfer to a membrane. Lane 2. Western blot with FI6 IgG1 antibodies. Lane 3. Western blot with FI6 IgA1 antibodies. Lane 4. Western blot with FI6 IgA2m1 antibodies. Lane 5. Conjugate control (Western blot in the absence of recombinant antibodies).



gel electrophoresis upon reducing conditions [21]. These results are consistent with the data of FI6 antibody epitope mapping presented in [8]. The broad specificity of FI6 antibody occurs because that FI6 targets a conserved epitope in the F-subdomain of hemagglutinin located between the H1 and H2 domains. Herein, the heavy chain of the antibody interacts with the H1 domain and the light chain – with the alpha helix from the H2 domain.

The ability of IgA-isotype antibodies to interact with different IAV subtypes was of interest. IgA1- and IgA2m1-isotype antibodies were compared by indirect ELISA using various inactivated H1N1 and H3N2 subtype influenza A strains immobilized in solid phase.

The immunochemical analysis (*Figs. 4 and 5*) indicates that recombinant IgA1- and IgA2m1-isotype antibodies recognize the strains of both isotypes from different phylogenetic groups. The affinity of recombinant IgA1- and IgA2m1-isotype antibodies to some strains of the investigated subtypes is different. The greatest difference is observed for strains of the H3N2 subtype; the intensity of H3N2 interaction with the IgA2m1-isotope antibodies is much lower than that with IgA1-isotype antibodies.

Our data agree with the data [8] showing that FI6 antibodies recognize 16 subtypes of IAV and exert different binding strengths on different virus subtypes.

For the three obtained recombinant antibodies, the dissociation constants of the antigen–antibody complex were estimated for the A(H1N1)/Solomon Islands/03/06 influenza strain antigen (*Table 2*).

The  $K_d$  values of the recombinant IgA1 and IgA2m1 antibodies differ considerably (4 times). Herewith, the  $K_d$  value of IgA1 is even slightly lower than that of IgG1, which indicates a greater binding strength and is probably caused by the greater flexibility of the antigen-binding sites of the variable domains associ-

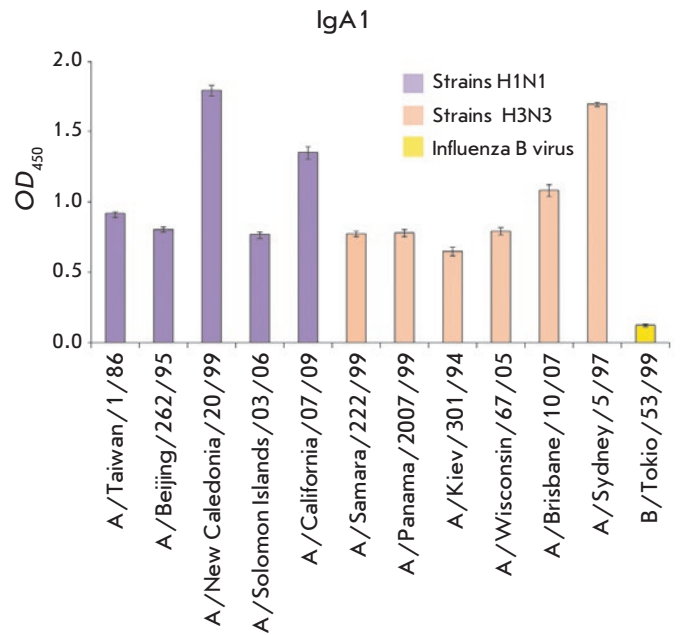


**Fig. 4.** Indirect ELISA of the interaction of influenza A strains of H1N1 and H3N2 subtypes with recombinant FI6 antibodies of IgA1 isotype.

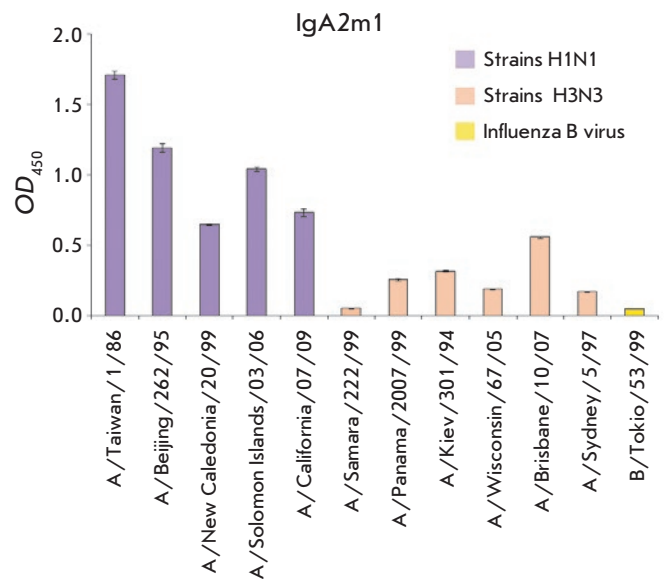


**Fig. 5.** Indirect ELISA of the interaction of influenza A strains of H1N1 and H3N2 subtypes with recombinant FI6 antibodies of IgA2m1 isotype.

**Table 2.** Comparison of  $K_d$  values for FI6 recombinant antibodies of IgG and IgA isotypes

| Antibody | $K_d$ , nM |
|----------|------------|
| IgG1     | 1.2–1.8    |
| IgA1     | 0.7–1.5    |
| IgA2m1   | 3.3–3.9    |

ated with the unique IgA1 hinge site structure. Overall, our study shows that production of the IgA isotype FI6 antibody does not deteriorate its antigen-binding properties. It is noted that retaining high degrees of antigen-binding and neutralizing properties when reformatting an antibody isotype is not an obvious result as indicated by the data in [22]. It was shown that the chimeric (mouse-human) antibody 9F4 of IgA1 isotype to H5N1 subtype hemagglutinin exerts a lower neutralizing activity compared to parental mouse antibody and the chimeric version of the IgG-isotype.

## CONCLUSION

Recombinant monomer antibodies of IgA1- and IgA2m1-isotypes on the basis of variable domains of the broad-spectrum antibody FI6 to influenza A virus hemagglutinin were obtained. These antibodies recognize 10 relic and current IAV strains in indirect ELISA and

are characterized by a  $K_d$  value of the antigen-antibody complex no higher than 4 nM. The affinity of the studied antibody samples to the IAV strains of the H1N1 subtype is higher than the affinity to the H3N2 subtype strain. Our data show that production of antibody FI6 of monomer IgA form does not change its antigen-binding properties, which is an important prerequisite for the use of IgA-isotype antibodies for therapeutic purposes. ●

*This study was supported by the Ministry of Education and Science of the Russian Federation (No. 14.607.21.0060) within the framework of a Federal Program "Research and Developments for Priority Areas of the Development of Scientific and Technological Complex in Russia for 2014–2020 years" (unique project identification RFMEFI60714X0060)*

## REFERENCES

- Gerhard W. // *Curr. Top. Microbiol. Immunol.* 2001. V. 260. P. 171–190.
- Lachmann P. // *Emerging Microbes Infections.* 2012. V. 1. e11; doi: 10.1038/emi.2012.2
- Throsby M., van den Brink E., Jongeneelen M., Poon L.L., Alard P., Cornelissen L., Bakker A., Cox F., van Deventer E., Guan Y., et al. // *PLoS One.* 2008. V. 3. e3942.
- Sui J., Hwang W.C., Perez S., Wei G., Aird D., Chen L.M., Santelli E., Stec B., Cadwell G., Ali M., et al. // *Nat. Struct. Mol. Biol.* 2009. V. 16. P. 265–273.
- Friesen R.H., Koudstaal W., Koldijk M.H., Weverling G.J., Brakenhoff J.P., Lenting P.J., Stittelaar K.J., Osterhaus A.D., Kompier R., Goudsmit J. // *PLoS One.* 2010. V. 5. e9106.
- Wrammert J., Koutsonanos D., Li G.M., Edupuganti S., Sui J., Morrissey M., McCausland M., Skountzou I., Hornig M., Lipkin W.I., et al. // *J. Exp. Med.* 2011. V. 208. № 1. P. 181–193.
- Grandea A.G., Olsen O.A., Cox T.C., Renshaw M., Hammond P.W., Chan-Hui P.Y., Mitcham J.L., Cieplak W., Stewart S.M., Grantham M.L., et al. // *Proc. Natl. Acad. Sci. USA.* 2010. V. 107. № 28. P. 12658–12663.
- Corti D., Voss J., Gamblin S.J., Codoni G., Macagno A., Jarrossay D., Vachieri S.G., Pinna D., Minola A., Vanzetta F., et al. // *Science.* 2011. V. 333. № 6044. P. 850–856.
- Tamura S., Kurata T. // *Jpn J. Infect. Dis.* 2004. V. 57. № 6. P. 236–247.
- Weltzin R., Monath T.P. // *Clin. Microbiol. Rev.* 1999. V. 12. № 3. P. 383–393.
- Jianqiang Y., Hongxia S., Perez D.R. // *Immunotherapy.* 2012. V. 4. № 2. P. 175–186.
- Bakema J.E., van Egmond M. // *MAbs.* 2011. V. 3. № 4. P. 352–361.
- Aliev T.K., Dement'yeva I.G., Toporova V.A., Bokov M.N., Pozdnyakova L.P., Rybchenko V.S., Dolgikh D.A., Sveshnikov P.G., Kirpichnikov M.P. // *Mocow Univ. Biol. Sci. Bull.* 2016. № 2. P. 25–31.
- Aliev T.K., Balabashin D.S., Dolgikh D.A., Kirpichnikov M.P., Panina A.A., Toporova V.A. Patent of the Russian Federation № 2555533. 2015.
- Kavran J.M., Leahy D.J. // *Methods Enzymol.* 2014. V. 541. P. 27–34.
- Friguet B., Chaffotte A.F., Djavadi-Ohanian L., Goldberg M.E. // *J. Immunol. Methods.* 1985. V. 77 (2). P. 305–319.
- Klotz I.M. // *Arch. Biochem.* 1946. V. 9. P. 109–117.
- Delacroix D.L., Dive C., Rambaud J.C., Vaerman J.P. // *Immunology.* 1982. V. 47. № 2. P. 383–385.
- Tomana M., Niedermeier W., Mestecky J., Skvaril F. // *Immunochemistry.* 1976. V. 13. № 4. P. 325–328.
- Chintalacheruvu K.R., Raines M., Morrison S.L. // *J. Immunol.* 1994. V. 152. № 11. P. 5299–5304.
- Feshchenko E., Rhodes D.G., Felberbaum R., McPherson C., Rininger J.A., Post P., Cox M.M.J. // *BMC Biotechnology.* 2012. 12:77 <http://www.biomedcentral.com/1472-6750/12/77>.
- Mak T.-M., Hanson B.J., Tan Y.-J. // *Antiviral Res.* 2014. V. 107. P. 76–83.

# Cognitive Tagging of Neurons: CRE-Mediated Genetic Labeling and Characterization of the Cells Involved in Learning and Memory

O. I. Ivashkina<sup>1,2</sup>, N. S. Vorobyeva<sup>1</sup>, A. M. Gruzdeva<sup>1</sup>, M. A. Roshchina<sup>3</sup>, K. A. Toropova<sup>1,2</sup>, K. V. Anokhin<sup>1,2,4\*</sup>

<sup>1</sup>Department of Neuroscience, National Research Center "Kurchatov Institute", Akademika Kurchatova pl. 1, Moscow, 123182, Russia

<sup>2</sup>Center for Neural and Cognitive Sciences, Lomonosov Moscow State University, Leninskie Gory 1, bldg. 27, Moscow, 119991, Russia

<sup>3</sup>Institute of Higher Nervous Activity and Neurophysiology of RAS, Butlerova Str. 5A, Moscow, 117485, Russia

<sup>4</sup>Laboratory for Neurobiology of Memory, P.K. Anokhin Institute of Normal Physiology, Baltiyskaya Str. 8, Moscow, 125315, Russia

\*E-mail: k.anokhin@gmail.com

Received November 27, 2017; in final form March 26, 2018

Copyright © 2018 Park-media, Ltd. This is an open access article distributed under the Creative Commons Attribution License, which permits unrestricted use, distribution, and reproduction in any medium, provided the original work is properly cited.

**ABSTRACT** In this study, we describe use of Cre-mediated recombination to obtain a permanent genetic labeling of the brain neuronal networks activated during a new experience in animals. This method utilizes bitransgenic Fos-Cre-eGFP mice in which a green fluorescent protein is expressed upon tamoxifen-induced Cre-recombination only in the cells where immediate early gene *c-fos* expression takes place due to the new experience. We used the classical fear conditioning model to show that *ex vivo* microscopy of the eGFP protein in Fos-Cre-eGFP mice enables mapping of the neurons of the various brain regions that undergo Cre-recombination during acquisition of a new experience. We exposed the animals to the new environment in brief sessions and demonstrated that double immunohistochemical staining enables a characterization of the types of neocortical and hippocampal neurons that undergo experience-dependent Cre-recombination. Notably, Fos-Cre-eGFP-labeled cells appeared to belong to excitatory pyramidal neurons rather than to various types of inhibitory neurons. We also showed that a combination of genetic Cre-eGFP labeling with immunohistochemical staining of the endogenous c-Fos protein allows one to identify and compare the neuronal populations that are activated during two different episodes of new experiences in the same animal. This new approach can be used in a wide spectrum of tasks that require imaging and a comparative analysis of cognitive neuronal networks.

**KEYWORDS** brain, neuronal networks, learning, immediate early genes, Cre-recombination, genetic labeling of neurons.

**ABBREVIATIONS** eGFP – enhanced green fluorescent protein; GFAP – glial fibrillary acidic protein; NeuN – neuronal nuclei; CaMKII – Ca<sup>2+</sup>/calmodulin-dependent protein kinase II; SOM – somatostatin; NPY – neuropeptide Y; PV – parvalbumin; IEGs – immediate early genes; PCR – polymerase chain reaction; FC – fear conditioning; FS – footshock.

## INTRODUCTION

The study of the mechanisms of formation and functioning of the neural networks involved in cognitive functions is one of the most important aspects of modern neuroscience. The development of new experimental methods for cell-resolution visualization of the neural substrates of cognitive processes throughout the whole brain plays a key role in addressing these problems.

Detection of immediate early gene expression is a classical method used to identify the neuronal populations involved in various types of cognitive activity in animals [1–3]. IEG is a family of genes that are rapidly activated in the cell through intracellular signaling cascades in response to certain external influences. This family includes genes that encode transcription factors, structural synaptic proteins, cytoplasmic enzymes, etc. [4]. Expression of some IEGs, for example *c-fos*, *zif268*

and *arc*, is induced in animals through a new experience and plays a key role in plastic rearrangements and the formation of long-term memory, storing the individual experience [1, 3, 5, 6]. These properties of IEGs form the basis for the methods of immunohistochemical and *in situ* hybridization mapping of the brain, which make it possible to identify the cognitive neural networks activated during learning [2, 7–9].

However, identification of IEG products using immunohistochemistry or *in situ* hybridization is laborious and limited to a narrow time window after cognitive exposure. Visualization of the populations of cognitively active neurons using expression of fluorescent protein genes controlled by IEG promoters is a promising way to address some of these problems. The use of controlled transgenic systems makes it possible to obtain mice in which the fluorescent protein is synthesized only in those neurons where IEG, for example *c-fos*, was expressed at a certain time [10]. In recent years, these technologies have become increasingly widespread. However, they suffer from a significant limitation: labeling of the population of cognitively active neurons is limited by the lifetime of the fluorescent protein.

Permanent genetic labelling of the population of neurons involved in a certain cognitive task may be a solution to this problem. The system of site-specific recombinases widely used in neurobiology [11–13], in particular the one with modified Cre-recombinase of P1 bacteriophage, which is bound to the mutant ligand-binding domain of the estrogen receptor, can be used for this purpose [14, 15]. Cre-recombinase recognizes homotypic loxP sites and excises the DNA flanked by these sites in the presence of tamoxifen, a synthetic estrogen antagonist. LoxP sites usually flank the STOP codon located before the reporter gene sequence that encodes the fluorescent protein (GFP, tdTomato, etc.),  $\beta$ -galactosidase, or channelrhodopsin [13, 16]. At present, dozens of transgenic mouse strains have been developed where Cre-recombinase is selectively expressed in different tissues or different cell types; for example, in certain types of interneurons [17] or at certain stages of neuronal progenitor development [13]. Thus, the technology of genetic labelling of neurons with Cre-recombinase is currently well developed, but it is primarily used for anatomical mapping of the nervous system or for embryonic research.

The work of Guenther et al. [18], who developed transgenic mice lines expressing Cre-recombinase under the control of the IEG promoters *c-fos* and *arc*, was a methodological innovation. Cross-breeding of Fos-Cre or Arc-Cre mice with reporter mice carrying the red fluorescent protein tdTomato for the first time provided permanent genetic labeling of neurons with activated IEGs [18].

We generated double transgenic Fos-Cre-eGFP mice which were used in this work to investigate the morphological and molecular phenotype of the neurons of various brain structures undergoing Cre-recombination when animals acquire a new experience. We also tested for the first time the possibility of using Fos-Cre-eGFP transgenic mice to label and compare two populations of neurons activated in the same animal in two different situations when gaining new experience.

## EXPERIMENTAL

### Preparation of bitransgenic Fos-Cre-eGFP mice

B6.129(Cg)-Fostm1.1(cre/ERT2)Luo/J transgenic mice (The Jackson Laboratory, stock Number: 021882) bearing Cre-recombinase under the *c-fos* promoter were interbred with TG(CAG-Bgeo/GFP)21Lbe/J mice (The Jackson Laboratory, Stock No. 003920) carrying the enhanced green fluorescent protein gene eGFP under loxP sites in order to produce Fos-Cre-eGFP mice. The mice were managed in individually ventilated cells, five animals per cell, with water and food ad libitum and a light cycle of 12/12 h. All experiments were carried out in accordance with the requirements of Order No. 267 of the Ministry of Health of the Russian Federation (19.06.2003) and also with the directive of the local ethical Committee on Biomedical Research of the Research Center of the Kurchatov Institute (Protocol No. 1 of 09/07/2015).

### Genotyping

The transgene was in a heterozygous state in both parental lines, and, therefore, genotyping for each transgene was used to identify bitransgenic animals. Tissue samples were collected from mice at the age of two months, and DNA was isolated by lysing with a proteinase K solution (Sigma) in 1% SDS buffer (Helicon), followed by precipitation with 96% ethanol. The DNA precipitate was dissolved in a TE buffer. The resulting DNA was used for a polymerase chain reaction (PCR) with primers to Cre-recombinase and eGFP in a ScreenMix medium (ZAO Eurogen). The following primers were used: for Cre – CACCAGTGTCTACCCCTGGA (common forward sequence for the wild type and transgene), CGGCTACACAAAGC-CAAAC (reverse wild-type sequence), CGCGCCTGAAGATATAGAAGA (reverse transgene sequence); for GFP – TGGACGGCGACGTAAACGGC (first transgene sequence), GGCGGTCACGAACTCCAGCA (second transgene sequence), CTAGGCCACAGAATTGAAAGATCT (forward sequence of the internal positive control), GTAGGTGGAAATTCTAGCATCATCC (reverse sequence of the internal positive control). PCR conditions are shown in *table*. PCR products were de-

tected in 2.5% agarose gel in a TAE buffer with ethidium bromide.

### Induction of Cre-recombination with tamoxifen

A single intraperitoneal injection of tamoxifen (Sigma) dissolved in corn oil (Sigma) was used at a dose of 150 mg/kg to induce Cre-recombination as previously described [18]. For experience-induced Cre-recombination, tamoxifen was injected 24 hours before the animal gained a new experience.

### Context exploration

For new context exploration, the mice were placed in an experimental chamber for 5 minutes and allowed to freely explore it. It is known that such an exploration leads to the formation of long-term memory in animals [19].

Two contexts were used in this work. Context A was a chamber illuminated with diffused white light (average illumination level 87 lux) size 20 × 30 × 20 cm and equipped with an electrode floor; the noise level in the chamber was 7 dB. The chamber was wiped with a 40% solution of ethyl alcohol before placing each animal in it. Context B was a chamber size 20 × 15 × 20 cm with an electrode floor; the camera was illuminated only with a near-infrared light source, which is invisible to mice; the noise level in the chamber was 25 dB. The chamber was wiped with a 3% acetic acid solution before placing each animal in it.

### Immediate footshock

Footshock (FS) was applied 3 days after the exploration of context A. For this purpose, the mice were

placed in context A or context B and immediately administered FS with an intensity of 1 mA and duration of 2 seconds and then immediately returned to their home cage.

### Fear conditioning (FC) training

For the purpose of FC training, the mice were placed in context A, followed by a sound signal (90 dB, 5 kHz) lasting 30 s for 120 seconds. The last 2 seconds of sound were combined with a 1 mA FS. The mice were returned to their home cage 30 seconds after the end of the FC.

### Experimental groups

Two groups of animals were used to evaluate the baseline and experience-induced eGFP expression: “Learning” group animals ( $n = 4$ ) were fear-conditioned as described above; “control” group mice ( $n = 4$ ) stayed in their home cages and were not exposed to any influences.

The animals that explored context A for 5 min ( $n = 5$ ) were taken to determine the phenotype of the cells undergoing experience-dependent Cre-recombination.

The A - A + FS ( $n = 5$ ) and A - B + FS ( $n = 5$ ) groups were used to identify two populations of cognitively active neurons in one brain. A - A + FS group mice explored context A and then received immediate FS for 3 days in the same context; A - B + FS group mice explored context B and then received immediate FS for 3 days in context B.

### Brain sample harvesting and preparation of floating sections

Mouse brain samples were obtained 3 days after the animals had been exposed to a new experience which was accompanied by Cre-recombination. In the experiments aimed at identifying two populations of active neurons, mouse brain samples were collected 90 minutes after the second cognitive episode (FS application).

Mice were anesthetized by intraperitoneal injection of 15% chloral hydrate in saline, followed by intracardial perfusion with phosphate buffer and a 4% paraformaldehyde solution in phosphate buffer and brain harvesting. The resulting brain samples were post-fixed with a 4% paraformaldehyde solution in phosphate buffer: 2 h at room temperature and 14–18 h at +4°C. After that, the samples were placed in a phosphate buffer for 2 hours and 50- $\mu$ m thick frontal sections of the brain were prepared using a Leica VT1200S (Leica) vibratome. Sections were taken at a distance of +2.46 and -1.34 mm from the bregma. The coordinates of the sections were determined using a stereotactic mouse brain atlas [20].

### PCR conditions for genotyping

| Step | Temperature, °C | Time  | Remark                                     |
|------|-----------------|-------|--|
| 1    | 94              | 2 min |  |
| 2    | 94              | 20 s  |  |
| 3    | 65              | 15 s  | Decrease in temperature by 0.5°C per cycle |
| 4    | 68              | 10 s  |  |
| 5    |                 |       | Repeating steps 2 to 4 for 10 cycles       |
| 6    | 94              | 15 s  |  |
| 7    | 60              | 15 s  |  |
| 8    | 72              | 10 s  |  |
| 9    |                 |       | Repeating steps 6 to 8 for 28 cycles       |
| 10   | 72              | 2 min |  |
| 11   | 10              |       | Stop                                       |

### Detection of the fluorescent protein eGFP and double immunohistochemical staining

The cells subjected to Cre-recombination in the experiments aimed at determining the baseline and experience-induced eGFP expression were detected based on intrinsic fluorescence of the eGFP protein. The prepared brain sections were placed under cover glass using the Fluoromount™ Aqueous Mounting Medium (Sigma-Aldrich) and digitized as described below.

In the experiments aimed at determining the phenotype and proportion of cells undergoing experience-induced Cre-recombination, as well as the identification of two populations of cognitively active neurons, Cre-recombined cells were detected using immunohistochemistry based on eGFP protein staining. Brain sections were subjected to the permeabilization procedure in a 1% Triton-X100 solution (Sigma) in the phosphate buffer with 5% normal donkey serum (Sigma) and 5% normal goat serum (Abcam) for 60 min, followed by triple washing with a 0.2% Triton-X100 solution in phosphate buffer for 5 minutes and incubation with primary antibodies for 18 hours at +4°C. The following primary antibodies were used in different reactions to identify various markers: eGFP (Rabbit Anti-GFP Antibody, Life Technologies, 1:250 dilution), eGFP (Chicken Anti-GFP Antibody, Aves Labs, 1:500 dilution), c-Fos Goat Anti-c-Fos Antibody (Santa Cruz Biotechnology, 1:150 dilution), GFAP (Chicken Anti-GFAP Antibody, Abcam, 1:500 dilution), NeuN (Mouse Anti-NeuN Antibody, EMD Millipore, 1:500 dilution), CaMKII (Mouse Anti-CaMKII Antibody, EMD Millipore, 1:200 dilution), SOM (Rabbit Anti-Somatostatin Antibody, Santa Cruz Biotechnology, 1:1000 dilution), NPY (Rabbit Anti-Neuropeptide Y Antibody, Novus Biologicals; 1:10000 dilution), and PV (Rabbit Anti-Parvalbumin Antibody, Abcam; 1:10000 dilution). At the end of the incubation, the sections were washed with a 0.2% Triton-X100 solution in phosphate buffer 3 times for 5 minutes. The sections were then incubated with secondary antibodies for 2 hours at room temperature in the dark. The following secondary antibodies were used in different reactions: AlexaFluor® 488 Donkey Anti-Goat Antibody (Life Technologies, 1:500 dilution), AlexaFluor® 488 Goat Anti-Chicken Antibody (Life Technologies, 1:500 dilution), AlexaFluor® 568 Donkey Anti-Rabbit Antibody (Life Technologies, 1:500 dilution), AlexaFluor® 568 Goat Anti-Chicken Antibody (Life Technologies, 1:500 dilution), or AlexaFluor® 568 Donkey Anti-Mouse Antibody (Life Technologies, 1:500 dilution). After incubation with secondary antibodies, sections were washed 3 times for 5 minutes in a 0.2% Triton-X100 solution in phosphate

buffer. After the end of staining, the sections were placed under the cover glass using the Fluoromount™ Aqueous Mounting Medium (Sigma-Aldrich). The sections were digitized on a confocal microscope Olympus FV1000BW61WI (Olympus) with ×20 magnification. Each brain section was used to produce 10–13 optical sections with 5 μm increments along the Z axis.

### Counting of eGFP-positive cells and colocalization analysis

The resulting images were processed, and further analysis was carried out using the Imaris 7.1.0 software (Bitplane). Since eGFP staining is cytoplasmic and involves not only the bodies but also the processes of the cells, the automated counting of eGFP-positive neurons is complicated. Because of this, eGFP-positive cells were marked manually and then counted automatically. NeuN and c-Fos staining is nuclear, and, therefore, automated marking and counting of NeuN-positive and c-Fos-positive cells was used based on the size and threshold level of red-channel color intensity. In the case of eGFP, NeuN, and c-Fos staining, all positive cells whose soma was fully located within the slice along the Z axis were counted; the cells whose soma was located on the upper and lower boundaries of brain sections along the Z axis were not counted. Expert evaluation of eGFP colocalization with NeuN or c-Fos was carried out in three projections for each cell. The cells whose NeuN- or c-Fos-positive nucleus was completely surrounded with eGFP-stained cytoplasm were considered as double positive. Double-positive cells were marked manually and then counted automatically. Positive cells were counted over the entire area of the frontal associative cortex on the brain slice and, in the case of concomitant staining with NeuN, also separately in the layers 1, 2/3, 5, and 6. The boundaries of the frontal association cortex were determined using a stereotaxic mouse brain atlas [20]. The boundaries of the layers were determined according to the Allen Mouse Brain Atlas, <http://mouse.brain-map.org/static/atlas>. Three sections of the frontal association cortex per animal were analyzed. The results of positive cell counting were averaged for the right and left hemispheres in one section and three sections of one brain.

### Statistical data analysis

Statistical data processing was carried out with the Prism 7 (GraphPad) software package using a two-sample *t*-test, as well as two-way ANOVA variance analysis or ANOVA variance analysis with repeated measurements and the Sidak *t*-test. The significance level was  $p < 0.05$ .

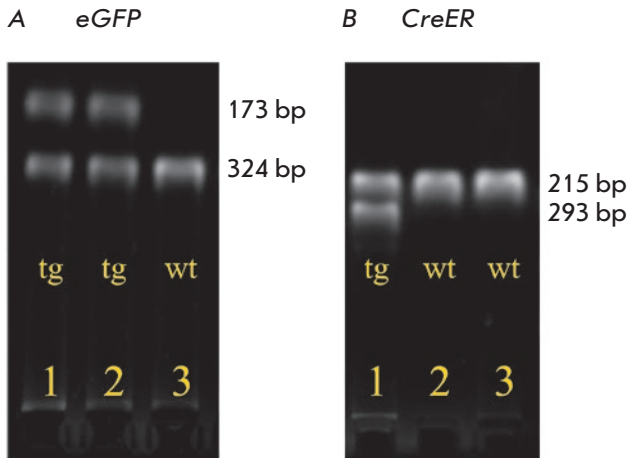


**Fig. 1.** Electrophoretic analysis of PCR products for identification of bitransgenic Fos-Cre-eGFP mice carrying both the eGFP (A) and Cre-recombinase (B) genes. 173 bp – the fragment corresponding to the eGFP transgene; 324 bp – internal positive control; 215 bp – the fragment corresponding to the wild-type Cre-recombinase gene; 293 bp – the fragment corresponding to epy Cre-recombinase transgene; wt – wild-type animal, tg – transgenic animal; 1, 2, 3 – animal number. Only mouse No 1 is bitransgenic.

## RESULTS AND DISCUSSION

### Baseline and experience-induced expression of the green fluorescent protein in the brain of Fos-Cre-eGFP bitransgenic mice

Cross-breeding of B6.129(Cg)-Fostm1.1(cre/ERT2) Luo/J and Tg(CAG-Bgeo/GFP)21Lbe/J mice resulted in offspring which partially consisted of bitransgenic animals simultaneously carrying the Cre-recombinase gene under the *c-fos* promoter and an enhanced fluorescent protein eGFP gene under the loxP-flanked stop signal (Fig. 1). Transgenic mice were injected with tamoxifen, followed by FC training 24 hours after injection (“Learning” group) or left in the home cells (“Control” group) in order to assess the baseline level of Cre-recombination and experience-dependent induction of recombination. In 3 days, eGFP was detected on the mouse brain sections (Fig. 2). The neurons where the green fluorescent protein was detected were the neurons involved in the activation of the *c-fos* gene promoter, followed by Cre-recombination.

“Learning”-group mice showed a large number of eGFP-positive neurons in all the structures specifically related to FC learning [21], namely in the olfactory nu-

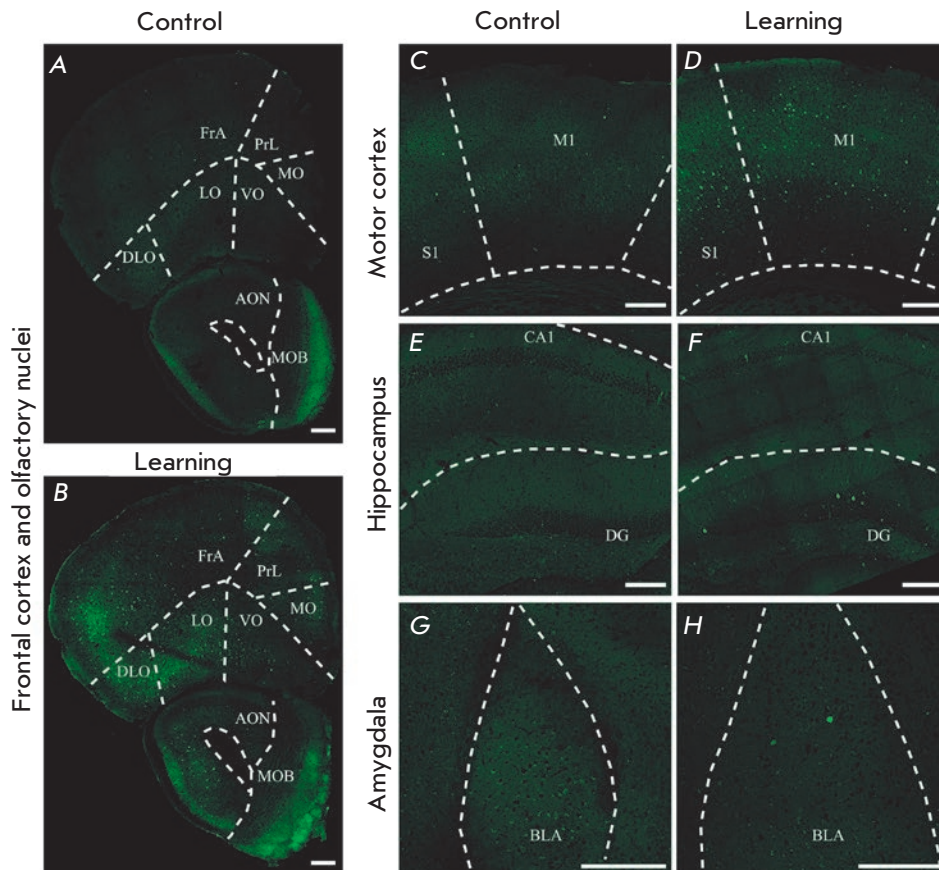


**Fig. 2.** Baseline level of Cre-recombination in the “Control” group naïve mice (A, C, E, G) vs experience-induced Cre-recombination in the “Learning” group of fear-conditioned mice (B, D, F, H). AON – anterior olfactory nucleus; BLA – basolateral amygdala; CA1 – CA1 area of the hippocampus; DG – dentate gyrus of the hippocampus; DLO – dorsolateral orbital cortex; FrA – frontal association cortex; LO – lateral orbital cortex; M1 – primary motor cortex; MO – medial orbital cortex; MOB – main olfactory bulb; PrL – prelimbic cortex; S1 – primary somatosensory cortex; VO – ventral orbital cortex. Scale – 100  $\mu$ m

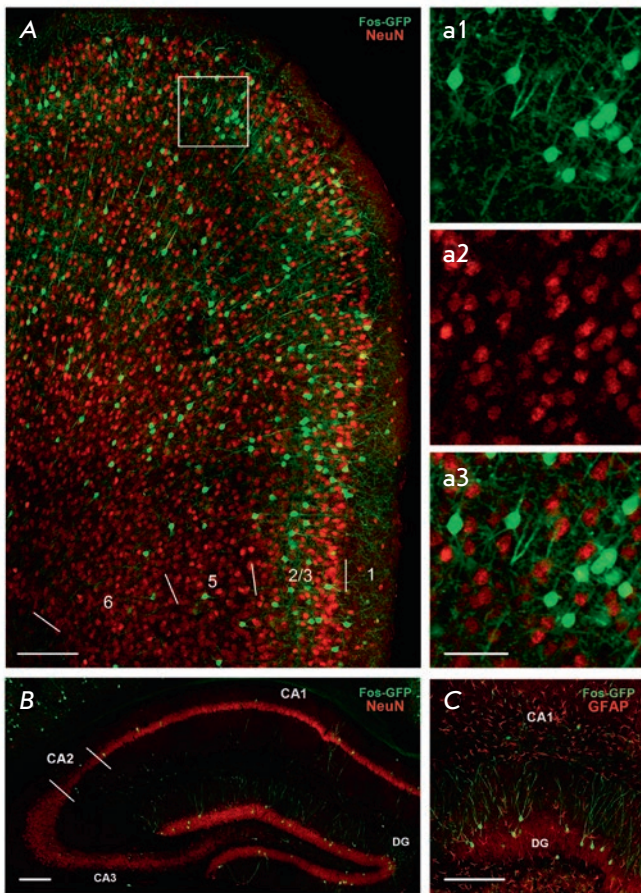


**Fig. 3.** Experience-dependent Cre-recombination takes place only in neurons. Green channel – eGFP. Red channel – NeuN neuronal marker (A, B) or astrocyte marker GFAP (C). A – neocortex (frontal association cortex); B, C – dorsal hippocampus; scale: 150  $\mu$ m. Microphotographs a1, a2, a3 show the area framed in A, separately in channels: a1 – cytoplasmic eGFP staining, a2 – nuclear NeuN staining, a3 – combination of the two; scale: 70  $\mu$ m.

clei, hippocampus, amygdala, ventral thalamus, and in various neocortical areas: frontal association, prelimbic, infralimbic, cingulate, retrosplenial, parietal association, temporal association, entorhinal, somatosensory, auditory, visual, motor, insular, and orbital cortices (Fig. 2B, 2D, 2F, 2H). At the same time, almost no eGFP-positive cells were detected in the aforementioned brain regions in the mice of the control group (Fig. 2A, 2C, 2E, 2G). Rare eGFP-positive cells were detected in the control animals only in some areas of the neocortex: frontal association, dorsolateral, orbital, motor, somatosensory, pyriform, and entorhinal. These results indicate that the method of genetic labeling of active neurons in Fos-Cre-eGFP mice enables successful vis-

ualization of the activation of a widely distributed population of neurons, involving a large number of various brain structures.

### Determining the phenotype of cells undergoing experience-dependent Cre-recombination

In the experiment aimed at determining the type of cells undergoing experience-induced Cre-recombination, mice were injected with tamoxifen and then placed into the new context A. In 3 days, pairs of markers (eGFP and one of the specific cell type markers) were identified.

The NeuN protein, which is localized in the nuclei of virtually all types of neurons in the central nervous system of mammals, except for the Purkinje cells of the cerebellum, mitral cells of the olfactory bulb, and photoreceptor retinal cells, was selected as the marker of mature neurons [22]. The GFAP protein was selected as a cellular marker of astrocytes [23]. In all the examined structures, all eGFP-positive cells were also NeuN-positive (Fig. 3A, B); there were no cases of eGFP colocalization with the GFAP protein (Fig. 3B).

Brain neurons can be classified as excitatory (pyramidal) and inhibitory (interneurons). CaMKII may be used as a marker of excitatory neurons. This enzyme is involved in the functions of excitatory synapses and is never synthesized in GABAergic interneurons [24]. Interneurons are highly variable in their morphological, electrophysiological, and biochemical properties, and, therefore, they are classified into several different types, for example, based on the synthesis of specific biochemical markers: PV, SOM, and NPY [25]. We evaluated colocalization of the eGFP protein and the marker of excitatory pyramidal neurons CaMKII or one of the markers of inhibitory interneurons (PV, SOM, and NPY) to determine which neuronal type corresponds to the cells that undergo Cre-recombination.

We found no colocalization of eGFP with any of the interneuron markers (Fig. 4–6). At the same time, eGFP-positive neurons were also CaMKII-positive; i.e., they belonged to the class of excitatory pyramidal cells (Fig. 7). CaMKII-positive eGFP-positive neurons were detected in various layers of the neocortex (Fig. 7A), as well as in the pyramidal layer of the CA1 zone and the granular layer of the hippocampal dentate gyrus (Fig. 7B). Immunohistochemical detection of the eGFP protein showed staining of not only cell bodies, but also a significant part of the processes. Visual analysis of the morphology of these eGFP-positive cells also confirmed the conclusion that experience-induced Cre-recombination occurred in pyramidal cells (Fig. 7C, D).

Therefore, molecular phenotyping of the cells showed that the experience-induced Cre-recombination occurs only in neurons, but not in the glial cells of

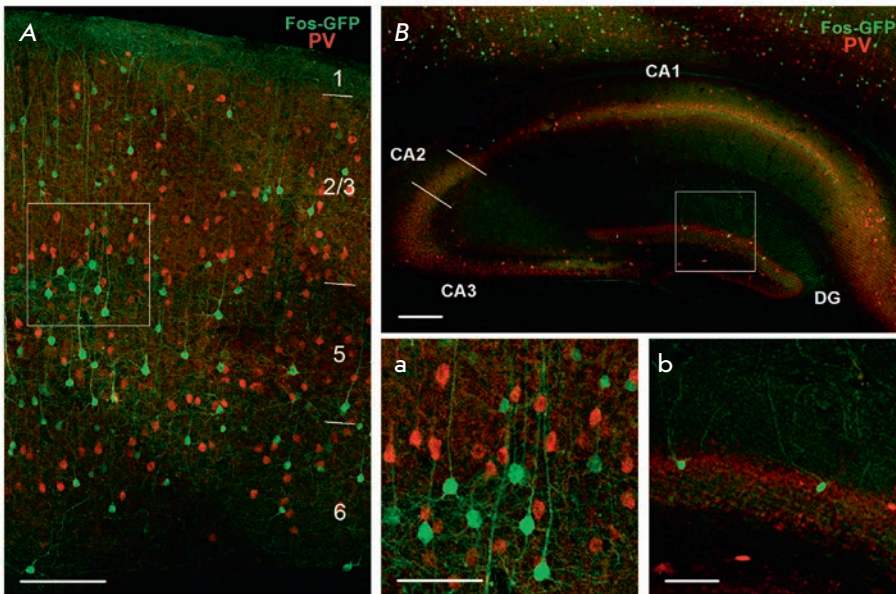


**Fig. 4.** Combined staining for eGFP (neurons that underwent experience-dependent Cre-recombination) and interneuron marker parvalbumin (PV, red channel). A – neocortex (frontal association cortex), neocortical layers are numbered; B – dorsal hippocampus; scale: 150  $\mu$ m. Microphotographs a and b show the neocortical and hippocampal areas framed in A and B, respectively; scale: 70  $\mu$ m. CA1 – CA1 area of the hippocampus; CA2 – CA2 area of the hippocampus; CA3 – CA3 area of the hippocampus; DG – dentate gyrus of the hippocampus.

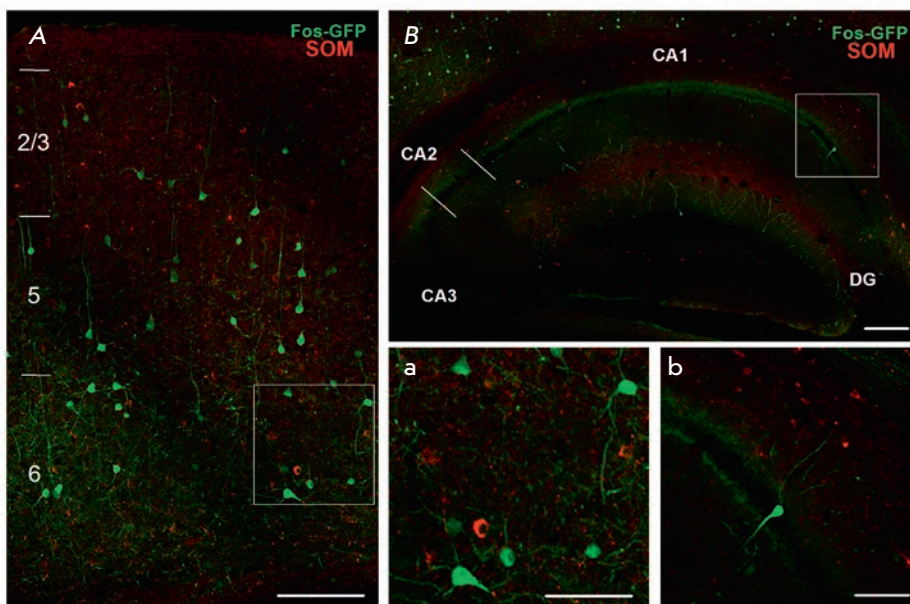


**Fig. 5.** Combined staining for eGFP (neurons that underwent experience-dependent Cre-recombination) and interneuron marker somatostatin (SOM, red channel). A – neocortex (frontal associative cortex), neocortical layers are numbered; B – dorsal hippocampus; scale: 150  $\mu$ m. Microphotographs a and b depict the neocortical and hippocampal areas framed in A and B, respectively; scale: 70  $\mu$ m. CA1 – CA1 area of the hippocampus; CA2 – CA2 area of the hippocampus; CA3 – CA3 area of the hippocampus; DG – dentate gyrus of the hippocampus.

Fos-Cre-eGFP mice, and that the neurons undergoing Cre-recombination belong to the family of excitatory pyramidal cells.

#### Determining the proportion of cells that undergo Cre-recombination in animals after they explore a new environment

The number of eGFP-positive neurons was assessed in different layers of the frontal association cortex in mice that had explored the context after tamoxifen in-

jection ( $n = 5$ ) in order to determine the proportion of neurons undergoing experience-induced Cre-recombination when the animals gained new experience and to analyze the patterns of distribution of those cells in the brain. Concomitant detection of the eGFP and NeuN mature neuron marker was carried out to assess the percentage of eGFP-positive cells among all the neurons in this layer [22].

eGFP-positive cells were found in all the layers of the frontal association cortex, but their number was

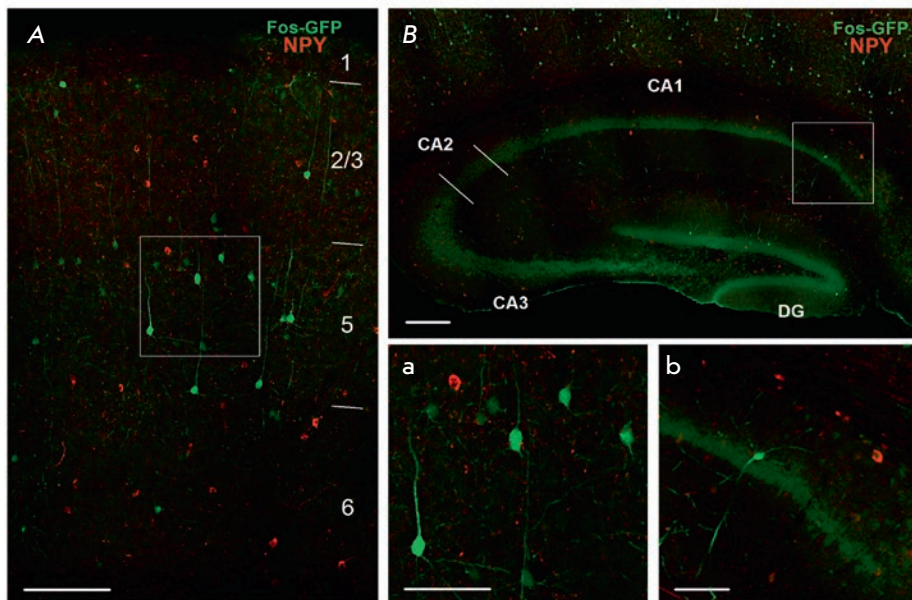


**Fig. 6.** Combined staining for eGFP (neurons that underwent experience-dependent Cre-recombination) and interneuron marker neuropeptide Y (NPY, red channel). A – neocortex (frontal association cortex), neocortical layers are numbered; B – dorsal hippocampus; scale: 150  $\mu$ m. Microphotographs a and b depict the neocortical and hippocampal areas framed in A and B, respectively; scale: 70  $\mu$ m. CA1 – CA1 area of the hippocampus; CA2 – CA2 area of the hippocampus; CA3 – CA3 area of the hippocampus; DG – dentate gyrus of the hippocampus.

highest in layers 2/3 and 5 ( $F(1.298,5.191) = 41.47$ ,  $p = 0.0009$ ; pairwise comparison of layers 2/3 and 5 with other layers:  $p < 0.02$ ), whereas only rare neurons that underwent Cre-recombination were detected in layer 1 (Fig. 8A). At the same time, the proportion of eGFP-positive cells among all the NeuN-labeled neurons was also highest in layers 2/3 and 5 ( $F(1.203,4.812) = 7.122$ ,  $p = 0.0425$ ; pairwise comparisons of layers 2/3 and 5 with layer 6:  $p < 0.02$ ), and it averaged 11.0% for the entire frontal association cortex (Fig. 8B).

### The use of Cre-recombination to identify two populations of cognitively active neurons in one brain

Cre-recombinase activity leads to permanent labeling of the neurons that are active within the time window defined by the action of tamoxifen. This opens the possibility of repeated placement of an animal with genetically labeled neurons in the situation of acquiring a new experience or reactivation of a previous one, followed by the detection of two separate populations of neurons activated upon two different cognitive loads within one brain. In this case, the neurons that underwent Cre-recombination after the first cognitive episode can be detected based on the presence of the eGFP protein and the neurons activated after the second episode can be visualized using immunohistochemistry based on the presence of the c-Fos protein.

A high degree of overlap of neuronal populations labeled in mice that explored a new context (the first cognitive episode) and those that underwent subsequent immediate FS in the same context 25 min later (the second cognitive episode) was previously detected

in the frontal association cortex. In our experiment, the mice were allowed to explore a new context after administration of tamoxifen and, 3 days later, received an immediate FS in order to visualize the two populations of neurons involved in the various cognitive episodes. Double immunohistochemical staining was used to detect the neurons activated when exploring the context (using eGFP protein) or receiving immediate FS (using c-Fos protein), as well as the neurons that were active in both cognitive episodes (eGFP and c-Fos) in various regions of the mouse brain (Fig. 9).

We assessed the number of neurons that were activated when exploring the context with application of subsequent immediate FS, as well as the overlap of these neuronal populations in the frontal associative cortex of A – A + FS group mice and control A – B + FS group mice (Fig. 10). Exploration of the new context and application of immediate FS activated similar-in-size populations of neurons in the frontal association cortex. However, a larger number of neurons were activated when FS was applied in the previously explored context A than in the new context B (“group” factor:  $F(1, 8) = 12.33$ ,  $p = 0.0080$ ; “cognitive episode” factor:  $F(1, 8) = 11.37$ ,  $p = 0.0098$ ; interaction between factors:  $F(1, 8) = 3.947$ ,  $p = 0.0404$ ; comparison of the number of c-Fos-positive cells in the groups A – A + FC and A – B + FC:  $p = 0.0212$ , Fig. 10A). In addition, FS application in a familiar context activated more neurons than it did in its initial exploration (comparing the number of c-Fos-positive and eGFP-positive cells in the group A – A + FS:  $p = 0.01924$ ). In this case, the proportion of neurons activated when exploring the new context and then re-activated when applying

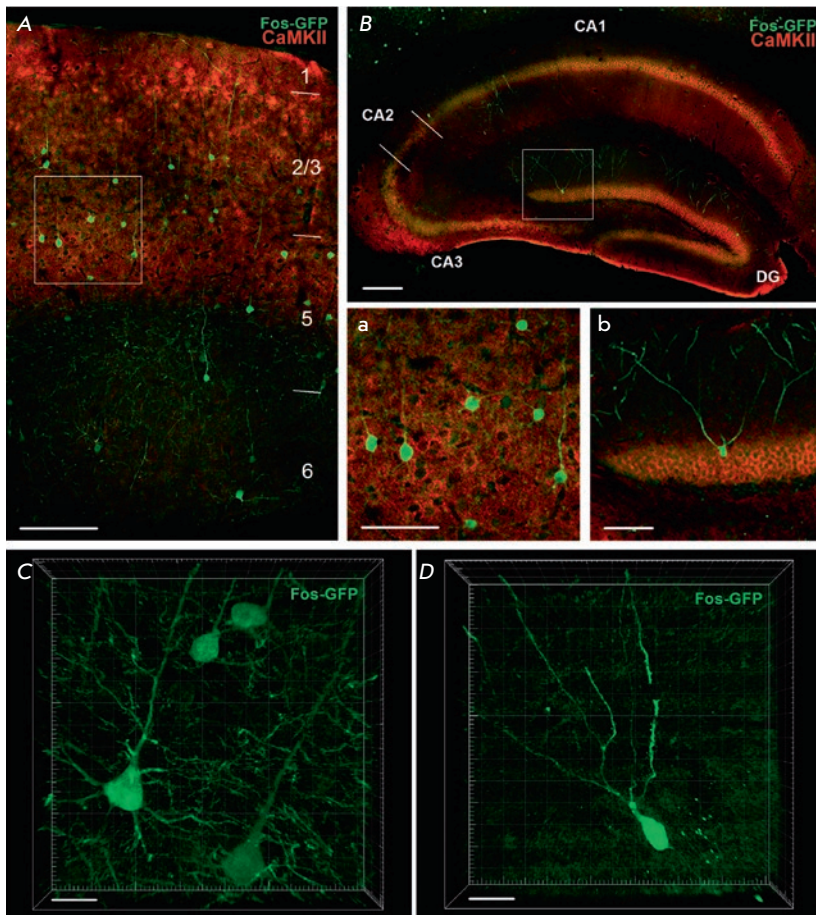


**Fig. 7.** Colocalization of the eGFP-positive neurons that underwent experience-dependent Cre-recombination (green channel) with the pyramidal neuronal marker CaMKII (red channel). A – neocortex (frontal association cortex), numbers indicate neocortical layers; B – dorsal hippocampus, areas CA1, CA2, CA3 and dentate gyrus (DG); scale: 150  $\mu$ m. Microphotographs a and b show the neocortical and hippocampal areas framed in A and B, respectively; scale: 70  $\mu$ m. C and D – microphotographs of several neurons that underwent experience-dependent Cre-recombination in the neocortex and the hippocampus, respectively. Dendritic trees and axons branching out from soma are visible; scale: 20  $\mu$ m. Colocalization of the eGFP-positive neurons that underwent experience-dependent Cre-recombination (green channel) with the pyramidal neuronal marker CaMKII (red channel). A – neocortex (frontal association cortex), numbers indicate neocortical layers; B – dorsal hippocampus, areas CA1, CA2, CA3 and dentate gyrus (DG); scale: 150  $\mu$ m. Microphotographs a and b show the neocortical and hippocampal areas framed in A and B, respectively; scale: 70  $\mu$ m. C and D – microphotographs of several neurons that underwent experience-dependent Cre-recombination in the neocortex and the hippocampus, respectively. Dendritic trees and axons branching out from soma are visible; scale: 20  $\mu$ m.

FS was significantly higher in the group A – A + FS (48.8%) than in the group A – B + FS (4.2%),  $p < 0.0001$ . A similar result was obtained for the proportion of neurons activated in both cognitive episodes among all neurons activated upon application of FS (Fig. 10B).

The results of this experiment indicate that it is possible to use Cre-induced genetic labelling of neurons to identify and then analyze the populations of neurons activated in the same brain during two different cognitive episodes.

Previously, a transgenic technology based on the tTA-tetO system was used to label two populations of cognitively active neurons. Rejmers et al. used the tTA-tetO system to analyze overlapping of neuronal populations activated during memory formation and reactivation [27]. Two different genetic markers of transcriptional cell activation, *c-fos* and *zif268*, were used to compare these populations. However, it is known that these two genes have different baseline expression levels, different cellular functions, different specificities with respect to brain cell types, and

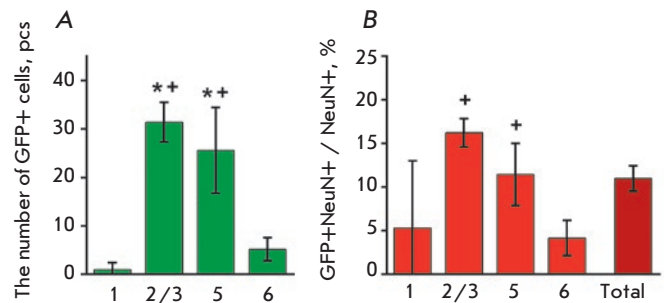


**Fig. 8.** Analysis of the distribution patterns of the neurons that underwent experience-dependent Cre-recombination after exploration of a new context by layers of the frontal association cortex. A – the number of eGFP-positive cells; B – the proportion of eGFP-positive cells among all NeuN-labeled neurons. The numbers indicate neocortical layers, “total” – the value averaged over the whole frontal associative cortex. \* –  $p < 0.02$ , + –  $p < 0.02$  compared to layers 1 and 6, respectively, Sidak t-test. Data are shown as a mean value  $\pm$  95% CI

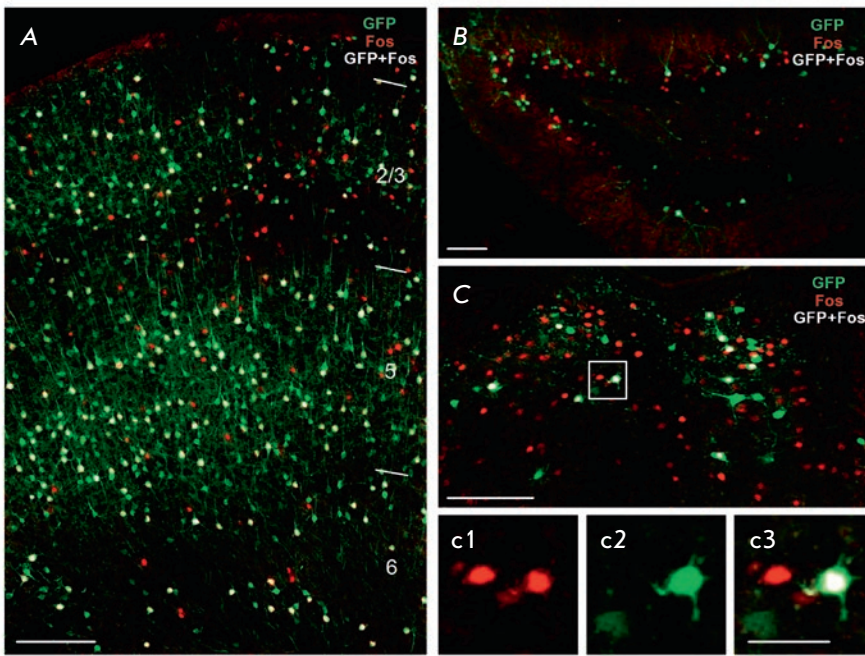


**Fig. 9.** Immunohistochemical identification of the neurons activated during two cognitive episodes. Neurons activated during the first episode, exploration of a new environment, are labeled with eGFP (green channel); cells activated during the second episode, electric shock, are labeled with endogenous c-Fos protein (red channel). White pseudocolor labels the cells that are both eGFP- and c-Fos-positive, meaning that they were active in both cognitive episodes. A – neocortex (frontal association cortex), numbers indicate neocortical layers; B – dentate gyrus of the hippocampus; C – paraventricular thalamic nucleus; scale: 100  $\mu$ m. Microphotographs c1, c2, c3 show the area framed in C, separately in channels: a1 – cytoplasmic eGFP staining, a2 – nuclear c-Fos staining, a3 – combination of the two; scale: 70  $\mu$ m.

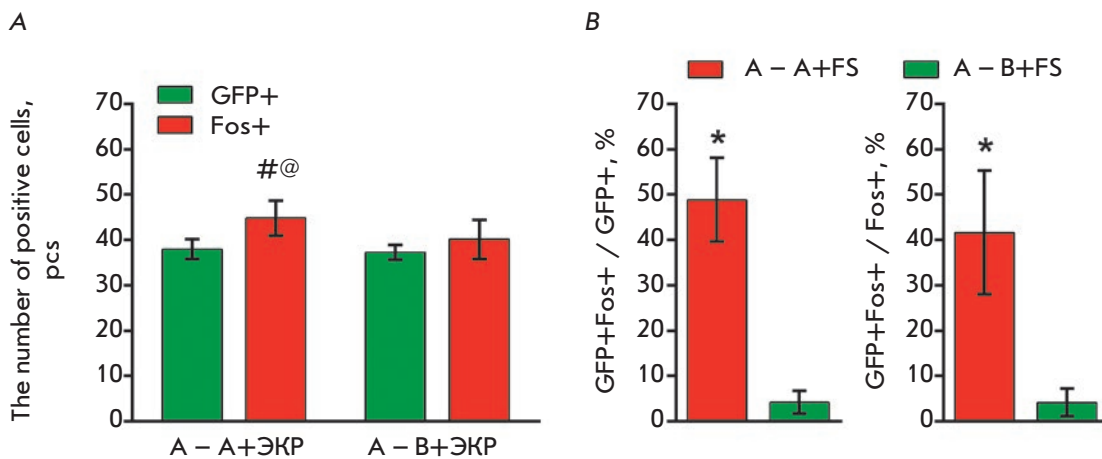


**Fig. 10.** Quantitative analysis of the overlap between neuronal populations of the frontal association cortex that were active during two cognitive episodes. A – neuronal populations active during exploration of context A (eGFP-positive cells) and immediate shock (c-Fos-positive cells); B – proportion of neurons active during both cognitive episodes among all the neurons involved in the new context exploration (GFP+Fos+ / GFP+) or all the neurons involved in immediate shock (GFP+Fos+ / Fos+). # –  $p = 0.0192$  compared to c-Fos-positive cells for “A – A+FS”, @ –  $p = 0.0212$  compared to “B – A+FS”, Sidak t-test; \* –  $p < 0.0001$  compared to “B – A+FS”, Student’s t-test. Data are shown as mean values  $\pm$  95% CI

that they are activated in response to different types of cognitive activity by animals [28]. Therefore, the comparison of the involvement of neuronal populations in two cognitive activity episodes for these two distinct markers poses great theoretical difficulties and draws serious objections. Furthermore, the tTA-tetO system has a number of methodological limitations: tTA-tetO

transgenic mice require lifetime administration of doxycycline, while genetic labeling of neurons is possible only during the period of drug withdrawal. At the same time, the system activation time window after doxycycline withdrawal can take several days, which leads to a large number of nonspecifically marked neurons [27, 29]. Therefore, the transgenic system with Cre-re-

combinase seems to be more adequate for application in experiments aimed at identifying two neuronal networks activated in the same brain in different cognitive episodes.

## CONCLUSION

We generated bitransgenic Fos-Cre-eGFP mice in which experience-induced Cre-recombination resulted in genetic labelling of the neurons active during the action of tamoxifen. These mice demonstrated a low baseline level of Cre-recombination in a quiet state and significant increase in the number of eGFP-expressing genetically labelled neurons after acquisition of a new experience. In these mice, experience-induced Cre-recombination occurred in a large number of brain

structures. Cre-recombination occurred in pyramidal excitatory neurons, but not in inhibitory interneurons. We also showed that Cre-induced genetic labelling of neuronal networks can be successfully used to identify activity by two different neuronal populations associated with different cognitive episodes within one nervous system and also to analyze overlapping of these populations of neurons. ●

*This study was supported by a Russian Science Foundation grant (project No. 14-15-00685). The study was carried out using the equipment of the Resource Center for Neurocognitive Studies of the Kurchatov Complex of Nano-bio-info-cognito-socio-technologies.*

## REFERENCES

- Anokhin K.V. // Zh. Vyssh. Nerv. Deiat. Im. I. P. Pavlova. 1997. V. 47. № 2. P. 261–286.
- Kaczmarek L. // Handbook of Chem. Neuroanatomy. Amsterdam: Elsevier, 2002. V. 19. P. 189–215.
- Korb E., Finkbeiner S. // Trends Neurosci. 2011. V. 34. № 11. P. 591–598.
- Pérez-Cadahía B., Drobic B., Davie J.R. // Biochem. Cell Biol. 2011. V. 89. № 1. P. 61–73.
- Anokhin K.V., Rose S.P. // Eur. J. Neurosci. 1991. V. 3. № 2. P. 162–167.
- Alberini C.M. // Physiol. Rev. 2009. V. 89. P. 121–145.
- Abramova A.B., Anokhin K.V. // Neurosci. Behav. Physiol. 1998. V. 28. № 6. P. 616–619.
- Zvorykina S.V., Anokhin K.V. // Neurosci. Behav. Physiol. 2004. V. 34. № 8. P. 869–872.
- Kuptsov P.A., Pleskacheva M.G., Voronkov D.N., Lipp Kh.P., Anokhin K.V. // Neurosci. Behav. Physiol. 2006. V. 36. № 4. P. 341–350.
- Barth A.L., Gerkin R.C., Dean K.L. // J. Neurosci. 2004. V. 24. № 29. P. 6466–6475.
- Branda C.S., Dymecki S.M. // Dev. Cell. 2004. V. 6. P. 7–28.
- Nagy A. // Genesis. 2000. V. 26. P. 99–109.
- Wu S., Ying G., Wu Q., Capecchi M.R. // Nat. Genet. 2007. V. 39. P. 922–930.
- Metzger D., Clifford J., Chiba H., Chambon P. // Proc. Natl. Acad. Sci. USA. 1995. V. 92. P. 6991–6995.
- Feil R., Wagner J., Metzger D., Chambon P. // Biochem. Biophys. Res. Commun. 1997. V. 237. P. 752–757.
- Imayoshi I., Sakamoto M., Kageyama R. // Front. Neurosci. 2011. V. 5. № 64. P. 1–11.
- Taniguchi H., He M., Wu P., Kim S., Paik R., Sugino K., Kvitsani D., Fu Y., Lu J., Lin Y., et al. // Neuron. 2011. V. 71. P. 998–1013.
- Guenther C.J., Miyamichi K., Yang H.H., Heller H.C., Luo L. // Neuron. 2013. V. 78. № 5. P. 773–784.
- Vorobyeva N.S., Ivashkina O.I., Toropova K.A., Anokhin K.V. // Zh. Vyssh. Nerv. Deiat. Im. I. P. Pavlova. 2016. V. 66. № 3. P. 352–360.
- Franklin K.B.J., Paxinos G. The mouse brain in stereotaxic coordinates. 3rd ed. N.Y.: Acad. Press, 2007. 346 p.
- Tovote P., Fadok J.P., Lüthi A. // Nat. Rev. Neurosci. 2015. V. 16. P. 317–331.
- Mullen R.J., Buck C.R., Smith A.M. // Development. 1992. V. 116. № 1. P. 201–211.
- Funchs E., Weber K. // Annu. Rev. Biochem. 1994. V. 63. P. 345–382.
- Liu X.B., Murray K.D. // Epilepsia. 2012. V. 53. P. 45–52.
- Markram H., Toledo-Rodriguez M., Wang Y., Gupta A., Silberberg G., Wu C. // Nat. Rev. Neurosci. 2004. V. 5. № 10. P. 793–807.
- Nakayama D., Baraki Z., Onoue K., Ikegaya Y., Matsuki N., Nomura H. // Curr. Biol. 2015. V. 25. № 1. P. 117–123.
- Reijmers L.G., Perkins B.L., Matsuo N., Mayford M. // Science. 2007. V. 317. P. 1230–1233.
- Lee J.L., Everitt B.J., Thomas K.L. // Science. 2004. V. 304. № 5672. P. 839–843.
- Glazewski S., Bejar R., Mayford M., Fox K. // Neuropharmacology. 2001. V. 41. P. 771–778.

# Characterization of the T-cell Repertoire after Autologous HSCT in Patients with Ankylosing Spondylitis

E. A. Komech<sup>1\*</sup>, I. V. Zvyagin<sup>1</sup>, M. V. Pogorelyy<sup>1</sup>, I. Z. Mamedov<sup>1</sup>, D. A. Fedorenko<sup>2</sup>, Y. B. Lebedev<sup>1</sup>

<sup>1</sup>Shemyakin–Ovchinnikov Institute of Bioorganic Chemistry, Miklukho–Maklaya Str. 16/10, Moscow, 117997, Russia

<sup>2</sup>A.A. Maximov Hematology and Cell Therapy Department, National Pirogov Medical Surgical Center, Nizhnaya Pervomaiskaya Str. 70, Moscow, 105203, Russia

\*E-mail: ekomech@gmail.com

Received October 24, 2017; in final form, April 16, 2018

Copyright © 2018 Park-media, Ltd. This is an open access article distributed under the Creative Commons Attribution License, which permits unrestricted use, distribution, and reproduction in any medium, provided the original work is properly cited.

**ABSTRACT** Autologous hematopoietic stem cell transplantation (HSCT), a safer type of HSCT than allogeneic HSCT, is a promising therapy for patients with severe autoimmune diseases (ADs). Despite the long history of medical practice, structural changes in the adaptive immune system as a result of autologous HSCT in patients with various types of ADs remain poorly understood. In this study, we used high-throughput sequencing to investigate the structural changes in the peripheral blood T-cell repertoire in adult patients with ankylosing spondylitis (AS) during two years after autologous HSCT. The implementation of unique molecular identifiers allowed us to substantially reduce the impact of the biases occurring during the preparation of libraries, to carry out a comparative analysis of the various properties of the T-cell repertoire between different time points, and to track the dynamics of both distinct T-cell clonotypes and T-cell subpopulations. In the first year of the reconstitution, clonal diversity of the T-cell repertoire remained lower than the initial one in both patients. During the second year after HSCT, clonal diversity continued to increase and reached a normal value in one of the patients. The increase in the diversity was associated with the emergence of a large number of low-frequency clonotypes, which were not identified before HSCT. Efficiency of clonotypes detection after HSCT was dependent on their abundance in the initial repertoire. Almost all of the 100 most abundant clonotypes observed before HSCT were detected 2 years after transplantation and remained highly abundant irrespective of their CD4+ or CD8+ phenotype. A total of up to 25% of peripheral blood T cells 2 years after HSCT were represented by clonotypes from the initial repertoire.

**KEYWORDS** autologous HSCT, TCR repertoire, NGS, ankylosing spondylitis.

**ABBREVIATIONS** HSCT – hematopoietic stem cell transplantation; TCR – T-cell receptor; AD – autoimmune disease; AS – ankylosing spondylitis; HD – healthy donors; RepSeq – repertoire sequencing; TNF $\alpha$  – tumor necrosis factor alpha.

## INTRODUCTION

Ankylosing spondylitis (AS), also known as Bekhterev's disease, is a chronic autoimmune disorder affecting the joints of the axial skeleton. The strong association between the risk of developing AS and the HLA-B\*27 allele, as well as alleles of the other genes involved in antigen presentation to T cells, suggests that T cells are actively involved in the pathogenesis of this disease. Nonsteroidal anti-inflammatory drugs (NSAIDs) or their combinations with monoclonal antibodies, usually anti-TNF $\alpha$  monoclonal antibodies, are currently used to treat AS. Alas, this therapy has proved ineffective for 40% of patients [1]. Autologous hematopoietic stem cell transplantation (HSCT) has been used over the past

two decades in patients with severe autoimmune diseases. This therapy has proved to be effective in patients with multiple sclerosis (MS), systemic lupus erythematosus, juvenile idiopathic arthritis, and systemic scleroderma [2–5]. The currently available data demonstrate that the clinical effect of this therapy is based on a significant reformation of the T- and B-cell repertoires as a result of deep immunosuppression, followed by the formation of a new T-cell repertoire. The pivotal role of T cells in the normal functioning and regulation of the immune system, as well as their involvement in autoimmune processes, reinforces the importance of studying the reformation of the T-cell repertoire during HSCT. Investigation of the clonal repertoire of

hypervariable T-cell receptors by high-throughput parallel sequencing (Repseq) is a state-of-the-art and informative approach for monitoring the dynamics of a T-cell pool at the level of individual T-cell clones. To date, a few studies have been published on T cell repertoire reconstitution after autologous HSCT [4, 6], including two papers that analyzed the repertoire in a patient with AS after autologous HSCT [7, 8]. In this study, we performed a longer-term and more thorough investigation of the reconstitution of the T-cell repertoire in patients with AS following autologous HSCT: for the first time, we tracked the clonal dynamics of T cells during 2 years following transplantation. The cDNA barcoding technique allowed us to evaluate the clonal diversity of the repertoire in the samples more accurately than in previous studies by setting an equal analysis depth, reducing the PCR bias, and eliminating most of the incorrect sequences that emerge during PCR and sequencing.

## MATERIALS AND METHODS

### Patients

Peripheral blood samples were collected from two patients with AS at several time points: before HSCT (point 0) and 4, 12, and 25 months post HSCT. The patients were diagnosed with AS according to the modified New York criteria [9]. All the patients provided an informed consent to participate in the study; the study was conducted in compliance with current ethical and regulatory requirements.

Patient ash-110 - a 26-year-old male, HLA-B\*27+. Before HSCT, disease duration was > 3 years; the patient was treated with methotrexate (7.5 mg/week, i.m. injections) and non-steroidal anti-inflammatory drugs (NSAIDs). At the time point when HSCT was conducted, the patient had grade 2 ankylosing spondylitis and a grade 2 impaired functional status. A month after HSCT, the patient's condition had improved and he was discharged to receive outpatient care. Acute relapse occurred one year after HSCT (point 12); after that, the patient started receiving chronic therapy with adalimumab (Humira®). Another relapse occurred two years after HSCT (point 24).

Patient ash-111 - a 28-year-old female, HLA-B\*27+. Before HSCT, disease duration was > 10 years; the patient was treated with infliximab (Remicade®). At the time point when HSCT was conducted, the patient had grade 2–3 ankylosing spondylitis and a grade 2 impaired functional status. A month after HSCT, the patient's condition had improved and she was discharged to receive outpatient care. Acute relapse occurred one year after HSCT (point 12); after that, the patient started receiving chronic therapy with etanercept (Enbrel®).

### HSCT

Autologous HSCT was conducted according to the following protocol: immunosuppressive chemotherapy with cyclophosphamide (200 mg/kg for 4 days), followed by infusion of a cryopreserved autologous isolate of hematopoietic stem cells ( $2.4 \times 10^6$  blood stem cells/kg body weight). The autologous stem cell transplant was mobilized using a granulocyte colony-stimulating factor (G-CSF, 10 mg/kg body weight); no CD34+ enrichment was performed. Antithymocyte globulin was transfused simultaneously with the graft to ensure *in vivo* T-cell depletion.

### Isolation of the lymphocytes and cell sorting

Peripheral blood samples (8 ml) were collected into Vacutainer tubes with K<sub>3</sub>EDTA (BD Biosciences) 0 (before HSCT and chemotherapy), 4, 9 (ash-111) or 12 (ash-110), and 24 months post-HSCT. The mononuclear cell fraction was isolated by conventional density gradient centrifugation using Ficoll (1.077 g/cm<sup>3</sup>, PanEco, Russia). Two equal-volume samples of peripheral blood (R1 and R2) were collected from both patients to analyze the clonal repertoire reproducibility at 24 months. In the same time frame (24 months post-HSCT), individual fractions of CD4+ and CD8+ T cells were obtained simultaneously with R1 and R2 samples using the Dynabeads reagent kits for immunomagnetic separation (Invitrogen, USA).

### Preparation of TCRβ cDNA libraries and sequencing

RNA was isolated using the TRIzol reagent (Invitrogen, USA) in compliance with the manufacturer's protocol. The cDNA libraries were prepared using the previously published technique [10], with some modifications: after cDNA synthesis, TCR alpha and beta cDNA were pre-amplified with the primers BCuni2R TGCTTCTGATGGCTCAAACAC and M1S AAGCAGTGGTATCAACGCAGAGT (94°C, 20 s; 60°C, 15 s; 72°C, 60 s – 18 cycles). Each reaction mixture contained BCuni2R and M1S oligonucleotides (5 pmol each), 1× Tersus buffer, 0.1 mM of each dNTP, and 0.2 μl of Tersus polymerase (Evrogen, Russia); the total volume of the mixture was 15 μl. The amplification product was purified using the QIAquick PCR Purification Kit (Qiagen, USA) according to the manufacturer's protocol. The entire purified PCR product was used for subsequent amplification.

Sequencing was carried out using an Illumina HiSeq 2000/2500 in pair-end mode with a 100 bp read length.

### Sequence data processing

Sequencing data pre-processing included a correction of sequencing errors and counting of the number of molecular events (UMI) in the library using the MiGEC software [11]. The MiTCR software was employed to

## Sequencing statistics

| Patient | Point / T-cell population | Number of reads | Number of UMI <sup>§, #</sup> | Total clonotype count <sup>#</sup> | Clonotype count per 90,000 UMI <sup>#</sup> |
|---------|---------------------------|-----------------|-------------------------------|------------------------------------|---|
| ash-110 | 0/F*                      | 10671513        | 301277                        | 226383                             | 77160                                       |
|         | 4/F                       | 13657155        | 90985                         | 47119                              | 46803                                       |
|         | 12/F                      | 1011932         | 125640                        | 72925                              | 55413                                       |
|         | 24/R1**                   | 7366741         | 964274                        | 519425                             | 69397                                       |
|         | 24/R2**                   | 7533711         | 1263464                       | 625152                             | 69244                                       |
|         | 24/CD4+                   | 2776546         | 587713                        | 329331                             | 71870                                       |
|         | 24/CD8+                   | 2964049         | 653168                        | 183735                             | 42679                                       |
| ash-111 | 0/F                       | 11194792        | 308159                        | 222555                             | 74115                                       |
|         | 4/F                       | 17725492        | 138299                        | 68398                              | 48533                                       |
|         | 12/F                      | 23807978        | 225397                        | 134596                             | 61615                                       |
|         | 24/R1                     | 7366741         | 957406                        | 414203                             | 63755                                       |
|         | 24/R2                     | 4597521         | 367849                        | 210597                             | 64547                                       |
|         | 24/CD4+                   | 3144715         | 435297                        | 218230                             | 64026                                       |
|         | 24/CD8+                   | 2850176         | 552005                        | 163602                             | 43519                                       |

\*F – the fraction of peripheral blood mononuclear cells.

\*\*R1, R2 – fractions of peripheral blood mononuclear cells from two parallel blood samples.

§UMI – unique molecular identifier.

#Each UMI was read at least twice.

determine the V, D, and J gene segments and CDR3 sequences, to count the number of clonotypes, and to generate a list of the clonotypes identified in each sample. When reconstituting the clonal repertoire of a sample, we used the TCR cDNA sequences read at least twice according to the UMI analysis, which allowed us to eliminate most of the erroneous sequences [11, 13]. The sequencing statistics are listed in *Table*. Further bioinformatic and statistical analysis of the results was performed using the R programming language and the tcR package [14, 15].

Matching between the nucleotide sequences in the CDR3 region and the V segment of TCR in the reconstituted repertoires was employed to establish whether a clone had a CD4 or CD8 phenotype and to search for specific clonotypes in individual repertoires at different time points.

In order to calculate the clonal diversity, the estimated lower bound of frequency of the clonotypes stably detected in a sample and the degree of repertoire renewal, the analysis depth for the repertoire of the samples being compared, was aligned by random selection of 90,000 UMI from the sequence dataset for each sample.

The clonal diversity of the T-cell repertoire was evaluated using the Chao1 diversity index [16].

## RESULTS

### The dynamics of T-cell repertoire reconstitution

When studying the changes in the T-cell repertoire by high-throughput parallel sequencing, it is very important to maximally reduce the artificial diversity effected by sequencing errors and to ensure a comparable depth of analysis for the repertoires in the samples under comparison [17]. In order to perform TCR high-throughput sequencing and reconstructions of peripheral T-lymphocyte repertoires for two AS patients before and after autologous HSCT, we applied the cDNA barcoding technique for preparing TCR cDNA libraries [18, 19]. The use of unique molecular identifiers (UMI) in the processing of the sequencing data allows one to eliminate most PCR and sequencing errors, to reduce the artificial diversity, and to quantify the frequency of each T-cell clonotype in the sample [11, 13]. Five peripheral blood samples were collected from each patient at 5 time points (one week before HSCT (point 0) and 4, 12, and 24 (a pair of parallel samples) months after HSCT). From  $1 \times 10^6$  to  $23 \times 10^6$  sequences corresponding to at least  $9 \times 10^4$  unique TCR  $\beta$ -chain cDNA molecules were obtained after sequencing of each sample; the minimal threshold was two reads per TCR cDNA molecule (*Table*). The selected threshold allowed us to eliminate most of the erroneous cDNA se-

quences that emerged during PCR and sequencing from further analysis [20].

We used the Chao1 index as a measure of the clonal diversity of a repertoire: this index is determined by estimating the number of low-frequency clonotypes in a sample and takes into account the richness of naïve T cell clonotypes, which underlie the diversity of the T-cell repertoire in the sample [16, 21]. Taking into account the sensitivity of this metric to the analysis depth, 90,000 TCR cDNA sequences with unique molecular identifiers were arbitrarily chosen for each sample from the dataset when we studied the dynamics of clonal diversity. Earlier evaluation of the efficiency of the technique for T-cell repertoire reconstitution used in this study demonstrated that the selected number roughly corresponds to an analysis of 90,000 T cells [13, 21].

Four months post-HSCT, the diversity (by Chao1 index) significantly decreased ( $p < 2.2 \times 10^{-16}$ , Mann–Whitney U test) with respect to its initial value in both patients (Fig. 1). The total count of the identified TCR $\beta$  clonotypes was more than twice as low as that before HSCT (77391 and 46797, 73880 and 48505 clonotypes in the samples at time points 0 and 4 months in patients ash-110 and ash-111, respectively). After the 1-year-long reconstitution period, the clonal diversity of the repertoire in both patients had not returned to its initial level. The rate of clonal diversity reconstitution was different in these two patients. Two years post-HSCT, the clonal diversity of the repertoire in patient ash-110 had returned to its initial level and corresponded to that of healthy donors of the same age (Fig. 1). One year post-HSCT, the clonal diversity in patient ash-111 was only 50% of its initial value. No significant changes were observed during the second year of the reconstitution period, and a normal value was not reached. Unlike in other autoimmune diseases where the clonal diversity of the T-cell repertoire before HSCT is significantly reduced [2, 4], the initial clonal diversity of repertoires in both patients in this study was similar to that in healthy donors and/or in patients with AS of comparable age ( $p = 0.284$  and  $p = 0.0$ , respectively, Mann–Whitney U test).

### Effect of HSCT on the clonotypes presented in the initial T-cell repertoire

When studying the dynamics of the initial repertoire during 2 years post-HSCT, we tracked the frequencies of clonotypes from the repertoire at point 0 detected in all subsequent samples (i.e., 4, 12, and 24 months post-HSCT). According to our findings, the clonotypes from the initial repertoire provisionally divided into two groups: the ones being constantly present at all points after HSCT and the ones detected at some of the sub-

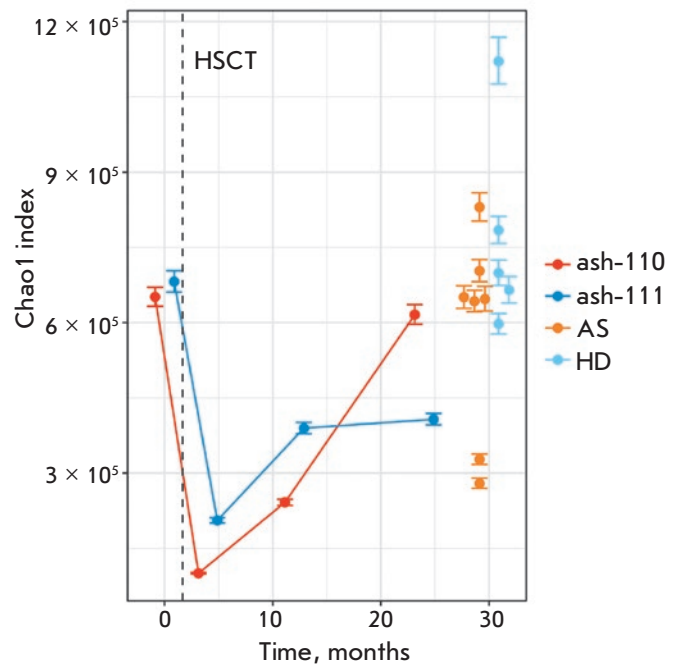


**Fig. 1.** Dynamics of T-cell diversity during 2 years after HSCT. Estimation of the lower bound of clonal diversity using the Chao1 index [16]. Blue dots represent healthy donors ( $n=6$ , age 22–34 years; the data were reported by Britanova et al. 2014 [21]); orange dots – patients with AS ( $n=5$ , age 22–34; the data were reported by Komech et al. 2018 [22]). The dashed vertical line shows the time point of HSCT. The 95% confidence interval for each value is marked with an error bar.

sequent time points, only. The first group consisted of 3,188 clonotypes in ash-110 repertoire and 6,126 clonotypes in ash-111 repertoire (1.4 and 3.0% of the overall diversity, respectively), corresponding to approximately 10% (ash-110) or 15% (ash-111) of peripheral blood T cells before HSCT (Fig. 2). The clonotypes in the second group (i.e., the ones either not detected at all or observed only at some time points post-HSCT) predominated among peripheral blood T cells before HSCT (~90%). The initial frequencies were significantly different in these groups: the first group contained most of the high-abundance clonotypes in the sampled repertoire (the median clonotype frequency in the initial repertoire was 0.001%; the interquartile range for each patient was 0.0007–0.003%), while the second group mostly contained the low-abundance clonotypes (median frequency, 0.0003%; the interquartile range was 0.0003–0.0003%). An interesting fact was that some initially low-abundance clonotypes were still detected in the first group (i.e., were present in all repertoires post-HSCT), while the high-abundance clonotypes in the initial repertoire could disappear after HSCT.

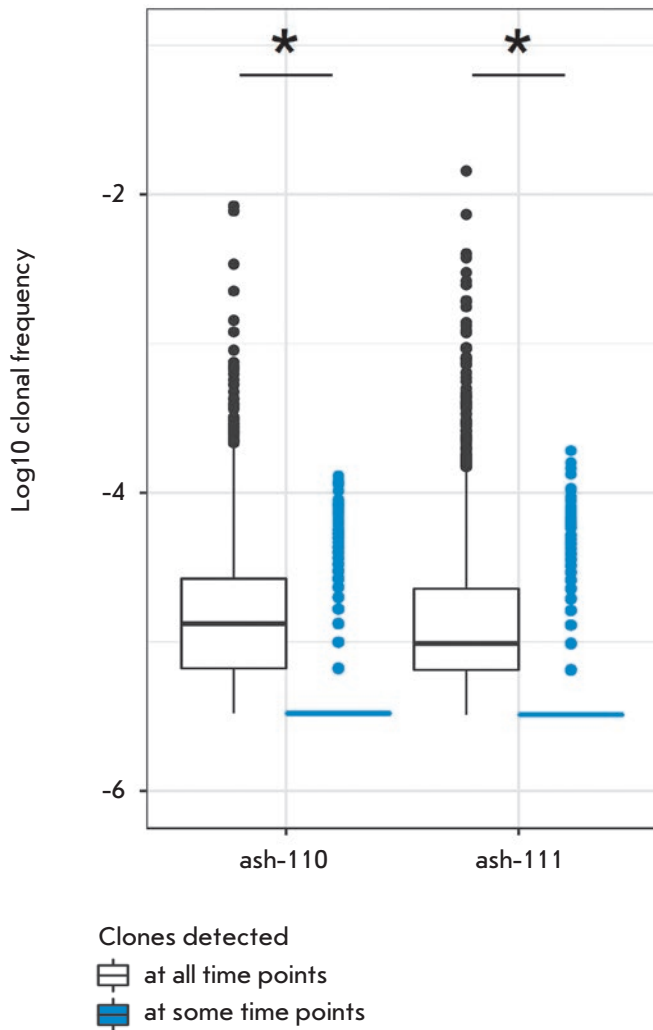


**Fig. 2.** Clonal frequency distribution in the initial repertoire according to the detection of clonotypes in samples after HSCT. White box plots show the frequency distribution of clonotypes found in all the analyzed samples, including the time point before HSCT; blue box plots show the frequency distribution of clonotypes present at point 0 but not found in at least one sample after HSCT (points 4, 12 or 24). \*The p-value  $< 2.2 \times 10^{-16}$  (Mann–Whitney U-test).

When studying the dynamics of individual clonotypes over a long time frame, one should take into account the fact that the probability of detecting a clonotype in a sample depends on the count of clonotype cells in the repertoire: clonotypes with a larger cell count (i.e., the so-called high-abundance clonotypes) have a higher probability of being detected in several independently collected blood samples, unlike the low-abundance ones. In order to determine the bound of abundance of clonotypes that were stably detected in

the sample under analysis and were revealed in the sequencing data, we carried out a comparative analysis of the clonal repertoires of parallel blood samples collected at the same time point. In order to eliminate any influence of the sequencing dataset sizes, we randomly sampled 90,000 TCR cDNA sequences from each dataset. In both patients, only clonotypes with abundance  $> 0.01\%$  (100–150 of the most high-abundance clonotypes in the repertoire) were observed in each replica at the same analysis depth (Fig. 3A). We used this estimation of reproducibility and tracked the 100 most high-abundance (“top 100”) clonotypes from point 0 at all time points post-HSCT in each patient to characterize the degree of renewal of the initial repertoire. We assumed that the absence or presence of these clonotypes in post-HSCT repertoires will reflect changes in the cell count for a given clonotype. In full consistency with their high abundance, all “top 100” clonotypes, except for two clonotypes in patient ash-111, proved to belong to the group of clonotypes that were constantly present in repertoires during the reconstitution period. Meanwhile, approximately 50% of the “top 100” clonotypes in each patient (45 clonotypes in ash-110 and 52 clonotypes in ash-111) remained abundant and were among the top 100 high-abundance clonotypes 2 years post-HSCT. In a similar manner, we tracked the dynamics of the 100 most high-abundance clonotypes in three healthy donors of comparable age during 2 years. In the healthy donors, who had no HSCT, 85–95% of the initial top 100 high-abundance clonotypes still remained among the “top 100” clonotypes after 2 years.

We attributed each “top 100” clonotype to subpopulations of CD8<sup>+</sup> cytotoxic or CD4<sup>+</sup> helper T cells by cross-analysis of the repertoires of corresponding T cell fractions. We found no significant differences in whether or not a clonotype still remained among the “top 100” clonotypes 2 years post-HSCT depending on their cytotoxic or T-helper phenotype (Fig. 3B).

These results allowed us to conclude that autologous HSCT did not result in complete renewal of high-abundance clonotypes in the analyzed patients:  $> 50\%$  of the clonotypes remained in the repertoire and retained their high frequency. However, the HSCT-induced rearrangement of high-abundance clonotypes was more significant compared to the dynamics of the corresponding part of the repertoires in healthy donors within the same time frame. The detectability of clonotypes from the initial repertoire in post-HSCT repertoires depended mostly on clonotype abundance in the initial repertoire. Meanwhile, many clonotypes with low abundance before HSCT were still detected in the individual repertoire 2 years post-HSCT. The latter finding suggests that other factors besides initial abundance may affect the fate of T-cell clones after HSCT.

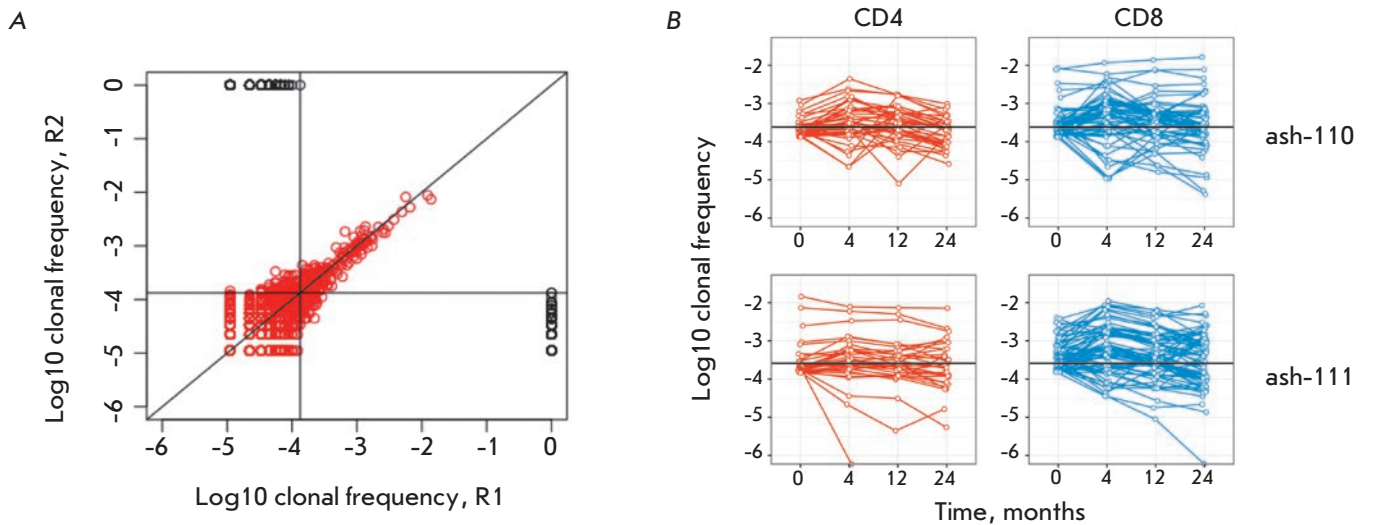


**Fig. 3.** Clonal dynamics of the initial T-cell repertoire. (A) Reproducibility of clonal frequency in two parallel blood samples collected from one donor. Each dot represents a TCR $\beta$  clonotype. Black dots represent the clonotypes that do not reproduce in replica. (B) The dynamics of the top 100 clonotypes from the initial repertoire. CD4+ clonotypes are shown in red; CD8+ clonotypes, in blue. The black horizontal line represents the lower bound of clonal frequency for the top 100 clonotypes at point 24.

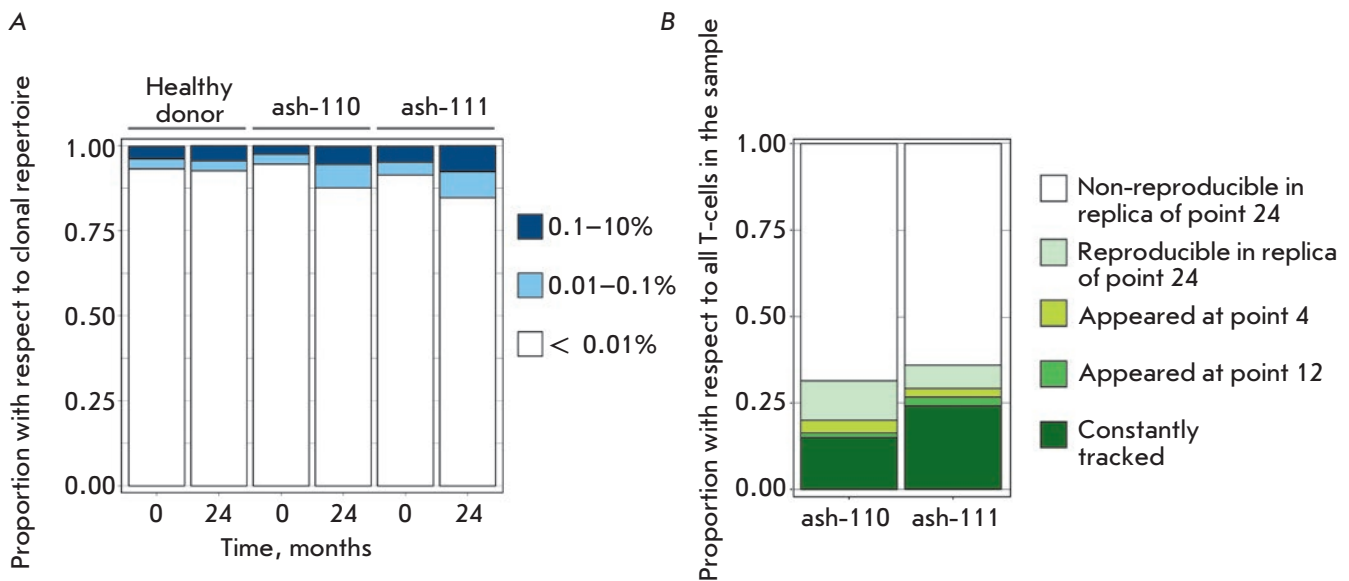


**Fig. 4.** The structure of the clonal repertoire two years after HSCT. (A) Proportion of clonotypes belonging to different frequency groups with respect to the total number of clonotypes in the sample: high-abundance (0.1–10%), medium-abundance (0.01–0.1%), and low-abundance (<0.01%). Structures of T-cell repertoires are given for two patients with AS before and 2 years after HSCT (points 0 and 24) and for one representative healthy donor. (B) All clones at point 24 are divided into groups according to the time point when they were detected for the first time. Y-axis: the cumulative proportion of clonotypes from each group with respect to all cells in a sample 2 years after HSCT.

### Structure of the clonal repertoire 2 years post-HSCT

Renewal of the clonal composition of the T-cell repertoire is one of the putative sequelae of HSCT determining the therapeutic potential of the procedure. In order to assess the changes that had taken place in the rep-

ertoire structure 2 years post-HSCT, we analyzed the clonal composition of the repertoire at points 0 and 24 in both patients. For the sake of comparison, we studied the repertoire structures in healthy donors of comparative age ( $n = 3$ ) using the same analysis (Fig. 4A; the

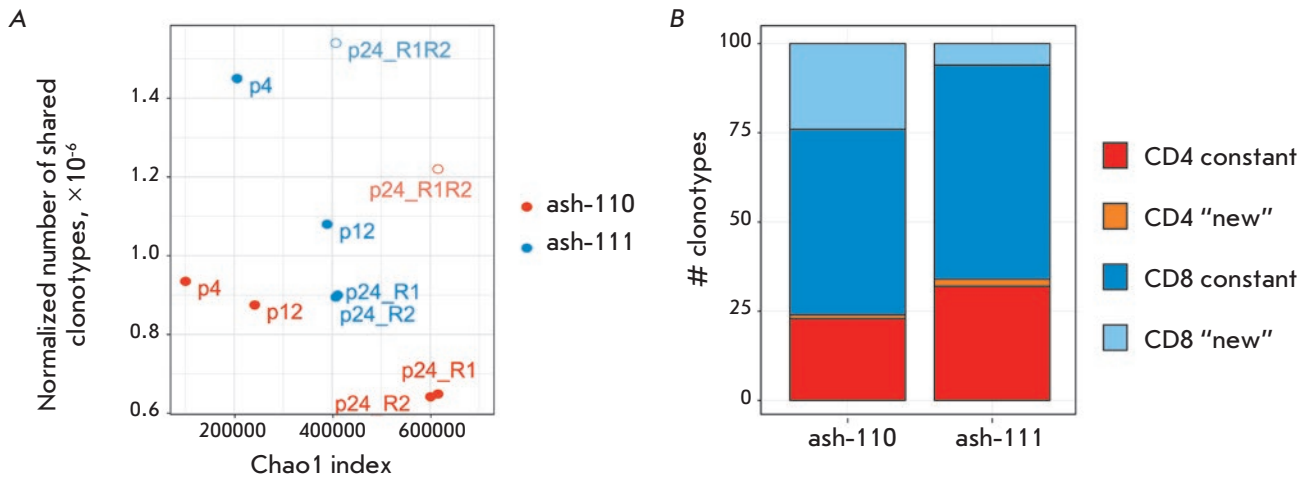


**Fig. 5.** Degree of clonal repertoire renewal after HSCT. (A) Correlation between the normalized number of the clonotypes shared between point 0 and points 4 (p4), 12 (p12), 24 (in two replicas: p24\_R1 and p24\_R2) and the diversity of a reference sample. Points p24\_R1R2 represent the comparison of replicas of point 24. (B) Composition of the 100 most abundant clonotypes in the repertoire of point 24. CD8+ cytotoxic clonotypes are shown in blue and light blue; CD4+ T-helper clonotypes are shown in red and orange.

left panel shows the repertoire structures for one representative donor). Two years after HSCT, the structures of the clonal repertoire in patients were almost identical to the normal structure: a small fraction (up to 10%) of the repertoire was represented by high- and medium-abundance clonotypes, while the remaining fraction (approximately 90%) was represented by low-abundance clonotypes. Meanwhile, the T-cell repertoires of patients post-HSCT were more oligoclonal than before the transplantation (Fig. 4A).

In order to evaluate the degree of repertoire renewal, we analyzed the clonal composition 2 years post-HSCT in comparison with repertoires at all preceding time points. Fifteen and twenty-four percent (ash-110 and ash-111, respectively) of all T cells were represented by clonotypes that had been detected in the repertoire before HSCT and in all post-HSCT repertoires (Fig. 4B). Such clonotypes originated both from the pool of T cells that had survived in the patient's organism after pretransplantation chemotherapy and/or from the T cells of the graft, which contains the almost complete pre-HSCT repertoire of a patient, since no specific depletion of mature T cells had been conducted. The high abundance of these clonotypes within the post-HSCT repertoires may have been caused by an intense proliferation of T cells, which would have enabled them to overcome the significant decline in lymphocyte count after pretransplantation chemotherapy. Meanwhile, in parallel with the increase in repertoire diversity, the percentage of clonotypes originated from the initial repertoire declined during 2 years post-HSCT in

both patients (Fig. 5A). This evidence, in combination with the observation of increased clonotype sharing between replicates at point 24 (p24\_R1R2 in Fig. 5A) in comparison with clonal sharing between point 24 and point 0, suggests that newly developed clones fill up the T-lymphocyte repertoire during the reconstitution period.

In order to analyze the degree of renewal of the repertoire of high-abundance clonotypes, we tracked the presence of the 100 most abundant clonotypes of the repertoire at point 24 in the repertoires at all earlier points. Seventy-five and ninety-two clonotypes out of 100 were detected in the pre-HSCT repertoire in patients ash-110 and ash-111, respectively (Fig. 5B). Among the "top 100", 24 CD8+ and one CD4+ clonotypes in patient ash-110 and six CD8+ and two CD4+ clonotypes in patient ash-111 had not been detected before HSCT.

Hence, the fraction of medium- and high-abundance T-cell clonotypes increased and the clonal composition of low-abundance T-cell clonotypes was significantly renewed two years post-HSCT. Meanwhile, most of the high-abundance clonotypes in the 2-years-post-HSCT repertoire originated from the initial T-cell repertoire.

## DISCUSSION

Ankylosing spondylitis, also known as Bekhterev's disease, is a chronic systemic autoimmune disorder characterized by periodic remission and relapse stages. Specific treatment for AS does not exist; disease-modifying therapy involves nonspecific nonsteroidal anti-inflam-

matory drugs. The conventional therapy has recently been combined with application of anti-TNF $\alpha$  monoclonal antibodies: infliximab (Remicoid<sup>®</sup>) and adalimumab (Humira<sup>®</sup>). However, up to 40% of patients either are resistant or stop responding to antibody-based therapy [23]. If the disease-modifying therapy proves ineffective, autologous hematopoietic stem cell transplantation can be one of the promising therapies for patients with progressive AS. Meanwhile, questions regarding the selection of an effective HSCT protocol and the overall effectiveness of this therapeutic approach are still to be answered.

Here, we continued our previous studies [7, 24] and investigated the dynamics of the clonal repertoire of peripheral T-lymphocyte during 2 years after autologous HSCT in 2 patients with AS. During the entire reconstitution period, the thymus produced new naïve T cells, thus increasing the diversity of the TCR repertoire: although it had significantly decreased short-term after HSCT, by the end of the first year the diversity of the TCR repertoire in both patients had reached 50% of its initial level and continued to accrue during the second year (*Fig. 1*). Similar dynamics of repertoire reconstitution have also been reported in adult patients with other autoimmune diseases [2, 25]. We found that the rates of clonal diversity reconstitution in the two patients differed noticeably: after 2 years, patient ash-110 had a count of clonotypes that was nearly the same as the initial one, while the count of clonotypes in patient ash-111 was only ~50% of its initial level.

The molecular mechanisms responsible for the effectiveness of HSCT in treating autoimmune diseases remain to be elucidated. It has been demonstrated in several studies that despite chemotherapy some T cells remain within the repertoire after HSCT but have no effect on the development of stable remission of the underlying disease during 2–5 years post-HSCT [4–7]. In the patients in our study, the clones that had survived HSCT made up to 25% of the T cells within the repertoire 2 years post-HSCT. Most of the clonotypes that had survived HSCT were high-abundant clonotypes of the initial repertoire, with a mean abundance of > 0.001% (*Fig. 2*). These clonotypes could have remained in the organism after the course of chemotherapy or originated from the cells of a non-T-cell-depleted graft. Interestingly, a small fraction of initially low-abundance clonotypes was also revealed in all repertoires post-HSCT, while some high-abundance clonotypes had totally disappeared after the transplantation. In other words, clonotype survival depends not only on its abundance, but also on the functional status of various T cells. Kanakry et al. demonstrated that CD4+CD25+FoxP3+ regulatory T cells are resistant to medium doses (50–100 mg/kg) of cyclophosphamide *in*

*vitro* due to an enhanced expression of aldehyde dehydrogenase, which neutralizes the cytotoxic activity of cyclophosphamide [26]. It is reasonable to assume that the low-abundant clonotypes detected after HSCT in our study were a subpopulation of regulatory T cells.

Having focused on the clonotypes stably in the samples, we followed with an assessment of the degree of renewal of the T-cell repertoire post-HSCT. In our study, approximately 50% of the clonotypes from the “top 100” ones in the initial repertoire remained in the “top 100” 2 years post-HSCT. This state was independent of whether the clonotype had a CD4+ or CD8+ phenotype. After two years, new clonotypes were detected among the “top 100” ones in both patients; these clonotypes were not detected before HSCT and mostly consisted of CD8+ T cells. In the older (45-year-old) patient with AS who had undergone HSCT according to an identical protocol and achieved long-lasting remission (> 5 years), more than one-third of the clonotypes that had been highly abundant before HSCT were still among the “top 100” clonotypes 2 years post-transplantation (data reported by Britanova et al. [7]). Hence, the patients whose T-cell repertoires were investigated in this study did not display a deep rearrangement of high-abundance T-cell clones. Reconstitution of the initial clonal structure of the repertoire could be related to the selected HSCT protocol, according to which graft preparation involved neither depletion of mature T cells nor CD34+ cell enrichment. Meanwhile, an identical HSCT protocol allowed the older patient to achieve long-lasting remission. A similar extent of renewal of high-abundance clonotypes was reported for patients with multiple sclerosis aged 27–53 years when a different protocol of autologous HSCT involving CD34+ cell enrichment was employed (about 40% of T-cell clonotypes from the “top 1000” CD4+ and CD8+ subpopulations remained within the “top 1000” corresponding fractions a year after transplantation) regardless of whether or not remission had been achieved [4]. Hence, one can only conclude that the therapeutic potential of HSCT significantly depends on other factors.

The subpopulation of regulatory T cells (T<sub>reg</sub>) is one of the T-cell subpopulations shown to play a crucial role in the pathogenesis of many autoimmune diseases (the data were summarized in [27, 28]). In particular, it has recently been demonstrated that renewal of this T-cell population is important for the therapeutic effectiveness of HSCT in patients with juvenile idiopathic arthritis and dermatomyositis: long-lasting remission was observed only in patients in whom HSCT had significantly increased the diversity of the clonal T<sub>reg</sub> repertoire [29]. It seems reasonable to suggest that the absence of a long-term therapeutic effect by HSCT in our two patients with AS was related to insufficient

reconstitution of the repertoire of the regulatory T-cell subpopulation. Further research into the dynamics of the clonal composition of various T-cell subpopulations, combined with the use of different HSCT protocols in a representative cohort of patients, will make it possible to evaluate the effectiveness of autologous HSCT as a method for treating severe forms of AS.

## CONCLUSIONS

HSCT is used increasingly often to treat patients with a severe course of autoimmune disease who fail to respond to the conventional therapy. We employed high-throughput sequencing and the cDNA barcoding technique to quantify the frequency of the clonotypes of peripheral blood T cells and, for the first time, to track the dynamics of reconstitution of the T-lymphocyte clonal repertoire during 2 years after autologous HSCT in two patients with ankylosing spondylitis. Reconstitution of the diversity of the T-cell repertoire in patients with AS lasted over two years, which is

consistent with the dynamics of repertoire reconstitution in adult patients previously reported by other researchers. Two years after HSCT, up to 25% of the cells in the repertoire of the examined patients were represented by clonotypes from the pre-transplantation repertoire. We have demonstrated that almost all the high-abundance and a small fraction of the low-abundance clonotypes in the initial repertoire survived HSCT. Our findings significantly broaden the database on the functioning of the immune system upon HSCT and can be applied to optimize and elaborate new efficient protocols for autologous HSCT employed to treat severe forms of AS. ●

*This work was supported by the Russian Foundation for Basic Research (grants Nos. 16-04-01881 and 17-04-01568) and the Scholarship of the President of the Russian Federation awarded to E.A. Komech (No. SP-1264.2016.4).*

## REFERENCES

1. Sieper J., Poddubnyy D. // *Nat. Rev. Rheumatol.* 2016. V. 12. № 5. P. 282–295.
2. Farge D., Arruda L.C.M., Brigant F., Clave E., Douay C., Marjanovic Z., Deligny C., Maki G., Gluckman E., Toubert A., et al. // *J. Hematol. Oncol.* 2017. V. 10. № 1. P. 21.
3. Leone A., Radin M., Almarzooqi A.M., Al-Saleh J., Roccatello D., Sciascia S., Khamashta M. // *Autoimmun. Rev.* 2017. V. 16. № 5. P. 469–477.
4. Muraro P.A., Robins H., Malhotra S., Howell M., Phippard D., Desmarais C., de Paula Alves Sousa A., Griffith L.M., Lim N., Nash R.A., et al. // *J. Clin. Inv.* 2014. V. 124. № 3. P. 1168–1172.
5. Wu Q., Pesenacker A.M., Stansfield A., King D., Barge D., Foster H.E., Abinun M., Wedderburn L.R. // *Immunology.* 2014. V. 142. № 2. P. 227–236.
6. van Heijst J.W.J., Ceberio I., Lipuma L.B., Samilo D.W., Wasilewski G.D., Gonzales A.M.R., Nieves J.L., van den Brink M.R.M., Perales M.A., Pamer E.G., et al. // *Nat. Med.* 2013. V. 19. № 3. P. 372–377.
7. Britanova O.V., Bochkova A.G., Staroverov D.B., Fedorenko D.A., Bolotin D.A., Mamedov I.Z., Turchaninova M.A., Putintseva E.V., Kotlobay A.A., Lukyanov S.A., et al. // *Bone Marrow Transplant.* 2012. V. 47. P. 1479–1481.
8. Mamedov I.Z., Britanova O.V., Chkalina A.V., Staroverov D.B., Amosova A.L., Mishin A.S., Kurnikova M.A., Zvyagin I.V., Mutovina Z.Y., Gordeev A.V., et al. // *Autoimmunity.* 2009. V. 42. № 6. P. 525–536.
9. van der Linden S., Valkenburg H.A., Cats A. // *Arthritis Rheum.* 1984. V. 27. № 4. P. 361–368.
10. Zvyagin I.V., Mamedov I.Z., Tatarinova O.V., Komech E.A., Kurnikova E.E., Boyakova E.V., Brilliantova V., Shelihova L.N., Balashov D.N., Shugay M., et al. // *Leukemia.* 2017. V. 31. № 5. P. 1145–1153.
11. Shugay M., Britanova O.V., Merzlyak E.M., Turchaninova M.A., Mamedov I.Z., Tuganbaev T.R., Bolotin D.A., Staroverov D.B., Putintseva E.V., Plevova K., et al. // *Nat. Methods.* 2014. V. 11. № 6. P. 653–655.
12. Bolotin D.A., Shugay M., Mamedov I.Z., Putintseva E.V., Turchaninova M.A., Zvyagin I.V., Britanova O.V., Chudakov D.M. // *Nat. Methods.* 2013. V. 10. № 9. P. 813–814.
13. Egorov E.S., Merzlyak E.M., Shelenkov A.A., Britanova O.V., Sharonov G.V., Staroverov D.B., Bolotin D.A., Davydov A.N., Barsova E., Lebedev Y.B., et al. // *J. Immunol.* 2015. V. 194. № 12. P. 6155–6163.
14. R Core Team // *R Foundation for Statistical Computing.* Vienna, Austria. 2015.
15. Nazarov V.I., Pogorelyy M.V., Komech E.A., Zvyagin I.V., Bolotin D.A., Shugay M., Chudakov D.M., Lebedev Y.B., Mamedov I.Z. // *BMC Bioinformatics.* 2015. V. 16. № 1. P. 175.
16. Hughes J.B., Hellmann J.J., Ricketts T.H., Bohannon B.J. // *Appl. Environ. Microbiol.* 2001. V. 67. № 10. P. 4399–4406.
17. Hou X.-L., Wang L., Ding Y.-L., Xie Q., Diao H.-Y. // *Genes Immun.* 2016. V. 17. № 3. P. 153–164.
18. Kivioja T., Vähärautio A., Karlsson K., Bonke M., Enge M., Linnarsson S., Taipale J. // *Nat. Methods.* 2011. V. 9. № 1. P. 72–74.
19. Mamedov I.Z., Britanova O.V., Zvyagin I.V., Turchaninova M.A., Bolotin D.A., Putintseva E.V., Lebedev Y.B., Chudakov D.M. // *Front. Immunol.* 2013. V. 4. P. 456.
20. Britanova O.V., Shugay M., Merzlyak E.M., Staroverov D.B., Putintseva E.V., Turchaninova M.A., Mamedov I.Z., Pogorelyy M.V., Bolotin D.A., Izraelson M., et al. // *J. Immunol.* 2016. V. 196. № 12. P. 5005–5013.
21. Britanova O.V., Putintseva E.V., Shugay M., Merzlyak E.M., Turchaninova M.A., Staroverov D.B., Bolotin D.A., Lukyanov S., Bogdanova E.A., Mamedov I.Z., et al. // *J. Immunol.* 2014. V. 192. № 6. P. 2689–2698.
22. Komech E.A., Pogorelyy M.V., Egorov E.S., Britanova O.V., Rebrikov D.V., Bochkova A.G., Shmidt E.I., Shostak N.A., Shugay M., Lukyanov S., et al. // *Rheumatology (Oxford).* 2018. V. 57. № 6. P. 1097–1104.
23. Deodhar A., Yu D. // *Semin. Arthritis Rheum.* 2017. V. 47. № 3. P. 343–350.
24. Mamedov I.Z., Britanova O.V., Bolotin D.A., Chkalina

## RESEARCH ARTICLES

- A.V., Staroverov D.B., Zvyagin I. V., Kotlobay A.A., Turchaninova M.A., Fedorenko D.A., Novik A.A., et al. // *EMBO Mol. Med.* 2011. V. 3. № 4. P. 201–207.
25. Swart J.F., Delemarre E.M., van Wijk F., Boelens J.-J., Kuball J., van Laar J.M., Wulfraat N.M. // *Nat. Rev. Rheumatol.* 2017. V. 13. № 4. P. 244–256.
26. Kanakry C.G., Ganguly S., Luznik L. // *Oncoimmunology.* 2015. V. 4. № 3. P. e974393.
27. van Wijk F., Roord S.T., Vastert B., de Kleer I., Wulfraat N., Prakken B.J. // *Autoimmunity.* 2008. V. 41. № 8. P. 585–591.
28. Grant C.R., Liberal R., Mieli-Vergani G., Vergani D., Longhi M.S. // *Autoimmun. Rev.* 2015. V. 14. № 2. P. 105–116.
29. Delemarre E.M., van den Broek T., Mijnheer G., Meeding J., Wehrens E.J., Olek S., Boes M., van Herwijnen M.J.C., Broere F., van Royen A., et al. // *Blood.* 2016. V. 127. № 1. P. 91–101.

# 1-(4-Phenoxybenzyl) 5-Aminouracil Derivatives and Their Analogues – Novel Inhibitors of Human Adenovirus Replication

N. A. Nikitenko<sup>1</sup>, E. S. Gureeva<sup>2</sup>, A. A. Ozerov<sup>2</sup>, A. I. Tikhvatulin, F. M. Izhaeva<sup>1</sup>, V. S. Prassolov<sup>3</sup>, P. G. Deryabin<sup>1</sup>, M. S. Novikov<sup>2</sup>, D. Y. Logunov<sup>1</sup>

<sup>1</sup>N.F. Gamaleya Federal National Research Center for Epidemiology and Microbiology, Gamaleya Str. 18, Moscow, 123098, Russia

<sup>2</sup>Volgograd State Medical University, Pavshih Bortsov Sq. 1, Volgograd, 400131, Russia

<sup>3</sup>Engelhardt Institute of Molecular Biology, Russian Academy of Sciences, Vavilova Str. 32, Moscow, 119991, Russia

\*E-mail: nanthalia@gmail.com

Received October 11, 2017; in final form April 26, 2018

Copyright © 2018 Park-media, Ltd. This is an open access article distributed under the Creative Commons Attribution License, which permits unrestricted use, distribution, and reproduction in any medium, provided the original work is properly cited.

**ABSTRACT** Adenovirus infections are characterized by widespread distribution. The lack of causal therapy, which is effective in treating this group of diseases, explains the need for new therapeutic drugs. Notably, anti-adenoviral activity of [4-(phenoxy)benzyl]-5-(phenylamino)-6-azauracil, 1-[4-(phenoxy)benzyl]-5-(morpholino) uracil, 1-[4-(4-chlorophenoxy)benzyl]-5-(morpholino) uracil, and 1-[4-(4-fluorophenoxy)-benzyl]-5-(morpholino) uracil was observed.

**KEYWORDS** Human adenovirus, 5-aminouracil derivatives, adenovirus replication, inhibitors of adenovirus replication.

**ABBREVIATIONS** HAdV – human adenovirus, HIV – human immunodeficiency virus, HMDS – hexamethyldisilazane.

## INTRODUCTION

Human adenoviruses (HAdV) are nonenveloped viruses, and their genome is linear nonsegmented double-stranded DNA [1]. Adenovirus infections, which affect persons of all ages, are widespread and highly contagious. Human adenoviruses most often affect the mucous membranes of the respiratory tract [2, 3], eye [4], gastrointestinal tract [5], and genitourinary system [6]. The most dangerous manifestations of adenovirus infections occur in immunocompromised patients (recipients of hematopoietic stem cell transplant, HIV-infected individuals, etc.) [7, 8], in whom they can lead to the development of acute infectious diseases resulting in fatal outcomes [9].

At the moment, there are no selective chemotherapeutic agents that are highly effective against adenoviral infections [10]. Typically, a broad spectrum of antiviral agents is used, such as interferon or interferon inducers and corticosteroid medications [11]. However, interferon inducers are not effective enough, since adenoviruses are insensitive to interferon. The derivatives of acyclonucleotides, such as cidofovir, also display low activity; e.g., the use of (S)-1-(3-hy-

droxy-2-phosphonylmethoxypropyl) cytosine [12] is limited by its high nephrotoxicity [13]. Therefore, the development of low-toxic chemotherapy drugs that are effective against adenoviral infections remains relevant.

The purpose of our work was to study the inhibitory properties of new 5-amino derivatives of uracil [14] against human adenoviruses. Based on an analysis of the relationship between the structure and biological activity of uracil derivatives studied earlier [15], new 5-aminouracil derivatives which can presumably inhibit DNA-containing viruses were constructed and synthesized. It was shown that these compounds are highly effective in suppressing the replication of human adenoviruses *in vitro*. In addition, we studied the relationships between anti-adenoviral effect and the presence of various substituents in the structure. For example, we identified the key role of the aromatic fragment in the potency of the anti-adenoviral activity. Therefore, a new type of inhibitors of human adenovirus replication has been identified. The data obtained can contribute to the development of novel antiviral therapy *in vivo*.

**EXPERIMENTAL**

The  $^1\text{H}$  and  $^{13}\text{C}$  NMR spectra were recorded on a Bruker Avance 400 spectrometer (Bruker, Germany) (400 MHz for  $^1\text{H}$  and 100 MHz for  $^{13}\text{C}$ ) in  $\text{DMSO}-\text{D}_6$ , with tetramethylsilane as the internal standard. Thin layer chromatography was performed on TLS Silica gel 60  $\text{F}_{254}$  (Merck, Germany) plates using ethyl acetate as the eluent. The plates were developed using a UV lamp VL-6.LC (Vilber, France). Melting points were measured in glass capillaries on a Mel-Temp 3.0 instrument (Laboratory Devices Inc., USA).

The starting 5-(phenylamino) uracils and -6-azauracils were synthesized according to [16], 5-(morpholino) uracil – according to [17], 4-(phenoxy)benzyl bromides were obtained by brominating the starting 4-(phenoxy)toluenes with molecular bromine by irradiation with light in boiling chloroform in accordance with [14]. Synthesis of the starting 1-[ $\omega$ -(phenoxy)-alkyl]-5-bromouracils was carried out by condensing equimolar amounts of 2,4-bis(trimethylsilyloxy)-5-bromopyrimidine and 1-bromo- $\omega$ -(phenoxy) alkane through heating to 160–170 °C for 1 hour according to [18].

**The general method for the synthesis of 1-[4-(phenoxy)benzyl]-5-amino-6-azauracil (compounds 1, 2) and -uracil derivatives (compounds 3 - 5).**

A suspension of 4.90 mmol of 5-amino-6-azauracil or 5-aminouracil and 0.1 g (1.87 mmol) of  $\text{NH}_4\text{Cl}$  in 30 ml of hexamethyldisilazane (HMDS) was boiled for 12 hours until a clear solution formed. Excess HMDS was removed under reduced pressure, the residue was dissolved in 50 ml of anhydrous 1,2-dichloroethane, and 4.94 mmol of 4-(phenoxy)benzyl bromide was added to the solution, after which the mixture was boiled for 24 hours while protected from air moisture. The reaction mass was cooled to room temperature, treated with 10 ml of isopropyl alcohol, evaporated under reduced pressure, and the residue was purified by flash chromatography, eluting with chloroform-methanol (10:1). The fractions containing the product were combined and evaporated to dryness under reduced pressure. The solid residue was recrystallized from ethyl acetate-hexane (2:1).

*1-[4-(Phenoxy)benzyl]-5-(phenylamino)-6-azauracil (1)*. Yield 67%,  $T_{\text{mp}}$  264–266°C,  $R_f$  0.76 (ethyl acetate).  $^1\text{H}$ -NMR ( $\text{DMSO}-\text{D}_6$ ),  $\delta$ , ppm: 4.95 (2H, s,  $\text{CH}_2$ ); 6.89–7.03 (5H, m, H-2', H-3', H-4', H-5', H-6'); 7.10 (1H, t,  $J = 7.1$  Hz, H-4''); 7.22 (2H, t,  $J = 7.6$  Hz, H-3''', H-5'''); 7.33 (2H, t,  $J = 7.7$  Hz, H-3'', H-5''); 7.38 (2H, d,  $J = 8.2$  Hz, H-2'', H-6''); 7.61 (2H, d,  $J = 7.8$  Hz, H-2''', H-6'''); 8.33 (1H, s,  $\text{N}^3\text{H}$ );  $^{13}\text{C}$ -NMR ( $\text{DMSO}-\text{D}_6$ ),  $\delta$ , ppm:

52.7; 119.0; 119.1; 119.3; 122.4; 123.9; 128.9; 130.3; 130.4; 132.5; 139.8; 140.0; 148.0; 154.7; 156.8; 157.3.

*1-[4-(Phenoxy)benzyl]-5-[(3,5-dichlorophenyl)amino]-6-azauracil (2)*. Yield 56%,  $T_{\text{mp}}$  224.5–226°C,  $R_f$  0.78 (ethyl acetate).  $^1\text{H}$ -NMR-spectrum ( $\text{DMSO}_6$ ),  $\delta$ , ppm: 4.95 (2H, s,  $\text{CH}_2$ ); 6.93–6.98 (4H, m, H-2''', H-4''', H-6''', NH); 7.10 (1H, t,  $J = 6.9$  Hz, H-4'); 7.22 (2H, t,  $J = 7.6$  Hz, H-3', H-5'); 7.33 (2H, d,  $J = 7.5$  Hz, H-2', H-6'); 7.39 (2H, d,  $J = 8.2$  Hz, H-3'', H-5''); 7.61 (2H, d,  $J = 7.8$  Hz, H-2'', H-6''); 8.33 (1H, s,  $\text{N}^3\text{H}$ );  $^{13}\text{C}$ -NMR-spectrum ( $\text{DMSO}-\text{D}_6$ ),  $\delta$ , ppm: 31.1; 36.1; 40.3; 51.9; 116.9; 118.9; 120.9; 123.8; 130.3; 130.5; 132.0; 134.2; 139.6; 142.1; 147.9; 154.3.

*1-[4-(Phenoxy)benzyl]-5-(morpholino)uracil (3)*. Yield 68%,  $T_{\text{mp}}$  182–184°C,  $R_f$  0.41 (ethyl acetate).  $^1\text{H}$ -NMR ( $\text{DMSO}-\text{D}_6$ ),  $\delta$ , ppm: 2.82 (4H, s,  $2 \times \text{CH}_2$ ); 3.64 (4H, t,  $J = 4.4$  Hz,  $2 \times \text{CH}_2$ ); 4.82 (2H, s,  $\text{CH}_2$ ); 6.96 (2H, d,  $J = 8.3$  Hz, H-2', H-6'); 6.98 (2H, d,  $J = 8.0$  Hz, H-3'', H-5''); 7.13 (1H, t,  $J = 8.0$  Hz, H-4'); 7.18 (1H, s, H-6); 7.32–7.36 (4H, m, H-3', H-5', H-2'', H-6''); 11.37 (1H, s,  $\text{N}^3\text{H}$ ).  $^{13}\text{C}$ -NMR ( $\text{DMSO}-\text{D}_6$ ),  $\delta$ , ppm: 40.3; 50.2; 50.4; 66.3; 118.9; 119.0; 123.9; 127.2; 129.7; 130.2; 130.4; 132.3; 150.1; 156.5; 156.8; 161.2.

*1-[4-(4-Chlorophenoxy)benzyl]-5-(morpholino)uracil (4)*. Yield 81%,  $T_{\text{mp}}$  204–206°C,  $R_f$  0.32 (ethyl acetate).  $^1\text{H}$ -NMR-spectrum ( $\text{DMSO}-\text{D}_6$ ),  $\delta$ , ppm: 2.82 (4H, s,  $2 \times \text{CH}_2$ ); 3.64 (4H, s,  $2 \times \text{CH}_2$ ); 4.80 (2H, s,  $\text{CH}_2$ ); 6.80 (2H, d,  $J = 7.6$  Hz, H-2', H-6'); 7.12 (2H, d,  $J = 7.4$  Hz, H-3', H-5'); 7.39 (2H, d,  $J = 8.2$  Hz, H-3'', H-5''); 7.61 (2H, d,  $J = 7.8$  Hz, H-2'', H-6''); 7.70 (1H, s, H-6); 11.42 (1H, s,  $\text{N}^3\text{H}$ ).  $^{13}\text{C}$ -NMR-spectrum ( $\text{DMSO}-\text{D}_6$ ),  $\delta$ , ppm: 50.1; 50.5; 67.0; 118.8; 121.1; 122.5; 123.2; 124.5; 134.0; 134.1; 138.5; 149.8; 154.2; 160.1; 164.2.

*1-[4-(4-Fluorophenoxy)benzyl]-5-(morpholino)uracil (5)*. Yield 74%,  $T_{\text{mp}}$  220–222°C,  $R_f$  0.34 (ethyl acetate).  $^1\text{H}$ -NMR-spectrum ( $\text{DMSO}-\text{D}_6$ ),  $\delta$ , ppm: 2.85 (4H, s,  $2 \times \text{CH}_2$ ); 3.66 (4H, s,  $2 \times \text{CH}_2$ ); 4.79 (2H, s,  $\text{CH}_2$ ); 6.79 (2H, d,  $J = 7.9$  Hz, H-2', H-6'); 7.11 (2H, d,  $J = 7.4$  Hz, H-3', H-5'); 7.36 (2H, d,  $J = 8.2$  Hz, H-3'', H-5''); 7.60 (2H, d,  $J = 7.9$  Hz, H-2'', H-6''); 7.69 (1H, s, H-6); 11.47 (1H, s,  $\text{N}^3\text{H}$ ).  $^{13}\text{C}$ -NMR-spectrum ( $\text{DMSO}-\text{D}_6$ ),  $\delta$ , ppm: 50.2; 50.6; 67.0; 118.8; 121.1; 122.5; 123.2; 124.5; 134.0; 134.1; 138.5; 149.8; 154.0; 154.2; 158.8; 160.1; 164.2.

**The general method for the synthesis of 1-[ $\omega$ -(phenoxy)alkyl]-5-(morpholino)uracil (compounds 6–8).**

A mixture of 4.61 mmol of 5-bromo-1-[ $\omega$ -(phenoxy)alkyl]uracil and 1 ml (11.56 mmol) of morpholine was boiled in a solution of 50 ml of anhydrous ethylene glycol for 2 hours, cooled down to room temperature, 250 ml of cold water was added to the mixture, and it

was left overnight at a temperature of 4 °C. The precipitate formed was filtered and recrystallized from ethyl acetate-hexane (3:1).

**1-[3-(Phenoxy)propyl]-5-(morpholino)uracil (6).** Yield 66%,  $T_{mp}$  169–170 °C,  $R_f$  0.31 (ethyl acetate). <sup>1</sup>H-NMR-spectrum (DMSO- $D_6$ ),  $\delta$ , ppm: 2.04 (2H, q,  $J$  = 6.3 Hz,  $CH_2$ ); 3.77 (2H, t,  $J$  = 6.0 Hz,  $NCH_2$ ); 3.87 (2H, t,  $J$  = 5.7 Hz,  $CH_2$ ); 2.82 (4H, c,  $2 \times CH_2$ ); 3.69 (4H, c,  $2 \times CH_2$ ); 6.82–6.86 (3H, m, H-2', H-4', H-6'); 7.19 (2H, t,  $J$  = 8.0 Hz, H-3', H-5'); 7.63 (1H, s, H-6); 11.37 (1H, s,  $N^3H$ ). <sup>13</sup>C-NMR-spectrum (DMSO- $D_6$ ),  $\delta$ , ppm: 28.0; 45.4; 50.1; 50.5; 64.6; 100.9; 112.2; 122.3; 138.6; 145.8; 151.0; 158.4; 163.9.

**1-[4-(Phenoxy)butyl]-5-(morpholino)uracil (7).** Yield 78%,  $T_{mp}$  156–159 °C,  $R_f$  0.65 (ethyl acetate). <sup>1</sup>H-NMR-spectrum (DMSO- $D_6$ ),  $\delta$ , ppm: 1.64 (4H, s,  $CH_2$ ); 3.67 (2H, t,  $J$  = 6.2 Hz,  $CH_2$ ); 3.89 (2H, t,  $J$  = 6.2 Hz,  $CH_2$ ); 2.85 (4H, s,  $2 \times CH_2$ ); 3.66 (4H, s,  $2 \times CH_2$ ); 6.79–6.83 (3H, m, H-2', H-4', H-6'); 7.13 (2H, t,  $J$  = 8.1 Hz, H-3', H-5'); 7.64 (1H, s, H-6); 11.41 (1H, s,  $N^3H$ ). <sup>13</sup>C-NMR-spectrum (DMSO- $D_6$ ),  $\delta$ , ppm: 25.3; 25.7; 47.3; 50.4; 51.0; 66.8; 100.9; 114.4; 120.5; 129.5; 145.7; 151.0; 158.6; 165.8.

**1-[5-(Phenoxy)pentyl]-5-(morpholino)uracil (8).** Yield 71%,  $T_{mp}$  162–163.5 °C,  $R_f$  0.78 (ethyl acetate). <sup>1</sup>H-NMR-spectrum (DMSO- $D_6$ ),  $\delta$ , ppm: 1.39 (2H, q,  $J$  = 5.3 Hz,  $CH_2$ ); 1.63 (2H, q,  $J$  = 7.2 Hz,  $CH_2$ ); 1.72 (2H, q,  $J$  = 7.2 Hz,  $CH_2$ ); 3.67 (2H, t,  $J$  = 7.2 Hz,  $CH_2$ ); 3.93 (2H, t,  $J$  = 6.5 Hz,  $CH_2$ ); 2.88 (4H, s,  $2 \times CH_2$ ); 3.67 (4H, s,  $2 \times CH_2$ ); 6.83–6.88 (3H, m, H-2', H-4', H-6'); 7.22 (2H, t,  $J$  = 8.0 Hz, H-3', H-5'); 7.55 (1H, s, H-6); 11.29 (1H, s,  $N^3H$ ). <sup>13</sup>C-NMR-spectrum (DMSO- $D_6$ ),  $\delta$ , ppm: 22.9; 28.6; 28.7; 47.8; 50.5; 51.0; 67.5; 101.2; 114.8; 120.8; 129.9; 146.2; 151.4; 159.0; 164.3.

## Viruses

A recombinant human type 5 adenovirus, expressing an enhanced green fluorescent protein (HAdV5-eGFP), was used in the study [19, 20].

## Cell culture

HEK293 (human embryonic kidney) cells were used in the study [21]. HEK293 cells were cultivated in DMEM (Life Technologies UK) containing 10% fetal bovine serum (Life Technologies, UK), 4 mM *L*-glutamine, 1 mM sodium pyruvate, streptomycin/penicillin at a concentration of 100 µg/ml and 100 units/ml, respectively, at a temperature of 37 °C in an atmosphere of 5%  $CO_2$ .

## MTT Assay

HEK293 cells were incubated in the absence (control) or presence of various concentrations of the

test compounds. After 24–72 h, 3-[4,5-dimethylthiazolyl-2-yl]-2,5-diphenyltetrazolium bromide (MTT) was added to the cells; the final concentration of MTT was 0.5 mg/ml. After 2 hours of incubation at 37 °C, the living cells reduced the yellow MTT to dark-purple formazan granules. The culture medium was removed. The formazan granules were dissolved in DMSO, the amount of the reduced product was measured photometrically on a multi-function plate reader Synergy 2 Multi-Mode Reader (BioTek Instruments, USA) at 540 and 630 nm wavelengths [22].

## Resazurin Assay

HEK293 cells were incubated in the absence (control) or presence of various concentrations of the test compounds. After 24–72 h, a resazurin dye (Sigma, USA) was added to the cells and was reduced by mitochondrial dehydrogenases of living cells to a fluorescent resarufin product (at excitation and emission wavelengths of 530 and 590 nm). Fluorescence intensity was recorded on a multi-function plate reader Synergy 2 Multi-Mode Reader (BioTek Instruments, USA).

## Determination of human adenovirus genome copy number

To estimate the replication of HAdV5-eGFP 24 h after infection, the cells were harvested by trypsinization and total DNA was extracted with the QIAamp DNA Mini Kit (QIAGEN, Germany). Real-time qPCR was performed according to [23] on the CFX96™ Real-Time PCR Detection System (Bio-Rad, USA) using the iTaq™ Universal Probes Supermix reagent (Bio-Rad, USA).

## Titration of progeny viruses

HEK293 cells were transduced with HAdV5-eGFP at multiplicities of infection of 1 and 10 PFU/cell. Three hours post transduction, solutions of the compounds **1** and **3** in DMSO at a concentration of 25 µM were added. DMSO was used as the control, and its final concentration in the culture medium did not exceed 0.1%. After 48 hours, the culture medium was collected in microtubes and frozen at -70 °C. To destroy cells, the virus-containing medium was thawed at room temperature and again frozen at -70 °C. After repeated thawing, aliquots of 10-fold dilutions of virus stocks were added to the HEK293 cells.

## Statistical analysis

All data are presented as a mean  $\pm$  standard deviation (SD). The statistical significance was determined using the GraphPad Prism 6 software (GraphPad Software, USA). A value of  $p < 0.05$  was considered statistically significant.

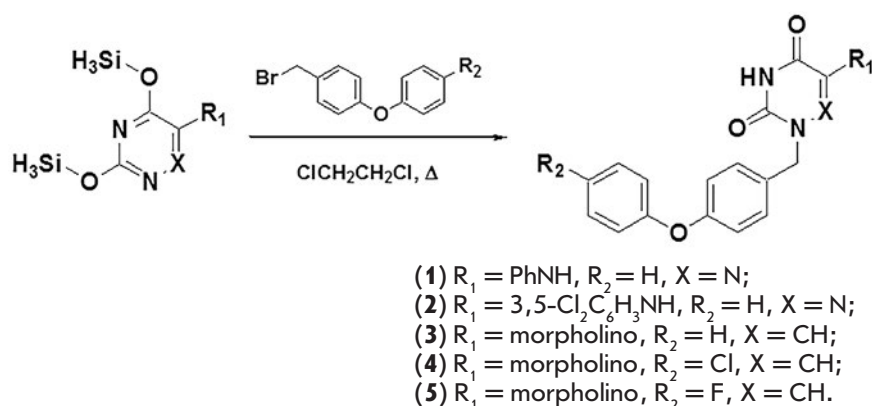


**Fig. 1.** Scheme for the synthesis of 1-[4-(phenoxy)benzyl]-5-(phenylamino)-6-azauracil (**1**), 1-[4-(phenoxy)benzyl]-5-[(3,5-dichlorophenyl)amino]-6-azauracil (**2**), and 1-[4-(phenoxy)benzyl]-5-[(3,5-dichlorophenyl)amino]-6-azauracil (**3**), 1-[4-(4-chlorophenoxy)benzyl]-5-(morpholino)uracil derivatives (**4**), 1-[4-(4-fluorophenoxy)benzyl]-5-(morpholino)uracil derivatives (**5**).

## RESULTS AND DISCUSSION

### Synthesis of the compounds

In terms of chemical structure, the synthesized compounds are most similar to 1-benzyl-5-(arylamino)uracil derivatives [15]. These derivatives are active against human immunodeficiency virus type 1 (HIV-1) and the Epstein-Barr virus. We assumed that the 5-aminouracil and 5-amino-6-azauracil derivatives containing a substituent on  $N^1$  and analogous to the described compounds can exhibit inhibitory activity against DNA-containing viruses: in particular, adenoviruses.

The synthesis of 1-[4-(phenoxy)benzyl]-5-(phenylamino)-6-azauracil (**1**) and 1-[4-(phenoxy)benzyl]-5-[(3,5-dichlorophenyl)amino]-6-azauracil (**2**), as well as 1-[4-(phenoxy)benzyl]-5-[(3,5-dichlorophenyl)amino]-6-azauracil (**3**), 1-[4-(4-chlorophenoxy)benzyl]-5-(morpholino)uracil (**4**) and 1-[4-(4-fluorophenoxy)benzyl]-5-(morpholino)uracil (**5**) derivatives, was accomplished by condensation of 6-amino-3,5-bis(trimethylsilyloxy)-1,2,4-triazine or 5-amino-2,4-bis(trimethylsilyloxy)pyrimidine with an equimolar amount of the corresponding 4-(phenoxy)benzyl bromides through boiling in an anhydrous 1,2-dichloroethane solution in accordance with the previously de-

scribed method [24]. The yield of compounds **1–5** was 56–81% (Fig. 1).

In order to study the relationships between the structure and antiviral activity, we synthesized analogues of the 5-(morpholino) derivative **3** in which the 4-(phenoxy)benzyl fragment at  $N^1$  was replaced with a  $\omega$ -(phenoxy)alkyl substituent. The synthesis of this group of compounds was carried out by amination of 5-bromo-1- $\omega$ -(phenoxy)alkyluracil by morpholine through boiling in an ethylene glycol solution in accordance with the previously described method [15]. The yield of the target 5-(morpholino)uracil derivatives **6–8** was 66–78% (Fig. 2).

### Cytotoxicity of the test compounds

The cytotoxicity of the compounds was assessed by intravital staining of the HEK293 cells with MTT or trypan blue [25]. The test compounds in DMSO were added to the cells in a concentration range of 2.5–200  $\mu\text{M}$ . The cells to which the appropriate amount of DMSO was added were used as a control.

Intravital staining of the HEK293 cells by MTT was carried out 48 hours after the administration of the compounds. The toxicity of different doses of the

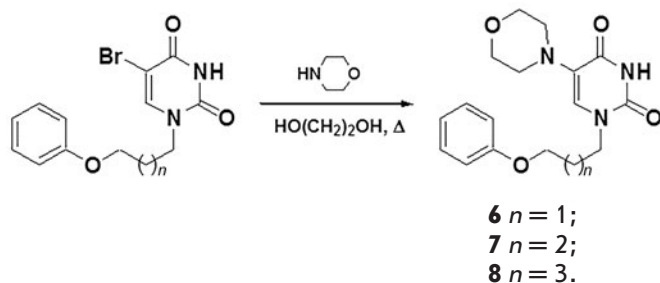


**Fig. 2.** Scheme for the synthesis of 5-(morpholino)uracil derivatives **6–8**

**Table 1.** Anti-adenoviral activity of 5-aminouracil derivatives

| Compound | $\text{IC}_{50}$ , $\mu\text{M}^a$ | $\text{TC}_{50}$ , $\mu\text{M}^b$ | $\text{SI}^c$ |
|----------|------------------------------------|------------------------------------|---------------|
| 1        | 9.2                                | 53.6                               | 5.8           |
| 3        | 0.5                                | 47.6                               | 95            |
| 4        | 8.7                                | 103.1                              | 11.9          |
| 5        | 13.1                               | 64.8                               | 4.9           |

<sup>a</sup>Concentration of half maximal inhibition at which the relative HAdV5-eGFP genome copy number is reduced by 50% compared to the control.

<sup>b</sup>Concentration at which the number of living cells is reduced by 50%.

<sup>c</sup>Ratio of the compound  $\text{TC}_{50}$  to its  $\text{IC}_{50}$ .

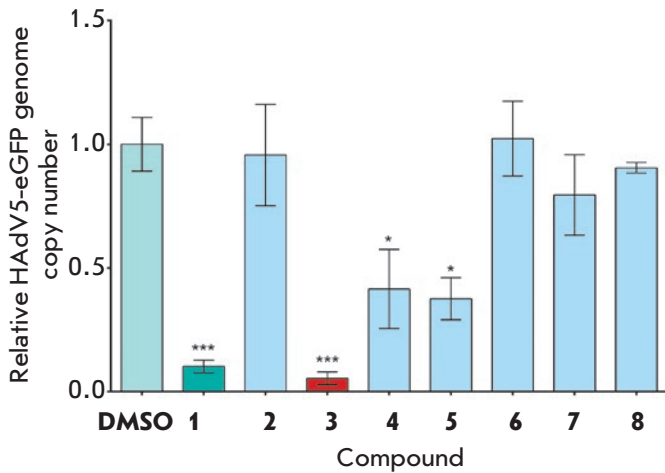


**Fig. 3.** Assessment of the relative HAdV5-eGFP genome copy number in HEK293 cells treated with the test compounds. The differences between experimental and control samples were statistically significant at \*  $p < 0.05$ ; \*\*\*  $p < 0.001$ .

compounds was determined by the viability of the cells compared to the control. All compounds at concentrations of up to 25  $\mu\text{M}$  had no toxic effect on HEK293 cells. In addition, a concentration at which the number of living cells reduced by 50% was determined for the compounds showing inhibitory activity against human adenoviruses ( $\text{TC}_{50}$ ). To this end, the cells selectively stained with trypan blue were counted 48 hours after the addition of the compounds. The results are shown in *Table 1*.

#### Anti-adenoviral activity of 5-aminouracil derivatives

During the evaluation of the anti-adenoviral activity of 5-aminouracil derivatives, the HEK293 cells were transduced with recombinant type 5 human adenovirus expressing the enhanced green fluorescent protein HAdV5-eGFP with a multiplicity of infections of 1 PFU/cell. The test compounds were added to the cells at a concentration of 25  $\mu\text{M}$  3 h post-transduction to give the recombinant adenovirus enough time to un-

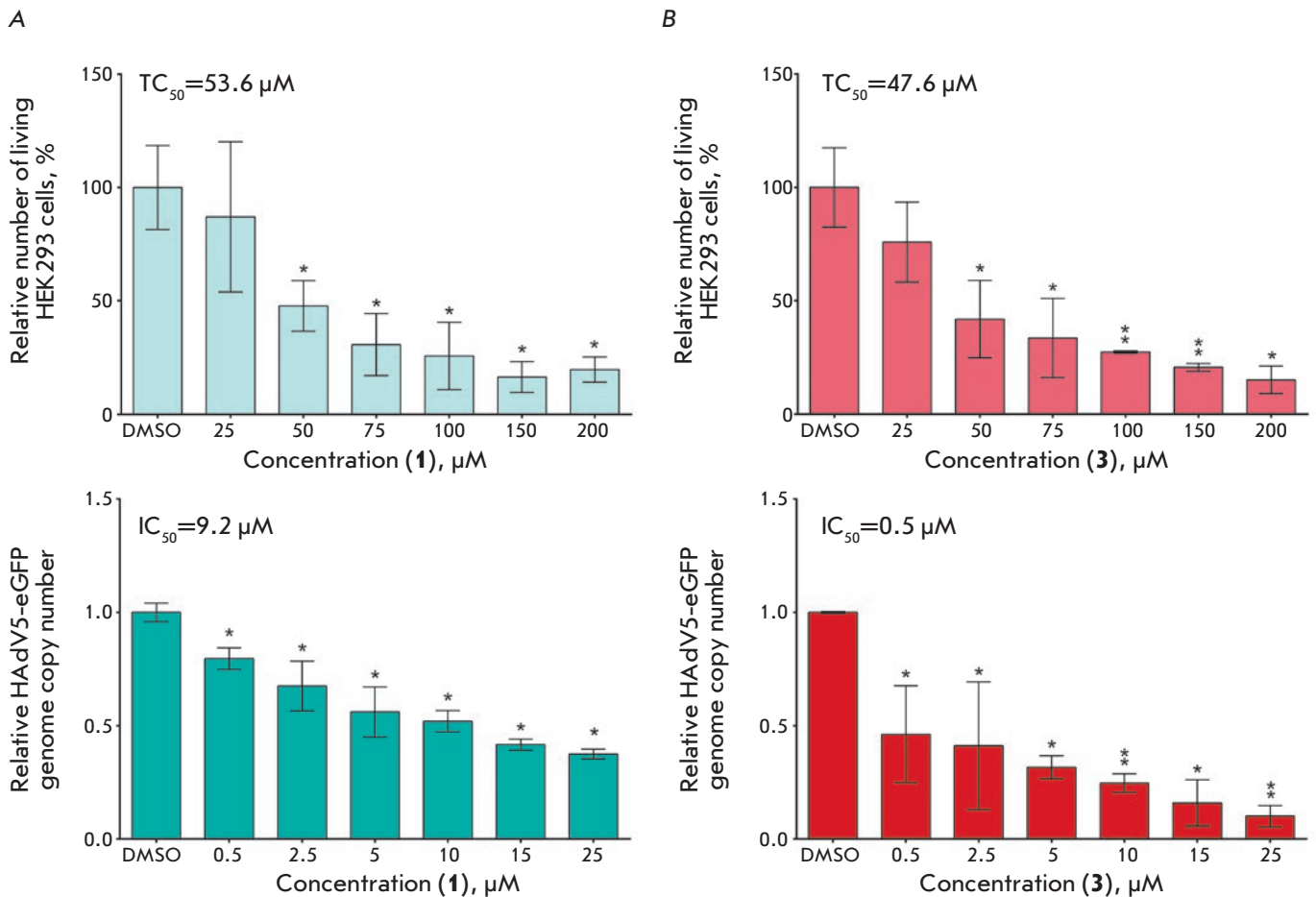


**Fig. 4.** Anti-adenoviral activity of 5-aminouracil derivatives.  $\text{TC}_{50}$  and  $\text{IC}_{50}$  of compounds **1** (A) and **3** (B). Differences between experimental and control samples were statistically significant at \*  $p < 0.05$ ; \*\*\*  $p < 0.001$ .

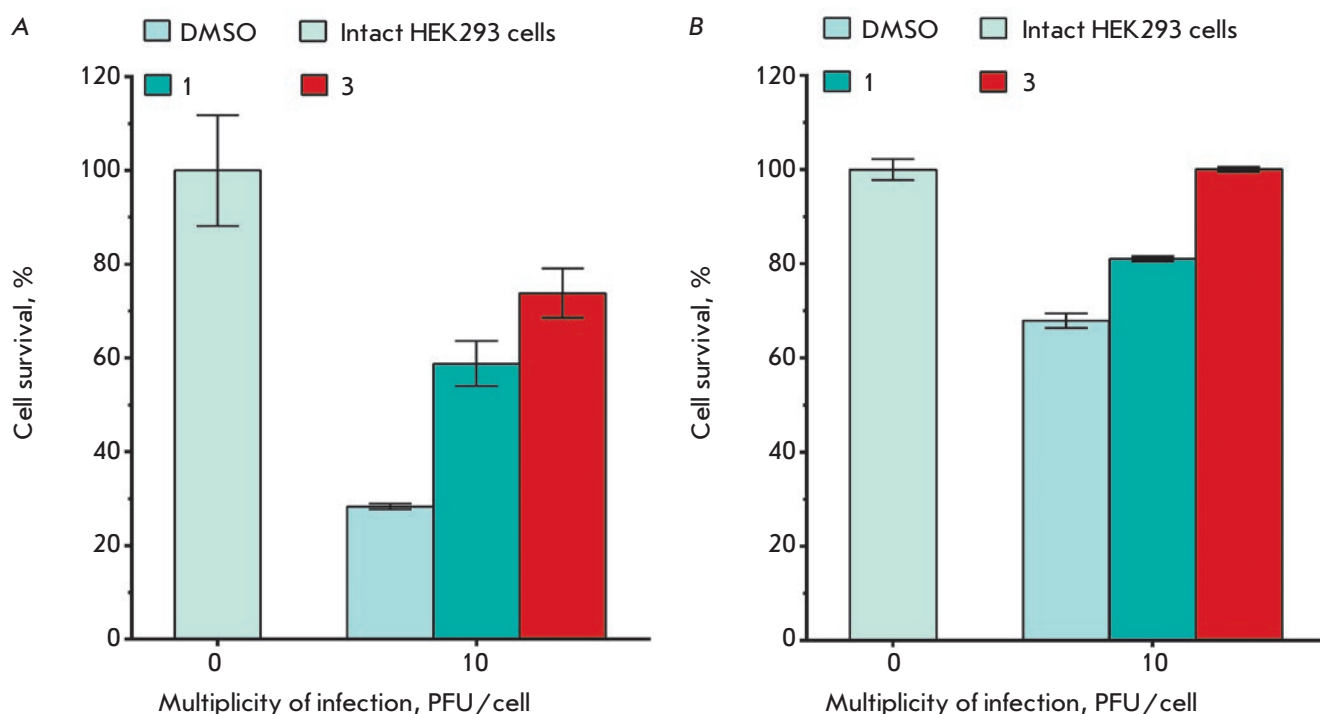


**Fig. 5.** The survival of HEK293 cells transduced with HAdV5-eGFP and treated with the 5-aminouracil derivatives **1** and **3**. (A) The results were obtained using the MTT assay. 100% corresponds to optical density value of intact HEK293 cells (control sample). All reported values are means of three independent measurements with standard deviations. The differences between experimental and control samples were statistically significant in all cases ( $p < 0.05$ ). (B) Data was obtained using the resazurin assay. One hundred percent corresponds to the fluorescence intensity of intact HEK293 cells (control sample). All reported values are means of three independent measurements with standard deviations. The differences between DMSO samples and other samples were statistically significant in all cases ( $p < 0.05$ ). The differences between intact cells samples and samples of group "3" were statistically insignificant.

dergo the initial stage of the replication cycle (the interaction of the virus with cell surface receptors and penetration into the cell). DMSO was used as a negative control. The concentration of DMSO in all samples did not exceed 0.1%. To assess the inhibitory activity of the compounds, newly synthesized HAdV5-eGFP genomes were detected via real-time qPCR 24 hours later [23]. It has been shown that compounds **1**, **3**, **4** and **5** display marked inhibitory activity with respect to HAdV5-eGFP replication (*Fig. 3*).

A concentration corresponding to the half-maximal inhibition ( $IC_{50}$ ) at which the relative HAdV5-eGFP genome copy number was reduced by 50% compared to the control was determined for compounds **1**, **3**, **4** and **5**, which display inhibitory activity against human adenovirus. HEK293 cells were transduced by HAdV5-eGFP with a multiplicity of infections of 1 PFU/cell. Three hours post-transduction, the test compounds were added to the cells at concentrations of 0.5, 2.5, 5, 10, 15 and 25  $\mu$ M. The concentration of DMSO in all samples did not exceed 0.1%. The inhibitory activity of the compounds was assessed 24 hours later by the de-

**Table 2.** Progeny HAdV5-eGFP titer in HEK293 cells

| Multiplicity of infection | Compound          |                   |                   |
|---------------------------|-------------------|-------------------|-------------------|
|                           | DMSO              | 1                 | 3                 |
| MOI 1                     | $1 \times 10^4$   | $5.1 \times 10^3$ | $2.3 \times 10^3$ |
| MOI 10                    | $2.7 \times 10^6$ | $1.7 \times 10^5$ | $3.7 \times 10^5$ |

termination of the HAdV5-eGFP genome copy number via qPCR (*Fig. 4*). The selectivity index (SI) was calculated as the ratio of  $TC_{50}$  of the compound to its  $IC_{50}$  (*Table 1*). These quantitative indices of inhibition can be used as a measure of the tested compounds' effectiveness; i.e., the degree of suppression of HAdV5-eGFP replication in HEK293 cells.

It has been demonstrated that the most potent antiviral effect is exhibited by 5-(morpholino)-derivative **3** with  $IC_{50}$  of 0.5  $\mu$ M, and  $SI = 95$ . The 6-azauracil derivatives were either an order of magnitude less active (compound **1**) or did not display any inhibitory properties at all (compound **2**). It has also been shown that the introduction of a chlorine atom (compound **4**) or a

fluorine atom (compound **5**) into the *para*-position of the 4-(phenoxy)benzyl moiety significantly reduces inhibitory activity. At the same time, the replacement of benzyl in the 4-(phenoxy)benzyl moiety by an aliphatic chain leads to compounds **6–8** which have no anti-adenoviral activity. This fact indicates the high importance of the aromatic fragment in the antiviral properties of series of the tested compounds.

In addition, the impact of the most effective 5-aminouracil derivatives, compounds **1** and **3**, on the production of progeny infectious HAdV5-eGFP was evaluated. A decrease in progeny virus titer was observed for these compounds (Table 2).

Based on the data presented, it can be assumed that the mechanism of action of the series of tested compounds is associated with the inhibition of viral replication key factors, i.e. viral DNA polymerase and products of the *E1A* gene [26, 27].

During the experiment, survival of the HEK293 cells infected with HAdV5 at a multiplicity of infection of 10 PFU/cell in the presence of compounds **1** and **3** was also assessed (Fig. 5). Three hours post infection, solutions of the compounds **1** and **3** in DMSO at a concentration of 25  $\mu$ M were added to the cells. According to

the MTT assay, cell survival 48 hours post infection at a multiplicity of 10 PFU/cell was 74 and 59% in the presence of compounds **1** and **3**, respectively, compared to the control. These data are consistent with the results obtained in a similar analysis of cell survival during adenovirus infection (MOI 10 PFU/cell) using resazurin. For example, after exposure to compounds **1** and **3**, the proportion of living cells did not differ significantly from the proportion in the control sample (Fig. 5). The obtained data indicate that the test compounds possess antiviral properties.

## CONCLUSION

Thus, a new type of anti-adenoviral agents of a non-nucleoside nature has been discovered that exhibit an inhibitory effect on human adenoviruses. Compounds of this series may be promising candidates for the development of drugs effective against adenoviral infections. ●

*This work is supported by grants from the President of the Russian Federation for state support of young Russian scientists (grants MK-1746.2017.7 and MK-2480.2017.7).*

## REFERENCES

- Ghebremedhin B. // Eur. J. Microbiol. Immunol. 2014. V. 4. № 1. P. 26–33.
- Gupta P., Tobias J.D., Goyal S., Hervie P., Harris J.B., Sadot E., Noviski N. // J. Intensive Care Med. 2011. V. 26. № 4. P. 267–272.
- Lu X., Trujillo-Lopez E., Lott L., Erdman D.D. // J. Clin. Microbiol. 2013. V. 51. № 4. P. 1089–1093.
- Gonzalez-Lopez J.J., Morcillo-Laiz R., Munoz-Negrete F.J. // Arch. Soc. Esp. Oftalmol. 2013. V. 88. № 3. P. 108–115.
- Eckardt A.J., Baumgart D.C. // Recent Pat Antiinfect Drug Discov. 2011. V. 6. № 1. P. 54–63.
- Lynch J.P., 3rd, Fishbein M., Echavarria M. // Semin. Respir. Crit. Care Med. 2011. V. 32. № 4. P. 494–511.
- Echavarria M. // Clin. Microbiol. Rev. 2008. V. 21. № 4. P. 704–715.
- Florescu D.F., Hoffman J.A., the AST Infectious Diseases Community of Practice // Am. J. Transplant. 2013. V. 13 Suppl 4. P. 206–211.
- Robinson C.M., Seto D., Jones M.S., Dyer D.W., Chodosh J. // Infect. Genet. Evol. 2011. V. 11. № 6. P. 1208–1217.
- Pihos A.M. // J. Optometry. 2013. V. 6. № 2. P. 69–74.
- Meyer-Rusenberg B., Loderstadt U., Richard G., Kaulfers P.M., Gesser C. // Dtsch Arztebl. Int. 2011. V. 108. № 27. P. 475–480.
- De Clercq E. // Antiviral Res. 2007. V. 75. № 1. P. 1–13.
- Piscitelli S.C., Penzak S.R., Flexner C. // AIDS and Other Manifestations of HIV Infection / Ed. Wormser G. San Diego: Acad. Press, 2004. P. 913–930.
- Novikov M.S., Nikitenko N.A., Ozerov A.A., Gureeva E.S., Prassolov V.S., Prokofjeva M.M., Dzharullaeva A.S., Tukhvatulin A.I., Logunov D.Y. // Patent. 2628456 Russian-Federation. C07D 239/545 (2006.01), A61K 31/513 (2006.01), A61P 31/14 (2006.01) 2016.
- Novikov M.S., Buckheit R.W., Jr., Temburnikar K., Khandzhinskaya A.L., Ivanov A.V., Seley-Radtke K.L. // Bioorg. Med. Chem. 2010. V. 18. № 23. P. 8310–8314.
- Gerns F.R., Perrotta A., Hitchings G.H. // J. Med. Chem. 1966. V. 9. № 1. P. 108–115.
- Phillips A.P. // J. Am. Chem. Soc. 1951. V. 73. № 3. P. 1061–1062.
- Novikov M.S., Babkov D.A., Paramonova M.P., Khandzhinskaya A.L., Ozerov A.A., Chizhov A.O., Andrei G., Snoeck R., Balzarini J., Seley-Radtke K.L. // Bioorganic Med. Chem. 2013. V. 21. № 14. P. 4151–4157.
- Shmarov M.M., Chernova L.V., Shashkova E.V., Logunov D. Y., Verkhovskaya L.V., Kapitonov A.V., Neugodova G.L., Doronin K.K., Naroditsky B.S. // Molecular Genetics, Microbiology and Virology. 2002. V. 17. № 2. P. 30–35.
- Logunov D.Y., Zubkova O.V., Karyagina-Zhulina A.S., Shuvalova E.A., Karpov A.P., Shmarov M.M., Tutykhina I.L., Alyapkina Y.S., Grezina N.M., Zinovieva N.A., et al. // J. Virol. 2007. V. 81. № 18. P. 9641–9652.
- Graham F.L., Smiley J., Russell W.C., Nairn R. // J. Gen. Virol. 1977. V. 36. № 1. P. 59–74.
- Mosmann T. // J. Immunol. Methods. 1983. V. 65. № 1–2. P. 55–63.
- Heim A., Ebnet C., Harste G., Pring-Akerblom P. // J. Med. Virol. 2003. V. 70. № 2. P. 228–239.
- Babkov D.A., Chizhov A.O., Khandzhinskaya A.L., Corona A., Esposito F., Tramontano E., Seley-Radtke K.L., Novikov M.S. // Synthesis. 2015. V. 47. № 10. P. 1413–1422.
- Strober W. // Curr. Protoc Immunol. 2001. Appendix 3. Appendix 3B.
- Nikitenko N.A., Speiseder T., Lam E., Rubtsov P.M., Tonaeva K.D., Borzenok S.A., Dobner T., Prassolov V.S. // Acta Naturae. 2015. V. 7. № 3. P. 100–107.
- Nikitenko N.A., Speiseder T., Groitl P., Spirin P.V., Prokofjeva M.M., Lebedev T.D., Rubtsov P.M., Lam E., Riecken K., Fehse B., et al. // Biochimie. 2015. V. 113. P. 10–16.

# Reversible Cyclic Thermal Inactivation of Oligopeptidase B from *Serratia proteamaculans*

M. V. Ovchinnikova<sup>1,2</sup>, A. G. Mikhailova<sup>1\*</sup>, D. M. Karlinsky<sup>1</sup>, V. A. Gorlenko<sup>2</sup>, L. D. Rumsh<sup>1</sup>

<sup>1</sup>Shemyakin–Ovchinnikov Institute of Bioorganic Chemistry, Russian Academy of Sciences, Miklukho–Maklaya Str. 16/10, Moscow, 117997, Russia

<sup>2</sup>Moscow State Pedagogical University, M. Pirogovskaya Str. 1, bldg. 1, Moscow, 119991, Russia

\*E-mail: anna.mikhailova@ibch.ru

Received January 29, 2018; in final form, May 11, 2018

Copyright © 2018 Park-media, Ltd. This is an open access article distributed under the Creative Commons Attribution License, which permits unrestricted use, distribution, and reproduction in any medium, provided the original work is properly cited.

**ABSTRACT** A unique property was found for oligopeptidase B from *Serratia proteamaculans* (PSP) as well as its mutants: they can undergo reversible thermal inactivation at 37°C, with activity being restored or even increased with respect to the initial one upon subsequent cooling. The process can be repeated several times, with the same results achieved (up to 5 cycles). This effect can be explained by a shift in the equilibrium between the inactive open form of the enzyme and the active closed one upon variation of the incubation temperature.

**KEYWORDS** oligopeptidase B, *Serratia proteamaculans*, thermal inactivation.

**ABBREVIATIONS** PSP – protease from *Serratia proteamaculans*; OpdB – oligopeptidase B; BAPNA – *N*<sub>α</sub>-benzoyl-*D,L*-arginine *p*-nitroanilide; DMSO – dimethyl sulfoxide.

## INTRODUCTION

Oligopeptidase B (OpdB) [EC 3.4.21.83] is a trypsin-like serine peptidase belonging to the prolyl oligopeptidase family. OpdB is present in unicellular eukaryotes, such as trypanosomes *Trypanosoma cruzi* [1], *T. brucei* [2], and *T. evansi* [3], and in leishmania spp. (*Leishmania major* and *L. amazonensis* [4]). OpdB or the genes encoding this enzyme have been detected in prokaryotes, such as *Escherichia coli* [5], *Moraxella lacunata* [6], *Salmonella enterica* serovar *typhimurium* [7], *Yersinia pestis* [7], *Serratia marcescens*, *Stenotrophomonas maltophilia* and *Rhodococcus erythropolis* [8], in mycobacteria *Mycobacterium tuberculosis* and *M. leprae* [7], and in spirochetes *Treponema denticola* [9]. Members of the oligopeptidase B group are also found in some higher plants (e.g., *Ambrosia artemisiifolia* [10]). To date, protozoan OpdB have been the most extensively studied, and the crystal structures of OpdB from *L. major* [11] and *T. brucei* were determined in [12]. Neither the crystal structure nor the enzymological characteristics of most bacterial oligopeptidases B have been determined; only the nucleotide sequences of the genes coding for them are known.

Our study focused on oligopeptidase B from *Serratia proteamaculans* (PSP). The *OpdB S. proteamaculans* 94 gene has been cloned, sequenced, and expressed in *E. coli*; the substrate specificity of OpdB, inhibition, and

effect of calcium ions, pH, and temperature on enzyme activity have been studied [13–18].

All the previously investigated oligopeptidases B, both protozoan and bacterial, are characterized by high thermal stability [5, 19]. PSP is the first known psychrophilic oligopeptidase B. This enzyme is rather quickly inactivated at 37°C; thermal inactivation is independent of buffer nature and occurs identically in the phosphate, imidazole, and Tris-buffers at pH 7.5–8.0 [17]. The intrinsic fluorescence spectra demonstrate that heating at 37°C forces the PSP molecule to unfold, which is accompanied by a reduction in enzyme activity. Calcium ions accelerate and enhance PSP inactivation [17].

When experimentally studying thermal inactivation of PSP, Mikhailova et al. [17] revealed that enzyme activity was restored after some enzyme samples had been incubated at low temperatures. In this work, we thoroughly investigated this phenomenon at  $[Ca^{2+}] = 0$  and 50 mM.

## EXPERIMENTAL

The reagents used were *N*<sub>α</sub>-benzoyl-*D,L*-arginine *p*-nitroanilide (BAPNA) (Sigma, USA); Tris and NaCl (Merck, Germany), glycerol (ICN, USA); dimethyl sulfoxide (DMSO), and *p*'-guanidine benzoic acid *p*-nitrophenyl ester (Fluka, Germany).

Wild-type PSP and point mutants expressed in *E. coli* BL21(DE3) (Novagen) were obtained and purified according to the procedure described in [17, 20].

Optical density was measured on an Eppendorf BioSpectrometer® kinetic spectrophotometer (Germany). Protein concentration was determined by the Bradford protein assay using the Bio-Rad Protein Assay reagent, with BSA used as a reference protein. Molarity of the enzyme solutions was measured by titrating active sites with *p*'-guanidine benzoic acid *p*-nitrophenyl ester [21].

**Activity of the PSP samples** was studied spectrophotometrically at 25°C, using BAPNA (0.2 mM) as a substrate, in 0.1 M Tris-HCl buffer, pH 8.0, containing 50 mM CaCl<sub>2</sub> and 2% DMSO. The increase in optical density at 405 nm, which took place as soon as free *p*-nitroaniline ( $\Delta\epsilon_{405} = 10400 \text{ M}^{-1}\text{cm}^{-1}$ ) had formed, was measured. The initial hydrolysis rates of the substrate (two or three replicas for each reading; the rates differed by no more than 5–10%) were determined from the initial linear section of the kinetic curve (the degree of hydrolysis was  $\leq 10\%$ ).

#### Investigation of the thermal stability of PSP samples

The initial activities of the wild-type enzyme and its mutant variants (0.05 mg/ml = 0.65  $\mu\text{M}$ ) were determined by diluting the stock solution of the enzyme heated to 25°C in the incubation buffer at the same temperature, collecting 5–10  $\mu\text{l}$  aliquots, and measuring the initial hydrolysis rate of BAPNA substrate (0.2 mM; total volume, 1.5 ml). The aliquots of the enzyme solutions (100  $\mu\text{l}$ ; 0.65  $\mu\text{M}$ ) were incubated for a corresponding time at a corresponding temperature: 5–10  $\mu\text{l}$  aliquots were collected in a quartz cell containing BAPNA, and residual activity was measured immediately according to the procedure described above. The control samples of all PSP variants with the same concentration (0.05 mg/ml = 0.65  $\mu\text{M}$ ) were incubated at 25 and 4°C for a corresponding time according to the same procedure as the one used for the experimental specimens (except for heating), and their activity was determined.

## RESULTS AND DISCUSSION

A typical feature of the enzymes belonging to the prolyl oligopeptidase family, including OpdB, is that they contain the N-terminal  $\beta$ -propeller domain, which prevents penetration of bulky globular proteins into the active site, and the catalytic domain residing in the C-terminal portion of the molecule. Studies focused on the crystal structures of the enzymes belonging to the prolyl oligopeptidase family demonstrated that these proteins exist in the open (inactive) and closed (active)

forms, which exist in equilibrium. The identified crystal structures of protozoan OpdB from *L. major* [11] and *T. brucei* [12] showed that the function of these enzymes depends not only on the amino acid residues comprising the catalytic triad in its active site and the primary substrate-binding site, but also on five inter-domain salt bridges – SB1–SB5 – that involve nine charged amino acid residues. The salt bridge SB1 – E172/179-R650/664 (trypanosomes/leishmania spp.) plays a crucial role: the catalytic triad is either formed or destroyed as the bridge closes or opens when the molecule conformation changes from the open inactive form to the closed active one, respectively, and vice versa. The salt bridges SB1–SB5 are strictly conserved in all protozoan OpdB.

The amino acid sequence of PSP is 35% homologous with respect to those of OpdB from *L. major* and *T. brucei*; the degree of homology is higher in the C-terminal catalytic domain (50%). Meanwhile, the regions of the active site and the primary substrate-binding site in all these enzymes are virtually identical. It turned out, however, that the five functionally important inter-domain salt bridges detected in the protozoan enzymes are not conserved. Only one of them (SB3) is found in PSP and in other known bacterial OpdB. In PSP and the other investigated bacterial OpdB, either uncharged or oppositely charged amino acid residues occupy positions corresponding to five out of the seven charged residues of OpdB from *L. major* and *T. brucei*, which form the salt bridges SB1, SB2, SB4, and SB5. The key salt bridge responsible for enzyme activity is also absent.

In order to elucidate the mechanism of action of PSP, we simulated the crystal structure of the protein in its closed and open forms [20].

As a result, we revealed 12 charged residues forming the structure consisting of inter- and intra-domain salt bridges that are responsible for the structure and activity of PSP. Eight of those (E75, E96, E125, D647, D649, K655, R658, and K660) were replaced with uncharged residues by site-directed mutagenesis. The corresponding mutant enzymes were obtained and characterized; the residues listed above were shown to play an important role. Removal of charged a.a.r. 75, 96, 655, and 658 resulted in enzyme inactivation, while its activity was enhanced after a.a.r. 125 and 649 had been removed. Depending on the substrate used, substitution of a.a.r. 647 and 660 resulted in either a 2- to 3-fold reduction or a 1.5–2 increase in enzyme activity [20].

In this study, we compared the thermal stability of wild-type PSP (wt), four point mutants (D647A, D649A, K655A, and K660A; the charged residues in the His652-loop of PSP being replaced with uncharged ones) and two point mutants (E75A and E125A; the

acidic residues localized in the N-terminal  $\beta$ -propeller domain being replaced with uncharged ones) at  $[Ca^{2+}] = 0$  and 50 mM.

As we have repeatedly demonstrated earlier, activity of wild-type PSP samples [15, 17, 18] and its mutant variants [20] in 0.1 Tris-HCl buffer, pH 8.0, at  $T \leq 25^\circ C$  remains virtually unchanged for an appreciably long time (up to 10–14 days) irrespective of whether  $Ca^{2+}$  ions are absent or present (50 mM). In this study, activity of the initial PSP samples stored at both  $4^\circ C$  and  $25^\circ C$  also remained constant during the entire experiment.

The data shown in Fig. 1 A,B illustrate that calcium ions are a destabilizing factor for all PSP variants. Thermal stability of the E75A and E125A mutants at  $[Ca^{2+}] = 0$  is 20–25 % higher than that of the wild-type enzyme, while the thermal stability of D649A, K655A, K660A and especially D647A mutants is 1.5–2-fold lower (Fig. 1A). At  $[Ca^{2+}] = 50$  mM, the difference in the thermal stability of all PSP variants was less marked, but the E75A mutant was the most thermally labile one (Fig. 1B).

According to the data on the inactivation of PSP and the corresponding mutant variants of this enzyme shown in Fig. 1, we chose to perform incubation at  $37^\circ C$  for 3 h to study the reactivation of PSP variants. After determining the residual activity, enzyme samples were incubated at  $25^\circ C$  (0.5 and 1 h) and their activities were determined; the samples were then left at  $4^\circ C$  for 18–20 h. The activities of the wild-type enzyme and all the mutant variants were found to increase (Fig. 2A–D); for the wt, E125A, and E75A variants; a 1.2–1.8-fold increase in the initial activity of OpdB was systematically observed upon cooling of the partially thermally inactivated sample (Fig. 2A–C). Upon cooling, the activity of D649A was as high as 100–107% (Fig. 2D).

It is even more interesting that these heating–cooling cycles of an aliquot of PSP variants can be repeated (up to 5 times); each cycle involves a drop in activity observed upon heating ( $37^\circ C$ ) and a further increase upon cooling ( $25$  and  $4^\circ C$ ). Upon subsequent cycles (2–5), the restored activity exceeded the initial one to a lesser extent or was hardly higher; the activity of the D649A variants in cycles 4 and 5 after cooling was lower than its initial one (~80%) (Fig. 2D). Similar experiments on the reactivation of the D647A, K655A, and K660A variants also revealed that activity increased as the partially denatured enzyme was cooled; however, reactivation in the first two cycles did not exceed 75–80% of the initial activity of the samples or 45–50% in the subsequent cycles (data are not presented).

Cooling the partially inactivated samples in the presence of calcium ions also led to an increase in activity; however, the activity was lower than 100% of the initial value even after long-term incubation (for several

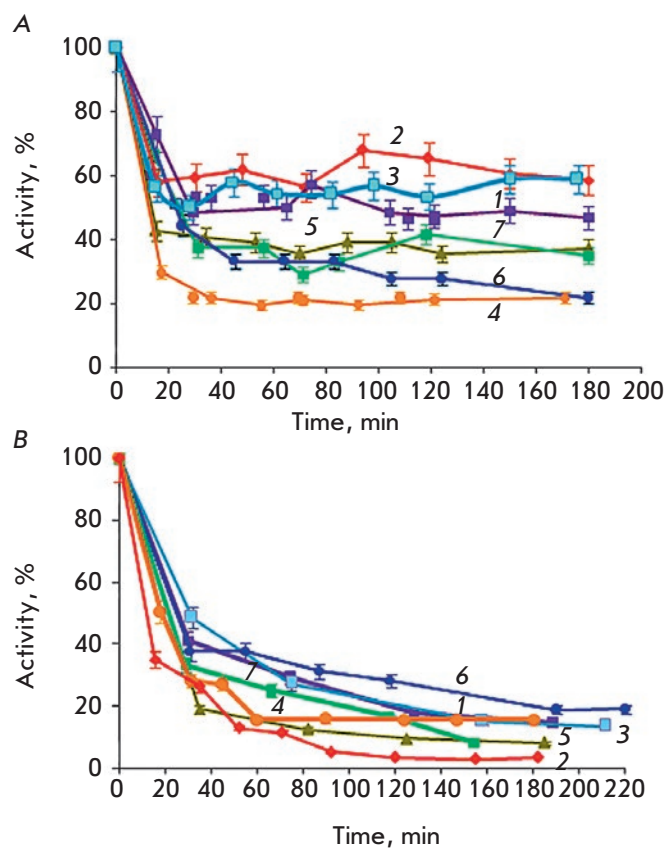


**Fig. 1.** Inactivation of PSP (wt) and the mutant variants of the enzyme (0.65  $\mu M$ ) during incubation at  $37^\circ C$  (0.1 M Tris-HCl buffer pH 8.0; BAPNA substrate) A –  $[Ca^{2+}] = 0$ ; B –  $[Ca^{2+}] = 50$  mM; 1 – wt; 2 – E75A; 3 – E125A; 4 – D647A; 5 – D649A; 6 – K655A; and 7 – K660A. Initial activity ( $v_0/[E]$ ,  $min^{-1}$ ): wt – 739; E75A – 200; E125A – 1846; D647A – 346; D649A – 923; K655A – 300; and K660A – 323.

days) at  $4^\circ C$ : 64% (wt), 36% (D649A), and 28% (E125A) (Fig. 3).

We had previously studied the thermal stability of a PSP molecule by high-sensitivity differential scanning calorimetry (HS-DSC); the results were indicative of a low thermal stability for PSP. The heat capacity curve for the protein featured two peaks with  $T_d = 43.1^\circ C$  (corresponding to the less stable C-terminal catalytic domain) and  $46.3^\circ C$  (the more stable N-terminal  $\beta$ -propeller) [17].

We studied the effect of incubation at  $43^\circ C$  (the denaturation temperature of the C-terminal catalytic domain) for 0.5 h, followed by cooling at  $37^\circ C$  according to the experimental scheme, on the activity of PSP (wt, E125A, and D649A). The residual activity after heating was a percentage of the initial value; nevertheless, sequential incubation at 25 and  $4^\circ C$  increased the ac-

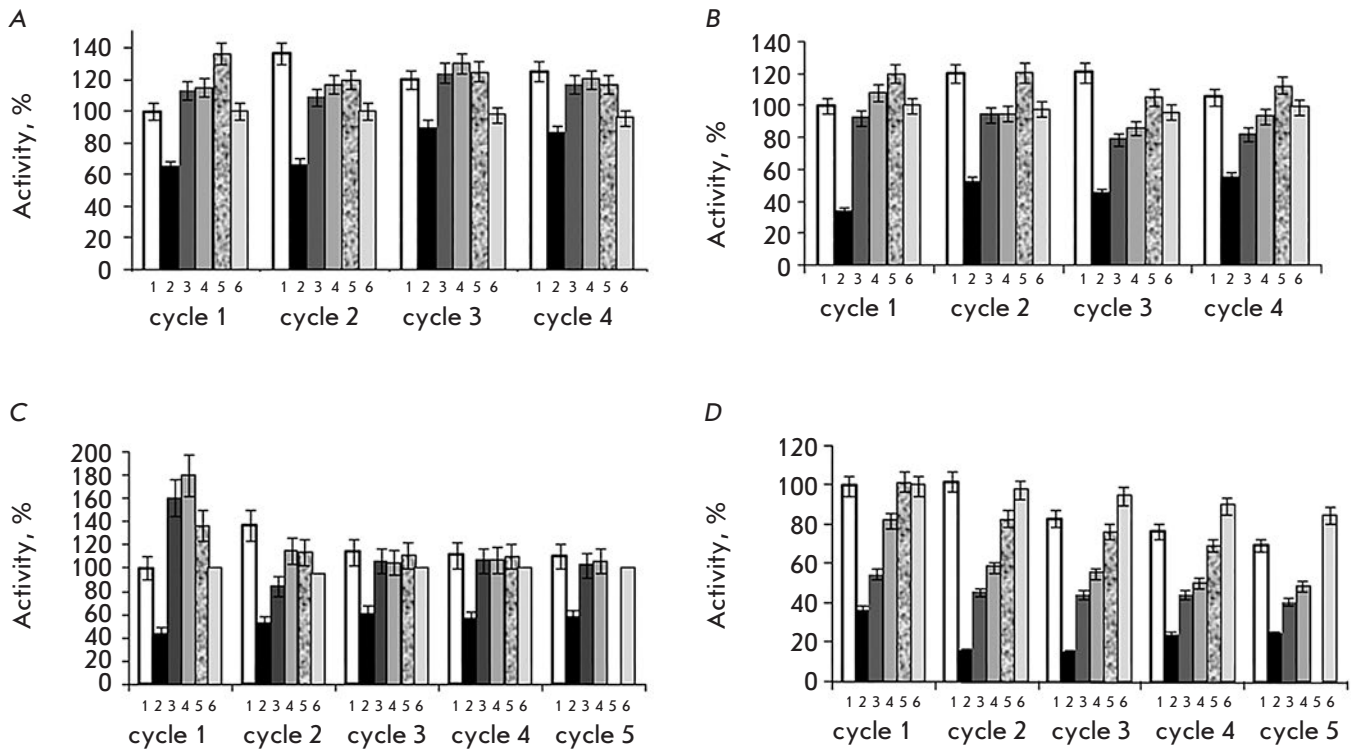


**Fig. 2.** Influence of the cyclic heating/cooling on the activity of mutant PSP variants ( $0.65 \mu\text{M}$ ) in  $0.1 \text{ M}$  Tris-HCl pH 8.0; A – wt; B – E125A; C – E75A; and D – D649A. 1 – initial activity; 2 –  $37^\circ\text{C}$ ; 3 h; 3, 4 –  $25^\circ\text{C}$ ; 0.5 and 1 h, respectively; 5 –  $4^\circ\text{C}$ ; 18–20 h; 6 – control:  $25^\circ\text{C}$ ; 4 h and  $4^\circ\text{C}$ ; 18–20 h. Initial activity ( $v_0/[E]$ ,  $\text{min}^{-1}$ ): wt – 739; E75A – 200; E125A – 1846; and D649A – 923.

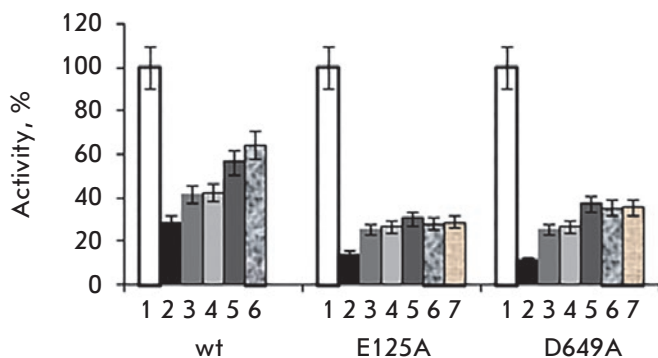


**Fig. 3.** Influence of heating at  $37^\circ\text{C}$  and subsequent cooling on the activity of PSP (wt), E125A and D649A ( $0.65$ ) in  $0.1 \text{ M}$  Tris-HCl, pH 8.0, containing  $50 \text{ mM}$   $\text{CaCl}_2$ . 1 – initial activity; 2 –  $37^\circ\text{C}$ ; 3 h; 3, 4 –  $25^\circ\text{C}$ ; 0.5 and 1 h, respectively; 5, 6, 7 –  $4^\circ\text{C}$ ; 18–20, 36–48 and 54–72 h, respectively.

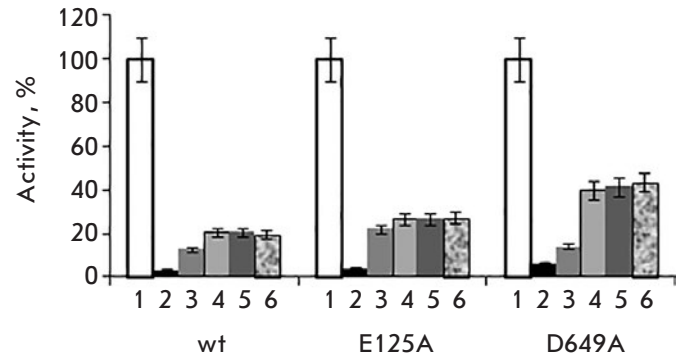


**Fig. 4.** Influence of heating at  $43^\circ\text{C}$  and subsequent cooling on the activity of PSP (wt), E125A and D649A ( $0.65$ ) in  $0.1 \text{ M}$  Tris-HCl pH 8.0. 1 – initial activity; 2 –  $43^\circ\text{C}$ ; 0.5 h; 3, 4 –  $25^\circ\text{C}$ ; 0.5 and 1 h, respectively; 5, 6, –  $4^\circ\text{C}$ ; 18–20 and 36–48 h, respectively.

tivity of PSP variants by an order of magnitude (up to 20–40%) (Fig. 4).

Incubation of wt, E125A, and D649A for 0.5 at  $46^\circ\text{C}$  (the temperature corresponding to the melting tem-

perature of the N-terminal  $\beta$ -propeller domain) fully inactivated the enzyme; subsequent incubation resulted in protein reactivation at neither  $25$  nor  $4^\circ\text{C}$  (data not presented).

## CONCLUSIONS

A unique property of oligopeptidase B from *S. proteamaculans* (PSP) has been revealed: it can undergo reversible thermal inactivation at 37°C, while subsequent cooling results in recovery of, or even an increase in, enzyme activity. The process can be repeated several times (up to five cycles), with the same results. This effect can be attributed to the fact that heating shifts the equilibrium between the inactive open enzyme form and the active closed one towards the open form. Subsequent cooling causes a reverse shift towards the closed active form. This hypothesis relies on the results of X-ray diffraction and NMR studies of the nature of reversible transitions between different forms of enzymes of the prolyl oligopeptidase family [12] and our earlier findings about the correlation between the thermal inactivation of PSP at 37°C and unfolding of its protein molecule (according to the intrinsic fluorescence spectra) [17]. Figure 5 shows the closed and open forms of PSP corresponding to an earlier obtained model of the enzyme [20]. It is clear that the inactive open form is an unfolded molecule (i.e., a denatured enzyme).

It is more difficult to explain the simultaneously occurring rise in activity. The intermediate, more active forms of the enzyme may form during the transition. Indeed, Canning et al. [12] conducted NMR studies of human prolyl oligopeptidase to find out that numerous conformations of this protein exist in solution, suggesting that the molecules of the enzymes of this family, including OpdB, are in constant movement and sequentially adopt a number of different conformations, including the completely open and completely closed ones.

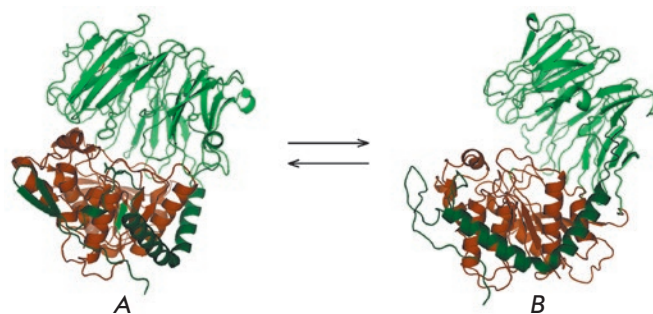


Fig. 5. Active closed (A) and inactive open (B) PSP structures. N-terminal peptide 1–80 is shown in dark green; N-terminal  $\beta$ -propeller domain 81–408 is shown in green; the C-terminal catalytic domain 409–677 is shown in brown.

Calcium ions impede the reverse transition to the closed form. The reduction in the thermal stability of PSP in the presence of  $\text{Ca}^{2+}$  can be attributed to the destruction of the salt bridges SB2 and SB3 that takes place as  $\text{Ca}^{2+}$  binds to the E494 and D460 residues partaking in bridge formation. Indeed, substitution of the corresponding charged amino acid residues for the uncharged ones in OpdB from *T. brucei* significantly reduced the thermal stability of these mutants. A conclusion has been drawn [22] that the salt bridges SB2 and SB3 play a structural role in and are responsible for the stability of the OpdB molecule. ●

*This work was supported by the Russian Science Foundation (grant No. 14-50-00131).*

## REFERENCES

- Burleigh B.A., Caler E.V., Webster P., Andrews N.W. // *J. Cell Biol.* 1997. V. 136. № 3. P. 609–620.
- Morty R.E., Shih A.Y., Fülöp V., Andrews N.W. // *FEBS Lett.* 2005. V. 579. № 10. P. 2191–2196.
- Morty R.E., Pelle R., Vadasz I., Uzcanga G.L., Seeger W., Bubis J.J. // *J. Biol. Chem.* 2005. V. 280. № 12. P. 10925–10937.
- de Matos Guedes H.L., Duarte Carneiro M.P., de Oliveira Gomes D.C., Rossi-Bergmann B., Giovanni De-Simone S. // *Parasitol. Res.* 2007. V. 101. № 4. P. 865–875.
- Yan J.B., Wang G.Q., Du P., Zhu D.X., Wang M.W., Jiang X.Y. // *Prot. Expr. Purif.* 2006. V. 47. № 2. P. 645–650.
- Yoshimoto T., Tabira J., Kabashima T., Inoue S., Ito K. // *J. Biochem.* 1995. V. 117. № 3. P. 654–660.
- Morty R.E., Fülöp V., Andrews N.W. // *J. Bacteriol.* 2002. V. 184. № 12. P. 3329–3337.
- Mustafa M.S.M., Nakajima Y., Oyama H., Iwata N., Ito K. // *Biol. Pharm. Bull.* 2012. V. 35. № 11. P. 2010–2016.
- Fenno J.C., Lee S.Y., Bayer C.H., Ning Y. // *Infect. Immun.* 2001. V. 69. № 10. P. 6193–6200.
- Bagarozzi D.A. Jr., Potempa J., Travis J. // *Am. J. Respir. Cell Mol. Biol.* 1998. V. 18. № 3. P. 363–369.
- McLuskey K., Paterson N.G., Bland N.D., Isaacs N.W., Mottram J.C. // *J. Biol. Chem.* 2010. V. 285. № 50. P. 39249–39259.
- Canning P., Rea D., Morty R.E., Fulop V. // *PloS One.* 2013. V. 8. № 11. e79349.
- Mikhailova A.G., Likhareva V.V., Khairullin R.F., Lubenets N.L., Rumsh L.D., Demidyuk I.V., Kostrov S.V. // *Biochemistry (Moscow)*. 2006. V. 71. № 5. P. 563–570.
- Khairullin R.F., Mikhailova A.G., Sebyakina T.Yu., Lubenets N.L., Ziganshin R.Kh., Demidyuk I.V., Gromova T.Yu., Kostrov S.V., Rumsh L.D. // *Biochemistry (Moscow)*. 2009. V. 74. № 10. P. 1164–1172.
- Mikhailova A.G., Khairullin R.F., Demidyuk I.V., Gromova T.Yu., Kostrov S.V., Rumsh L.D. // *Biochemistry (Moscow)*. 2011. V. 76. № 4. P. 480–490.
- Mikhailova A.G., Khairullin R.F., Kolomijtseva G.Ya., Rumsh L.D. // *Biochemistry (Moscow)*. 2012. V. 77. № 3. P. 300–306.
- Mikhailova A.G., Khairullin R.F., Demidyuk I.V., Kostrov S.V., Grinberg N.V., Burova T.V., Grinberg V.Ya., Rumsh L.D. // *Protein Exp. Purif.* 2014. V. 93. P. 63–76.
- Mikhailova A.G., Nekrasov A.N., Zinchenko A.A., Rakitina T.V., Korzhenevsky D.A.,

## RESEARCH ARTICLES

- Lipkin A.V., Razguljaeva O.A., Ovchinnikova M.V., Gorlenko V.A., Rumsh L.D. // *Biochemistry (Moscow)*. 2015. V. 80. № 11. P. 1331–1343.
19. Ismail N.I.M., Yuasa T., Yuasa K., Nambu Y., Nisimoto M., Goto M., Matsuki H., Inoue M., Nagahama M., Tsuji A. // *J. Biochem.* 2010. V. 147. № 2. P. 201–211.
20. Mikhailova A.G., Rakitina T.V., Timofeev V.I., Karlinsky D.M., Korzhenevsky D.A., Agapova Yu.K., Vlaskina A.V., Ovchinnikova M.V., Gorlenko V.A., Rumsh L.D. // *Biochimie*. 2017. V. 139. P. 125–136.
21. Walsh K.F., Wilcox P.E. // *Meth. Enzymol.* 1970. V. 19. P. 31–41.
22. Fukumoto J., Ismaliza N., Ismail M., Kubo M., Kinoshita K., Inoue M., Yuasa K., Nishimoto M., Matsuki H., Tsuji A. // *J. Biochem.* 2013. V. 154. № 5. P. 465–473.

# Soluble Guanylate Cyclase As the Key Enzyme in the Modulating Effect of NO on Metabotropic Glutamate Receptors

I. V. Ryzhova, A. D. Nozdrachev, T. V. Tobias, E. A. Vershinina

Pavlov Institute of Physiology, Russian Academy of Sciences, Makarova Embankment 6, St. Petersburg, 199034, Russia

\*E-mail: ireneryzhova@mail.ru

Received September 06, 2017; in final form April 25, 2018

Copyright © 2018 Park-media, Ltd. This is an open access article distributed under the Creative Commons Attribution License, which permits unrestricted use, distribution, and reproduction in any medium, provided the original work is properly cited.

**ABSTRACT** The synaptic plasticity of the afferent synapse of the vestibular apparatus is defined by the dynamic interaction of ionotropic and metabotropic glutamate receptors and the modulators of synaptic transmission. It was shown that nitric oxide modulates iGluR responses. In this paper, the effect of NO on the function of the afferent synapse mGluR was investigated. Inhibitor of nitric oxide synthase lowered the level of background activity but increased the amplitude of the responses of groups I and II mGluR agonist ACPD. Donor NO SNAP increased the level of background activity. Short-term perfusion of the synaptic region with low concentrations of SNAP led to a decrease in the amplitude of the answers of mGluR agonists ACPD and DHPG. The inhibitory effect of the NO donor was eliminated under blockade of soluble guanylate cyclase with a specific inhibitor ODQ. A prolonged application of NO did not cause a statistically significant change in the amplitude of the ACPD response. However, SNAP at concentrations of 10 and 100  $\mu\text{M}$  increased the amplitude of the mGluR agonist responses 30 and 15 minutes, respectively, after termination of the NO donor exposure. The obtained data show the multidirectional effect of NO on the function of mGluR and testify to the existence of a complex modulating mechanism of the afferent flow from vestibular organs to the central nervous system.

**KEYWORDS** nitric oxide, metabotropic glutamate receptors, vestibular apparatus, soluble guanylate cyclase, synaptic plasticity.

**ABBREVIATIONS** iGluR – ionotropic glutamate receptors, mGluR – metabotropic glutamate receptors, NO – nitric oxide, NOS – nitric oxide synthase, L-NAME – N-nitro-L-arginine methyl ester hydrochloride, sGC – soluble guanylate cyclase, cGMP – cyclic guanosine monophosphate, SNAP – S-Nitroso-N-acetyl-DL-penicillamine, IP3R – inositol trisphosphate receptors, RyR – ryanodine receptors, PKG – protein kinase G, ODQ – 1H-[1,2,4] Oxadiazolo[4,3-a]quinoxalin-1-one, ACPD – 1S,3R)-1-aminocyclopentane-trans-1,3-dicarboxylic acid, DHPG – (S)-3,5-dihydroxyphenylglycine, AMPA –  $\alpha$ -amino-3-hydroxy-5-methyl-4-isoxazolepropionic acid, NMDA – N-methyl-D-aspartate, CNS – central nervous system, EPSP – excitatory postsynaptic potential.

## INTRODUCTION

Hair cells, the secondary sensory receptors of the inner ear, contact the afferent fibers through an amino acid synapse. Glutamatergic synaptic plasticity is provided by the functional cross-talk between ionotropic and metabotropic glutamate receptors and the modulators of synaptic transmission released by hair cells, nerve terminals, or transported with the blood flow. Nitric oxide is of particular interest; it is a gaseous neuromodulator that functions as an intracellular and extrasynaptic signal messenger. L-arginine is the precursor of NO in humans and animals. NO-synthase and several cofactors catalyze the conversion of L-arginine in NO and L-citrulline. In the inner ear, nitric oxide can be synthesized under normal conditions by the neuronal

and endothelial NO-synthases located in hair cells, afferent and efferent nerve fibers [1–3]. Pathological processes in the inner ear (labyrinthectomy, excitotoxicity, infections and exposure to ototoxic substances) are accompanied by the activation of inducible NOS, leading to prolonged synthesis of high NO concentrations [4–9].

The important role of NO in the functioning of the vestibular epithelium is confirmed by clinical and experimental physiological data. The baseline synthesis of NO in hair cells was detected by using a NO-selective electrode [10, 11]. NO content was increased in response to the action of acetylcholine, glutamate, antibiotics, liposaccharides and cytokines. The effects of NO donors and NOS inhibitors have been revealed in the vestibular

epithelium of amphibians. It is shown that NO decreases the input resistance of vestibular afferent neuronal membranes, enhances the afferent resting discharge and increases the amplitude of the responses to adequate irritation and the magnitude of iGluR agonists' responses. In contrast to the effects of NO donors, NOS inhibitors diminish the frequency of background activity in afferent fibers and the frequency of the excitatory postsynaptic potentials but increase the response amplitude of glutamate and its agonists, AMPA and NMDA [12–14]. There is a suggestion that NOS inhibitors act at the presynaptic level and suppress neurotransmitter release. We have shown the postsynaptic effect of NO donors and NOS inhibitors under conditions of blockade of the presynaptic membrane with a hypermagnesium-hypocalcium solution [13]. Data on NO involvement in the afferent discharge and adaptive changes in the vestibular analyzer have been published [3, 8, 9, 11, 12, 14].

According to some researchers, the mechanism of NO action on synaptic transmission, synaptic plasticity, and neurodegenerative processes is associated with the modulation of ion channel activity in the plasma membrane [15–18]. In the vestibular epithelium of rats, using the patch-clamp method of whole and perforated cells, it has been shown that NO inhibits  $Ca^{2+}$  currents of the semicircular canal crista hair cells by nitrosylation of  $Ca^{2+}$  channels and activation of the sGCcGMP signaling pathway [18]. It has been shown that NO weakens  $Ca^{2+}$ -oscillations in frog saccular hair cells and increases the amplitude of the transients required to evoke these oscillations. This effect is associated with the inhibition of  $Ca^{2+}$ -dependent  $K^+$ - and  $Ca^{2+}$ -channels by the decreasing of their opening probability. Inhibition of  $K^+$ -channel transients by NO donors and by the membrane-permeable analogue of cGMP – 8-bromo-cGMP was observed in type I hair cells in rat semicircular canals [19, 20].

It is known that iGluR and mGluR are co-localized on the postsynaptic membrane. Taking into account the synthesis of NO during activation of NMDA receptors and rapid diffusion of NO along the concentration gradient, we hypothesized a possible effect of NO on the function of mGluR. Our pilot studies showed that the NO donor SNAP reduced the response amplitude of ACPD, a mGluR agonist, while the NOS inhibitor L-NAME had the opposite effect [21]. This work is devoted to a detailed study of the NO effect on the function of mGluR.

## EXPERIMENTAL

### Experimental procedure

Normal and pathological synaptic processes are associated with different concentrations of NO and differ-

ent times of its action. A physiologically functioning synapse is exposed to the short-term effects of low NO concentrations, whereas under pathological conditions a synapse is subjected to the long-term action of high NO concentrations. Our choice of an experimental model was based on data showing that the NO content in the utricle increases 5 min after the application of aminoglycoside antibiotic gentamicin [22]. Hence, we investigated 1) the short-term (1 min) and long-term (9 min) effects of NO donor SNAP (1–100  $\mu$ M) on the response amplitude of the mGluR agonists ACPD and DHPG and 2) proved the specificity of the NO effect on the function of mGluR via blockage of sGC, the receptor for NO, using a specific inhibitor, ODQ.

The frog vestibular system is a unique model that allows one to investigate the patterns of synaptic transmission in the bouton-like synaptic terminals between the hair cells and the afferent nerve fibers. The cartilage capsule of the labyrinth was excised and placed for further dissection in a chamber with a solution of the following composition (in mM): NaCl 117; KCl 2.5;  $NaHCO_3$  1.2;  $NaH_2PO_3 \cdot 2H_2O$  0.17;  $CaCl_2$  1.8; glucose 2.5. The tested substances were dissolved in a normal solution at the required concentrations (pH 7.4). The solutions were applied through external perfusion. The following substances manufactured by Sigma-Aldrich were used in the experiments: NO-synthase inhibitor L-NAME; NO donor SNAP; mGluR agonists: group I and II – ACPD, and selective group I (mGlu1, mGluR5) – DHPG; and selective sGC inhibitor ODQ.

The multiple impulse activity of the afferent fibers contacting the hair cells of the semicircular canal was recorded with a suction glass electrode. The impulse activity was applied to an amplifier A-M Systems Inc 3000 and converted into standard rectangular pulses of 2 ms duration, which were recorded on a computer online throughout the experiment using the original program. The responses of the mGluR agonists ACPD and DHPG were estimated as the ratio of the difference between the maximum and minimum of the response to the resting discharge rate (frequency, (max – min) of resting discharge, %). We compared the change in the response amplitude of the mGluR agonists ACPD and DHPG before, combined and after application of the NOS inhibitor and NO donor SNAP.

The data are presented as mean values and standard errors of the mean ( $M \pm SEM$ ). Data analysis was performed using one-way ANOVA for dependent variables (Repeated measurements) followed by multiple pair comparisons (Post hoc test). The factor is the stage of the process (control answer/application/recovery). In the absence of sufficient material in the recovery stage, only two stages were compared using the *t*-test. All calculations were duplicated with the Wilcoxon

rank test for dependent variables. A statistical decision was accepted at a 5% level of significance. Estimations were performed using the SPSS Inc. software complex. Illustrations were prepared using the MS-Excel software package.

## RESULTS

### The influence of NO donor SNAP on the background activity in afferent fibers

Perfusion of the synaptic area with a SNAP solution (0.01–100  $\mu\text{M}$ ) caused positive-negative changes in the frequency of the resting activity. The effect of the NO donor SNAP was characterized by a lack of dose-dependence. The dynamics of responses varied widely from one experiment to another, which was reflected in a different ratio of amplitude and duration of positive and negative response waves. Prolonged exposure to high SNAP concentrations (100  $\mu\text{M}$ ) slightly increased firing activity, followed by a decrease in the frequency of afferent discharges. Reduced level of firing activity was not restored to its initial level after 30-min exposure in a normal solution (*Fig. 1*).

### The short-term effect of the NO donor on the function of metabotropic glutamate receptors

The effect of NO on the response amplitude of groups I and II mGluR agonist ACPD and group I mGluR agonist DHPG were investigated in our work, because only groups I and II mGluR were revealed in the vestibular epithelium [23, 24].

ACPD, the agonist mGluR, increased spike frequency. To discriminate the changes in the excitatory wave of mGluR agonist responses from the excitatory effect of NO donor SNAP on the resting activity, ACPD was applied when a significant effect of the NO donor occurred. The amplitude of the ACPD-evoked response during SNAP application was lower compared to the control answer before SNAP application. The observed changes were reversible after 15-min washing in a normal solution (*Fig. 2*).

NO donor SNAP at low concentrations had a similar effect on the responses of the DHPG – group I mGluR specific agonist. DHPG application (200  $\mu\text{M}$ ) was accompanied by an increased spike frequency in afferent fibers. NO donor SNAP (1  $\mu\text{M}$ ) significantly reduced the amplitude of the group I mGluR agonist DHPG response (*Fig. 3*). Thus, the short-term impact of NO suppressed the function of groups I and II mGluR. The inhibitory effect was completely reversible.

### The long-term effect of NO on mGluR function

Prolonged influence of NO to mGluR function is of particular interest due to the long-term effect of a high

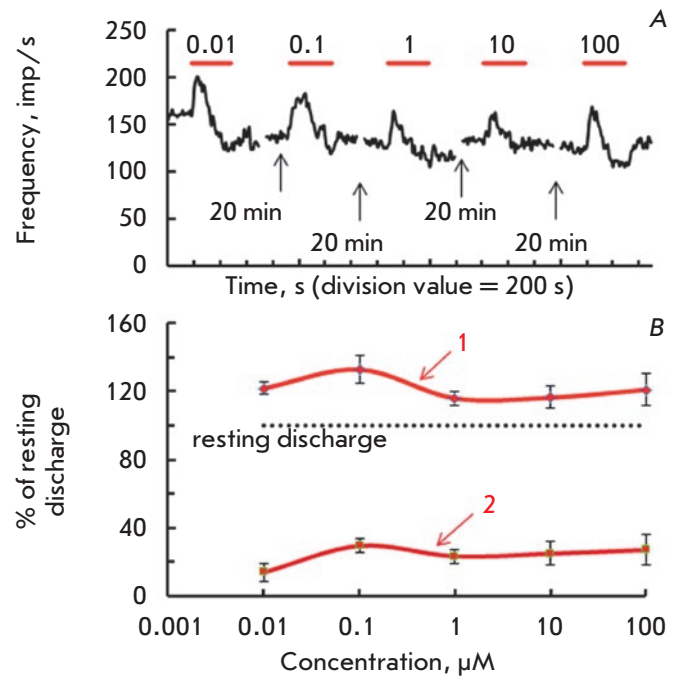


**Fig. 1.** Effects of long-term application of different concentrations of NO donor SNAP on the background activity in posterior semicircular canal nerve fibers of a frog. *A* – original recording of firing activity in the same experiment. Ordinate: spike frequency, imp/s; abscissa: time, s. The horizontal lines above the recording indicate the duration of drug applications. *B* – dose-response curves of the positive (1) and the negative (2) response waves for NO donor SNAP.  $N=5-6$

concentration of NO during pathological processes in the inner ear. In our experiments, the mGluR agonist ACPD (100  $\mu\text{M}$ ) was initially applied (control). After a 15-minute washing of the vestibular with a normal solution, a 5-minute perfusion of the NO donor SNAP (0.1–100  $\mu\text{M}$ ) was performed, against which the mGluR agonist ACPD was re-applied. Recovery of ACPD responses in a normal solution was monitored 15 and 30 minutes after cessation of the combined effect of SNAP and ACPD.

The long-term perfusion of the synaptic area with solutions of low SNAP concentration (0.1–1  $\mu\text{M}$ ) did not affect either the response value after 5-min perfusion or recovery of the response after 15 and 30 min. SNAP at a concentration of 10  $\mu\text{M}$  did not change either the response of the mGluR agonist after a 5-min perfusion or the response amplitude of the mGluR agonist after 15-min washing in a normal solution. However, the amplitude of the ACPD-evoked response increased significantly 30 min after the end of SNAP (10  $\mu\text{M}$ ) action and amounted to 169.9% compared to the background activity. Tendencies to differences were observed be-

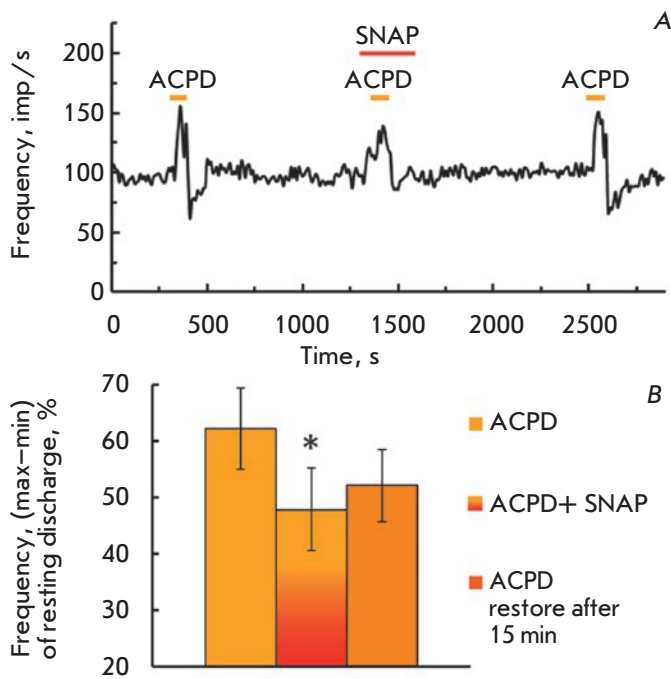


**Fig. 2.** Modification of the ACPD-evoked response before, combined and a short-time impact of NO donor SNAP (ACPD 100  $\mu$ M, SNAP 1  $\mu$ M). **A** – time course of firing activity in a typical experiment. The designations are the same as in Fig 1A. **B** – diagram of the decrease of the ACPD-evoked response combined short-term SNAP application. Abscissa: left to right – ACPD-control; SNAP+ACPD; ACPD recovery after 15 min in a normal solution. Ordinate: value of the response to ACPD, %, mean  $\pm$  SEM. (ANOVA  $F(2,18) = 3.9$ ,  $p = 0.039$ , Post hoc test  $p = 0.03$ )

tween responses to combined ACPD and SNAP exposure and its recovery after 15 min (Post hoc test = 0.082) and 30 min (Post hoc test = 0.059).

A 5-min SNAP application (100  $\mu$ M) did not change the amplitude of ACPD-evoked responses. But the ACPD induced response increased significantly in 15 min washing in a normal solution. This increase in the response amplitude remained at that level also 30 min after NO exposure, although it was statistically insignificant (Fig. 4).

Thus, the effect of NO on the mGluR function depended on the concentration and duration of the exposure. A short-term exposure to low NO concentrations inhibited the mGluR function. The long-term impact of high concentrations of the NO donor enhanced mGluR responses.

### The effect of a specific sGC inhibitor on the depressive effect of NO donor SNAP

The following protocol was used to investigate the involvement of sGC in the modulation of the mGluR

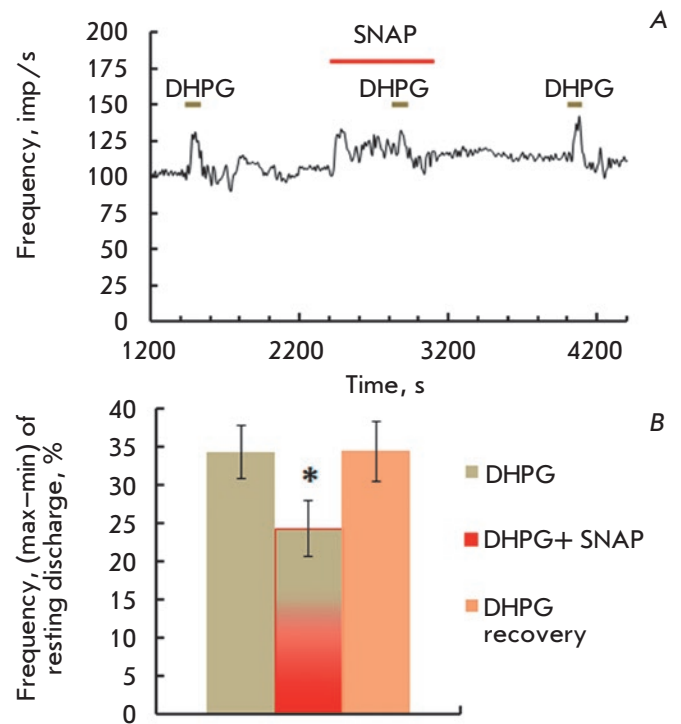


**Fig. 3.** Effects of NO donor SNAP (1  $\mu$ M) on the amplitude of mGluR I agonist DHPG (200  $\mu$ M). **A** – typical recording of the experiment. The designations are the same as in Fig. 1A. **B** – bar graph of reversible suppression of the DHPG-evoked response before, during and after SNAP application. Abscissa: left to right: DHPG – control; SNAP+DHPG; DHPG recovery in 15 min in a normal solution. Ordinate: mean  $\pm$  SEM for amplitude of DHPG-induced responses (%). (Wilcoxon  $p = 0.025$ )

function. Step 1 (Fig. 5A): application of mGluR agonist ACPD (control 1), washing of the vestibular apparatus in a normal solution, perfusion of the synaptic area with a solution of SNAP (1  $\mu$ M) plus ACPD (100  $\mu$ M) (inhibitory effect, application 1), recovery of ACPD-evoked response after 15 min washing in a normal solution. Step 2 (Fig. 5B): 20-min incubation of vestibular in a solution of the specific sGC inhibitor ODQ (15  $\mu$ M), then repeat stage 1 against ODQ perfusion [application of ACPD solution 100  $\mu$ M (control 2), SNAP (1  $\mu$ M) and ACPD solution (100  $\mu$ M) (application 2), recording of the ACPD response after 15 min of washing with ODQ (recovery 2)]. Stage 3: perfusion of the vestibular apparatus for 1 h in a normal solution and testing of the preservation of the ODQ influence on the inhibitory effect of SNAP to the ACPD-induced response (step 1 was repeated: control 3, application 3, recovery 3). To investigate the ODQ influence on the inhibitory effect of SNAP to mGluR agonist, the differences in the amplitudes of ACPD-evoked responses were estimated between control 1

and application 1 between control 2 and application 2. Preservation of the ODQ effect was expressed as the difference between control 3 and application 3 of stage 3. ANOVA and pairwise multiple comparisons revealed a significant decrease in the amplitude of mGluR agonist ACPD under the action of the NO donor SNAP (ANOVA  $F(2.18) = 3.9$ ,  $p = 0.039$ , Post hoc test –  $p = 0.03$ ) that was abolished after blockade of sGC with the specific inhibitor ODQ (ANOVA  $F(2.20) = 0.408$ ,  $p = 0.67$ ). The effect of ODQ persisted for 1 hour (Fig. 5).

## DISCUSSION

The functional role of mGluR in various CNS structures was studied in detail. mGluRs play a key role in CNS ontogenesis [25] and participate in the long-term potentiation, depression, learning, and formation of long-term memory [26–28]. mGluRs were revealed on glial cell membranes and on the pre- and postsynaptic membranes in the cortex, striatum, hippocampus, and cerebellum [26, 29–31]. To date, eight mGluR subtypes have been cloned. They are subdivided into three groups according to structure, pharmacological characteristics, and the second messengers involved [29, 32–34]. In all cases, the activation of mGluR is associated with  $Ca^{2+}$  release from intracellular stores and prolongation of the excitation wave triggered by iGluR.

There are two types of  $Ca^{2+}$ -channels with different functional and pharmacological characteristics on endoplasmic reticulum membranes. Ryanodine receptors (RyR) functionally interact with the potential-dependent  $Ca^{2+}$ -channels of the plasma membrane and are activated by low concentrations of ryanodine, ATP, heparin, and micromolar concentrations of  $Ca^{2+}$  cations. The function of the  $Ca^{2+}$ -channels of the ryanodine receptor can be inhibited by millimolar concentrations of  $Ca^{2+}$  and ryanodine, be modulated by NO, oxidants, protein kinases, and intracellular proteins [35, 36]. The inositol trisphosphate receptors (IP3R) located on endoplasmic reticulum membranes are activated by IP3 but are inhibited by calmodulin and the NO/cGMP-activated kinase I [37].

Information on the mGluR functions and the ways they are modulated in the acousticolateral system is scarce. Only groups I and II mGluR located on the pre- and postsynaptic membranes have been found in the vestibular epithelium of amphibians. The function of the mGluR2 and mGluR3 subtypes has not been studied yet [23, 24]. Evidence of a direct involvement of mGluR I in afferent synaptic transmission in the vestibular apparatus [23] and in the cochlea [38, 39] was obtained using methods of electrophysiology, immunohistochemistry, and molecular genetics.

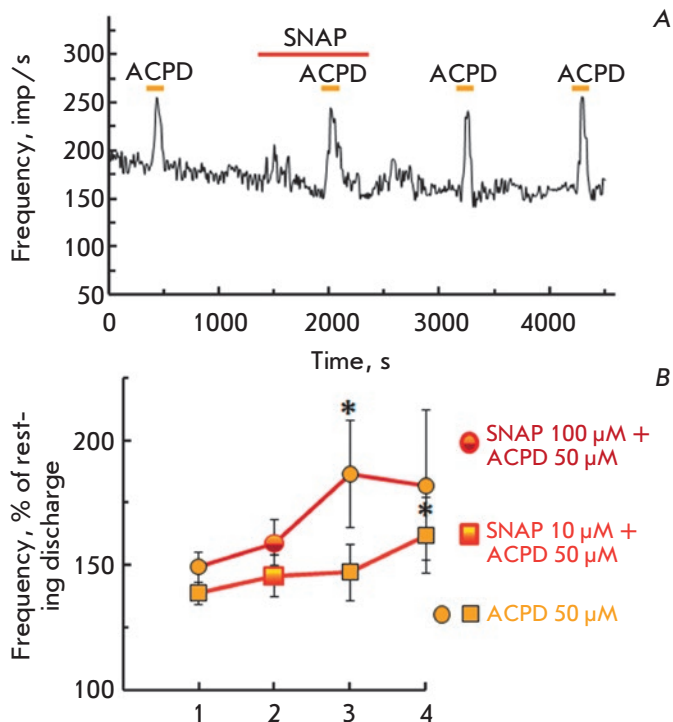


**Fig. 4.** Effects of a prolonged application of NO donor SNAP on the amplitude of group I and II mGluR agonist ACPD (50  $\mu$ M). **A** – original recording (SNAP 10  $\mu$ M). The designations are the same as in Fig. 1A. **B** – the increase in the amplitude of ACPD-evoked responses after prolonged exposure of different concentrations of NO donor SNAP in the vestibular. Abscissa: left to right: 1 – control; 2 – over 5-min application of SNAP; 3 – recovery 15 min after the end of drug application in normal solution; 4 – recovery in 30 min in a normal solution. Ordinate: mean  $\pm$  SEM for the amplitude of the ACPD-induced response (%). SNAP 10  $\mu$ M (ANOVA  $F(3.18) = 4.4$ ,  $p = 0.017$ , Post hoc test  $p = 0.047$ ) and SNAP 100  $\mu$ M (ANOVA  $F(2.16) = 4.58$ ,  $p = 0.027$ , Post hoc test  $p = 0.027$ )

The participation of group I mGluR in the functioning of glutamatergic synapses was demonstrated in frog semicircular canals [23, 40]. In those studies, the mGluR I–II agonist ACPD and mGluR I specific agonist DHPG produced an increase in the afferent firing rates of the ampullar nerve. It was proved that activation of presynaptic mGluR facilitates glutamatergic transmission due to intracellular  $Ca^{2+}$  release from IP3-sensitive and ryanodine/caffeine-sensitive intracellular  $Ca^{2+}$ -stores.

The functional relationship between group I mGluR and IP3R of the endoplasmic reticulum was revealed in the frog vestibular apparatus by immunocytochemistry and electrophysiology. The participation of IP3 in

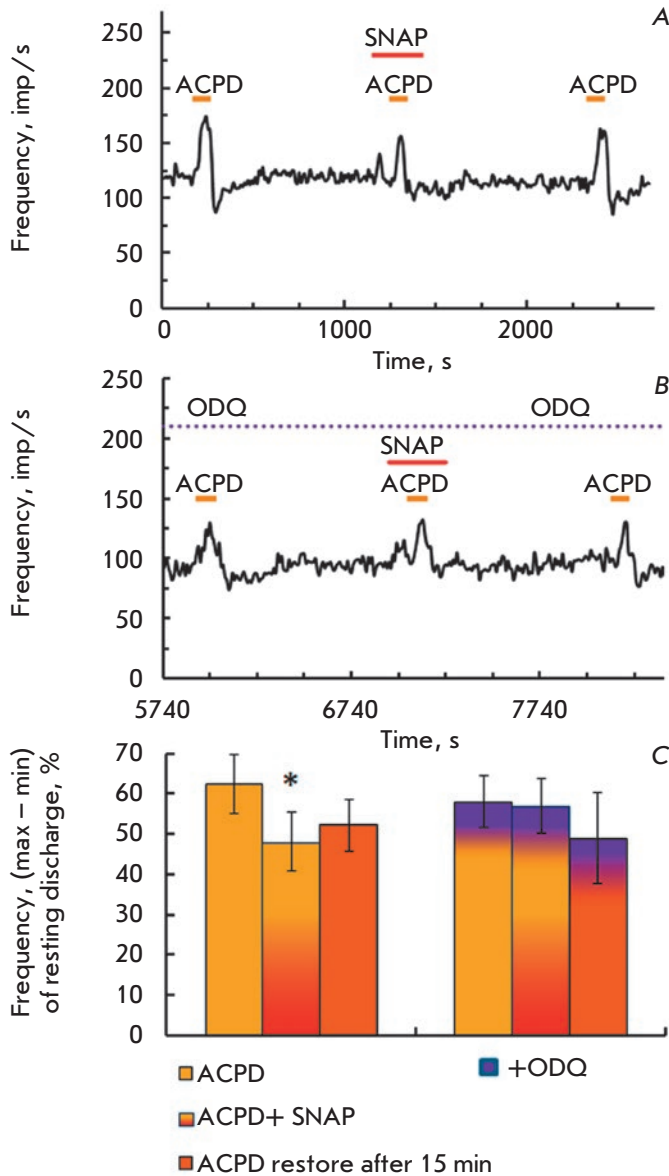


**Fig. 5.** Effects of the specific inhibitor of sGC ODO on SNAP ( $1 \mu\text{M}$ ) suppression of the ACPD-induced response. *A, B* – multiunit recording of firing activity in the posterior semicircular canal nerve before (*A*) and after (*B*) a 20-min perfusion on vestibular synapse by  $15 \mu\text{M}$  ODO. The designations are the same as in Fig 1A. *C* – lack of suppression of ACPD-evoked responses after inhibition of sGC by ODO. Abscissa: left to right: control; ACPD against SNAP; recovery 15 min after the end of drugs application in a normal solution; the same steps against ODO application. Ordinate: mean  $\pm$  SEM for the amplitude of the ACPD-induced response (%)

the modulation of the resting activity and mechanically evoked responses has also been proved [41]. The data observed show that the amphibian vestibular apparatus contains a heterogeneous population of mGluR the activation of which is associated with the formation of IP<sub>3</sub>, the activation of IP<sub>3</sub> and ryanodine receptors, and Ca<sup>2+</sup> release from endoplasmic reticulum cisterns. It is important to note that the ACPD-evoked response was caused by the activity of mGluR but was not due to the activity of ionotropic receptors, since specific iGluR antagonists did not change the amplitude of the ACPD response [23].

The afferent fibers of the vestibular epithelium produce a background activity, which reflects tonic release of glutamate from hair cells [42]. The sensitivity of the vestibular apparatus to adequate stimuli and informativity of the signal perceived by the CNS are mediated by the ratio between resting and evoked activity. According to current concepts, activation of mGluR in the vestibular epithelium of semicircular canals produces a positive feedback reinforcing the contrast between background and induced activity [23]. This hypothesis is confirmed by our data showing that application of the mGluR agonist ACPD increases the response amplitude of iGluR agonists [24].

The results of our pilot experiments and the presented data indicate that fluctuation of NO content can modulate the function of mGluR. In our experiments, NOS inhibitor L-NAME reduced afferent resting firing depending on its concentration but increased the response amplitude of ACPD [21]. These results confirm the hypothesis about the various mechanisms of background and evoked vestibular afferent firing [42]. Our data about the effect of NOS inhibitors on resting afferent nerve firing [13] are in line with the results received in various models of the -acousticolateral system: L-NAME inhibits the basal spike discharge in lateral line cells [43]. The NOS inhibitors L-NOARG and L-NAME elicited a decrease in the basal discharge and diminished the EPSP rates of the axolotl vestibular system [1, 12]. Using a specific fluorescent probe, the synthesis of NO was shown to be decreased in the presence of L-NAME in the vestibular epithelium of the frog saccule [11]. This data allows us to conclude that a small amount of NO is synthesized in the vestibular epithelium under normal physiological conditions. The decrease in resting activity and increase in the ACPD response amplitude under NOS blockade with the inhibitor L-NAME are specific.

The inhibitory effect of low NO donor concentrations on the mGluR agonists responses was studied with simultaneous and consecutive application of NO and mGluR agonists. This allowed us to separate the stimulating effect of mGluR agonists from the excitation

effect of the NO donor on basal activity and to compare the effect of NO donor SNAP on iGluR and mGluR. Our data showed that simultaneous short-term application of the NO donor increased the response amplitude of the iGluR agonists AMPA and NMDA [14] but reduced the response magnitude of the mGluR agonist ACPD. The inhibitory effect of SNAP on the ACPD-evoked response was dose-independent.

It was shown that NO can modify nerve cell excitation through two basic mechanisms: direct interaction with the ion channel protein (nitrosylation reaction) and by activating the NO/sGC/cGMP/PKG signaling cascade [15, 44]. Both pathways have been found in the hair cells of the inner ear [18]. To study the participation of soluble guanylate cyclase, and the possible involvement of the NO/sGC/cGMP signaling pathway in the inhibitory effect of NO on mGluR, we used the specific sGC blocker ODQ, since sGC is the specific cytosolic receptor for NO [45].

In our experiments, the specific blocker of sGC ODQ eliminated the inhibitory effect of NO donor SNAP, suggesting an involvement of the NO-sGC-cGMP signaling cascade in mGluR modulation. We failed to find direct data on the impact of NO on the mGluR function. However, it was found that NO can inhibit the G-protein-mediated signaling pathway. The possibility of IP3 receptor phosphorylation and a decrease in the intracellular  $Ca^{2+}$  concentration by the activation of PKG was shown in Chinese hamster ovary cells. In those experiments, increase in the intracellular  $Ca^{2+}$  concentration caused by the activation of the thrombin/G-protein/phospholipase C signaling cascade was fully prevented by 8-bromo-cGMP, which indicates a specific effect of cGMP-stimulated kinase [46].

Similar data were obtained on cell cultures transfected with IP3R and incubated in the presence of the cGKI-specific cGMP analogue 8-pCPT-cGMP. Pre-incubation of cells expressing IP3R, the IRAG complex and cGKI $\beta$  protein kinase with the specific analog 8-pCPT-cGMP, reduced bradykinin-stimulated release of  $Ca^{2+}$  from intracellular stores. The observed effect was linked to the phosphorylation of the IRAG protein complex and reduced IP3 synthesis [37].

Different experimental models revealed cGMP-dependent and cGMP-independent routes of NO impact on sarcoplasmic reticulum receptors. It is assumed

that NO can modify ryanodine and IP3 receptor functions. These two mechanisms differ in the activation kinetics and NO concentrations required for modulation. The NO-activated enzymatic pathway leading to PKG activation and inhibition of IP3 synthesis (or phosphorylation of IP3 receptors) is triggered by low NO concentrations within seconds. Nitrosylation of RyR is initiated by a higher concentration of NO, develops within several minutes, and is associated with a higher activity of the  $Ca^{2+}$ -channel connected with an increase in the probability of RyRs opening [47, 48]. Thus, efflux of  $Ca^{2+}$  ions from intracellular stores can be modulated in time through various mechanisms. The long-term exposure to high NO concentrations can cause nitrosylating stress, leading to pathology [47, 49].

Our data support the hypothesis that NO can modify the mGluR function with the modulating effect depending on the concentration and time of NO action. Short-term exposure to low NO concentrations suppresses mGluR agonist responses and, consequently, decreases  $Ca^{2+}$  efflux from intracellular stores. In our opinion, inhibition of the mGluR function with low NO concentrations can be proposed as one of the mechanisms of glutamatergic synaptic plasticity aimed at decreasing positive feedback [24]. Prolonged activation of the NO signaling cascade with high concentrations of a NO donor causes a low but statistically significant increase in the amplitude of the mGluR agonist response that may be hypothetically associated with the activation of ryanodine receptors. These assumptions require more experimental confirmation.

Thus, in this paper we showed the following:

NO affects the function of agonists of different mGluR groups (ACPD and DHPG).

Blocking a specific NO receptor eliminates the inhibitory effect of NO on the mGluR function, which suggests specificity of the NO influence. (We plan to search for evidence of the involvement of different links in the NO pathway in the modulation of the mGluR function in further experiments.)

The direction of the NO effect on the mGluR function is dynamic and depends on the concentration and time of influence. ●

*This study was supported by the Russian Foundation for Basic Research (grant No. 14-04-00409).*

## REFERENCES

1. Flores A., Leyn-Olea M., Vega R., Soto E. // *Neurosci. Lett.* 1996. V. 205. P. 131–134.
2. Lysakowski A., Singer M. // *J. Comp. Neurol.* 2000. V. 427. P. 508–521.
3. Takumida M., Anniko M. // *In vivo.* 2004. V. 18. P. 345–350.
4. Takumida M., Anniko M. // *ORL J. Otorhinolaryngol. Relat. Spec.* 1998a. V. 60. P. 67–72.
5. Popa R., Anniko M., Takumida M. // *Acta Otolaryngol.* 2000. V. 120. P. 350–358.

6. Takumida M., Anniko M. // *Eur. Arch. Otorhinolaryngol.* 1998b. V. 255. № 4. P. 184–188.
7. Park J.-S., Jeong H.-S. // *Jpn. J. Pharmacol.* 2000. V. 84. P. 425–430.
8. Smith P.F., Zheng Y., Paterson S., Darlington C.L. // *Acta Otolaryngol. Suppl.* 2001. V. 545. P. 57–60.
9. Hong S.H., Park S.K., Cho Y.-S., Lee H.-S., Kim K.R., Kim M.G., Chung W.-H. // *Hear. Res.* 2006. V. 211. P. 46–53.
10. Takumida M., Anniko M., Moncada S., Bolaños J.P. // *J. Neurochem.* 2006. V. 97. P. 1676–1689.
11. Lv P., Rodriguez-Contreras A., Kim H.J., Zhu J., Wei D., Choong-Ryoul S., Eastwood E., Mu K., Levic S., Song H., Petrov Y., et al. // *J. Neurophysiol.* 2010. V. 103. P. 2494–2505.
12. Flores A., Vega R., Soto E. // *Neurosci.* 2001. V. 103. P. 457–464.
13. Andrianov Yu.N., Ryzhova I.V., Tobias TV. // *Sens. Sys.* V. 25. № 4. P. 297–304.
14. Andrianov Yu.N., Ryzhova I.V., Tobias TV. // *Sens. Sys.* V. 26. № 3. P. 204–213.
15. Garthwaite J., Boulton C. // *Annu. Rev. Physiol.* 1995. V. 57. P. 683–706.
16. Rand M., Li C. // *Annu. Rev. Physiol.* 1995. V. 57. P. 659–682.
17. Schuman E.M., Madison D.V. // *Annu. Rev. Neurosci.* 1994. V. 17. P. 153–183.
18. Almanza A., Navarrete F., Vega R., Soto E. // *J. Neurophysiol.* 2007. V. 97. P. 1188–1195.
19. Behrend O., Schwark C., Kunihiro T., Strupp M. // *NeuroReport.* 1997. V. 8. P. 2687–2690.
20. Chen, J.W. Y., Eatock R.A. // *J. Neurophysiol.* 2000. V. 84. P. 139–151.
21. Ryzhova I.V., Nozdrachev A.D., Tobias TV., Orlov I.V., Chikhman V.N., and Solnushkin S.D. // *Doklady Biological Sciences.* 2016. V. 469. P. 1–3.
22. Takumida M., Anniko M. // *Acta Otolaryngol.* 2001. V. 121. P. 342–345.
23. Guth P.S., Holt J.C., Perin P., Athas G., Garcia M., Puri A., Zucca G., Botta L., Valli P. // *Hear. Res.* 1998a. V. 125. P. 154–162.
24. Andrianov G.N., Puyal J., Raymond J., Venteo S., Dememes D., Ryzhova I.V. // *Hear. Res.* 2005. V. 204. P. 200–209.
25. Puyal J., Grassi S., Dieni C., Frondali A., Demêmes D., Raymond J., Pettorossi V.E. // *J. Physiol.* 2003. V. 553. P. 427–443.
26. Anwyl R. // *Brain Res. Rev.* 1999. V. 29. P. 83–120.
27. Bellone C., Lüscher C., Mameli M. // *Cell. Mol. Life Sci.* 2008. V. 65. P. 2913–2923.
28. Pettorossi V.E., Dieni C.V., Scarduzio M., Grassi S. // *Neurosci.* 2011. V. 187. P. 1–14.
29. Nakanishi S. // *Neuron.* 1994. V. 13. P. 1031–1037.
30. Pin J.-P., Duvoisin R. // *Neuropharmacol.* 1995. V. 34. P. 1–26.
31. Conn P.J., Pin J.P. // *Annu. Rev. Pharmacol. Toxicol.* 1997. V. 37. P. 205–237.
32. Roberts M. // *Neuropharm.* 1995. V. 34. P. 813–819.
33. Kew J.N., Kemp J.A. // *Psychopharmacol.* 2005. V. 179. P. 4–29.
34. Niswender C.M., Conn P.J. // *Annu. Rev. Pharmacol. Toxicol.* 2010. V. 50. P. 295–322.
35. Fill M., Copello J.A. // *Physiol. Rev.* 2002. V. 82. P. 893–922.
36. Kakizawa S. // *Front. Endocrinol.* 2013. V. 4. P. 1–6.
37. Schlossmann J., Ammendola A., Ashman K., Zong H., Huber A., Neubauer G., Wang G.-X., Allescher H.D., Korth M., Wilms M., et al. // *Nature.* 2000. V. 404. P. 197–201.
38. Kleinlogel S., Oestereicher T.A., Ehrenberger K., Felix D. // *NeuroReport.* 1999. V. 10. P. 1879–1882.
39. Peng B.G., Li Q.X., Ren T.Y., Ahmad S., Chen S.P., Chen P., Lin X. // *Neurosci.* 2004. V. 123. P. 221–230.
40. Hendricson A.W., Guth P.S. // *Hear. Res.* 2002. V. 172. P. 99–109.
41. Rossi M.L., Prigioni I., Gioglio L., Rubbini G., Russo G., Martini M., Farinelli F., Rispoli G., Fesce R. // *Eur. J. Neurosci.* 2006. V. 23. P. 1775–1783.
42. Guth P.S., Perin P., Norris C.H., Valli P. // *Progr. Neurobiol.* 1998b. V. 54. P. 193–247.
43. Vega R., Ortega A., Almanza A., Soto E. // *Neurosci. Lett.* 2006. V. 393. P. 65–69.
44. Martínez-Ruiz A., Cadenas S., Lamas S. // *Free Radical Biol. Med.* 2011. V. 51. P. 17–29.
45. Garthwaite J., Southam E., Boulton C., Nielsen E., Schmidt K., Mayer B. // *Mol. Pharmacology.* 1995. V. 48. P. 184–188.
46. Ruth P., Wang G.-X., Boekhoff I., May B., Pfeir A., Pennert R., Korth M., Breer H., Hofmann F. // *Proc. Natl. Acad. Sci. USA.* 1993. V. 90. P. 2623–2627.
47. Ahern G., Klyachko V., Jackson M.B. // *Trends Neurosci.* 2002. V. 25. № 10. P. 510–517.
48. Stoyanovsky D., Murphy T., Anno P.R., Kim Y.-M., Salama G. // *Cell Calcium.* 1997. V. 21. № 1. P. 19–29.
49. Nakamura T., Lipton S.A. // *Neurochem. Res.* 2016. V. 41. № 3. P. 510–514.

# Phylogenetic Analysis and Molecular Typing of Trichothecene-Producing *Fusarium* Fungi from Russian Collections

A. A. Stakheev<sup>1</sup>, L. V. Samokhvalova<sup>1</sup>, O. D. Mikityuk<sup>2</sup>, S. K. Zavriev<sup>1</sup>

<sup>1</sup>M.M. Shemyakin and Yu.A. Ovchinnikov Institute of Bioorganic chemistry of the Russian Academy of Sciences, Miklukho-Maklaya Str. 16\10, Moscow, 117997, Russia

<sup>2</sup>All-Russian Research Institute of Phytopathology, Institut Str. 5, B. Vyazyomy, Moscow region, 143050, Russia

\*E-mail: Stakheev.aa@gmail.com

Received April 26, 2017; in final form March 27, 2018

Copyright © 2018 Park-media, Ltd. This is an open access article distributed under the Creative Commons Attribution License, which permits unrestricted use, distribution, and reproduction in any medium, provided the original work is properly cited.

**ABSTRACT** We performed a three-locus phylogenetic analysis of *Fusarium* strains presumably capable of trichothecene production, which were deposited in the Russian national collections. The intra- and interspecific polymorphism of partial sequences of the translation elongation factor 1 alpha (*TEF1α*) gene and two genes from the trichothecene cluster *TRI5* and *TRI14* was studied. A study of 60 strains of different origins using DNA markers confirmed, and in the case of several strains, clarified their taxonomic characteristics. As a result, a strain of *F. commune* (F-900) was identified in Russia for the first time. Furthermore, the strain F-846 proved to be phylogenetically distinct from any of the known *Fusarium* species. *F. equiseti* strains from Northwest Russia were found to belong to the North European group (I), whereas a strain from the North Caucasus – to the South European one (II). Partial *TRI14* sequences from 9 out of 12 species were determined for the first time. Their comparative analysis demonstrated a relatively high level of intraspecific variability in *F. graminearum* and *F. sporotrichioides*, but no correlation between the sequence polymorphism and the geographic origin of the strains or their chemotype was found. Specific chemotypes of trichothecene B producers were characterized using two primer sets. The chemotyping results were verified by HPLC.

**KEYWORDS** *Fusarium*, trichothecene mycotoxins, DNA markers, phylogenetic analysis, identification, chemotype.

**ABBREVIATIONS** PCR – polymerase chain reaction, TrMT – trichothecene mycotoxin, *TEF1α* – translation elongation factor 1-α gene, *TRI5* – trichodiene synthase gene, bp – base pairs.

## INTRODUCTION

Fungi of the genus *Fusarium* from the class *Ascomycetes* occupy various ecological niches and occur in various climatic zones. In Russia, *Fusarium* species are ubiquitous in all regions where agricultural crops, primarily cereals, are grown. This fungus causes significant damage to the agricultural and food industries, resulting in several hundred million dollar losses annually. In addition, the mycotoxins produced by members of the genus *Fusarium* pose a threat to human and animal health and also act as pathogenicity factors for plants [1].

Trichothecene mycotoxins (TrMTs) are the most extensive group of toxic metabolites produced by *Fusarium* fungi. Trichothecene mycotoxins are produced not only by members of the genus *Fusarium*, but also by those from the genera *Myrothecium*, *Trichoderma*, *Cephalosporium*, *Verticimonosporium*, and *Stachybotrys* [2]. To date, about 200 trichothecene toxins

have been identified [3–6]. TrMTs are sesquiterpene compounds consisting of three rings with an epoxide ring at the C-12–C-13 atoms and a double bond at the C-9–C-10 atoms: so, the group is called 12,13-epoxytrichotec-9-ens. Depending on the side group structure, trichothecene toxins are divided into four types (A–D), with only types A and B produced by *Fusarium* fungi. More toxic members of type A trichothecenes include diacetoxyscirpenol (DAS), as well as toxins T-2 and HT-2, and the main producers of these toxins are *F. sporotrichioides* and *F. langsethiae*. In 2015–2016, a new group of type A trichothecene toxins, named NX, was described [7, 8]. Interestingly, these compounds were identified in cultures of *F. graminearum*, a traditional producer of B-type TrMTs. Type B is represented by compounds such as nivalenol (NIV), deoxynivalenol (DON), and their acetylated derivatives (3- and 15-ADON and 4,15-ANIV) that are produced

by *F. graminearum*, *F. culmorum*, *F. cerealis*, and a group of species known as the *F. graminearum* species complex (FGSC) [9, 10]. In addition, *F. poae*, *F. venenatum*, and *F. equiseti* are capable of producing both type A and type B toxins [11]. The type of toxins produced by a particular strain is determined by the structure and functions of the genes present in the trichothecene cluster [12, 13]. In most trichothecene-producing *Fusarium* species, the main cluster comprises 12 genes that encode both of the enzymes responsible for different biosynthesis stages and regulatory factors, some of which control the expression of a large number of the genes associated with various aspects of the fungal metabolism and life activity [14]. Trichothecene toxins inhibit protein synthesis in eukaryotes [15], and trichothecenes such as DON are important aggressiveness factors promoting fungal spread within host plant tissues. Artificial inoculation of cereal ears with mutant *F. graminearum* strains with abolished DON synthesis has been shown to infect a smaller number of kernels compared to inoculation with wild-type strains [16].

The danger posed by *Fusarium* fungi and their mycotoxins necessitates the development of methods for a quick and reliable species-specific identification of the strains which will enable a determination of the spectrum of the compounds contained in a culture or batch of grain. At present, DNA polymorphism analysis methods play an important role in taxonomic studies of the genus *Fusarium* and in the identification of its members. Application of the molecular genetics approach has enabled a clarification of the standards and boundaries of species, as well as the characterization of several new taxa. In particular, a multilocus phylogenetic analysis using sequence-characterized amplified region (SCAR) markers [17] based on 13 housekeeping genes enabled the identification of 9 new species within the FGSC [10], which had been previously considered as a single-species *F. graminearum*. A little later, species *F. vorosii* and *F. gerlachii* were also included in this complex [18]. In total, 16 phylogenetic species can be distinguished in the FGSC [19]. The phylogenetic approach was used to confirm the status of *F. pseudograminearum* and *F. culmorum* as separate species [20, 21]. In Russia, an analysis of polymorphic DNA markers enabled the identification of strain groups that were subsequently described as two new species: *F. ussuriianum*, morphologically and phenotypically similar to *F. graminearum* [22], and *F. sibiricum*, closely related to *F. sporotrichioides* [23]. A number of recent phylogenetic studies have determined an intricate structure of the *F. equiseti*–*F. incarnatum* species complex (FIESC) and identified several new species within the complex [24]. In addition, investigation of inter- and intraspecific DNA polymorphisms has made possible the devel-

opment of several highly specific diagnostic and identification systems for the main *Fusarium* pathogens, which are primarily based on PCR and its modifications [25–29]. The use of modern molecular biological and bioinformatic methods, including whole genome sequencing [30, 31], has significantly accelerated the investigation of the genetic diversity of the genus *Fusarium* and the functional characterization of genomic elements, but the search for effective methods of molecular typing and informative DNA barcodes still remains topical [32, 33].

The genus *Fusarium* is different from most other taxa of the kingdom Fungi. The “gold standard” of molecular fungal taxonomy is the ribosomal DNA internal transcribed spacer (ITS) region [34]. However, these markers in the genome of members of the genus *Fusarium* are represented by two nonorthologous copies and do not possess a sufficient level of interspecific polymorphism [35]. Today, the *TEF1α* gene is most often used as a marker in phylogenetic and taxonomic studies [36, 37]. It seems promising to use the genes involved in mycotoxin biosynthesis as phylogenetic markers. For example, the trichodiene synthase gene (*TRI5*) has been used to develop species-specific primer systems [38] and to study intraspecific polymorphism in members of the *F. equiseti* species complex [39, 40]. However, the phylogenetic characteristics of the *TRI5* gene have not been compared with those of “classical” markers, such as *TEF1α*. Among other genes that comprise the trichothecene cluster and are used in phylogenetic studies, it is necessary to emphasize the role of *TRI1* encoding cytochrome P450 monooxygenase and *TRI12* encoding a trichothecene efflux pump [41]. A phylogenetic analysis of the *TRI1* gene helped to identify a group of *F. graminearum* strains capable of producing the NX-2 toxin [7]. *TRI12* polymorphism was used to design primers for the detection of type B TrMT-producing strains based on their chemotype (3/15-ADON, NIV) [42]. The trichothecene cluster also includes a number of genes that have not been characterized either structurally or functionally; e.g., *TRI9* and *TRI14* [43].

*Fusarium* strains from Russian national collections, which are potentially capable of producing TrMTs and represent different climatic and geographic regions of Russia, have not been characterized by molecular genetic methods. Therefore, the main objectives of this study were as follows: (1) a SCAR marker-based analysis of the accuracy of the taxonomic identification of the trichothecene-producing *Fusarium* strains deposited in Russian national collections; (2) an investigation of the molecular genetic diversity of strains of different geographical origin, isolated in different years and from different sources; (3) determination of the inter-

and intraspecific polymorphism of the *TRI14* gene, one of the least studied genes of the trichothecene cluster; and (4) determination of chemotypes of type B TrMT-producing strains using specific PCR primers, with verification of the data by HPLC.

## EXPERIMENTAL

### Fungal strains

We analyzed 60 strains of 12 *Fusarium* genus species deposited in Russian national collections and presumably possessing ability for TrMT biosynthesis. The choice of the strains was based on maximum coverage of various natural and geographical zones of Russia. In addition, the study included strains from a number of neighboring countries, as well as from Moldova and Germany. We also studied the *F. graminearum* strain F-892 (VKPM) deposited in the StrainInfo database (<http://www.straininfo.net>; ATCC 36015). The list of strains with indication of their geographical origin, host plant species, year of isolation, and the particular collection are given in *Table 1*. In addition, the morphological features of several strains the initial identification of which had not been confirmed by molecular methods were determined using a MIKMED 6 laboratory microscope (Lomo, Russia). For the microscopic analysis, the fungal strains were grown on carnation leaf agar (CLA) and synthetic nutrient deficient agar (SNA; Nirenberg) for 10–14 days.

### DNA isolation

Prior to DNA isolation, monospore cultures of fungi were grown on potato sucrose agar (PSA) at room temperature for 10 days, until abundant mycelium was obtained. DNA was isolated from monospore fungal cultures by a method based on the use of cetyltrimethylammonium bromide as a detergent, with allowance for the modifications described earlier [28]. The concentration and purity of DNA samples were evaluated using a NanoVue spectrophotometer (GE HealthCare, USA).

### Design of universal primers, PCR, and sequencing

To amplify partial sequences of the *TEF1 $\alpha$* , *TRI5*, and *TRI14* genes, we constructed the following primer pairs: TEF50F (5'-CGACTCTGGCAA-GTCGACCAC-3') and TEF590R (5'-CTCGGCT-TTGAGCTTGTC AAG-3'); TRI5F (5'-ACACT-GGTTCTGGACGACAGCA-3') and TRI5R (5'-CCATCCAGTTCTCCATCTGAG-3'); TRI14F (5'-GAAGCTGCCTCGACATGGCTC-3') and TRI14R (5'-AATAATATTATGGGGAACAATCAT-3').

The primers were designed using the ClustalW algorithm [44]. The physicochemical properties of the primers were evaluated using the Oligo 6.71 software.

PCR was performed using the following amplification programs.

Primers TEF50F–590R: 93°C, 90 s; 93°C, 20 s; 64°C, 5 s; 67°C, 5 s (5 cycles); 93°C, 1 s; 64°C, 5 s; 67°C, 5 s (40 cycles).

Primers TRI5F–R and TRI14F–R: 93°C, 90 s; 93°C, 10 s; 55°C, 15 s; 72°C, 10 s (40 cycles).

PCR and electrophoretic analysis were performed according to [27, 28].

PCR products were cloned using an InstA Clone PCR cloning kit (Fermentas, Lithuania) according to the manufacturer's protocol. DNA was sequenced at the Evrogen JSC using an ABI PRISM BigDye Terminator v.3.1 kit, followed by an analysis of the reaction products on an ABI PRISM 3730 automatic sequencer (Applied Biosystems).

The nucleotide sequences characterized in the present work are deposited in the NCBI GenBank under the accession numbers MG989711–989751 (*TEF1 $\alpha$* ), MH001611–001651 (*TRI5*), and MH001652–001692 (*TRI14*).

### Phylogenetic analysis

DNA markers with a characterized nucleotide sequence were compared with sequences deposited in the NCBI GenBank and *Fusarium* MLST databases (<http://www.westerdijkinstituut.nl/fusarium/>) using the BLAST algorithm. Phylogenetic trees were constructed with the maximum likelihood (ML) method and GTR+G (General Time Reversible) nucleotide substitution model [45] using the MEGA5.1 software [46]. In addition to the studied strains, several sequences of the appropriate genes of typical strains from international collections deposited in databases were used in the phylogenetic analysis. The reliability of phylogenetic tree topologies was confirmed by bootstrap analysis from 1,000 replicates. Insertions and deletions were omitted from the analysis. The number of variable, parsimony informative nucleotides and haplotypes for each marker was calculated with the DnaSP v6 software [47] using a sample of 41 strains.

### Molecular typing of type B TrMT producers

To determine the chemotypes of the type B TrMT producers, we analyzed *F. graminearum*, *F. culmorum*, *F. cerealis*, and *F. ussurianum* strains. Chemotype-specific PCR was performed using three primer sets: two sets of primers for the polymorphic regions of the *TRI12* gene [42] (the set is denoted as 12-1), [48] (12-2), and a pair of primers for the amplification of *TRI13* gene fragments with different lengths, depending on the chemotype [49] (13-1). The structure of primers and their melting temperatures are presented in *Table 2*.

Table 1. *Fusarium* fungal strains used in the study.

| No. | Accession number     | Species                           | Origin                       | Source         | Year of isolation |
|-----|----------------------|-----------------------------------|------------------------------|----------------|-------------------|
| 1   | M-99-43*             | <i>F. culmorum</i>                | Moscow Region                | Wheat          | 1999              |
| 2   | 09-1/7*              | <i>F. culmorum</i>                | Moscow Region                | Wheat          | 2009              |
| 3   | M-99-9*              | <i>F. culmorum</i>                | Moscow Region                | Wheat          | 1999              |
| 4   | M-10-1*              | <i>F. culmorum</i>                | Moscow Region                | Wheat          | 2010              |
| 5   | BR-03-19*            | <i>F. culmorum</i>                | Bryansk Region               | Wheat          | 2003              |
| 6   | BR-0453*             | <i>F. culmorum</i>                | Bryansk Region               | Wheat          | 2004              |
| 7   | OM-0233*             | <i>F. culmorum</i>                | Omsk Region                  | Wheat          | 2002              |
| 8   | OR-02-37*            | <i>F. culmorum</i>                | Orel Region                  | Wheat          | 2002              |
| 9   | CM-9864*             | <i>F. culmorum</i>                | Smolensk region              | Wheat          | 1998              |
| 10  | KP-1136-66*          | <i>F. culmorum</i>                | Kirov region                 | Wheat          | 1995              |
| 11  | KP-1599-25/3*        | <i>F. culmorum</i>                | Kirov Region                 | Wheat          | 1996              |
| 12  | KS-1384-1*           | <i>F. culmorum</i>                | Kirov Region                 | Wheat          | 2007              |
| 13  | M-05-111*            | <i>F. culmorum</i>                | Moscow Region                | Wheat          | 2005              |
| 14  | KC-1716-8*           | <i>F. culmorum</i>                | Kirov Region                 | Wheat          | 1997              |
| 15  | 58801**              | <i>F. culmorum</i>                | Moscow Region                | Wheat          | 2004              |
| 16  | Kz-27*               | <i>F. culmorum</i>                | Kostanay Region, Kazakhstan  | Unknown        | 2014              |
| 17  | 74007**              | <i>F. culmorum</i>                | Arkhangelsk Region           | Potato         | Unknown           |
| 18  | 58030**              | <i>F. culmorum</i>                | Rostov Region                | Cirsium        | 2004              |
| 19  | 70505**              | <i>F. culmorum</i>                | Belarus                      | Wheat          | 2003              |
| 20  | 50106**              | <i>F. culmorum</i>                | Leningrad Region             | Cirsium        | 2006              |
| 21  | 64722**              | <i>F. cerealis</i>                | Khabarovsk Region            | Wheat          | 2006              |
| 22  | 39295**              | <i>F. cerealis</i>                | Heilongjiang province, China | Wheat          | 2003              |
| 23  | 37032**              | <i>F. cerealis</i>                | Heilongjiang Province, China | Wheat          | 2003              |
| 24  | 39142**              | <i>F. cerealis</i>                | Heilongjiang Province, China | Wheat          | 2003              |
| 25  | 37031**              | <i>F. cerealis</i>                | Heilongjiang Province, China | Wheat          | 2003              |
| 26  | 41727**              | <i>F. cerealis</i>                | North Ossetia                | Cirsium        | 2004              |
| 27  | G.8-8**              | <i>F. graminearum</i>             | Germany                      | Wheat          | 1998              |
| 28  | 41806**              | <i>F. graminearum</i>             | North Ossetia                | Wheat          | 2004              |
| 29  | 48702**              | <i>F. graminearum</i>             | Tula Region                  | Wheat          | Unknown           |
| 30  | 58033**              | <i>F. graminearum</i>             | Leningrad Region             | Wheat          | 2002              |
| 31  | 70725**              | <i>F. graminearum</i>             | Orel Region                  | Wheat          | 2006              |
| 32  | 58212**              | <i>F. ussurianum</i> <sup>1</sup> | Primorsky Krai               | Wheat          | Unknown           |
| 33  | 29813**              | <i>F. ussurianum</i>              | Jewish Autonomous Oblast     | Wheat          | 2002              |
| 34  | MM-7*                | <i>F. sporotrichioides</i>        | Moscow Region                | Wheat          | 2010              |
| 35  | KG-9744*             | <i>F. sporotrichioides</i>        | Kirov Region                 | Wheat          | Unknown           |
| 36  | 78105**              | <i>F. sporotrichioides</i>        | Orel Region                  | Wheat          | 2006              |
| 37  | SK-1506*             | <i>F. sporotrichioides</i>        | North Ossetia                | Wheat          | 2010              |
| 38  | 64706**              | <i>F. sporotrichioides</i>        | Primorsky Krai               | Barley         | 2006              |
| 39  | 33100**              | <i>F. sporotrichioides</i>        | Primorsky Krai               | Wheat          | 2003              |
| 40  | 74006**              | <i>F. sporotrichioides</i>        | Leningrad Region             | Barley         | 2006              |
| 41  | 11007**              | <i>F. sibiricum</i>               | Krasnoyarsk Region           | Barley         | 2000              |
| 42  | 11014**              | <i>F. sibiricum</i>               | Amur Region                  | Oat            | 2001              |
| 43  | 55201**              | <i>F. langsethiae</i>             | Kaliningrad Region           | Oat            | 2005              |
| 44  | 82901**              | <i>F. langsethiae</i>             | Orel Region                  | Oat            | 2003              |
| 45  | 47401**              | <i>F. poae</i>                    | Moscow Region                | Wheat          | 2004              |
| 46  | 61701**              | <i>F. poae</i>                    | Saratov Region               | Wheat          | 2005              |
| 47  | 58242**              | <i>F. venenatum</i>               | Germany                      | Unknown        | Unknown           |
| 48  | 58514**              | <i>F. venenatum</i>               | Leningrad Region             | Oat            | 2013              |
| 49  | 58455**              | <i>F. venenatum</i>               | Novgorod Region              | Wheat          | 2001              |
| 50  | F-842**              | <i>F. sambucinum</i>              | Kiev region, Ukraine         | Potato         | 1965              |
| 51  | F-3966***            | <i>F. sambucinum</i> <sup>2</sup> | Tula Region                  | Soil           | 2006              |
| 52  | F-4360***            | <i>F. sambucinum</i> <sup>2</sup> | Buryatia                     | Wood           | 2005              |
| 53  | 64414**              | <i>F. equiseti</i>                | Kaliningrad Region           | Barley         | 2006              |
| 54  | 65901**              | <i>F. equiseti</i>                | Leningrad Region             | Barley         | 2006              |
| 55  | 97001**              | <i>F. equiseti</i>                | North Ossetia                | Wheat          | 2007              |
| 56  | F-3549***            | <i>F. equiseti</i> <sup>4</sup>   | Negev Desert, Israel         | Soil           | 1995              |
| 57  | F-2681***            | <i>F. incarnatum</i>              | Moscow Region                | Unknown        | 1966              |
| 58  | F-846***             | <i>F. sp</i> <sup>3</sup>         | Moldova                      | Melon          | 1958              |
| 59  | F-892 (ATCC36015)*** | <i>F. graminearum</i>             | USA                          | Unknown        | 1977              |
| 60  | F-900****            | <i>F. sambucinum</i> <sup>2</sup> | Krasnoyarsk Region           | Larix sibirica | Unknown           |

\* – strains from the collection of the All-Russian Research Institute of Phytopathology; \*\* – strains from the collection of the All-Russian Institute of Plant Protection; \*\*\* – strains from the All-Russian Collection of Microorganisms; \*\*\*\* – strains from the All-Russian Collection of Industrial Microorganisms.

<sup>1</sup> – initially identified as *F. graminearum*;

<sup>2</sup> – initial identification was not confirmed;

<sup>3</sup> – initially identified as *F. poae*.

**Table 2.** Primers used for the chemotyping of type B trichothecene-producing strains.

| Primer set | Sequence   | Product length, bp | $T_m$ , °C | Chemotype                | Reference |
|------------|--|--------------------|------------|--------------------------|-----------|
| 12-1       | 12CON (univ.): 5'-CATGAGCATGGTGATGTC-3'  |                    |            |                          | [48]      |
|            | 12 NF: 5'-TCTCCTCGTTGTATCTGG-3'  | 840                | 60         | NIV                      |           |
|            | 12-15F: 5'-TACAGCGGTCGCAACTTC-3'   | 670                | 60         | 15-ADON                  |           |
|            | 12-3F: 5'-CTTTGGCAAGCCCCTGCA-3'  | 410                | 60         | 3-ADON                   |           |
| 12-2       | 3ADONf: 5'-AACATGATCGGTGAGGTATCGA-3'<br>3ADONr: 5'-CCATGGCGCTGGGAGTT-3'                | 60                 | 60         | 3-ADON                   | [42]      |
|            | 15ADONf: 5'-GTTTCGATATTCATTGGAAAGCTAC-3'<br>15ADONr: 5'-CAAATAAGTATCGTCTGAAATTGGAAA-5' | 57                 | 60         | 15-ADON                  |           |
|            | NIVf: 5'-GCCCATATTCGCGACAATGT-5'<br>NIVr: 5'-GGCGAACTGATGAGTAACAAAACC-3'               | 77                 | 60         | NIV                      |           |
| 13-1       | Tri13P1: 5'-CTCSACCGCATCGAAGASTCTC-3'<br>Tri13P2: 5'-GAASGTGCGARGACCTTGTTC-3'          | 859<br>644<br>583  | 62         | 15-ADON<br>3-ADON<br>NIV | [49]      |

un. – universal primer

$T_m$  – melting temperature

In the case of system 12-2, the analysis was performed with each pair of primers separately, not in a multiplex PCR [48] format, to increase analysis specificity and avoid the formation of nonspecific amplicons.

The obtained results were confirmed by quantitative PCR (qPCR) with primer pairs from systems 12-1 and 12-2. In addition to standard components, 1.5  $\mu$ L of 20 $\times$  EvaGreen dye (Biotium, USA) was added to the reaction mixture. Amplification and fluorescent signal detection were performed in a DT-96-detecting amplifier (DNA-Technology, Russia). The PCR results were expressed as quantification cycles ( $C_q$ , [50]). Each sample was analyzed in two independent replicates.

#### HPLC analysis of toxin production by type B TrMT-producing strains

To determine the type of TrMTs produced by the studied strains, fungal cultures were grown on a MYRO liquid medium [51] at 25 °C and 220 rpm for 5 days. The ability of isolates to produce DON and its monoacetylated derivatives was determined by reverse phase high pressure liquid chromatography of the culture filtrate supernatant separated from the mycelium by centrifugation [52, 53]. An 8 mL aliquot of the culture liquid supernatant was diluted with a acetonitrile : water (1 : 1) mixture to 10 mL and passed through a 0.22  $\mu$ m Millipore membrane filter; 10  $\mu$ L of the sample was introduced into the injector of a Waters 1525 Breeze HPLC system equipped with a Waters 2487 UV detector (Waters, USA). Separation was carried out on a Symmetry C18 (150  $\times$  4.6 mm) column thermostated at 27°C. Mycotoxins were eluted with an acetonitrile : methanol : water (1 : 1 : 8 v/v/v – mobile phase)

mixture at a flow rate of 0.5 mL/min and detected at 254 nm. Commercial DON, 3-AcDON, and 15-AcDON (Sigma-Aldrich, USA) were used as standards; as a control, we used the filtrate of the MYRO uninoculated medium that was incubated simultaneously with cultivation of submerged fungal cultures under the above conditions.

## RESULTS

### Phylogenetic properties of genes, analysis of their partial sequences using the BLAST algorithm, and microscopic analysis of the morphology of strains with controversial identification

The main phylogenetic properties of the analyzed genes are given in Table 3. The DNA of all strains was amplified with a TEF50F–590R primer pair, which resulted in a single 452 to 483 bp amplification product containing two 80 to 100 and 236 to 254 bp introns. Except for the insertions and deletions omitted in the evaluation of the phylogenetic properties, the length of the analyzed sequences was 392 bp, including 129 (32.9%) variable nucleotides. The number of parsimony informative characters was 115 (29.3%), and the number of haplotypes was 17. An analysis of the *TEF1 $\alpha$*  gene sequences using the BLAST algorithm confirmed the initial species identification for 54 strains. Of the six strains without confirmed identification, three were initially classified as *F. sambucinum*. The *TEF1 $\alpha$*  sequences of strains F-3966 (No. 51, Table 1), NRRL 52726 relating to the *F. tricinctum* species complex, and NRRL 52727 (*F. avenaceum*) were shown to be 99.3% similar. Similarity for the strain F-4360 (No. 52) to the *F. acuminatum* strain, NRRL 52789 was 99.545%. The *TEF1 $\alpha$*

Table 3. Phylogenetic characteristics of analyzed sequences.

| Locus                   | SL, bp | GC, % | VS, % | PIS, % | HT | H <sub>d</sub> | P <sub>i</sub> |
|-------------------------|--------|-------|-------|--------|----|----------------|----------------|
| <i>TEF1α</i>            | 392    | 53.2  | 32.9  | 29.3   | 17 | 0.933          | 0.08872        |
| <i>TRI5</i>             | 379    | 48.5  | 37.2  | 36.1   | 13 | 0.907          | 0.13586        |
| <i>TRI14</i>            | 650    | 49.1  | 36.7  | 34.5   | 23 | 0.96           | 0.13510        |
| <i>TEF1α+TRI5+TRI14</i> | 1421   | 50    | 35.9  | 33.5   | 28 | 0.976          | 0.1233         |

SL – sequence length

VS – variable sites

PIS – parsimony informative sites

HT –haplotypes

H<sub>d</sub> – haplotype diversity

P<sub>i</sub> – nucleotide diversity

gene sequence from the F-900 strain (No. 60) was 100% similar to a fragment of this gene from the *F. commune* strain NRRL 52764. The initial morphological species identification of strain F-3549 (No. 56) as *F. equiseti* was not confirmed: the BLAST analysis revealed 99% similarity to the sequence of strain NRRL 34033 from a relatively rare species, *F. brachygibbosum*. The strain 58212 (No. 32), initially identified as *F. graminearum*, had 100% similarity of the *TEF1α* sequence to that of CBS 123751–123745 strains typical of *F. ussurianum*. The most interesting result was obtained through a marker sequence analysis of the strain F-846 initially identified as *F. poae*. Comparison with the *TEF1α* sequences of typical strains deposited in databases did not reveal 100% similarity to any of them. The closest sequence was that from the *F. polyphialidicum* strain F-0016 (DQ295144, 97% similarity).

*TRI5*F-R primer pair provided DNA amplification for all studied strains except for Nos. 51, 52, 56, and 60. An amplification product of the *TRI5* gene was 431–440 bp long and contained one intron of 52–61 bp in length. The length of the analyzed sequences was 379 bp, including 141 (37.2%) variable sites and 137 (36.1%) parsimony informative sites; the number of haplotypes was 13. The BLAST-based sequence analysis confirmed the accuracy of species identification for 54 strains. A DNA amplification product of the strain 58212 had 99% similarity with a *TRI5* gene fragment from *F. asiaticum* (strains NRRL 26156 and 28720). It should be noted that none of the databases contained records of complete or partial structures of this gene in *F. ussurianum* strains, but given the close relationship between *F. asiaticum* and *F. ussurianum* [7], this result seems reliable. A DNA amplification product of the strain F-846 was 98% similar to a partial *TRI5* gene sequence from the *F. langsethiae* strain KF2640 (JF966259).

PCR with the *TRI14*F-R primer pair revealed no DNA amplification products in samples Nos. 51, 52, 56, and 60 (as in the case of the *TRI5*F-R pair), as well as

No. 58 (F-846). The DNA of the other strains was amplified with the formation of 698 to 705 bp products containing a single 50- to 59-bp intron. The analyzed sequence length (without insertions and deletions) was 650 bp, of which 239 bp (36.8%) were variable, and 224 bp (34.5%) were parsimony informative; the number of haplotypes was 23. The search for similar sequences in the GenBank and Fusarium MLST databases showed that the studied strains of *F. graminearum* constitute two groups: the first group comprising Nos. 30 and 58 showed 100% similarity with the *TRI14* sequence of strain CBS 138562 (KU572434.1), while the second group (Nos. 27–29, 31) was completely identical to the sequence of strain CBS 138561 (KU572429.1), with the sequence similarity in these two groups being 97%.

We performed a microscopic analysis of the main morphological structures of strains whose initial identification was not confirmed by the marker sequence analysis. In strains F-3966 and F-4360 growing on CLA, elongated curved macroconidia with three to four septa typical of *F. avenaceum*, *F. tricinctum*, and *F. acuminatum* [54] were revealed. The strain F-900 also formed curved macroconidia with four septa and oval microconidia about 10 μm in size – features typical of the species *F. commune* [55]. In the strain F-846, thick-walled microconidia with four to five septa, as well as oval and clavate microconidia, were found. This result confirms the suggestion about erroneous initial identification of the strain as *F. poae*, because this species is characterized by spherical or spinulose microconidia and rarely forms macroconidia, usually with three septa [54].

#### Analysis of phylogenetic tree topology

The phylogenetic trees generated on the basis of the structures of the three studied genes were characterized by both similarity and several significant topological differences. The *TEF1α* gene dendrogram (Fig. 1) comprises four large clusters supported by high bootstrap values (98 to 99%). Each cluster includes strains

**Fig. 1.** Phylogenetic tree constructed based on the alignment of partial *TEF1 $\alpha$*  gene sequences of trichothecene-producing species using the maximum likelihood method (74 sequences). Only bootstrap values higher than 50% from 1,000 replicates are shown. 21 sequences from the NCBI GenBank are also included.

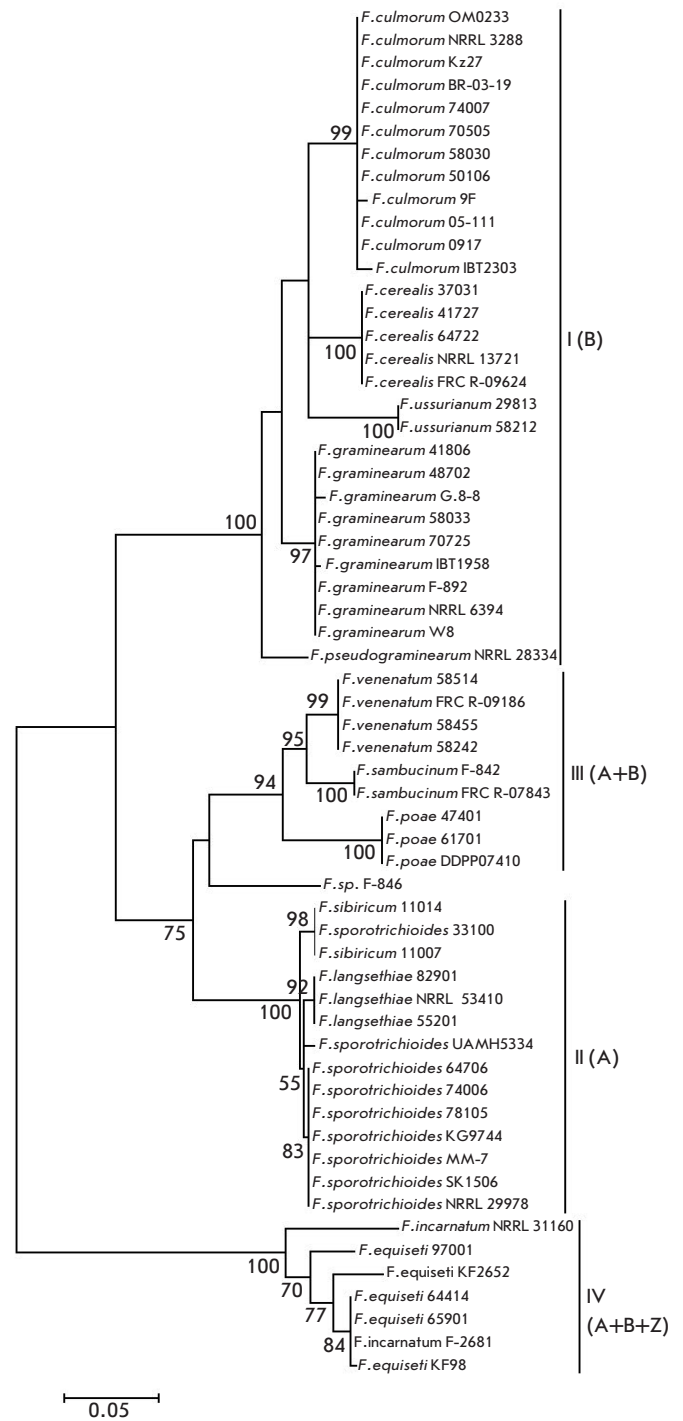
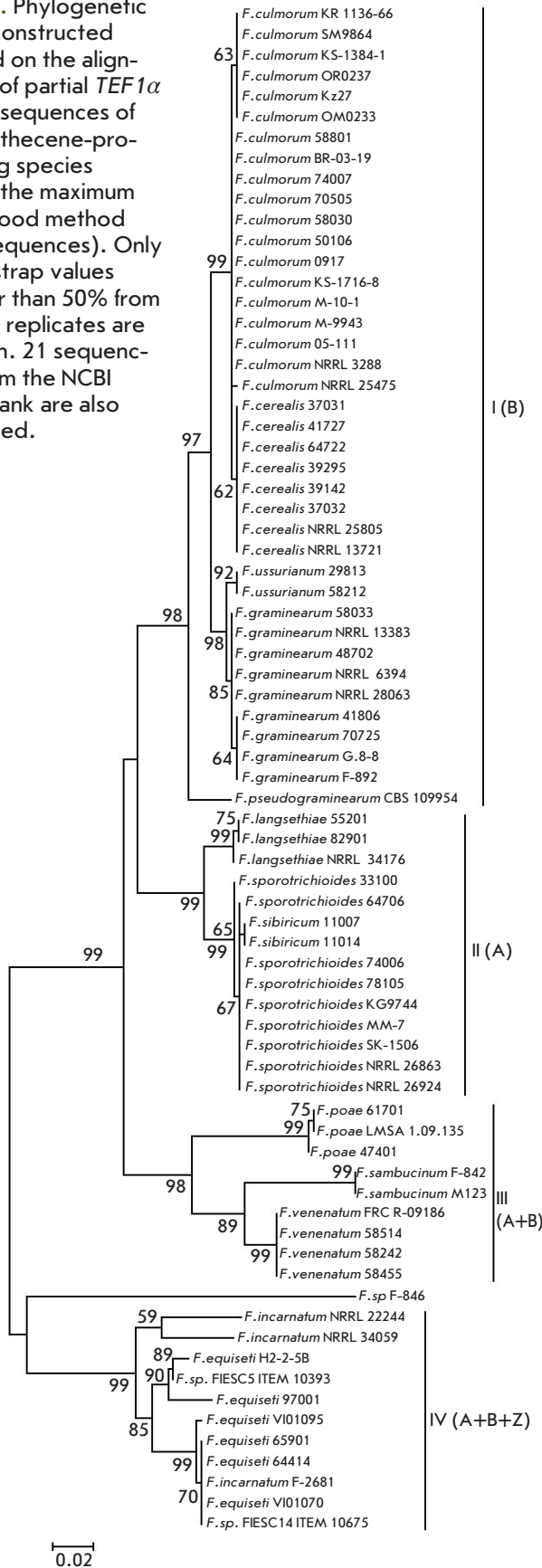


**Fig. 2.** Phylogenetic tree constructed based on the alignment of partial *TR15* gene sequences of trichothecene-producing species using the maximum likelihood method (60 sequences). Only bootstrap values higher than 50% from 1,000 replicates are shown. 18 sequences from the NCBI GenBank are also included.

of species characterized by similar spectra of the produced mycotoxins. Cluster I (bootstrap support of 98%) is represented by type B TrMT-producing species (including *F. pseudograminearum* CBS109954, No. KM434220); cluster II (99%) is formed by type A TrMT producers; cluster III (98%) is represented by species producing both TrMT types; and cluster IV (99%) is represented by the species *F. equiseti* and *F. incarnatum* that are also capable of producing both type A and B toxins; however, unlike *F. poae* and closely related species, they also possess the ability to produce zearalenone and some other mycotoxins. It should be noted that clusters I–III and IV form separate groups supported by high bootstrap values (99%), and “*F. sp.*” (*Fusarium sp.* strain F-846) located in an intermediate position between these two groups. Clusters I and II include two subgroups: the first subgroup of cluster I (support 99%) comprises strains of the species *F. culmorum* and *F. cerealis*, and the second subgroup (98%) contains *F. graminearum* and *F. ussurianum*. Subgroups of cluster II are represented by the species *F. langsethiae* and *F. sporotrichioides*/*F. sibiricum* (bootstrap support of 99% each). Cluster IV is the most heterogeneous and represented by *F. equiseti* and *F. incarnatum* species. Two typical strains of *F. incarnatum* (NRRL 22244 and NRRL 34059) form a separate group supported by a bootstrap value of 59%, which, however, does not include the F-2681 strain investigated in this study. The *F. equiseti* strain 97001, together with strains H2-2-5B (JF496575) and 10393 (LN901566), forms a subgroup (90%), and strains 65901 and 64414 are included in another subgroup (99%) that also comprises strains VI01095 (AJ543560), VI01070 (AJ543562), and 10675 (LN901573).

On the *TRI5* gene dendrogram (Fig. 2), the bootstrap support of the main clusters corresponding to the toxigenic profiles of the studied species ranges from 94 (cluster III) to 100% (clusters I, II, and IV). In contrast to the *TEF1 $\alpha$*  gene dendrogram, “*F. sp.*” is located in an intermediate position between clusters II and III. In addition, *F. sporotrichioides* strains do not form a single group but are distributed within cluster II; in particular, the strain 33100 belongs to the same subgroup as *F. sibiricum* strains (support of 98%). Cluster I lacks the *F. graminearum*-*ussurianum* subgroup characteristic of the *TEF1 $\alpha$*  dendrogram. On the *TRI14* gene phylogenetic tree (Fig. 3), *F. ussurianum* strains, together with *F. cerealis* strains, form a subgroup (bootstrap support of 95%), while *F. graminearum* strains are divided into two subgroups supported by bootstrap values of 99 and 100%, respectively. Cluster II includes the subgroups *F. langsethiae* (98%) and *F. sporotrichioides*/*sibiricum* (91%); therefore, the topology of this cluster on the *TRI14* dendrogram corresponds to the topology

of *TEF1 $\alpha$*  rather than the *TRI5* dendrogram. It should be noted that in cluster IV, the *F. equiseti* strains 64414 and 65901 and *F. incarnatum* strain F-2681, on the one hand, and the *F. equiseti* strain 97001, on the other, form separate branches on the dendrograms of both *TRI* genes.

The structure of a phylogenetic tree generated based on the analysis of the combined sequence of the genes *TEF1 $\alpha$* , *TRI5*, and *TRI14* (Fig. 4) involves four large clusters supported by 100% bootstrap values. Of particular interest is a common group comprising clusters II and III (bootstrap support of 96%).

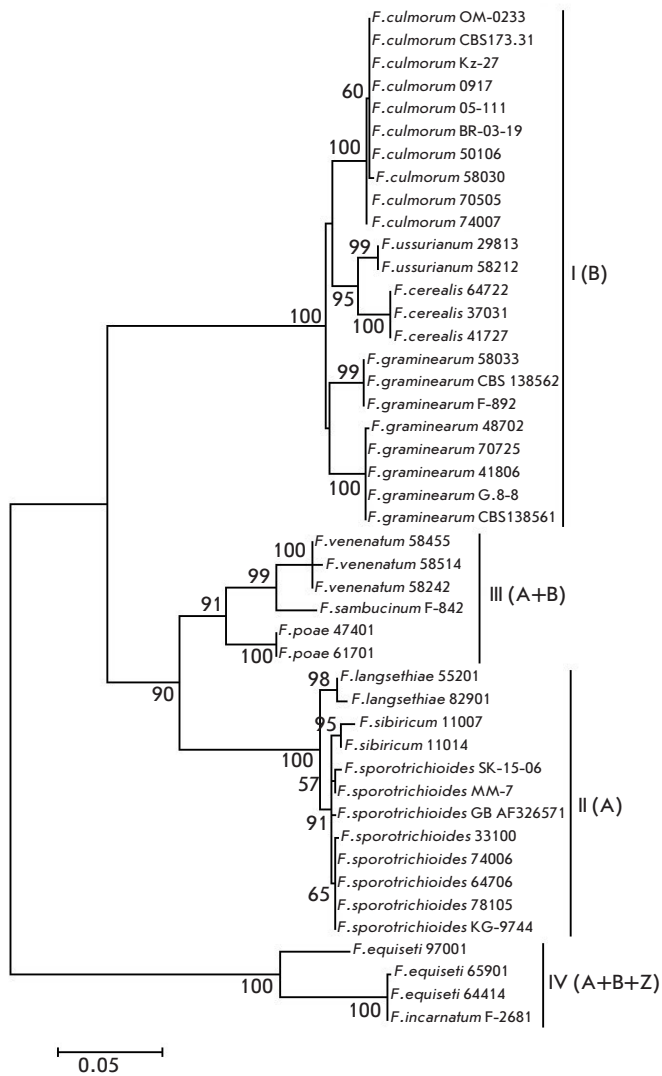
### Chemotyping of type B TrMT-producing strains and determination of mycotoxins by HPLC

Table 4 presents the results of the analysis of 33 type B TrMT-producing strains using qPCR with the primer sets 12-1 and 12-2. During the study, we decided to exclude set 13-1 from the use because an electrophoretic analysis of amplification products revealed two specific bands in all samples (data not shown): i.e., it was not possible to separate 3-ADON and 15-ADON chemotypes in *F. graminearum*. According to the chemotyping results, all analyzed *F. culmorum* and *F. ussurianum* strains belong to the 3-ADON chemotype, and the *F. graminearum* strains 58033 and 70725 also belong to it. The DNA of the *F. graminearum* strains G.8-8, 41806, and 48702 was amplified using a pair of 12CON-12-15F primers, indicating that they belong to the 15-ADON chemotype (however, minor bands were also detected in samples of *F. graminearum* 14-17, which was probably related to PCR conditions).

An HPLC-based analysis of strains for the toxin-forming ability confirmed the molecular typing data for most samples (Table 4). In most cultures, DON quantitatively predominated over acetylated derivatives; no derivatives were detected in strains *F. graminearum* G.8-8, *F. culmorum* KP-1599-25/3 and KS-1384-1, and *F. ussurianum* 58212. Figure 5 shows an example chromatogram of the culture liquid of the *F. ussurianum* strain 29813, with peaks corresponding to DON (retention time, 4.453 min) and 3-ADON (retention time, 5.483 min).

### DISCUSSION

The main objective of this work was to study the genetic diversity and toxigenic characteristics of *Fusarium* fungal strains potentially capable of producing TrMTs, which were isolated in different regions of Russia and deposited in Russian national collections. Another important aspect of the study was to extend information about the structural features of the trichothecene cluster genes associated with the synthesis of the toxins and pathogenic properties of fungi.



**Fig. 3.** Phylogenetic tree constructed based on the alignment of partial *TR14* gene sequences of trichothecene-producing species using the maximum likelihood method (45 sequences). Only bootstrap values higher than 50% from 1,000 replicates are shown. 4 sequences from the NCBI GenBank are also included.

Because the *TEF1 $\alpha$*  gene is now considered to be the most studied and phylogenetically informative SCAR marker of genus *Fusarium* members, an analysis of its sequences has become the basis for verification of the taxonomic status of collection strains. The initial identification of six out of the 60 samples was not confirmed. The use of a combination of molecular genetic and morphological approaches enabled a highly reliable species identification for “controversial” strains. The strain 58212 (initially *F. graminearum*) was identified as *F. ussuriarum*, and this fact correlates well with its geographic origin (Primorye region) and with the

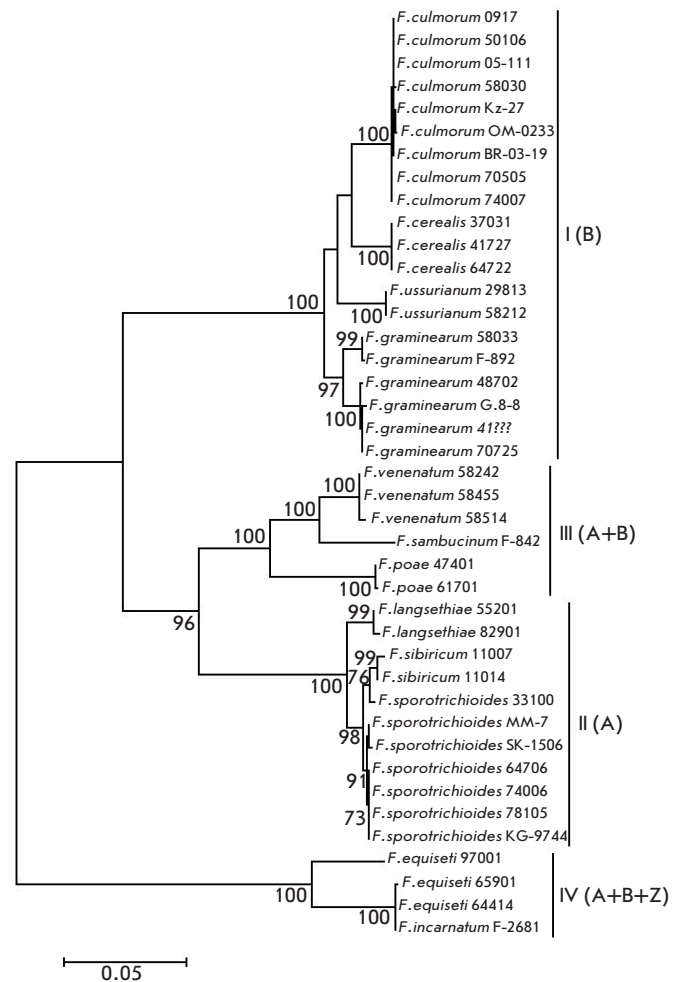


**Fig. 4.** Phylogenetic tree constructed based on the alignment of combined (*TEF1 $\alpha$* +*TR15*+*TR14*) sequences of trichothecene-producing species using the maximum likelihood method (41 sequences). Only bootstrap values higher than 50% from 1,000 replicates are shown.

fact that species *F. graminearum* and *F. ussuriarum* are almost indistinguishable by morphological features. Strains F-3966 and F-4360 deposited in collections as *F. sambucinum* were identified as *F. avenaceum* and *F. acuminatum*, respectively. Species *F. acuminatum* and *F. avenaceum* do not produce trichothecene mycotoxins; however, according to their ecological niches and growth pattern on potato sucrose agar, they are similar to *F. sambucinum*. There are no data on similar errors, but it is argued that *F. torulosum*, closely related to these two species, has been misidentified as *F. sambucinum* [54]. The strain F-900 isolated from forest tree nursery soil in the Krasnoyarsk region was identified as *F. commune* based on the results of a comprehensive study. The species *F. commune* described in 2003 [55] has not been detected to date in

**Table 4.** Results of qPCR with primer sets 12-1 and 12-2 for 33 strains of trichothecene B-producing *Fusarium* species. «?» - minor bands on electrophoresis gel or minor amplification on last cycles are detected; «n/a» - not analyzed.

| Strain                          | 3-ADON |      | 15-ADON |      | NIV  |      | HPLC    |
|---------------------------------|--------|------|---------|------|------|------|---------|
|                                 | 12-1   | 12-2 | 12-1    | 12-2 | 12-1 | 12-2 |         |
| Primer set                      |        |      |         |      |      |      |         |
| <i>F. culmorum</i> M-99-43      | +      | +    | -       | -    | -    | -    | 3-ADON  |
| <i>F. culmorum</i> 09-1/7       | +      | +    | -       | -    | -    | -    | 3-ADON  |
| <i>F. culmorum</i> M-99-9       | +      | +    | -       | ?    | -    | -    | 3-ADON  |
| <i>F. culmorum</i> M-10-1       | +      | +    | -       | -    | -    | -    | n/a     |
| <i>F. culmorum</i> BR-03-19     | +      | +    | -       | -    | -    | -    | n/a     |
| <i>F. culmorum</i> BR-0453      | +      | +    | -       | -    | -    | -    | n/a     |
| <i>F. culmorum</i> OM-0233      | +      | +    | -       | -    | -    | -    | n/a     |
| <i>F. culmorum</i> OR-02-37     | +      | +    | -       | -    | -    | -    | 3-ADON  |
| <i>F. culmorum</i> CM-9864      | +      | +    | -       | -    | -    | -    | 3-ADON  |
| <i>F. culmorum</i> KP-1136-66   | +      | +    | -       | -    | -    | -    | n/a     |
| <i>F. culmorum</i> KP-1599-25/3 | +      | +    | -       | -    | -    | -    | DON     |
| <i>F. culmorum</i> KS-1384-1    | +      | +    | -       | -    | -    | -    | DON     |
| <i>F. culmorum</i> M-05-111     | +      | +    | -       | -    | -    | -    | 3-ADON  |
| <i>F. culmorum</i> KC-1716-8    | +      | +    | -       | -    | -    | -    | n/a     |
| <i>F. culmorum</i> 58801        | +      | +    | -       | -    | -    | -    | 3-ADON  |
| <i>F. culmorum</i> Kz-27        | +      | +    | -       | -    | -    | -    | n/a     |
| <i>F. culmorum</i> 74007        | +      | +    | -       | -    | -    | -    | 3-ADON  |
| <i>F. culmorum</i> 58030        | +      | +    | -       | -    | -    | -    | 3-ADON  |
| <i>F. culmorum</i> 70505        | +      | +    | -       | -    | -    | -    | 3-ADON  |
| <i>F. culmorum</i> 50106        | +      | +    | -       | -    | -    | -    | 3-ADON  |
| <i>F. cerealis</i> 64722        | -      | -    | -       | -    | +    | +    | n/a     |
| <i>F. cerealis</i> 39295        | -      | -    | -       | -    | +    | +    | n/a     |
| <i>F. cerealis</i> 37032        | -      | -    | -       | -    | +    | +    | n/a     |
| <i>F. cerealis</i> 39142        | -      | -    | -       | -    | +    | +    | n/a     |
| <i>F. cerealis</i> 37031        | -      | -    | -       | -    | +    | +    | n/a     |
| <i>F. cerealis</i> 41727        | -      | -    | -       | -    | +    | +    | n/a     |
| <i>F. graminearum</i> G.8-8     | -      | -    | +       | +    | -    | -    | DON     |
| <i>F. graminearum</i> 41806     | ?      | ?    | +       | +    | -    | -    | 15-ADON |
| <i>F. graminearum</i> 48702     | -      | ?    | +       | +    | -    | -    | 15-ADON |
| <i>F. graminearum</i> 58033     | +      | +    | -       | -    | -    | -    | 3-ADON  |
| <i>F. graminearum</i> 70725     | +      | +    | -       | -    | -    | -    | 3-ADON  |
| <i>F. ussurianum</i> 58212      | +      | +    | -       | -    | -    | -    | DON     |
| <i>F. ussurianum</i> 29813      | +      | +    | -       | -    | -    | -    | 3-ADON  |

Russia. According to the available data, *F. commune* can be both a soil saprophyte and a pathogen of various plants, including economically important crops. *F. commune* is considered to be taxonomically close to the *F. oxysporum* species complex, but it is incapable of producing TrMTs [56], which is confirmed by the absence of PCR amplification products with primer pairs to the *TRI5* and *TRI14* genes. Based on an analysis of *TEF1α* and *TRI5* gene sequences, the strain F-846 isolated from melon (Moldova, 1958), which was referred to as *F. poae* according to the Russian National Collection of Microorganisms, had no 100% similarity with

any of the sequences deposited in databases. According to its marker gene structure, the strain was most close to the strains *F. polyphialidicum* F-0016 (*TEF1α*) and *F. langsethiae* F2640 (*TRI5*). The relationship between F-846 and *F. polyphialidicum* was not confirmed by an analysis of their morphological structures. Regarding the strain F2640 deposited in the GenBank, there are doubts about the accuracy of its identification as *F. langsethiae*, which are confirmed by significant differences in the *TRI5* gene structure between this strain and typical strains of *F. langsethiae*. On dendrograms of the *TEF1α* and *TRI5* genes, F-846 was located in an

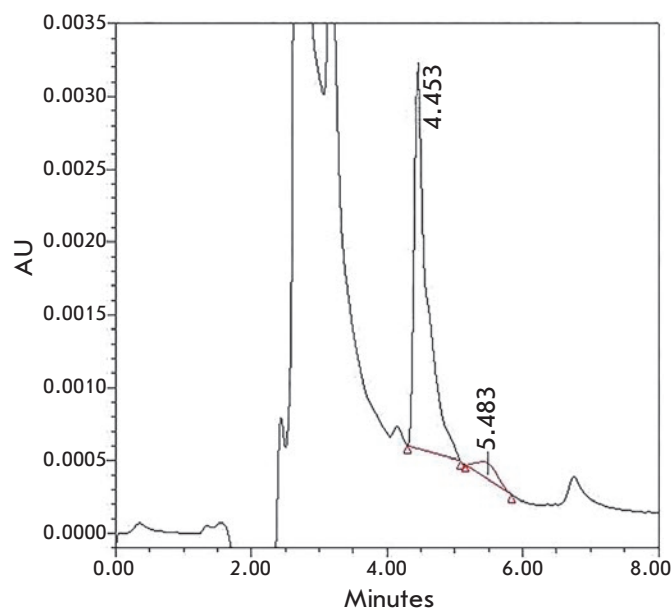


**Fig. 5.** An HPLC chromatogram of a liquid culture medium of *F. ussurianum* 29813. DON has a retention time of 4.453 min; 3-ADON has a retention time of 5.483 min.

intermediate position and was not assigned to any of the large clusters. We may tentatively suggest that the strain F-846 is a separate phylogenetic species; however, confirmation of this suggestion requires additional analysis using a broader spectrum of DNA markers, investigation of its toxin-producing ability, and additional morphological and physiological data.

In recent years, the species *F. equiseti*, together with the closely related *F. incarnatum*, has been shown to have a complex phylogenetic structure, forming a heterogeneous group called the *F. incarnatum-equiseti* species complex (FIESC). *F. equiseti* strains from Northern and Southern Europe form two different groups named type I and II [57]. In the present study, marker sequences of the *TEF1 $\alpha$*  gene of strains from different regions of Russia were compared with sequences of this gene from strains VI01070 and VI01095 belonging to type I, strain H2-2-5B belonging to type II, and strains 10675 and 10393 analyzed in [40]. Sequence comparison and phylogenetic analysis of *TEF1 $\alpha$*  demonstrated that the strain 97001 appears to belong to type II (Southern Europe), which correlates with its geographic origin (North Ossetia), while strains 64414 and 65901 (Kaliningrad and Leningrad Region, respectively) belong to the North European type I. An exception to this rule was the strain 10675 (LN901573) isolated from wheat in Spain in 2009, assigned, however, according to the constructed tree topology, to type I. The *F. incarnatum* strain F-2681 also belonged to type I.

The use of structures of the genes responsible for various stages of mycotoxin biosynthesis in phylogenetic studies has been a controversial issue, because most of these genes have been acquired through horizontal transfer. Usually, a comparative analysis of these markers does not correctly reflect the evolutionary relationships among taxa, but it may be useful in identifying the features of toxin formation or the pathogenic properties of the strains. In this study, we investigated the partial structures of two trichothecene cluster genes: *TRI5* encoding trichodiene synthase responsible for the first stage of TrMT biosynthesis, and *TRI14* the exact function of which is unknown but is presumably associated with the regulation of DON biosynthesis or its transport beyond the cell during the development of the fungus in infected plant tissues [16]. The information on the sequences of the trichothecene cluster genes presented in databases is rather limited. For example, one *TRI5* gene sequence from *F. venenatum* and *F. incarnatum* and two gene copies from *F. sambucinum* are deposited. There are only three *TRI14* gene annotations for *F. sporotrichioides*, one annotation for *F. pseudograminearum*, and seven and four annotations among complete sequences of the trichothecene cluster of *F. graminearum* and *F. culmorum*, respectively. Therefore, for the first time, partial sequences of the *TRI14* gene for 9 of 12 examined species were determined and deposited in the GenBank database. A characteristic feature of the *TRI5* and *TRI14* genes is the fact that a significant portion of the variable sites in the genes is located in the coding part, which is reflected in the differences in the amino acid sequences of appropriate proteins among and within species. The reverse is observed for the *TEF1 $\alpha$*  gene, in which all variable sites occur in introns, and the coding part is highly conserved. We believe that these differences may reflect the different evolutionary history of these genes and also the fact that the translation elongation factor does not belong to proteins specific to the genus *Fusarium*, while the polymorphism of the amino acid sequences of the proteins encoded by the *TRI* genes has an important adaptive value. This may also explain the differences in topology of phylogenetic trees constructed based on *TEF1 $\alpha$* , *TRI5*, and *TRI14*. One of the differences is common branches formed by clusters II (type A TrMT producers) and III (TrMT A+B) on the dendrograms of the *TRI5* and *TRI14* genes, respectively, and supported by high bootstrap values (90 and 75%). In turn, on the *TEF1 $\alpha$*  gene dendrogram, cluster II, along with cluster I (type B TrMT producers), forms a common branch, although the bootstrap support of this branch is low (less than 50%). Also, on dendrograms of the *TRI5* and *TRI14* genes, *F. ussurianum* strains form common clusters with strains of the species *F. culmo-*

*rum* and *F. cerealis*; this contradicts the evolutionary data according to which *F. ussurianum* is most close to the species *F. graminearum* [22], which is confirmed by a phylogenetic analysis of *TEF1α*. On the *TRI14* gene dendrogram, the studied strains of *F. graminearum* were divided into two clusters with high bootstrap support, but we could not refer this grouping either to the chemotype of the strains or to their geographical origin. We could assume a relationship between the *TRI14* gene polymorphism and differences in the aggressiveness of different strains with respect to the host plant. However, similar studies were not performed in the present work. For the *TRI5* gene, no correlation between *F. graminearum* chemotypes (3/15-ADON) and the species' phylogenetic structure was found. In addition, none of the analyzed *F. graminearum* and *F. culmorum* strains contained an 8-nucleotide deletion (TGGAACAA), a marker for weakly toxigenic strains of these species [58].

Despite an approximately identical content of variable and phylogenetically informative sites, as well as haplotypic diversity of the three genes, an analysis of *TEF1α* more accurately reflected the phylogenetic structure and presumable evolutionary development of a group of *Fusarium* genus species TrMT producers. This result agrees with the data in an earlier study of the polymorphism of other genes involved in mycotoxin biosynthesis, e.g. *TRII* [7], or the gene of enniatin synthetase (*Esyn1*), a key enzyme of enniatin biosynthesis in *F. avenaceum* and closely related species [28, 59].

The belonging to a particular chemotype is a specific feature of a B-trichothecene producing strain. In recent years, studies have been published on the occurrence of chemotypes of B-trichothecene producers (primarily *F. graminearum*) in various regions of the world, e.g., in South America [60], Africa [61], and Europe [62, 63]. In 2016, the results of an extensive study conducted by experts from 17 European countries, including Russia, were published [64], which led to the creation of a European database ([www.catalogueeu.luxmcc.lu](http://www.catalogueeu.luxmcc.lu)). This database contains information on 187 strains isolated on the territory of Russia; however, it lacks information about strains from several regions, such as Western Siberia and the Volga-Vyatka Region, as well as information on the chemotypes of collection samples isolated in previous years. In the present study, the TrMT type was analyzed using a combined approach involving chemotyping with the chemotype-specific primers described earlier (see Molecular typing of type B TrMT producers) and an analysis of the culture fluids of some strains by HPLC. By using sets of primers (12-1 and 12-2) specific to the polymorphic regions of the *TRI12* gene, we identified the chemotypes of the strains of four type BTrMT-producing species. It was

demonstrated that the *F. culmorum* and *F. ussurianum* strains belong to the 3-ADON chemotypes, the *F. cerealis* strains belong to the NIV chemotype, and that there were both 3-ADON and 15-ADON producers among *F. graminearum* strains. It should be taken into account that PCR analysis data in some cases may not coincide with the actual toxigenic profile of a strain, which emphasizes the need to confirm genetic data by chemical methods [65]. HPLC confirmed the results of chemotyping for 16 out of 20 strains selected for chromatographic analysis. The culture liquids of four strains contained only DON, and acetylated derivatives were absent. The data published in recent years have demonstrated that 3-ADON producers predominate among *F. graminearum* strains of different geographical origins, which is mainly related to their higher aggressiveness compared to that of 15-ADON and NIV producers [66, 67]. An analysis of European strains of *F. graminearum* has demonstrated that the 3-ADON chemotype is common in Northern Europe, while the 15-ADON chemotype is more common in Central and Southern Europe [62–64]. Of the three studied *F. graminearum* strains with the 15-ADON chemotype, two may be assigned to the Central European group (G.8-8 – Germany, 48702 – Tula Region), and one may be assigned to the South European group (41806 – North Ossetia). 3-ADON chemotype strains may be assigned to the North European (58033 – Leningrad Region) and Central European (70725 – Orel Region) groups. All the studied cultures of the species *F. culmorum* were assigned to the 3-ADON chemotype. It is believed that only two of the three known B chemotypes, 3-ADON and NIV, are characteristic of *F. culmorum*, with 3-ADON being much more ubiquitous [61, 64], which was confirmed in the present study. The *F. ussurianum* strain 29813 representing the 3-ADON chemotype produced the largest amount of DON among all the analyzed cultures. The relation of *F. cerealis* strains to the NIV chemotype is also in line with the data in [68]. We believe that the results obtained in the present study can partially compensate for information absent in the European database on the chemotypes of strains from certain regions of Russia. For example, strains from the Volga-Vyatka Region (No. 10–12), as well as Western Siberia and its neighboring Kostanay Region of Kazakhstan (No. 7, 16), were characterized for the first time.

## CONCLUSION

The findings in this study have both a basic and applied significance. The fundamental significance is associated with the great expansion of information on the molecular genetic diversity of trichothecene-producing strains of the genus *Fusarium*, which have different origins

and represent different regions of Russia. The use of a complex approach combining the classical study of morphological structures with the analysis of highly informative DNA markers made it possible to verify and clarify species identification for a number of collection samples, in particular, to discover the first *F. commune* strain on the territory of Russia. For the first time, the *TRI14* gene was used for phylogenetic studies; the gene analysis revealed, on the one hand, a high level of inter- and intraspecific polymorphism and, on the other hand, the need for further investigations of its structure and functions, which would provide better understanding of its role in pathogenesis and mycotoxin biosynthesis. The applied significance of this study is related to the possibility of using the studied markers for developing monitoring systems for food contamination by TrMT producers. A combined study of the relation of type B

TrMT producers to the main chemotypes using specific PCR and HPLC enabled an evaluation of their occurrence in Russia, including regions where TrMT producers had not been previously found. ●

*The authors are grateful to T.Yu. Gagkaeva (All-Russian Research Institute of Plant Protection) for valuable comments on morphological characterization of studied strains.*

*The study was supported by the Russian Foundation for Basic Research, grants No. 15-29-02527 (L.S., S.Z.; selection of collection samples, phylogenetic analysis of *TEF1α* and *TRI5* genes, and microscopy) and 16-34-01369 (A.S.; structural and phylogenetic analysis of the *TRI14* gene and analysis of the toxin-producing ability of strains by HPLC).*

## REFERENCES

- Moretti A., Susca A., Mule G., Logrieco A.F., Proctor R.H. // *Int. J. Food Microbiol.* 2013. V. 167. P. 57–66.
- Ueno Y. // *Adv. Food Nutr. Res.* 1989. V. 3. P. 301–305.
- Desjardins A.E. *Fusarium* mycotoxins: chemistry, genetics and biology. APS Press, St. Paul, Minnesota, 2006.
- Grovey J.F. / The trichothecenes and their biosynthesis. // *Progress in the Chemistry of Organic Natural Products*. Eds Herz W., Falk H., Kirby G.W. Vienna: Springer-Verlag, 2007. P. 63–130.
- McCormick S.P., Stanley A.M., Stover N.A., Alexander N.J. // *Toxins*. 2011. V. 3. P. 802–814.
- Nesic K., Ivanovic S., Nesic V. // *Rev. Environ. Contam. Toxicol.* 2014. V. 228. P. 101–120.
- Kelly A., Proctor R.H., Belzile F., Chulze S.N., Clear R.M., Cowger C., Elmer W., Lee T., Obanor F., Waalwijk C., Ward T.J. // *Fungal Genet. Biol.* 2016. V. 95. P. 39–48.
- Varga E., Wiesenberger G., Hametner C., Ward T.J., Dong Y., Schöffbeck D., McCormick S., Broz K., Stückler R., Schuhmacher R., et al. // *Environ. Microbiol.* 2015. V. 17. № 8. P. 2588–2600.
- O'Donnell K., Kistler H.C., Tacke B.K., Casper H.H. // *Proc. Natl. Acad. Sci. USA.* 2000. V. 97. P. 7905–7910.
- O'Donnell K., Ward T.J., Geiser D.M., Kistler H.C., Aoki T. // *Fungal Genet. Biol.* 2004. V. 41. P. 600–623.
- Moss M.O., Thrane U. // *Toxicol. Lett.* 2004. V. 153. № 1. P. 23–28.
- Brown D.W., Dyer R.B., McCormick S.P., Kendra D.F., Plattner R.D. // *Fungal Genet. Biol.* 2004. V. 41. P. 454–462.
- Alexander N.J., McCormick S.P., Waalwijk C., van der Lee T., Proctor R.H. // *Fungal Genet. Biol.* 2011. V. 48. № 5. P. 485–495.
- Nasmith C.G., Walkowiak S., Wang L., Leung W.W.Y., Gong Y., Johnston A., Harris L.J., Guttman D.S., Subramaniam R. // *PLoS Pathog.* 2011. V. 7. № 9. e1002266.
- Cundliffe E., Cannon M., Davies J. // *Proc. Natl. Acad. Sci. USA.* 1974. V. 71. № 1. P. 30–34.
- Dyer R.B., Plattner R.D., Kendra D.F., Brown D.R. // *J. Agric. Food Chem.* 2005. V. 53. P. 9281–9287.
- Paran I., Michelmore R.W. // *Theor. Appl. Genet.* 1993. V. 85. № 8. P. 985–993.
- Starkey D.E., Ward T.J., Aoki T., Gale L.R., Kistler H.C., Geiser D.M., Suga H., Toth B., Varga J., O'Donnell K. // *Fungal Genet. Biol.* 2007. V. 44. P. 1191–1204.
- Aoki T., Ward T.J., Kistler H.C., O'Donnell K. // *JSM Mycotoxins*. 2012. V. 62. P. 91–102.
- Obanor F., Erginbas-Orakci G., Tunali B., Nicol J.M., Chakraborty S. // *Fungal Biol.* 2010. V. 114. P. 753–765.
- Scott J.B., Chakraborty S. // *Mycol. Res.* 2006. V. 110. P. 1413–1425.
- Yli-Mattila T., Gagkaeva T., Ward T.J., Aoki T., Kistler H.C., O'Donnell K. // *Mycologia*. 2009. V. 101. № 6. P. 841–852.
- Yli-Mattila T., Ward T.J., O'Donnell K., Proctor R.H., Burkin A.A., Kononenko G.P., Gavrilova O.P., Aoki T., McCormick S.P., Gagkaeva T.Yu. // *Int. J. Food Microbiol.* 2011. V. 147. P. 58–68.
- O'Donnell K., Sutton D.A., Rinaldi M.G., Gueidan C., Crous P.W., Geiser D.M. // *J. Clin. Microbiol.* 2009. V. 47. P. 3851–3861.
- Fernandez-Ortuno D., Waalwijk C., van der Lee T., Fan J., Atkins S., West J.S., Fraaije B.A. // *Int. J. Food Microbiol.* 2013. V. 166. P. 148–154.
- Nicolaisen M., Surponiene S., Nielsen L.K., Lazzaro I., Spliid N.H., Justensen A.F. // *J. Microbiol. Meth.* 2009. V. 76. P. 234–240.
- Stakheev A.A., Ryazantsev D.Yu., Gagkaeva T.Yu., Zavriev S.K. // *Food Control*. 2011. V. 22. P. 462–468.
- Stakheev A.A., Khairulina D.R., Zavriev S.K. // *Int. J. Food Microbiol.* 2016. V. 225. P. 27–37.
- Yli-Mattila T., Nayaka S.C., Venkataramana M., Yörük E. // *Methods Mol. Biol.* 2017. V. 1542. P. 269–291.
- Walkowiak S., Rowland O., Rodrigue N., Subramaniam R. // *BMC Genomics*. 2016. V. 17. P. 1014.
- Lysøe E., Frandsen R.J.N., Divon H.H., Terzi V., Orru L., Lamontanara A., Kolseth A.-K., Nielsen K.F., Thrane U. // *Int. J. Food Microbiol.* 2016. V. 221. P. 29–36.
- Al-Hatmi A.M.S., van den Ende A.H.G.G., Stielow J.B., van Diepeningen A.D., Seifert K.A., McCormick W., Assabgui R., Gräfenhan T., de Hoog G.S., Levesque C.A. // *Fungal Biol.* 2016. V. 120. P. 231–245.
- Nirmaladevi D., Venkataramana M., Srivastava R.K., Uppalapati S.R., Gupta V.K., Yli-Mattila T., Clement Tsui

- K.M., Srinivas C., Niranjana S.R., Chandra N.S. // *Sci. Rep.* 2016. V. 6. P. 21367.
34. Schoch C.L., Seifert K.A., Huhndorf S., Robert V., Spouge J.L., Levesque C.A., Chen W., Fungal Barcoding Consortium. // *Proc. Natl. Acad. Sci. USA.* 2012. V. 109. P. 6241–6246.
35. O'Donnell K., Cigelnik E. // *Mol. Phylogenet. Evol.* 1997. V. 7. № 1. P. 103–116.
36. Kristensen R., Torp M., Kosiak B., Holst-Jensen A. // *Mycol. Res.* 2005. V. 109. № 2. P. 173–186.
37. Geiser D.M., Jimenez-Case M., Kang S., Makalowska I., Veeraraghavan N., Ward T., Zhang N., Kuldau G.A., O'Donnell K. // *Eur. J. Plant Pathol.* 2004. V. 110. P. 473–479.
38. Niessen L., Schmidt H., Vogel R.F. // *Int. J. Food Microbiol.* 2004. V. 95. P. 305–319.
39. Stepień L., Gromadzka K., Chelkowski J. // *J. Appl. Genet.* 2012. V. 53. P. 227–236.
40. Villani A., Moretti A., De Saeger S., Han Z., Di Mavungu J.D., Soares C.M.G., Proctor R.H., Venancio A., Lima N., Stea G., et al. // *Int. J. Food Microbiol.* 2016. V. 234. P. 24–35.
41. Menke J., Dong Y., Kistler H.C. // *Mol. Plant Microbe In.* 2012. V. 25. № 11. P. 1408–1418.
42. Nielsen L.K., Jensen J.D., Rodriguez A., Jorgensen L.N., Justensen A.F. // *Int. J. Food Microbiol.* 2012. V. 157. P. 384–392.
43. Wachowska U., Packa D., Wiwart M. // *Toxins.* 2017. V. 9. № 12. P. 408.
44. Thompson J.D., Higgins D.G., Gibson T.J. // *Nucl. Acids Res.* 1994. V. 22. P. 4673–4680.
45. Nei M., Kumar S. *Molecular Evolution and Phylogenetics.* New York: Oxford University Press, 2000.
46. Tamura K., Peterson D., Peterson N., Stecher G., Nei M., Kumar S. // *Mol. Biol. Evol.* 2011. V. 28. № 10. P. 2731–2739.
47. Rozas J., Ferrer-Mata A., Sánchez-DelBarrio J.C., Guirao-Rico S., Librado P., Ramos-Onsins S.E., Sánchez-Gracia A. // *Mol. Biol. Evol.* 2017. V. 34. № 12. P. 3299–3302.
48. Ward T.J., Bielawski J.P., Kistler H.C., Sullivan E., O'Donnell K. // *Proc. Natl. Acad. Sci. USA.* 2002. V. 99. P. 9278–9283.
49. Wang J.H., Li H.-P., Qu B., Zhang J.-B., Huang T., Chen F.-F., Liao Y.-C. // *Int. J. Mol. Sci.* 2008. V. 9. P. 2495–2504.
50. Bustin S.A., Benes V., Garson J.A., Hellemans J., Huggett J., Kubista M., Mueller R., Nolan T., Pfaffl M.W., Shipley G.L., Vandesompele J., Wittwer C.T. // *Clin. Chem.* 2009. V. 55. P. 611–622.
51. Farber J.M., Sanders G.W. // *Appl. Environ. Microbiol.* 1986. V. 51. № 2. P. 381–384.
52. Gupta V.K., Chattopadhyay P., Kalita M.C., Chaurasia A.K., Gogoi H.K., Singh L. // *Pharm. Methods.* 2011. V. 2. № 1. P. 25–29.
53. Han Z., Tangni E.K., Huybrechts B., Munaut F., Scauf-laire J., Wu A., Callebaut A. // *Mycotoxin Res.* 2014. V. 30. P. 231–240.
54. Leslie J.F., Summerell B.A. *The Fusarium laboratory manual.* Blackwell Publ., 2006. P. 266–267.
55. Skovgaard K., Rosendahl S., O'Donnell K., Hirenberh H.I. // *Mycologia.* 2003. V. 95. P. 630–636.
56. Zhu Z., Zheng L., Pan L. // *Plant Disease.* 2014. V. 98. № 7. P. 977–987.
57. Marin P., Moretti A., Ritieni A., Jurado M., Vazquez C., Teresa Gonzalez-Jaen M. // *Food Microbiol.* 2012. V. 31. P. 229–237.
58. Bakan B., Giraud-Delville C., Pinson L., Richard-Molard D., Fournier E., Brygoo Y. // *Appl. Environ. Microbiol.* 2002. V. 68. № 11. P. 5472–5479.
59. Kulik T., Pszczolkowska A., Lojko M. // *Int. J. Mol. Sci.* 2011. V. 12. P. 5626–5640.
60. Pan D., Mionetto A., Calero N., Reynoso M.M., Torres A., Bettucci L. // *Gen. Mol. Res.* 2016. V. 15. № 1. 15017270.
61. Laraba I., Boureghda H., Abdallah N., Bouaicha O., Obanor F., Moretti A., Geiser D.M., Kim H.-S., McCormick S.P., Proctor R.H., et al. // *Fungal Genet. Biol.* 2017. V. 103. P. 34–41.
62. Yli-Mattila T., Rämö S., Hietaniemi V., Hussien T., Carlobos-Lopez A.L., Cumagun C.J.R. // *Microorganisms.* 2013. V. 1. P. 162–174.
63. Surponiene S., Sakalauskas S., Mankeviciene A., Barcauskaite K., Jonaviciene A. // *Zemdirbyste-Agriculture.* 2016. V. 103. № 3. P. 281–287.
64. Pasquali M., Beyer M., Logrieco A., Audenaert K., Balmas V., Basler R., Boutigny A.L., Chrpova J., Czembor E., Gagkaeva T., et al. // *Front. Microbiol.* 2016. V. 7. P. 406.
65. Kulik T., Busko M., Bilka K., Ostrowska-Kolodziejczak A., van Diepeningen A.D., Perkowski J., Steinglein S. // *Toxins.* 2016. V. 8. № 11. 330.
66. Covarelli L., Beccari G., Prodi A., Generotti S., Etruschi F., Juan C., Ferrer E., Manes J. // *J. Sci. Food Agric.* 2014. V. 95. P. 540–551.
67. Pasquali M., Giraud F., Brochot C., Cocco E., Hoffmann L., Bohn T. // *Int. J. Food Microbiol.* 2010. V. 137. P. 246–253.
68. Amarasinghe C.C., Tittlemier S.A., Fernando W.G.D. // *Plant Pathol.* 2014. V. 64. № 4. P. 988–995.

# ATP Reduces the Entry of Calcium Ions into the Nerve Ending by Blocking L-type Calcium Channels

E. F. Khaziev<sup>1,2,3</sup>, D. V. Samigullin<sup>1,2,3</sup>, A. N. Tsentssevitsky<sup>1,2\*</sup>, E. A. Bukharaeva<sup>1,2</sup>, E. E. Nikolsky<sup>1,2</sup>

<sup>1</sup>Kazan Institute of Biochemistry and Biophysics, FRC Kazan Scientific Center of RAS, P.O. Box 30, Kazan, 420111, Russia

<sup>2</sup>Institute of Fundamental Biology and Medicine, Kazan Federal University, Open Lab

"Neuropharmacology", Kremlevskaya Str. 18, Kazan 420008, Russia

<sup>3</sup>National Research Technical University named after A.N. Tupolev, K. Marx Str. 31/7, Kazan 420111, Russia

\*E-mail: atsen@list.ru

Received October 16, 2017; in final form April 09, 2018

Copyright © 2018 Park-media, Ltd. This is an open access article distributed under the Creative Commons Attribution License, which permits unrestricted use, distribution, and reproduction in any medium, provided the original work is properly cited.

**ABSTRACT** At neuromuscular junctions, ATP inhibits both the evoked and spontaneous acetylcholine release and inward calcium current operating via presynaptic P2Y receptors. It was shown in experiments with the frog neuromuscular synapse using specific calcium-sensitive dye Oregon Green Bapta 1 that exogenous ATP reduces the amplitude of calcium transient, which reflects the changes in the entry of calcium ions in response to the nerve pulse. The depressing effect of ATP on the transient was prevented by suramin, the blocker of P2 receptors. Nitrendipine, a specific blocker of L-type calcium channels, *per se* decreased the calcium transient amplitude and significantly attenuated the effect of ATP on the calcium signal. Contrariwise, the preliminary application of ATP to the neuromuscular junction completely eliminated the depressing effect of nitrendipine on the calcium response. The obtained data suggest that an essential component in the inhibitory action of ATP on the calcium transient amplitude is provided by reduction of the entry of calcium ions into a frog nerve ending via L-type voltage-gated calcium channels.

**KEYWORDS** ATP, calcium transient, calcium channels, neuromuscular junction.

## INTRODUCTION

ATP reduces the amplitude of multiquantal endplate currents (EPCs) in the neuromuscular junction by activating presynaptic P2Y receptors [1]. The inhibitory activity of ATP on the amplitude of postsynaptic currents is a presynaptic effect and can be caused by changes in the activity of calcium channels, the input of calcium ( $\text{Ca}^{2+}$ ) through which exocytosis of synaptic vesicles is triggered. Indeed, ATP reversibly reduces the  $\text{Ca}^{2+}$  current in the perisynaptic region of axon [2] and decreases the amplitude of  $\text{Ca}^{2+}$  transient recorded in various regions of a frog nerve terminal [3]. A change in the transient amplitude reflects changes in the concentration of free  $\text{Ca}^{2+}$  ions in the terminal [4, 5], while its decrease in association with ATP action may be indicative of the effect of this purine on the activity of presynaptic calcium channels. There are several types of voltage-gated calcium channels that function in a frog nerve terminal [4]. It remains unknown the activity of which type of channels is altered by ATP. The data regarding the effect of ATP on L-type voltage-gated calcium channels are quite

contradictory. It has been shown on various objects that ATP is capable of both enhancing the entry of calcium ions through L-type channels [6] and inhibiting these channels [7]. In this study, we used the fluorescent method of recording  $\text{Ca}^{2+}$  transient in a frog nerve terminal to find whether or not presynaptic L-type voltage-gated calcium channels are involved in ATP-induced reduction of the  $\text{Ca}^{2+}$  transient amplitude. It was established that the decrease in the transient amplitude upon activation of purine receptors is partially due to a reduction in the entry of  $\text{Ca}^{2+}$  ions through L-type calcium channels.

## EXPERIMENTAL SECTION

The study was performed using an isolated neuromuscular specimen of the *m. cutaneus pectoris* obtained from the frog *Rana ridibunda*. The relative change in the  $\text{Ca}^{2+}$  level in the nerve terminal ( $\text{Ca}^{2+}$  transient) was evaluated using the Oregon Green Bapta 1 fluorescent dye. The technique of dye loading through the nerve stump and the protocols of recording and processing fluorescent signals were described in detail in [8]. The

experimental protocol was as follows. After the fluorescent dye was loaded into the nerve terminals, the specimen was placed in a 3-ml reservoir through which a perfusion solution was fed at a rate of 3 ml/min. In order to prevent contractions of muscle fibers upon motor nerve stimulation, a Ringer's solution with a reduced content of  $\text{Ca}^{2+}$  ions and increased concentration of  $\text{Mg}^{2+}$  ions (113.0 mM NaCl, 2.5 mM KCl, 3.0 mM  $\text{NaHCO}_3$ , 6.0 mM  $\text{MgCl}_2$ , 0.9 mM  $\text{CaCl}_2$ ; pH 7.2–7.3; temperature,  $20.0 \pm 0.3^\circ\text{C}$ ) was used. The experiments were conducted in accordance with the ethical principles and guidelines recommended by the European Science Foundation (ESF) and the Declaration on Animal Welfare. A total of 6–21 synapses obtained from 3–5 animals were used in each series of experiments.

Stimulation of the motor nerve with rectangular pulses 0.2 ms long, with a frequency of 0.5 imp/s, was performed by a stimulator (A-M Systems 2100) using a suction electrode. A total of 60 consecutive fluorescent signals were recorded along the entire length of the selected nerve terminal under control conditions; the test substance was then added to the perfusion solution. Registration of 60 signals from the same terminal as the one used in the control was initiated 20–25 min after substance application. If necessary, the next test substance was added to the perfusion solution in the presence of the first substance, and all signals from the same nerve terminal were recorded again 20–25 min later. Preliminary experiments were conducted; the results indicated that the amplitude-time parameters of the fluorescent signal in response to infrequent stimulation of the motor nerve do not undergo any changes for a period of 3–4 h.

Fluorescent signals in response to a nerve stimulus were recorded using a photometric unit based on an Olympus BX-51 microscope with a 60 $\times$  water immersion lens and the Turbo-SM software. A Polychrome V monochromator (Till Photonics, Munich, Germany), tuned to the excitation wavelength of the dye, 488 nm, was used as a source of illumination. The fluorescent signal was isolated using the following set of filters: 505DCXT dichroic mirror, E520LP emission (Chroma). The area of illumination was restricted by a diaphragm in order to reduce background illumination. The data were analyzed using a Neuro CCD camera and the ImageJ software. The terminal and background areas were defined using the ImageJ software. Background fluorescence was subtracted from all the fluorescence values of the terminal area. The data are represented as a  $(\Delta F / F_0 - 1) \times 100\%$  ratio, where  $\Delta F$  is the fluorescence intensity in response to the stimulus and  $F_0$  is the fluorescence intensity at rest.  $F_0$  was registered before each recording of fluorescent signals in response to a nerve stimulus.

The statistical significance of the differences between the samples was estimated using the Student's t-test and the Mann–Whitney U test. Differences between the samples were considered statistically significant at  $p = 0.05$  (where  $n$  is the number of studied synapses).

## RESULTS AND DISCUSSION

Exogenous ATP at a concentration of 10  $\mu\text{M}$  decreased the amplitude of  $\text{Ca}^{2+}$  transient in response to a nerve stimulus by an average of  $13.2 \pm 1.9\%$  ( $p = 0.0003$ ,  $n = 8$ ; Fig. 1A,C). An increase in ATP concentration to 100  $\mu\text{M}$  did not affect the intensity of this effect: the  $\text{Ca}^{2+}$  transient was decreased by  $13.6 \pm 1.4\%$  ( $p = 0.000003$ ,  $n = 21$ ) relative to the reference values (Fig. 1C).

Suramin, a non-selective P2 receptor antagonist, at a dose of 300  $\mu\text{M}$  increased the  $\text{Ca}^{2+}$  transient value by an average of  $20.5 \pm 9.0\%$  ( $p = 0.037$ ,  $n = 8$ ; Fig. 1C) relative to the control values. Addition of 100  $\mu\text{M}$  ATP to the medium containing suramin did not significantly alter the  $\text{Ca}^{2+}$  transient, which was equal only to  $103.4 \pm 3.1\%$  ( $p = 0.27$ ,  $n = 5$ ; Fig. 1B,C). Thus, the effect of ATP on the amplitude of  $\text{Ca}^{2+}$  transient is associated with the activation of P2 receptors.

A specific L-type calcium channel blocker, nitrendipine, at a concentration of 5  $\mu\text{M}$  reduced the amplitude of  $\text{Ca}^{2+}$  transient by  $12.4 \pm 3.6\%$  ( $p = 0.0003$ ,  $n = 12$ ; Fig. 2), indicative of the contribution of L-type channels to the overall calcium current caused by the action potential (see also [4]). The change in the  $\text{Ca}^{2+}$  transient amplitude caused by ATP under L-type calcium channel blockade was only  $4.2 \pm 1.1\%$  ( $p = 0.016$ ,  $n = 7$ ; Fig. 2), which is much less than the effect of intrinsic ATP (Mann–Whitney U test,  $p = 0.011$ ). Thus, the blockade of L-type calcium channels alleviated the decrease in the  $\text{Ca}^{2+}$  transient amplitude through ATP action. One can assume that activation of purine receptors by ATP leads to the suppression of L-type calcium channels. If this assumption is true, then a decrease in the transient amplitude induced by nitrendipine should be less pronounced in the presence of ATP. Indeed, nitrendipine did not affect the  $\text{Ca}^{2+}$  transient amplitude after preliminary ATP application: the amplitude only changed by  $2.0 \pm 1.9\%$  ( $n = 6$ ; Fig. 2).

We have showed earlier that exogenous ATP at a concentration of 100  $\mu\text{M}$  reduces the  $\text{Ca}^{2+}$  transient amplitude equally in different regions of the extended nerve terminal of a frog [3]. The reduction in the transient caused by ATP corresponds to a decrease in the amplitude of induced EPC at normal calcium content [1] and the quantal content of EPC at reduced  $\text{Ca}^{2+}$  ion concentration in solution [9]. The data on the ATP-induced decrease in the input of  $\text{Ca}^{2+}$  ions into the terminal in response to a nerve impulse are consistent with

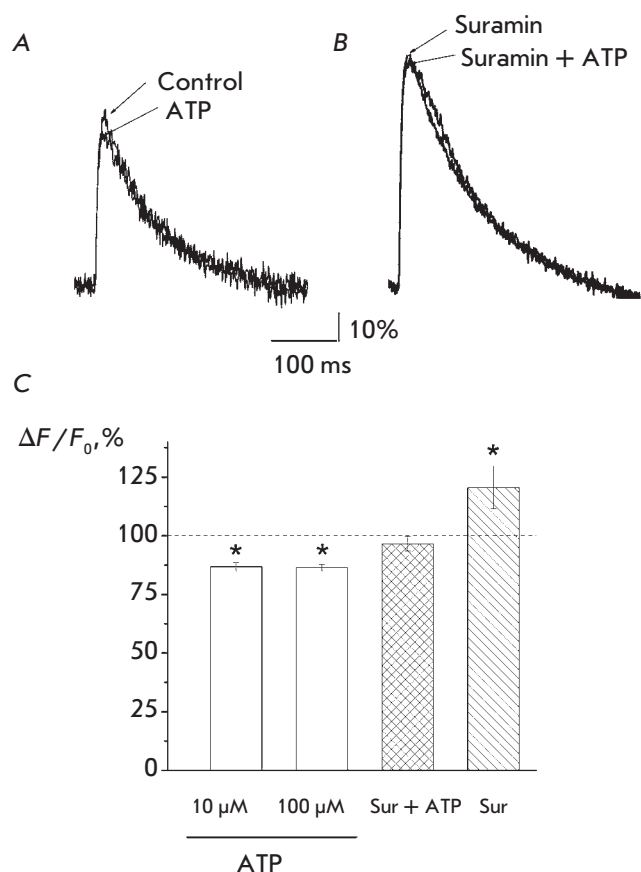


**Fig. 1.** ATP reduces the amplitude of calcium transient operating via P2 receptors. *A* – The effect of 10 μM ATP on Ca<sup>2+</sup> transient. *B* – The absence of ATP effect on transient in the presence of suramin. *A, B* – the averaging of 60 fluorescence signals. *C* – Effect of ATP (10 and 100 μM), suramin (Sur), and ATP in the presence of suramin on the amplitude of Ca<sup>2+</sup> transient. The averaged changes in the Ca<sup>2+</sup> transient amplitude for ATP and suramin (Sur) are expressed as a percentage of related calcium signal amplitudes under control conditions. In the case of combined action of suramin and ATP (Sur+ATP), the amplitude of Ca<sup>2+</sup> transient under suramin was taken as 100%. \*  $p < 0.05$

the results reported in [2], where ATP was shown to cause a reversible decrease in the presynaptic calcium current.

Exogenous ATP reduced the amplitude of EPC as a result of the activation of presynaptic P2Y receptors, since the effect was prevented by preliminary incubation of the specimen in suramin [1]. In our experiments, the ATP-induced decrease in the Ca<sup>2+</sup> transient amplitude was also prevented by suramin (Fig. 1*B,C*). At the same time, suramin *per se* enhanced Ca<sup>2+</sup> transient (Fig. 1). This effect can be associated with the possibili-

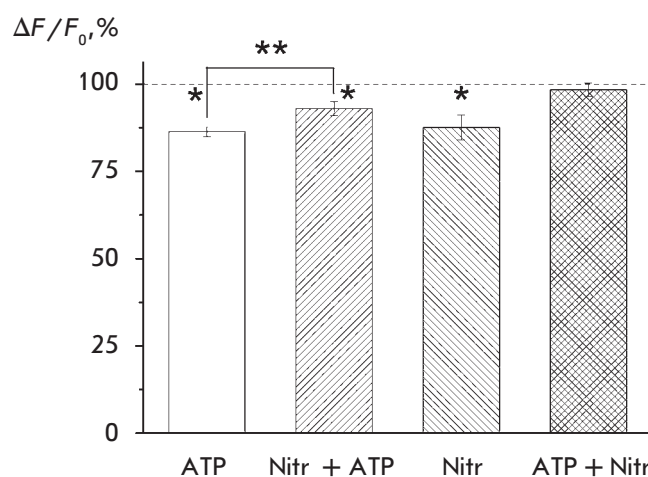


**Fig. 2.** ATP-induced reduction in the calcium transient amplitude is associated with blockade of presynaptic L-type voltage-gated calcium channels. The depressing effect of ATP is attenuated after the preliminary blocking of L-type calcium channels by nitrendipine (Nitr+ATP). Nitrendipine *per se* decreases the amplitude of Ca<sup>2+</sup> transient (Nitr). Nitrendipine does not alter the amplitude of transient under conditions when P2 receptors are activated by ATP (ATP+Nitr). \*  $p < 0.05$

ty of increasing the concentration of Ca<sup>2+</sup> ions in the cytoplasm as a result of its release from the sarcoplasmic reticulum [10]. It is shown that suramin increases not only the probability of an open state, but conductance of single ryanodine-sensitive channels as well [11]. The suramin-induced elevation of the Ca<sup>2+</sup> transient amplitude is consistent with the data on the increase in the quantal content of EPC observed upon blockade of P2 receptors [12].

The data on the effect of ATP on L-type voltage-gated calcium channels are quite contradictory. In micromolar concentrations, ATP is capable of suppressing the current through the L-type Ca<sup>2+</sup> channels in cardiomyocytes in a reversible, dose-dependent manner [7]. Meanwhile, activation of purine receptors can enhance the entry of Ca<sup>2+</sup> ions through the L-type channels in the perisynaptic glial cells of a frog [6]. Our results demonstrate that ATP-induced decrease in the Ca<sup>2+</sup> transient amplitude is influenced by a suppression of the L-type Ca<sup>2+</sup> channel activity. This is evidenced by a significant decrease in the effect of ATP on Ca<sup>2+</sup> transient in the presence of nitrendipine, a specific blocker of L-type channels (Fig. 2). An additional confirmation to the fact that L-type Ca<sup>2+</sup> channels contribute to the ATP action is that their specific blocker, nitrendipine, does not affect the transient amplitude after the pre-

liminary action of ATP (*Fig. 2*). Under these conditions, when the activity of L-type  $\text{Ca}^{2+}$  channels has been already reduced by ATP, nitrendipine does not have any target for action.

Our results demonstrate that the activity of L-type voltage-gated calcium channels plays a crucial role in the

inhibitory effect of ATP on the  $\text{Ca}^{2+}$  entry into the nerve terminal of a frog in response to a nerve stimulus. ●

*This work was partially supported by the Russian Foundation for Basic Research (grant № 16-04-01051 A).*

---

#### REFERENCES

1. Sokolova E., Grishin S., Shakirzyanova A., Talantova M., Giniatullin R. // *Eur. J. Neurosci.* 2003. V. 18. P. 1254–1264.
2. Grishin S., Shakirzyanova A., Giniatullin A., Afzalov R., Giniatullin R. // *Eur. J. Neurosci.* 2005. V. 21. P. 1271–1279.
3. Khaziev E., Golovyahina A., Bukharaeva E., Nikolsky E., Samigullin D. // *BioNanoSci.* 2017. V. 7. P. 254–257.
4. Tsentsevitsky A.N., Samigullin D.V., Nurullin L.F., Khaziev E.F., Nikolsky E.E., Bukharaeva E.A. // *Frogs: genetic diversity, neural development and ecological implications* / Ed. Lambert H. New York: NOVA Publ., 2014. P. 179–194.
5. Khaziev E., Samigullin D., Zhilyakov N., Fatikhov N., Bukharaeva E., Verkhatsky A., Nikolsky E. // *Front. Physiol.* 2016. V.7. P. 621. doi: 10.3389/fphys.2016.00621. eCollection 2016.
6. Robitaille R. // *J. Neurosci.* 1995. V. 15. P. 7121–7131.
7. Yamamoto T., Habuchi Y., Nishio M., Morikawa J., Tanaka H. // *Cardiovascular Res.* 1999. V. 41. P. 166–174.
8. Samigullin D.V., Khaziev E.F., Zhilyakov N.V., Bukharaeva E.A., Nikolsky E.E. // *J. Vis. Exp.* 2017. V. 125. P. 55122.
9. Tsentsevitsky A., Nikolsky E., Giniatullin R., Bukharaeva E. // *Neuroscience.* 2011. V. 189. P. 93–99.
10. Emmick J.T., Kwon S., Bidasee K.R., Besch K.T., Besch H.R. Jr // *J. Pharmacol. Exp. Ther.* 1994. 269. P. 717–724.
11. Hill A.P., Kingston O., Sitsapesan R. // *Mol. Pharmacol.* 2004. V. 65. № 5. P. 1258–1268.
12. Sugiura Y., Ko C.P. // *Neuroreport.* 2000. V. 11. № 13. P. 3017–3021.

# Role of the Scaffold Protein MIM in the Actin-Dependent Regulation of Epithelial Sodium Channels (ENaC)

L. S. Shuyskiy<sup>1,2\*</sup>, V. V. Levchenko<sup>2</sup>, Y. A. Negulyaev<sup>1,3</sup>, A. V. Staruschenko<sup>2</sup>, D. V. Ilatovskaya<sup>2,4</sup>

<sup>1</sup>Institute of Cytology of RAS, Tikhoretskij Ave. 4, St. Petersburg, 194064, Russia

<sup>2</sup>Department of Physiology, Medical College of Wisconsin, 8701 Watertown Plank Road, Milwaukee, WI 53226, USA

<sup>3</sup>Department of Medical Physics, Peter the Great St. Petersburg Polytechnic University, Politekhnikeskaya Str. 2, St. Petersburg, 195251, Russia

<sup>4</sup>Medical University of South Carolina, Department of Medicine, Division of Nephrology, 96 Jonathan Lucas St, MSC 629 CSB 822, Charleston, SC 29425, USA

\*E-mail: leonid.shuyskiy@gmail.com

Received November 09, 2017; in final form April 03, 2018

Copyright © 2018 Park-media, Ltd. This is an open access article distributed under the Creative Commons Attribution License, which permits unrestricted use, distribution, and reproduction in any medium, provided the original work is properly cited.

**ABSTRACT** Epithelial Sodium Channels (ENaCs) are expressed in different organs and tissues, particularly in the cortical collecting duct (CCD) in the kidney, where they fine tune sodium reabsorption. Dynamic rearrangements of the cytoskeleton are one of the common mechanisms of ENaC activity regulation. In our previous studies, we showed that the actin-binding proteins cortactin and Arp2/3 complex are involved in the cytoskeleton-dependent regulation of ENaC and that their cooperative work decreases a channel's probability of remaining open; however, the specific mechanism of interaction between actin-binding proteins and ENaC is unclear. In this study, we propose a new component for the protein machinery involved in the regulation of ENaC, the missing-in-metastasis (MIM) protein. The MIM protein contains an IMD domain (for interaction with PIP<sub>2</sub>-rich plasma membrane regions and Rac GTPases; this domain also possesses F-actin bundling activity), a PRD domain (for interaction with cortactin), and a WH2 domain (interaction with G-actin). The patch-clamp electrophysiological technique in whole-cell configuration was used to test the involvement of MIM in the actin-dependent regulation of ENaC. Co-transfection of ENaC subunits with the wild-type MIM protein (or its mutant forms) caused a significant reduction in ENaC-mediated integral ion currents. The analysis of the F-actin structure after the transfection of MIM plasmids showed the important role played by the domains PRD and WH2 of the MIM protein in cytoskeletal rearrangements. These results suggest that the MIM protein may be a part of the complex of actin-binding proteins which is responsible for the actin-dependent regulation of ENaC in the CCD.

**KEYWORDS** ENaC, MIM, cortactin, Arp2/3 complex, cytoskeleton.

**ABBREVIATIONS** ENaC – epithelial sodium channel; mENaC – mouse epithelial sodium channel; MIM (missing-in-metastasis) – adaptor protein; *mtss1* – gene encoding MIM protein.

## INTRODUCTION

In epithelial cells, microfilaments (MF, fibrillar actin, or F-actin) are involved in the regulation of cell contacts, the formation of lamellipodia and filopodia, modulation of ion channel activity, and other processes [1, 2]. The cytoskeleton is directly or indirectly (with involvement of actin-binding proteins) associated with the cytoplasmic regions of ion channels and regulates their gating properties, incorporation, internalization, etc. [3–11]. Direct interaction between the cytoskeleton and epithelial sodium channels (ENaC) [11–14], aquaporin-2 (AQP2) water channels [15–17], CFTR channels [18–

20], etc. has been shown. Cytoskeletal reorganization has an impact on the activity of ion channels [7, 21–24]. The effect of cytochalasin D leads to an increase in the ENaC open-state probability ( $P_o$ ) [10]. It is assumed that it is rather short microfilaments – but not globular actin (G-actin) or the long fibrils of F-actin – that regulate the activity of various ion channels [5, 10, 25, 26].

ENaCs belong to the DEG/ENaC (degenerin/epithelial sodium channels) superfamily. These channels are expressed in various organs and tissues in humans and animals (epithelium of the kidneys, lungs, intestines, etc.) and are responsible for sodium ions transport into

the cell. A distinctive feature of DEG/ENaC channels is that they are inhibited by a nanomolar concentration of a diuretic amiloride [27]. According to current concepts, functional ENaC channels consist of three subunits:  $\alpha$ ,  $\beta$ , and  $\gamma$ , the ratio being 1 : 1 : 1 [28, 29]. In the kidneys, ENaC is expressed in the epithelial cells of the CCD, where it mediates the reabsorption of sodium ions and plays an important role in maintaining salt-water homeostasis and regulating blood pressure [30, 31]. ENaCs were found to co-localize with actin filaments [14, 32] and actin-binding proteins (ankyrin, spectrin, etc. [33]). Interaction of the channel with the  $\alpha$ -spectrin SH3 domain via the proline-rich site at the C-terminus of the ENaC  $\alpha$ -subunit has been shown [25, 33, 34]. The existing model of ENaC regulation is being constantly supplemented with new data: it was recently established that the cytoskeleton-binding protein ankyrin-G participates in the delivery of ENaC to the cell's apical membrane in CCD [35]. We have proposed a model where cortactin (with involvement of the Arp2/3 complex) is the link between the channel and the cytoskeleton of CCD cells in mouse kidneys [36]. The interaction between ENaC and the cytoskeleton through adaptor proteins plays an important functional role in the regulation of the reabsorption of sodium in distal nephron.

The adapter protein MIM (missing-in-metastasis), which is encoded by the *mtss1* (metastasis suppressor 1) gene, was discovered in 2002. MIM, which was originally thought to be an actin-binding protein [37], is a significant element in the metastasis of several types of malignant neoplasms. MIM has been determined as a transcript absent in metastatic SKBR3 breast cancer cells and metastatic prostatic adenocarcinoma cell lines (LNCaP and PC3) [37–39]. MIM was assumed to function as a suppressor of metastasis [37]. However, there is still no definitive opinion on this point [40, 41]. An increase in MIM expression levels has been found to correlate with certain types of malignant transformations: for instance, in melanoma and head and neck squamous cell carcinoma [42, 43]. An increase in MIM expression also correlates with hepatocarcinoma progression [44]. MIM includes several important domains, which appear to play a key role in interactions with other proteins (see Fig. 1). For instance, the N-terminal domain of IMD (IRSp53-MIM homology domain) binds actin filaments, PIP<sub>2</sub>-rich membrane regions, small Rac GTPases and participates in protein dimerization. The SRD domain (serine-rich domain) contains tyrosine phosphorylation sites; the PRD domain (proline-rich domain) binds to cortactin and tyrosine phosphatase delta; the C-terminal domain WH2 (WASP homology domain 2) binds G-actin. MIM is presumably involved in cytoskeleton regulation through two independent actin-binding domains: IMD and WH2 [37, 39]. Co-localization of MIM

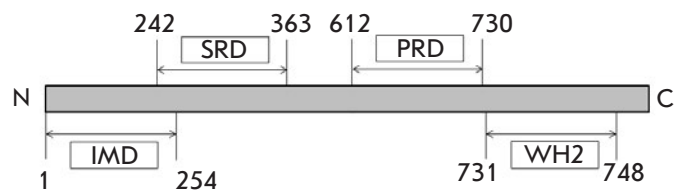


**Fig. 1.** Domain structure of the mouse MIM protein (encoded by *mtss1*, UniProt Q8R1S4). The IMD domain can bind to F-actin, PIP<sub>2</sub> rich membrane areas and Rac GTPases, and also plays an essential role in the dimerization of MIM. The SRD domain contains sites of Tyr phosphorylation. The PRD domain interacts with cortactin and tyrosine phosphatase delta. The WH2 domain binds G-actin

with cortactin has been shown, as well as their apparent interaction with the proline-rich domain (PRD) of MIM [45]. MIM is involved in cytoskeleton rearrangements [38, 45, 46]: increased expression of MIM is accompanied by the formation of actin-rich protrusions resembling ruffles and microspikes [47]. In mouse kidney epithelial cells, MIM is co-localized with the Arp2/3 complex, where it can mediate the assembly of actin filaments [48, 49]. Apparently, the functionally active protein is assembled into homodimers, with the IMD domain playing an important role in this process [50]. MIM is expressed in the kidneys of mouse embryos in the region of branching-collecting ducts, tubules, and glomeruli [51]. A significant expression level of MIM has been found in the cortical layer of newborn mouse kidneys, while a low MIM expression level has been shown in the brain area. Mice with a knockout *mtss1* gene (MIM<sup>-/-</sup>) were born healthy: however, about half of the animals developed large and numerous cysts in their kidneys by the age of 5, with signs of an autosomal-dominant polycystic kidney disease in [51]. MIM modulates the interaction between the cytoskeleton and the plasma membrane and facilitates maintenance of cellular contacts in renal epithelium [52]. Taking into account the important role of the MIM protein in the functioning of renal epithelial cells, a question arises regarding the involvement of this protein in the regulation of ENaC activity. The aim of our work was to study the involvement of the MIM protein in the actin-dependent regulation of ENaC and extend the model to ENaC regulation by actin-binding proteins.

## EXPERIMENTAL

### Cell lines

CHO (Chinese Hamster Ovary cells) cells of an immortalized line derived from Chinese hamster ovary epi-

thelial cells (CHO-K1, American collection of cell cultures) were used in the study. The cells were cultured in Petri dishes in a DMEM medium supplemented with 10% fetal bovine serum and 80 µg/ml of gentamicin.

### Transient transfection

Plasmids encoding the  $\alpha$ ,  $\beta$ , and  $\gamma$  subunits of mENaC [36, 53] and various forms of the mouse MIM protein (provided by Dr. Lappalainen and Dr. Zhao [45, 49, 54]) were used in the study. MIM full is the full-length protein; MIM PH is a chimeric protein containing an inactivated IMD domain conjugated to the PH (pleckstrin homology) domain of phospholipase C delta 1 (PLCD1) with impaired dimerization ability; MIM  $\Delta$ PRD is a protein lacking the PRD domain ( $\Delta$ 617–727), which does not interact with cortactin; MIM  $\Delta$ WH2 is a protein lacking the WH2 domain ( $\Delta$ 746–759), which does not polymerize G-actin; MIM/IMD-L is a plasmid that only encodes the long splice variant of the IMD domain, which is incapable of interacting with Rac GTPases (the rest of the protein is absent). All of the MIM plasmids encode the mouse protein and are based on the pEGFP-N5 vector. All information on plasmid design is contained in previously published articles [49, 54]. Reorganization of the cytoskeleton was analyzed using transient transfection of cells with various plasmids encoding the MIM protein and its mutant forms, with GFP transfection serving as a control. For electrophysiological experiments, cells were passaged on 4 × 4 mm coverslips with a density reaching 50–60% confluency on the day of transfection. The cells were co-transfected with the  $\alpha$ ,  $\beta$ , and  $\gamma$  subunits of mENaC (1: 1: 1 ratio) and various forms of the MIM protein 24 h prior to the experiments. The weight ratio of plasmid DNA is as follows:  $\alpha$ -mENaC, 0.33 µg;  $\beta$ -mENaC, 0.33 µg;  $\gamma$ -mENaC, 0.33 µg (total amount of mENaC-encoding plasmids, 1 µg); GFP in the control sample, 1 µg; MIM (with each of the forms carrying the GFP label), 1 µg. A total of 2 µg of plasmid DNA was used per transient transfection. All experiments were performed on CHO cells with the use of the PolyFect transfection reagent (Qiagen). GFP-encoding plasmid served as a marker of successful transfection in the control sample.

### Imaging of the cytoskeleton of fixed cells

Fixation and staining of the transfected CHO cells was performed according to a standard protocol [36]. Cells were passaged on the coverslips (12 × 12 mm), washed with PBS the next day, and then fixed with 3.7% formaldehyde for 10 minutes at room temperature. Then, the cells were perforated with 0.1% Triton X-100 (5 min, room temperature) and incubated in a 2 µM rhodamine-phalloidin solution (Sigma-Aldrich) for 15 min at 37 °C. Nuclei were stained with a Hoechst-33342 dye

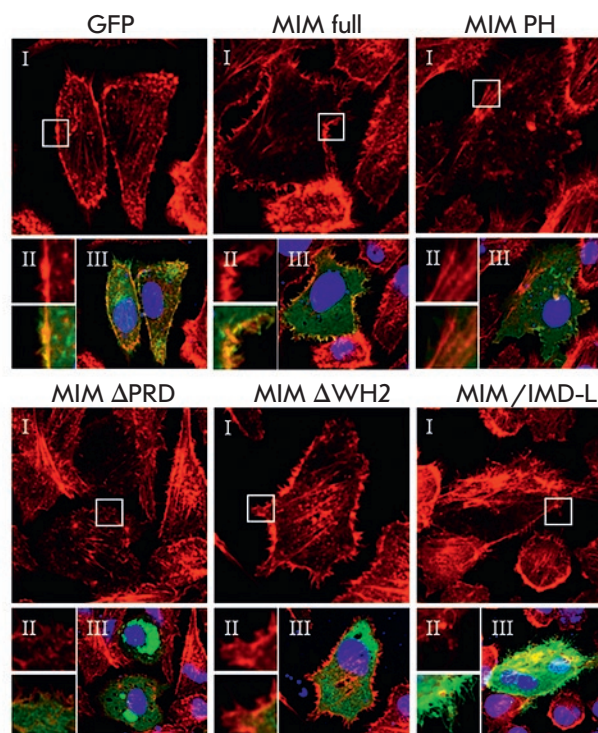
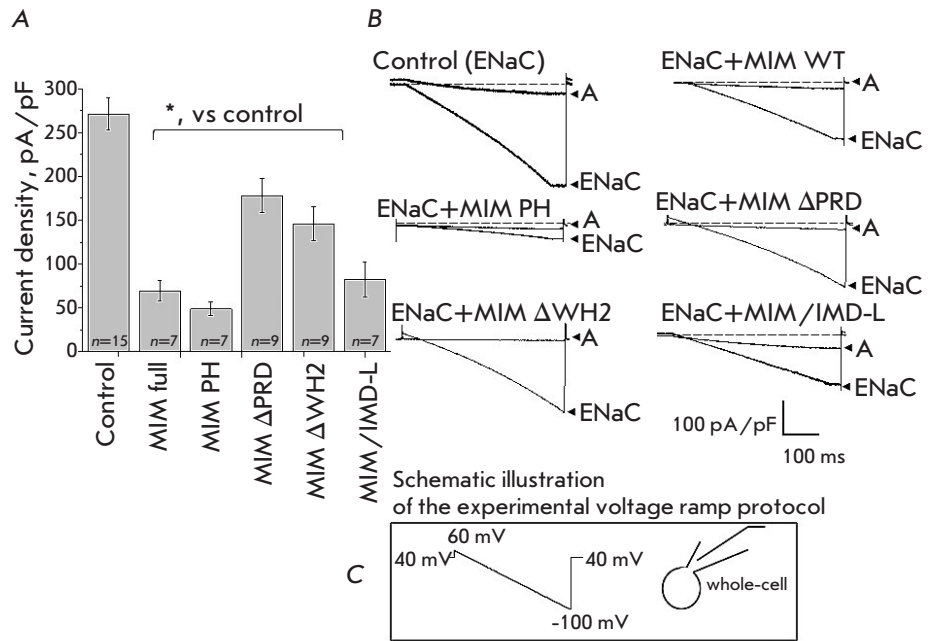


**Fig. 2.** Actin cytoskeleton arrangement after transfection with different types of the MIM protein. Images of the actin cytoskeleton acquired with a confocal microscope (typical micrographs from 3 independent experiments) in fixed CHO cells after transient transfection with plasmids encoding different forms of the MIM protein (each plasmid based on pEGFP vector). *GFP* – control transfection; *MIM full* – full-length protein; *MIM PH* – chimeric protein, where the inactive IMD domain is conjugated with the PH domain of PLCD1, which leads to MIM's inability to dimerize; *MIM  $\Delta$ PRD* – the PRD domain ( $\Delta$ 617–727) of MIM is removed, and the protein cannot interact with cortactin; *MIM  $\Delta$ WH2* – the WH2 domain ( $\Delta$ 746–759) of MIM is removed, and this form of MIM cannot polymerize G-actin; *MIM/IMD-L* – an isolated long splice variant of the IMD domain (the rest of the MIM protein is absent), which cannot interact with Rac GTPases. I – rhodamine-phalloidine emission (red). II – magnified images of selected areas: upper panel – rhodamine-phalloidine emission, lower panel – merged image. III – merged image of GFP (green), rhodamine-phalloidine (red) and Hoechst-33342 (nuclear acids dye, blue) emissions

(5 µg/ml, 5-min incubation, room temperature) and fixed on a slide using a Vectashield medium (Vector Laboratories). Addition of each reagent (pre-dissolved in PBS) was followed by washing with PBS. Imaging was carried out using a Nikon A-1R confocal microscope, ×100 lens, digital zoom. Lasers with excitation

**Fig. 3.** Effect of different forms of MIM on the amiloride-sensitive ENaC current density. **A** – summarized histogram of amiloride-sensitive current densities taken from electrophysiological experiments (patch-clamp in whole-cell configuration). CHO cells were co-transfected with mENaC plasmids, together with GFP (control), or mENaC with different types of the MIM protein ( $n$  – number of independent experiments; \* –  $p < 0.05$ ). **B** – representative traces of typical ENaC-mediated integral currents (ENaC – current magnitude, A – amiloride application at the end of the experiment ( $10 \mu\text{M}$ )). **C** – Schematic illustration of the experimental protocol



wavelengths of 405 nm (Hoechst-33342, emission maximum at 461 nm), 488 nm (GFP, emission maximum at 509 nm), and 561 nm (rhodamine-phalloidin, emission maximum at 565 nm) were used. Image analysis and processing were performed using the ImageJ software.

### Electrophysiology

Integral currents were recorded using the patch-clamp technique in the whole-cell configuration. In order to determine the maximum value of the ENaC-mediated integral current, the experiments were performed under fluid shear-stress conditions; for the determination of the minimum value at the end of the experiment, the ENaC-mediated integral current was inhibited by the addition of amiloride ( $10 \mu\text{M}$ ). An Axopatch 200B amplifier (Molecular Devices, Sunnyvale, CA, USA) connected via a Digidata 1440A A/D converter to a computer with installed pClamp 10.2 software (Molecular Devices) was used in the study. A Bessel filter (1 kHz) was used during the experiments. The currents were recorded at a fixed voltage using the previously described protocol [36] (schematic illustration of the voltage potential supply is shown in Fig. 3C): the potential was first held at +40 mV, followed by linear change from +60 mV to -100 mV (ramp, 500 ms duration). ENaC activity was defined as the current density value (current normalized to the cell capacitance) at -80 mV. Cells with a capacitance value in the range of  $6 \pm 10$  pF were used for the analysis (the electrical capacitance of the cells was compensated prior to the experiment). Co-transfection with  $\alpha$ -,  $\beta$ -, and  $\gamma$ -ENaC and a GFP-en-

coding plasmid (based on the pEGFP vector) was used as a negative control. The weight ratio of plasmid DNA was as follows:  $1 \mu\text{g}$  of  $\alpha$ -,  $\beta$ -, and  $\gamma$ -mENaC;  $1 \mu\text{g}$  of GFP. Intracellular solution composition was as follows (mM): 120 CsCl, 5 NaCl, 5 EGTA, 2  $\text{MgCl}_2$ , 2 Mg-ATP, 40 HEPES/Tris; pH 7.4. Extracellular solution composition was as follows (mM): 140 LiCl, 2  $\text{MgCl}_2$ , 10 HEPES/Tris, pH 7.4.

### Statistical analysis

All results are presented as a mean  $\pm$  standard error of the mean. Unpaired Student test calculated using the Microcal Origin 6.1 software (Microcal Software) was used for the analysis. Differences with  $p < 0.05$  were considered statistically significant.

## RESULTS AND DISCUSSION

### The effect of various mutant forms of the MIM protein on the structure of the cytoskeleton

We have studied the effect of the MIM protein (the domain structure of the protein is presented in Fig. 1) on cytoskeletal organization and ENaC activity. The effect of the MIM protein and its mutants on the cytoskeleton was analyzed in fixed CHO cells stained with rhodamine-phalloidin. The structure of the cytoskeleton in cells transfected with full-length MIM protein (Fig. 2, MIM full) was altered compared to the control transfection with GFP (Fig. 2, GFP): thickened actin filaments and formation of protrusions of the cell membrane (microspikes) in the sub-membrane region

were observed. Transfection with the chimeric protein (*Fig. 2, MIM PH*) resulted in similar changes in the cytoskeleton structure, whereas transfection with the protein lacking the proline-rich domain (which does not interact with cortactin; *Fig. 2, MIM ΔPRD*) or the protein lacking the WH2 domain (which is not capable of polymerizing G-actin; *Fig. 2, MIM ΔWH2*) did not cause such changes. Transfection with the long splice variant of the IMD domain only (which is incapable of interacting with Rac GTPases; *Fig. 2, MIM/IMD-L*) led to an uneven distribution of the cytoskeleton compared to transfection with a full-length protein. Our results are consistent with the data obtained using 3T3 fibroblast cells [38], where transfection with MIM-GFP resulted in the appearance of abnormal worm-like actin structures and a reduction in stress fibers. Similar rearrangements of the cytoskeleton were observed after transfection with MIM/IMD-L (long variant of the IMD domain only) in a study of the IMD domain in U2OS cells [49]. A suggestion has been made that this results from the deformation of the plasma membrane. Thus, the cytoskeleton reorganizations identified in our study are associated with the PRD and WH2 domains of the MIM protein. Since MIM interacts with cortactin via the proline-rich domain (PRD), it can be assumed that MIM modulates cortactin-dependent and Arp2/3-mediated actin polymerization [52], which is important for various cellular functions, including the formation of cellular protuberances [49].

### Effect of the MIM protein on the ENaC-mediated integral current

Dynamic rearrangements in the cytoskeleton are one of the mechanisms of ENaC activity regulation [14, 32]. According to data obtained by us using mouse kidney epithelial cells, the actin-binding proteins cortactin and Arp2/3 complex are involved in ENaC regulation [36]. MIM protein expression was detected in the kidney region expressing ENaC; its co-localization with cortactin and the proteins that form the Arp2/3 complex has been established [45, 52].

The following density values of the integral ENaC-mediated current were obtained in electrophysiological experiments (pA/pF): control,  $271.2 \pm 18.3$ ; co-transfection with MIM full,  $69.6 \pm 11.9$ ; MIM PH,  $48.9 \pm 7.8$ ; MIM ΔPRD,  $178.0 \pm 19.3$ ; MIM ΔWH2,  $146.0 \pm 19.4$ ; MIM/IMD-L,  $82.7 \pm 19.8$ . The summary diagram and representative current recordings are shown in *Fig. 3A,B*. As seen in *Fig. 3A*, the ENaC-mediated current was significantly lower upon co-transfection of channel subunits with full MIM protein. In addition, we showed that all of the tested mutants significantly reduce channel activity compared to the control values when channel subunits are expressed without MIM proteins.

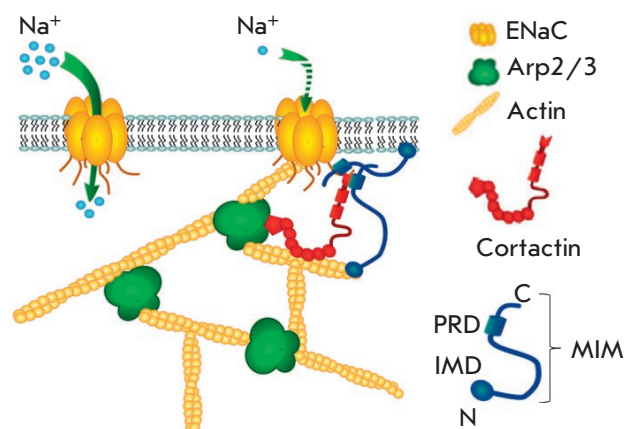


**Fig. 4.** Suggested scheme of actin-dependent regulation of ENaC by the actin-binding proteins MIM, cortactin, and the Arp2/3 complex

However, mutant forms of MIM (ΔPRD and ΔWH2) had the weakest effect on the integral current density. Thus, we can assume that the MIM protein (alongside the actin-binding proteins cortactin and Arp2/3 complex) is involved in the actin-mediated regulation of ENaC. Based on the obtained data, a hypothesis (*Fig. 4*) has been proposed according to which a multifunctional adapter protein MIM is involved in the cytoskeleton-mediated regulation of ENaC.

### CONCLUSION

Blood pressure in the body directly depends on the homeostasis of sodium ions ( $\text{Na}^+$ ). This process is regulated by kidneys through the re-absorption of  $\text{Na}^+$  and water via various ion channels and transporters, including the epithelial sodium channels (ENaC) in the aldosterone-sensitive distal nephron. The decrease in the ENaC open probability, as shown earlier [36], may be due to a cortactin-dependent and Arp2/3-mediated reorganization of the cytoskeleton. However, the exact mechanism of ENaC activity regulation by the cytoskeleton and adaptor proteins is not yet fully understood. The MIM adaptor protein can be a new actor in the multicomponent model of ENaC regulation. We established that MIM is involved in the cytoskeleton-mediated regulation of ENaC activity and showed the important role played by the PRD and WH2 domains using the patch-clamp electrophysiological technique. The resulting images of the cytoskeleton confirm the participation of the MIM protein in the processes of cytoskeleton organization. Thus, it is apparent that the activity of ENaC is regulated by cytoskeleton rearrangements with the participation of a multi-protein

complex which, alongside cortactin and the Arp2/3 complex, may also include MIM (Fig. 4). Studying the fine-tuning of this complex is important for understanding the molecular mechanisms that may underlie many pathophysiological conditions. ●

*The authors are grateful to Dr. Xi Zhan (University of Maryland School of Medicine) and Dr. Pekka Lappalainen (University of Helsinki) for providing the plasmids for the study of the MIM protein. We also*

*thank I.O. Vasilyeva, Dr. V.I. Chubinskiy-Nadezhdin, Dr. E.A. Morachevskaya (Institute of Cytology RAS) and Dr. Yu. Polina (Medical University of South Carolina) for critical comments, which were taken into account when writing this article.*

*This work was supported by grants from the National Heart, Lung, and Blood Institute (R35 HL135749 and R01 HL108880) and the National Institute of Diabetes and Digestive and Kidney Disease (R00 DK105160).*

## REFERENCES

- Janmey P.A. // *Physiol Rev.* 1998. V. 78. № 3. P. 763–781.
- Le Clairche C., Carlier M.F. // *Physiol Rev.* 2008. V. 88. № 2. P. 489–513.
- Wang Q., Zheng W., Wang Z., Yang J., Hussein S., Tang J., Chen X.Z. // *PLoS One.* 2015. V. 10. № 4. P. e0123018.
- Sudarikova A.V., Tsaplina O.A., Chubinskiy-Nadezhdin V.I., Morachevskaya E.A., Negulyaev Y.A. // *Biochem. Biophys. Res. Commun.* 2015. V. 461. № 1. P. 54–58.
- Karpushev A.V., Ilatovskaya D.V., Staruschenko A. // *BMC Res. Notes.* 2010. V. 3. P. 210.
- Alli A.A., Bao H.F., Liu B.C., Yu L., Aldrugh S., Montgomery D.S., Ma H.P., Eaton D.C. // *Am. J. Physiol. Renal Physiol.* 2015. V. 309. № 5. P. F456–463.
- Sasaki S., Yui N., Noda Y. // *Biochim. Biophys. Acta.* 2014. V. 1838. № 2. P. 514–520.
- Rooj A.K., Liu Z., McNicholas C.M., Fuller C.M. // *Am. J. Physiol. Cell Physiol.* 2015. V. 309. № 5. P. C308–319.
- Karpushev A.V., Levchenko V., Ilatovskaya D.V., Pavlov T.S., Staruschenko A. // *Hypertension.* 2011. V. 57. № 5. P. 996–1002.
- Karpushev A.V., Ilatovskaya D.V., Pavlov T.S., Negulyaev Y.A., Staruschenko A. // *PLoS One.* 2010. V. 5. № 1. P. e8827.
- Shin S.H., Lee E.J., Hyun S., Chun J., Kim Y., Kang S.S. // *Cell Signal.* 2012. V. 24. № 3. P. 641–651.
- Jovov B., Tousson A., Ji H.L., Keeton D., Shlyonsky V., Ripoll P.J., Fuller C.M., Benos D.J. // *J. Biol. Chem.* 1999. V. 274. № 53. P. 37845–37854.
- Copeland S.J., Berdiev B.K., Ji H.L., Lockhart J., Parker S., Fuller C.M., Benos D.J. // *Am. J. Physiol. Cell Physiol.* 2001. V. 281. № 1. P. C231–240.
- Mazzochi C., Bubien J.K., Smith P.R., Benos D.J. // *J. Biol. Chem.* 2006. V. 281. № 10. P. 6528–6538.
- Noda Y., Horikawa S., Katayama Y., Sasaki S. // *Biochem. Biophys. Res. Commun.* 2004. V. 322. № 3. P. 740–745.
- Noda Y., Sasaki S. // *Biochim. Biophys. Acta.* 2006. V. 1758. № 8. P. 1117–1125.
- Moeller H.B., Praetorius J., Rutzler M.R., Fenton R.A. // *Proc. Natl. Acad. Sci. USA.* 2010. V. 107. № 1. P. 424–429.
- Rogan M.P., Stoltz D.A., Hornick D.B. // *Chest.* 2011. V. 139. № 6. P. 1480–1490.
- Cantiello H.F. // *Exp. Physiol.* 1996. V. 81. № 3. P. 505–514.
- Chasan B., Geisse N.A., Pedatella K., Wooster D.G., Teintze M., Carattino M.D., Goldmann W.H., Cantiello H.F. // *Eur. Biophys. J.* 2002. V. 30. № 8. P. 617–624.
- Negulyaev Y.A., Vedernikova E.A., Maximov A.V. // *Mol. Biol. Cell.* 1996. V. 7. № 12. P. 1857–1864.
- Negulyaev Y.A., Khaitlina S.Y., Hinssen H., Shumilina E.V., Vedernikova E.A. // *J. Biol. Chem.* 2000. V. 275. № 52. P. 40933–40937.
- Chubinskiy-Nadezhdin V.I., Sudarikova A.V., Nikolsky N.N., Morachevskaya E.A. // *Dokl. Biochem, Biophys.* 2013. V. 450. P. 126–129.
- Chubinskiy-Nadezhdin V.I., Negulyaev Y.A., Morachevskaya E.A. // *Biochem. Biophys. Res. Commun.* 2011. V. 412. № 1. P. 80–85.
- Cantiello H.F., Stow J.L., Prati A.G., Ausiello D.A. // *Am. J. Physiol.* 1991. V. 261. № 5 Pt 1. P. C882–888.
- Staruschenko A., Negulyaev Y.A., Morachevskaya E.A. // *Biochim. Biophys. Acta.* 2005. V. 1669. № 1. P. 53–60.
- Kleyman T.R., Cragoe E.J., Jr. // *Semin, Nephrol.* 1988. V. 8. № 3. P. 242–248.
- Staruschenko A., Adams E., Booth R.E., Stockand J.D. // *Biophys. J.* 2005. V. 88. № 6. P. 3966–3975.
- Canessa C.M., Schild L., Buell G., Thorens B., Gautschi I., Horisberger J.D., Rossier B.C. // *Nature.* 1994. V. 367. № 6462. P. 463–467.
- Garty H., Palmer L.G. // *Physiol Rev.* 1997. V. 77. № 2. P. 359–396.
- Alvarez de la Rosa D., Canessa C.M., Fyfe G.K., Zhang P. // *Annu. Rev. Physiol.* 2000. V. 62. P. 573–594.
- Mazzochi C., Benos D.J., Smith P.R. // *Am. J. Physiol. Renal Physiol.* 2006. V. 291. № 6. P. F1113–1122.
- Rotin D., Bar-Sagi D., O’Brodivovich H., Merilainen J., Lehto V.P., Canessa C.M., Rossier B.C., Downey G.P. // *EMBO J.* 1994. V. 13. № 19. P. 4440–4450.
- Smith P.R., Saccomani G., Joe E.H., Angelides K.J., Benos D.J. // *Proc. Natl. Acad. Sci. USA.* 1991. V. 88. № 16. P. 6971–6975.
- Klemens C.A., Edinger R.S., Kightlinger L., Liu X., Butterworth M.B. // *J. Biol. Chem.* 2017. V. 292. № 1. P. 375–385.
- Ilatovskaya D.V., Pavlov T.S., Levchenko V., Negulyaev Y.A., Staruschenko A. // *FASEB J.* 2011. V. 25. № 8. P. 2688–2699.
- Lee Y.G., Macoska J.A., Korenchuk S., Pienta K.J. // *Neoplasia.* 2002. V. 4. № 4. P. 291–294.
- Mattila P.K., Salminen M., Yamashiro T., Lappalainen P. // *J. Biol. Chem.* 2003. V. 278. № 10. P. 8452–8459.
- Machesky L.M., Johnston S.A. // *J. Mol. Med. (Berl.).* 2007. V. 85. № 6. P. 569–576.
- Nixdorf S., Grimm M.O., Loberg R., Marreiros A., Russell P.J., Pienta K.J., Jackson P. // *Cancer Lett.* 2004. V. 215. № 2. P. 209–220.
- Bompard G., Sharp S.J., Freiss G., Machesky L.M. // *J. Cell. Sci.* 2005. V. 118. Pt. 22. P. 5393–5403.
- Dawson J.C., Bruche S., Spence H.J., Braga V.M., Machesky L.M. // *PLoS One.* 2012. V. 7. № 3. P. e31141.
- Mertz K.D., Pathria G., Wagner C., Saarikangas J., Sboner A., Romanov J., Gschaidner M., Lenz F., Neumann F., Schreiner W., et al. // *Nat. Commun.* 2014. V. 5. P. 3465.

44. Ma S., Guan X.Y., Lee T.K., Chan K.W. // *Hum. Pathol.* 2007. V. 38. № 8. P. 1201–1206.
45. Lin J., Liu J., Wang Y., Zhu J., Zhou K., Smith N., Zhan X. // *Oncogene*. 2005. V. 24. № 12. P. 2059–2066.
46. Yamagishi A., Masuda M., Ohki T., Onishi H., Mochizuki N. // *J. Biol. Chem.* 2004. V. 279. № 15. P. 14929–14936.
47. Woodings J.A., Sharp S.J., Machesky L.M. // *Biochem. J.* 2003. V. 371. Pt 2. P. 463–471.
48. Lee S.H., Kerff F., Chereau D., Ferron F., Klug A., Dominguez R. // *Structure*. 2007. V. 15. № 2. P. 145–155.
49. Mattila P.K., Pykalainen A., Saarikangas J., Paavilainen V.O., Vihinen H., Jokitalo E., Lappalainen P. // *J. Cell. Biol.* 2007. V. 176. № 7. P. 953–964.
50. Cao M., Zhan T., Ji M., Zhan X. // *Biochem. J.* 2012. V. 446. № 3. P. 469–475.
51. Xia S., Li X., Johnson T., Seidel C., Wallace D.P., Li R. // *Development*. 2010. V. 137. № 7. P. 1075–1084.
52. Saarikangas J., Mattila P.K., Varjosalo M., Bovellan M., Hakanen J., Calzada-Wack J., Tost M., Jennen L., Rathkolb B., Hans W., et al. // *J. Cell. Sci.* 2011. V. 124. Pt 8. P. 1245–1255.
53. Staruschenko A., Pochynyuk O.M., Tong Q., Stockand J.D. // *Biochim. Biophys. Acta*. 2005. V. 1669. № 2. P. 108–115.
54. Zhao H., Pykalainen A., Lappalainen P. // *Curr. Opin. Cell. Biol.* 2011. V. 23. № 1. P. 14–21.

## GENERAL RULES

*Acta Naturae* publishes experimental articles and reviews, as well as articles on topical issues, short reviews, and reports on the subjects of basic and applied life sciences and biotechnology.

The journal is published by the Park Media publishing house in both Russian and English.

The journal *Acta Naturae* is on the list of the leading periodicals of the Higher Attestation Commission of the Russian Ministry of Education and Science. The journal *Acta Naturae* is indexed in PubMed, Web of Science, Scopus and RCSI databases.

The editors of *Acta Naturae* ask of the authors that they follow certain guidelines listed below. Articles which fail to conform to these guidelines will be rejected without review. The editors will not consider articles whose results have already been published or are being considered by other publications.

The maximum length of a review, together with tables and references, cannot exceed 60,000 characters with spaces (approximately 30 pages, A4 format, 1.5 spacing, Times New Roman font, size 12) and cannot contain more than 16 figures.

Experimental articles should not exceed 30,000 symbols (approximately 15 pages in A4 format, including tables and references). They should contain no more than ten figures.

A short report must include the study's rationale, experimental material, and conclusions. A short report should not exceed 12,000 symbols (8 pages in A4 format including no more than 12 references). It should contain no more than four figures.

The manuscript and the accompanying documents should be sent to the Editorial Board in electronic form:

- 1) text in Word 2003 for Windows format;
- 2) the figures in TIFF format;
- 3) the text of the article and figures in one pdf file;
- 4) the article's title, the names and initials of the authors, the full name of the organizations, the abstract, keywords, abbreviations, figure captions, and Russian references should be translated to English;
- 5) the cover letter stating that the submitted manuscript has not been published elsewhere and is not under consideration for publication;
- 6) the license agreement (the agreement form can be downloaded from the website [www.actanaturae.ru](http://www.actanaturae.ru)).

## MANUSCRIPT FORMATTING

The manuscript should be formatted in the following manner:

- Article title. Bold font. The title should not be too long or too short and must be informative. The title should not exceed 100 characters. It should reflect the major result, the essence, and uniqueness of the work, names and initials of the authors.
- The corresponding author, who will also be working with the proofs, should be marked with a footnote \*.
- Full name of the scientific organization and its departmental affiliation. If there are two or more scientific organizations involved, they should be linked by digital superscripts with the authors' names. Ab-

stract. The structure of the abstract should be very clear and must reflect the following: it should introduce the reader to the main issue and describe the experimental approach, the possibility of practical use, and the possibility of further research in the field. The average length of an abstract is 20 lines (1,500 characters).

- Keywords (3 – 6). These should include the field of research, methods, experimental subject, and the specifics of the work. List of abbreviations.

• INTRODUCTION

• EXPERIMENTAL PROCEDURES

• RESULTS AND DISCUSSION

• CONCLUSION

The organizations that funded the work should be listed at the end of this section with grant numbers in parenthesis.

• REFERENCES

The in-text references should be in brackets, such as [1].

## RECOMMENDATIONS ON THE TYPING AND FORMATTING OF THE TEXT

- We recommend the use of Microsoft Word 2003 for Windows text editing software.
- The Times New Roman font should be used. Standard font size is 12.
- The space between the lines is 1.5.
- Using more than one whole space between words is not recommended.
- We do not accept articles with automatic referencing; automatic word hyphenation; or automatic prohibition of hyphenation, listing, automatic indentation, etc.
- We recommend that tables be created using Word software options (Table → Insert Table) or MS Excel. Tables that were created manually (using lots of spaces without boxes) cannot be accepted.
- Initials and last names should always be separated by a whole space; for example, A. A. Ivanov.
- Throughout the text, all dates should appear in the “day.month.year” format, for example 02.05.1991, 26.12.1874, etc.
- There should be no periods after the title of the article, the authors' names, headings and subheadings, figure captions, units (s – second, g – gram, min – minute, h – hour, d – day, deg – degree).
- Periods should be used after footnotes (including those in tables), table comments, abstracts, and abbreviations (mon. – months, y. – years, m. temp. – melting temperature); however, they should not be used in subscripted indexes ( $T_m$  – melting temperature;  $T_{pt}$  – temperature of phase transition). One exception is mln – million, which should be used without a period.
- Decimal numbers should always contain a period and not a comma (0.25 and not 0,25).
- The hyphen (“-”) is surrounded by two whole spaces, while the “minus,” “interval,” or “chemical bond” symbols do not require a space.
- The only symbol used for multiplication is “×”; the “x” symbol can only be used if it has a number to its

right. The “.” symbol is used for denoting complex compounds in chemical formulas and also noncovalent complexes (such as DNA·RNA, etc.).

- Formulas must use the letter of the Latin and Greek alphabets.
- Latin genera and species' names should be in italics, while the taxa of higher orders should be in regular font.
- Gene names (except for yeast genes) should be italicized, while names of proteins should be in regular font.
- Names of nucleotides (A, T, G, C, U), amino acids (Arg, Ile, Val, etc.), and phosphonucleotides (ATP, AMP, etc.) should be written with Latin letters in regular font.
- Numeration of bases in nucleic acids and amino acid residues should not be hyphenated (T34, Ala89).
- When choosing units of measurement, SI units are to be used.
- Molecular mass should be in Daltons (Da, KDa, MDa).
- The number of nucleotide pairs should be abbreviated (bp, kbp).
- The number of amino acids should be abbreviated to aa.
- Biochemical terms, such as the names of enzymes, should conform to IUPAC standards.
- The number of term and name abbreviations in the text should be kept to a minimum.
- Repeating the same data in the text, tables, and graphs is not allowed.

## GUIDENESS FOR ILLUSTRATIONS

- Figures should be supplied in separate files. Only TIFF is accepted.
- Figures should have a resolution of no less than 300 dpi for color and half-tone images and no less than 500 dpi.
- Files should not have any additional layers.

## REVIEW AND PREPARATION OF THE MANUSCRIPT FOR PRINT AND PUBLICATION

Articles are published on a first-come, first-served basis. The members of the editorial board have the right to recommend the expedited publishing of articles which are deemed to be a priority and have received good reviews.

Articles which have been received by the editorial board are assessed by the board members and then sent for external review, if needed. The choice of reviewers is up to the editorial board. The manuscript is sent on to reviewers who are experts in this field of research, and the editorial board makes its decisions based on the reviews of these experts. The article may be accepted as is, sent back for improvements, or rejected.

The editorial board can decide to reject an article if it does not conform to the guidelines set above.

The return of an article to the authors for improvement does not mean that the article has been accept-

ed for publication. After the revised text has been received, a decision is made by the editorial board. The author must return the improved text, together with the responses to all comments. The date of acceptance is the day on which the final version of the article was received by the publisher.

A revised manuscript must be sent back to the publisher a week after the authors have received the comments; if not, the article is considered a resubmission.

E-mail is used at all the stages of communication between the author, editors, publishers, and reviewers, so it is of vital importance that the authors monitor the address that they list in the article and inform the publisher of any changes in due time.

After the layout for the relevant issue of the journal is ready, the publisher sends out PDF files to the authors for a final review.

Changes other than simple corrections in the text, figures, or tables are not allowed at the final review stage. If this is necessary, the issue is resolved by the editorial board.

## FORMAT OF REFERENCES

The journal uses a numeric reference system, which means that references are denoted as numbers in the text (in brackets) which refer to the number in the reference list.

*For books:* the last name and initials of the author, full title of the book, location of publisher, publisher, year in which the work was published, and the volume or issue and the number of pages in the book.

*For periodicals:* the last name and initials of the author, title of the journal, year in which the work was published, volume, issue, first and last page of the article. Must specify the name of the first 10 authors. Ross M.T., Grafham D.V., Coffey A.J., Scherer S., McLay K., Muzny D., Platzer M., Howell G.R., Burrows C., Bird C.P., et al. // Nature. 2005. V. 434. № 7031. P. 325–337.

References to books which have Russian translations should be accompanied with references to the original material listing the required data.

References to doctoral thesis abstracts must include the last name and initials of the author, the title of the thesis, the location in which the work was performed, and the year of completion.

References to patents must include the last names and initials of the authors, the type of the patent document (the author's rights or patent), the patent number, the name of the country that issued the document, the international invention classification index, and the year of patent issue.

The list of references should be on a separate page. The tables should be on a separate page, and figure captions should also be on a separate page.

**The following e-mail addresses can be used to contact the editorial staff: vera.knorre@gmail.com, actanaturae@gmail.com, tel.: (495) 727-38-60, (495) 930-87-07**